File
NASW 1082
CONTRACT
RRL 3/28/67

FINAL REPORT
for Period
27 September 1964 to 28 September 1966

INVESTIGATIONS OF ELECTRON EMISSION CHARACTERISTICS OF LOW WORK FUNCTION SURFACES

by

L. W. Swanson
A. E. Bell
L. C. Crouser
B. E. Evans

Prepared for

Headquarters
National Aeronautics and Space Administration
Washington, D. C.

November 1966

CONTRACT NASw - 1082

Field Emission Corporation

McMinnville, Oregon

FINAL REPORT
for Period
27 September 1964 to 28 September 1966

INVESTIGATIONS OF ELECTRON EMISSION CHARACTERISTICS OF LOW WORK FUNCTION SURFACES

by

L. W. Swanson
A. E. Bell
L C Crouser
B. E. Evans

Prepared for

Headquarters
National Aeronautics and Space Administration
Washington, D. C.

November 1966

CONTRACT NASw-1082

FIELD EMISSION CORPORATION
Melrose Avenue at Linke Street
McMinnville, Oregon 97128

MEETINGS ATTENDED AND PAPERS GIVEN

The following list gives meetings attended, personnel who attended and titles of papers given during contract period:

Meeting	Paper	Given By
Twenty-Fifth Annual Conference on Physical Electronics, March 24-26, 1965, MIT.	Nottingham Effect in Field and T-F Emission: Heating and Cooling Domains, and Inversion Temperature.	L. W. Swanson
12th Annual Field Emission Symposium, Sept. 7-11, 1965, Pennsylvania State University.	1) Anomalies in the Nottingham Effect 2) Total Energy Distribution Measurements at Elevated Temperatures.	L. W. Swanson
13th Annual Field Emission Symposium, Sept. 6-10, 1966, Cornell University.	1) Total Energy Distribution from Clean and Zirconium-Coated Tungsten Field Emitters.	L. W. Swanson
	2) Single Plane Studies of Oxygen Adsorption on Tungsten.	A. E. Bell

PUBLICATIONS

1. Nottingham Effect in Field and T-F Emission: Heating and Cooling Domains, and Inversion Temperature, Physical Review Letters 13, 397 (1964).

2. Anomalous Total Energy Distribution for a Tungsten Field Emitter, Physical Review Letters 16, 389 (1966).

3. Energy Exchanges Attending Field Electron Emission from Tungsten, Phys. Rev. 151, 327 (1966).

TABLE OF CONTENTS

TABLE OF CONTENTS Cont'd

I PREFACE

This report describes work performed under support from NASA, Headquarters, Washington, D. C., for a two year period ending September 27, 1966. The primary purpose of this work has been to gain an improved fundamental understanding of

(1) the phenomena governing the production of low work function surfaces, and

(2) the factors affecting the quality and stability of electron emission characteristics.

It is anticipated that information generated from this investigation will be relevant to various kinds of electron emission (i. e., photo, thermionic and field emission), although the primary emphasis was placed upon field emission.

The formation of low work function surfaces was accomplished by;

(1) adsorption of appropriate electropositive adsorbates, and

(2) coadsorption of appropriate electropositive and electronegative adsorbates.

Various properties of these surfaces investigated in order to obtain a more fundamental understanding of them were the temperature dependency of the emission and work function, the various types of energy exchanges accompanying emission, the energy distribution of the field emitted electron, and various aspects of the surface kinetics of adsorbed layers such as binding energy, surface mobility and effect of external fields.

II ENERGY EXCHANGES ATTENDING FIELD ELECTRON EMISSION

INTRODUCTION

Electron emission is accompanied by energy exchanges between the conduction electrons and lattice, which become particularly important at the very high emission densities feasible with field and thermal-field (T-F) emission cathodes. Their study is of basic interest as it provides a complementary check, through a direct measurement of the average energy of emitted electrons, of the theory of field and T-F emission; it is also of practical importance because these energy exchanges control the cathode emitter tip temperature and set an upper limit on the feasible emission density. The work reported herein is an attempt to confirm, by direct measurement of the energy exchange, the theoretically predicted temperature dependence of the energy exchange and the reversal of its direction (from cathode heating to cooling) at high emitter temperatures.

There are two main emission induced energy exchange phenomena. The familiar resistive Joule heating effect was studied in the case of field emission by Dyke, et al [1], and Dolan, Dyke and Trolan [2]. In the usual case where resistivity increases rapidly with temperature, resistive heating by itself leads to an inherently unstable situation at high emission densities.

Since stable high density emission is observed [3], there must exist another factor having a strong and stabilizing influence on the cathode tip temperature.

Such a stabilizing factor is provided by the energy exchange resulting from the difference between the average energy of the emitted electrons, $\langle E \rangle$, and that of the replacement electron supplied from the Fermi sea, $\langle E' \rangle$. In the case of thermionic emission this phenomenon, discussed by Richardson [4] and later by Nottingham [5], is well known and produces cooling of a cathode with a work function ϕ by an average energy amount $e\phi + 2kT$ per emitted electron. The corresponding effect in field and T-F emission was first discussed by Fleming and Henderson [6], who were unable to detect it experimentally, and has been a subject of controversy [5,6] with respect to the correct value of $\langle E' \rangle$ and hence the direction of the effect (cathode cooling occurs when $\langle E \rangle > \langle E' \rangle$), and heating when $\langle E \rangle < \langle E' \rangle$). Preliminary data reported earlier [7] tended to support the view of Nottingham who took $\langle E' \rangle$ to be the Fermi energy E_f and, on that basis, predicted heating of the cathode in the case of field emission. Thus, the energy exchange corresponding to the replacement electron at energy E_f will be referred to as the "Nottingham Effect". The new experimental results discussed below for tungsten indicate that $\langle E' \rangle \neq E_f$, seeming at first glance to support the view of Fleming and Henderson. However, this agreement is thought to be fortuitous and the observed difference between $\langle E' \rangle$ and E_f is attributed to the fact that conduction processes in tungsten are not well described by the free-electron model.

The combined effect of resistive and Nottingham phenomena has been treated in the special case of tungsten field emitters initially at room temperature[8]; this work was later extended to other work functions and confirmed experimentally.[9] Levine[10] gave a theoretical analysis of a similar problem. Drechsler[11,12] has reported both departure and agreement with theoretical predictions for the temperature dependence of the Nottingham Effect and for the value of the inversion temperature for tungsten. The purpose of the present work was to permit a better check of existing theory through careful measurement of the Nottingham Effect for both clean and coated tungsten field emitters.

EXPERIMENTAL APPROACHES

The main difficulty in measuring energy-exchange phenomena in field and T-F emission is the strong localization of these phenomena and of the associated temperature changes; this localization results from the cathode geometry (very sharp needles with a conical shank and a tip radius well below one micron) with which controlled field emission is most reliably obtained. A determination of both the magnitude and the location of the energy transfer requires measurement of the temperature at the emitting area itself, which is of the order of 10^{-9} cm^2. For this purpose, temperature-sensitive coatings of materials which alter the cathode

work function can be used to sense the local tip temperature. Measurements of this type, discussed in this paper, conclusively established the existence of emission heating and cooling domains; within limit of experimental accuracy, they also confirm the magnitude of the energy exchange and its localization within a few tip radii of the cathode tip. However, the complex experimental conditions (pulsed emission, large field and temperature gradients near the tip, etc.) limit the accuracy of this approach; therefore, a more precise method has been used to measure the magnitude (but not the location) of the energy exchange and the inversion temperature, i.e., the temperature for which $\langle E \rangle = \langle E' \rangle$.

Temperature-Sensitive Coatings

One method of estimating the local temperature at the emitter tip consists of coating the emitter with adsorbates whose desorption or surface migration temperatures are determined in a separate experiment. We have employed this method primarily to establish the degree of localization of the energy exchange process and to obtain a qualitative estimate of the emitter tip temperature. The main difficulty in employing this method for quantitative temperature determination during emission arises from field effects [13] on the thermal desorption and surface migration rates.

The method employed by us consisted of depositing cesium, barium, or zirconium coadsorbed with oxygen, onto a tungsten emitter at low temperature in a standard field electron microscope tube. After migrating the adsorbate across the emitter by heating, the emitter was cooled and

a 1 μsec square wave pulsed voltage (at a repetition rate of 100 pps) was applied to the anode in order to draw a field emission current sufficient to heat the emitter tip. The high emission current (ca 30 to 100 mA) necessary to cause an appreciable temperature change, restricted the experiment to low duty factor pulsed emission since dc emission currents of such high levels will usually cause severe instability of the emission.

From the adsorbate coverage change after a specified emission time (as determined from work function variation) due to thermal desorption, the maximum temperature of the emitter could be inferred from previous thermal desorption data. Field electron emission patterns were also analyzed in order to ascertain the regions of the emitter which exhibited adsorbate removal.

Direct Measurement of the Energy Exchange

The method employed to obtain quantitative measurement of the energy exchange accompanying field emission is a refinement of that used by Drechsler [12] who obtained field and T-F emission from random protrusions on the surface of very thin wires. Briefly stated, the method is to provide an emitter-support filament of sufficient thermal impedance that the small heat input resulting from a low field electron emission current may be detected sensitively through the associated change in temperature and resistance of the filament. Reliance on emission from several random protrusions of unknown number, geometry and location creates uncertainties in the interpretation of the data which are avoided

here by confining emission to a single field-emission needle (whose precise geometry could be determined in an electron microscope and from field electron emission I-V characteristics) mounted at the center of a smooth wire one inch long and approximately 1.1 mil in diameter. The tip assembly shown in Figure 1 consists of two 40 mil moly rods a and a' supporting the emitter support wire b to which two 0.5 mil potential leads c and c' are spot welded for sampling resistance changes across a 200 mil portion of the emitter support filament. The central 1.1 mil diameter lead d carried the emission current in order to eliminate any IR drops on the emitter support filament due to the emission current itself. The temperature of the emitter e was controlled by adjusting a dc heating current through the filament b; the temperature was derived, to an accuracy of approximately 3%, from the resistance R of the 200 mil section of the emitter support filament. The thermal impedance of the structure was sufficiently large that emission-induced power inputs as low as 10 μw could be detected and measured. This had the advantage of permitting good measurements to be made at low dc current levels where the emission is highly stable and where the Nottingham Effect strongly predominates, resistive heating (which can be calculated only approximately) having only a relatively small effect. The emission-induced power input H at the emitter was derived from the change ΔR in support filament resistance caused by the associated change ΔT in support filament temperature. The experiment was confined to power inputs H small enough that ΔT and hence, ΔR could

be considered proportional to H. The experiment depended on the reliable determination of $c_o = \Delta R/H$ as a function of emitter temperature. This was extremely difficult to calculate because of the complex geometry of the emitter assembly and the importance of radiation losses at high temperatures. Hence, the tube was designed to permit direct experimental calibration of ΔR in terms of a known power input H. For this purpose the emitter could be bombarded by a fine 30 x 5 mil electron sheet beam generated by an auxiliary filament D of Figure 2 and focused by an 800 gauss magnetic field at the cathode tip; ΔR was measured as a function of bombarding beam power at various cathode temperatures. Alignment of the electron beam, so that it impinged on as small a section as possible of the 20 mil length field emitter, was accomplished by first aligning the emitter structure during fabrication so that only the very tip of the emitter protruded through the 30 mil circle defined by the aperture on plate A. The direction of the magnetic field was then adjusted during operation, while simultaneously measuring the beam current striking the emitter and the wire filaments C. The latter consisted of two 10 mil zirconium wires separated by 5 mils and served a two-fold purpose:

1) to determine the proper alignment and distribution of the bombarding beam during the emitter calibration, and
2) to serve as a source of zirconium which could be deposited onto the emitter for the purpose of changing the work function of the tip during the study of the Nottingham Effect.

The actual power calibration of the emitter assembly was performed by measuring ΔR vs the known power input H_b at the emitter due to the bombardment current I_b at various emitter temperatures ranging from 300 to 1100°K. For each temperature, a straight line was obtained and its slope yielded the value of c_o (as shown in Figure 3) as a function of temperature. As expected, c_o increased at low temperatures (as the thermal conductivity of tungsten decreases) then decreased at high temperatures as radiation losses became predominant. During the experimental measurements of ΔR vs H_b the potentials of the various tube elements were as follows: $V_D = -222$, $V_A = 0$, $V_B = -200$, $V_E = 0$ and $V_C = 0$ volts. This prevented secondary emission from the emitter and ensured that the only secondary electrons able to reach the emitter had originated at plate B and therefore possessed nearly full voltage. Furthermore, with careful beam alignment the number of such secondaries was very small since the beam was collimated by aperture A to a diameter much smaller than that of the apertures on B. Hence, H_b could without significant error be approximated by the product of V_D and the total current collected at the emitter.

The tube envelope was made of alumino-silicate glass in order to minimize helium diffusion in the tube after seal off. The tube embodiment was such that field electron patterns from the emitter could be displayed on a fluorescent screen in order to ascertain the orientation and cleanliness of the emitter surface. Tip cleaning was accomplished by a combination of electron bombardment and resistive heating of the emitter. The pressure

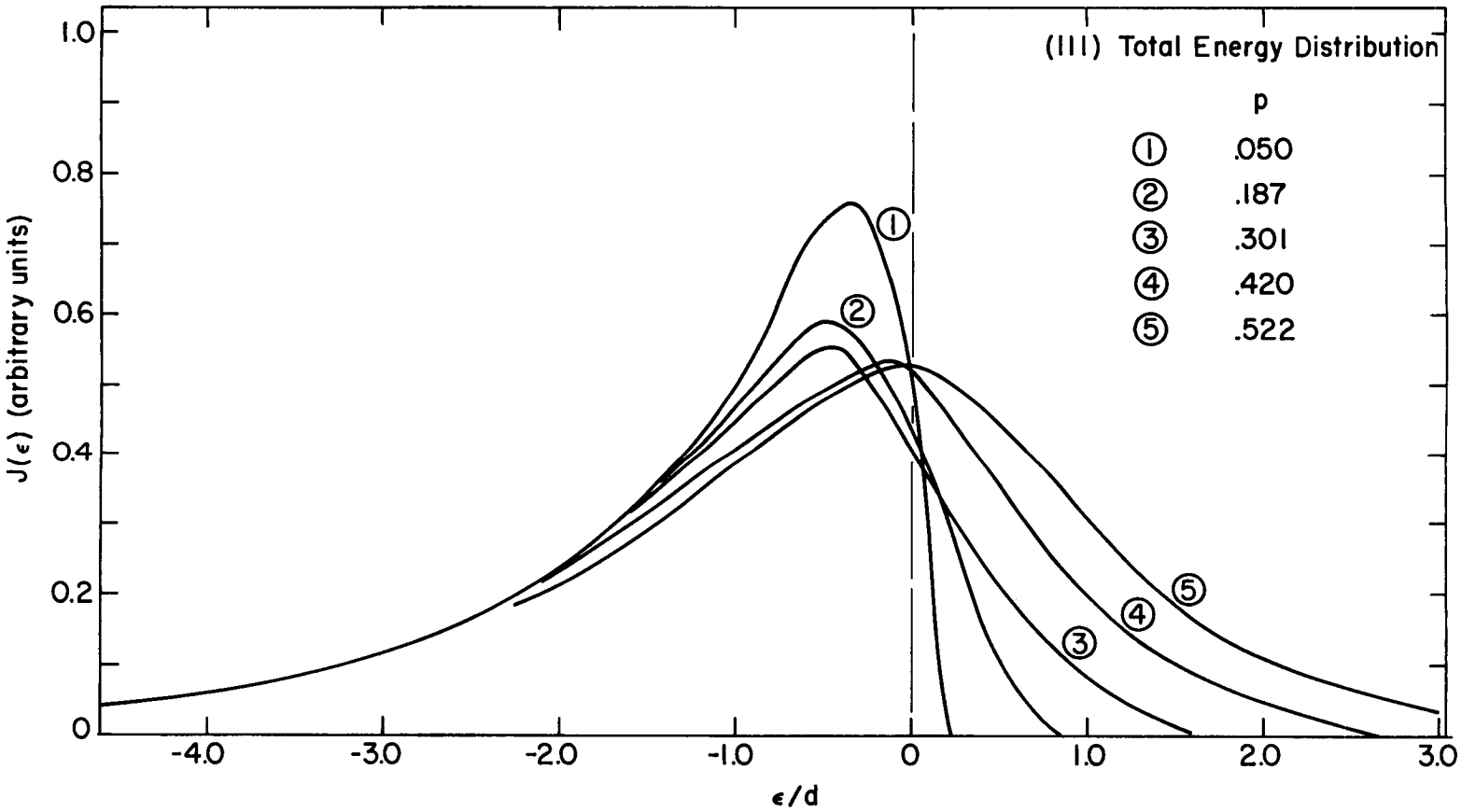

Figure 18. Experimental total energy distribution plots along the <111> direction of a W emitter as a function of p, where d = 0.134 eV and F = 2.99 x 10^7 V/cm.

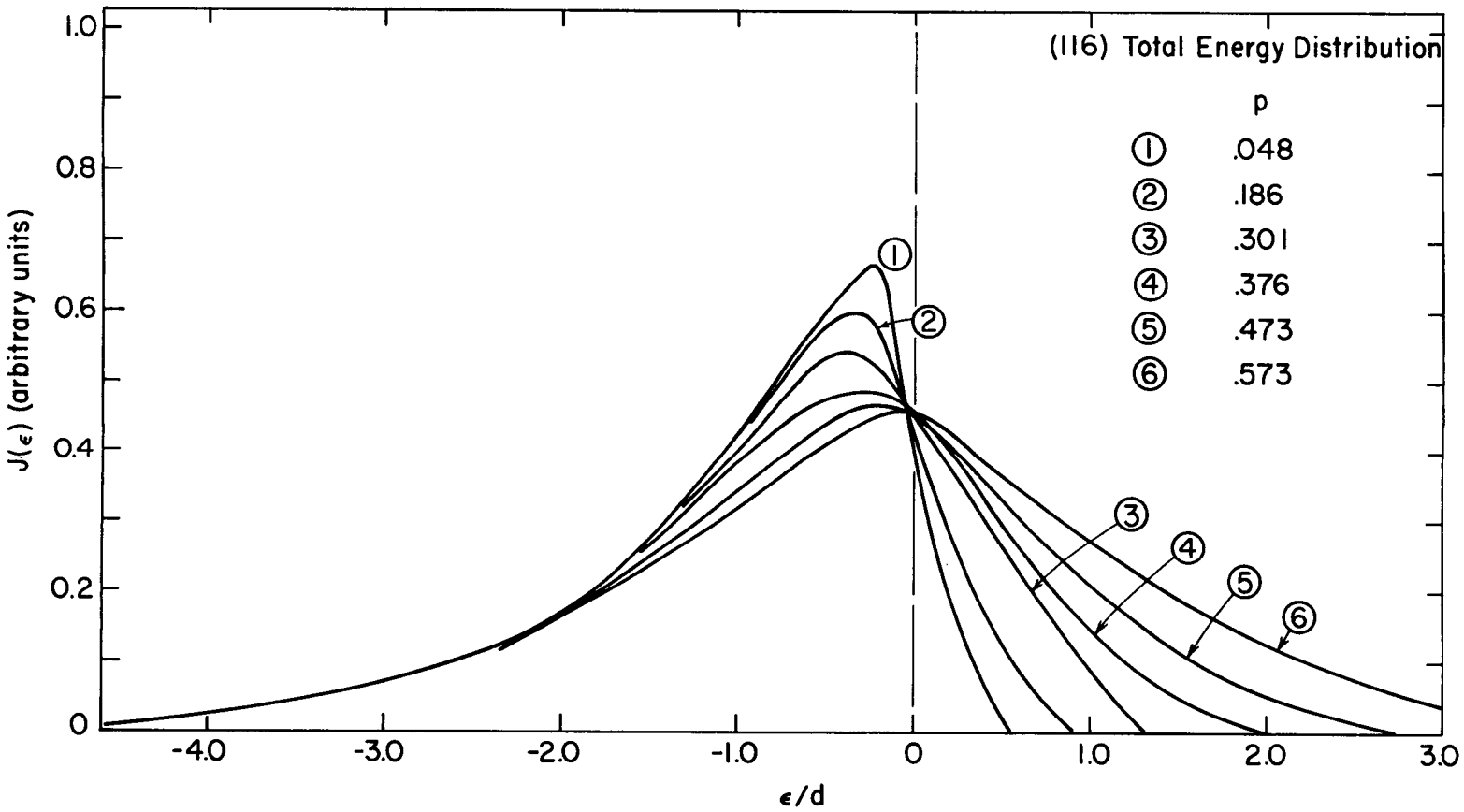

Figure 17. Experimental total energy distribution plots along the ⟨116⟩ direction of a W emitter as a function of p, where d = 0.138 eV and F = 3.04×10^7 V/cm.

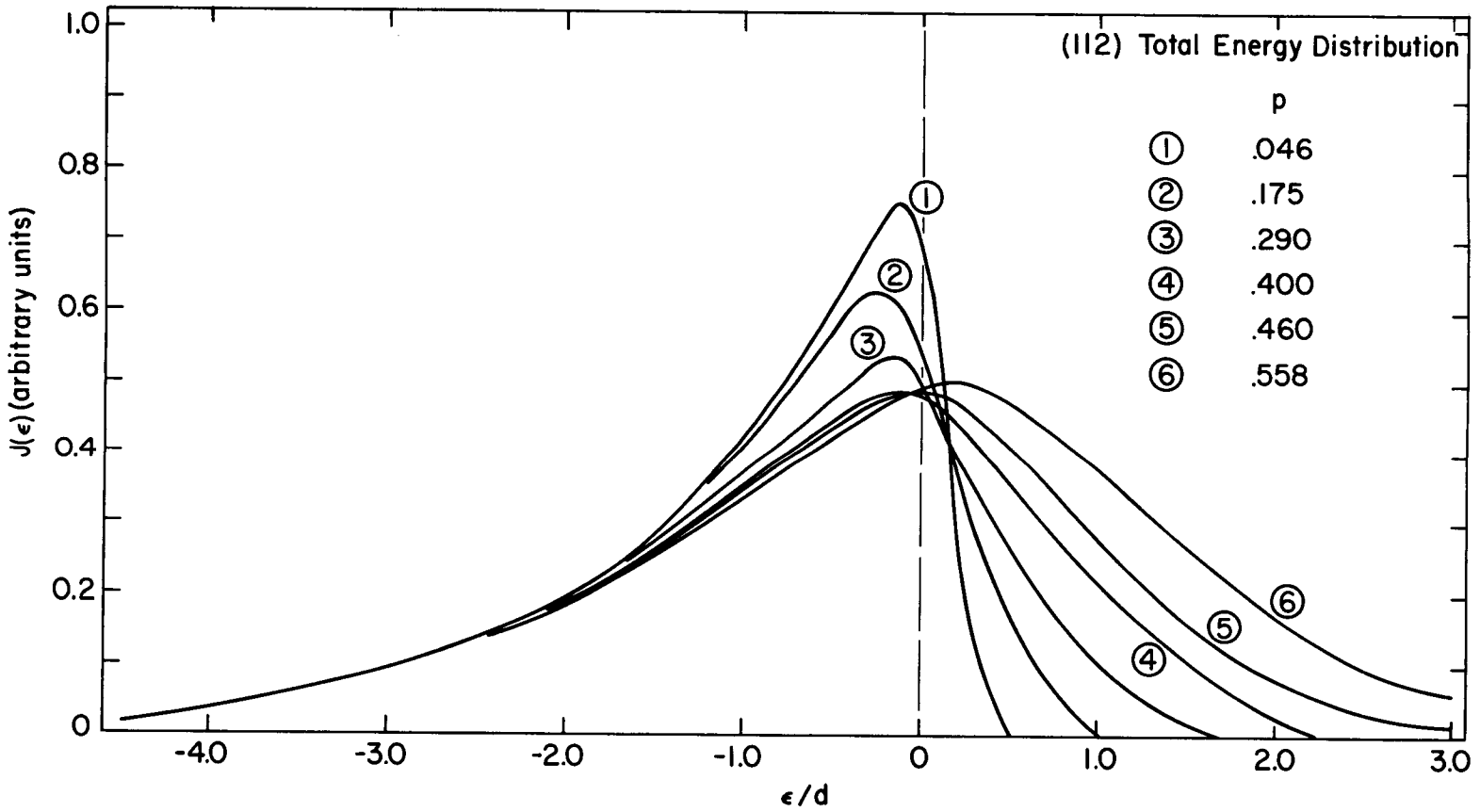

Figure 16. Experimental total energy distribution plots along the ⟨112⟩ direction of a W emitter as a function of p, where d = 0.146 eV and F = 3.48 x 10^7 V/cm.

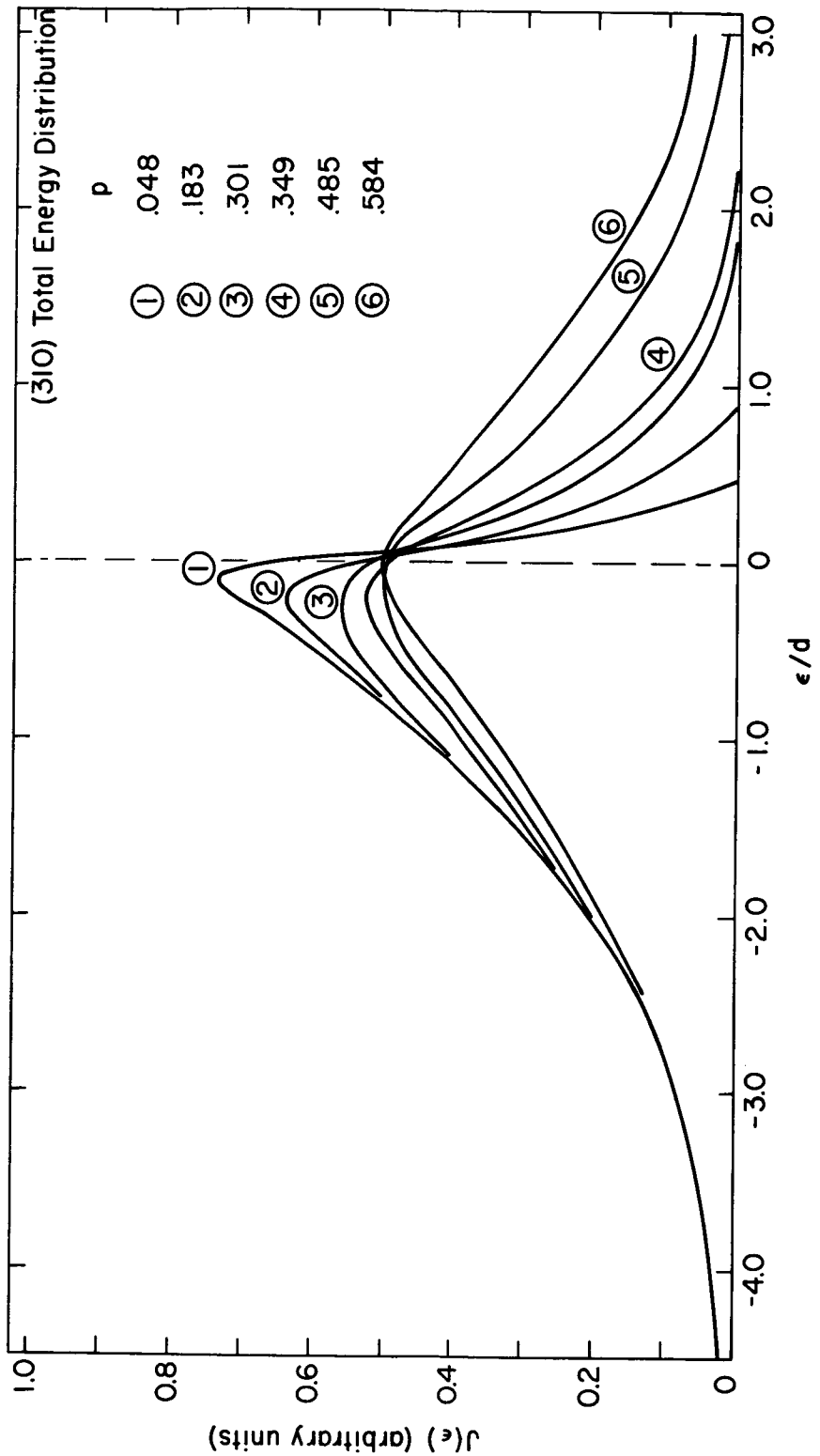

Figure 15. Experimental total energy distribution plots along the <310> direction of a W emitter as a function of p, where d = 0.137 eV and F = 3.06×10^7 V/cm.

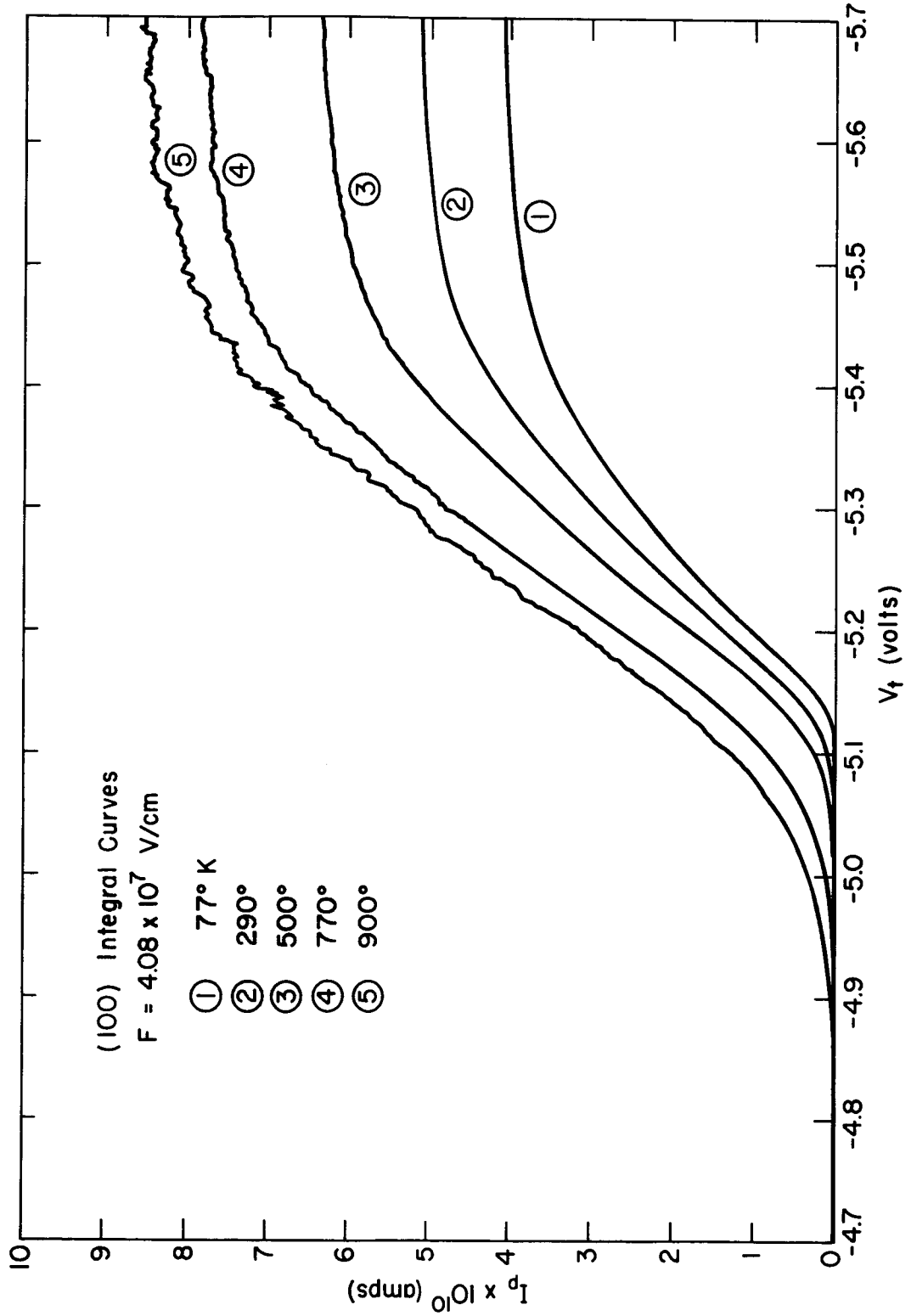

Figure 14. Recorder plots of the probe current I_p as a function of emitter bias voltage V_t at various temperatures.

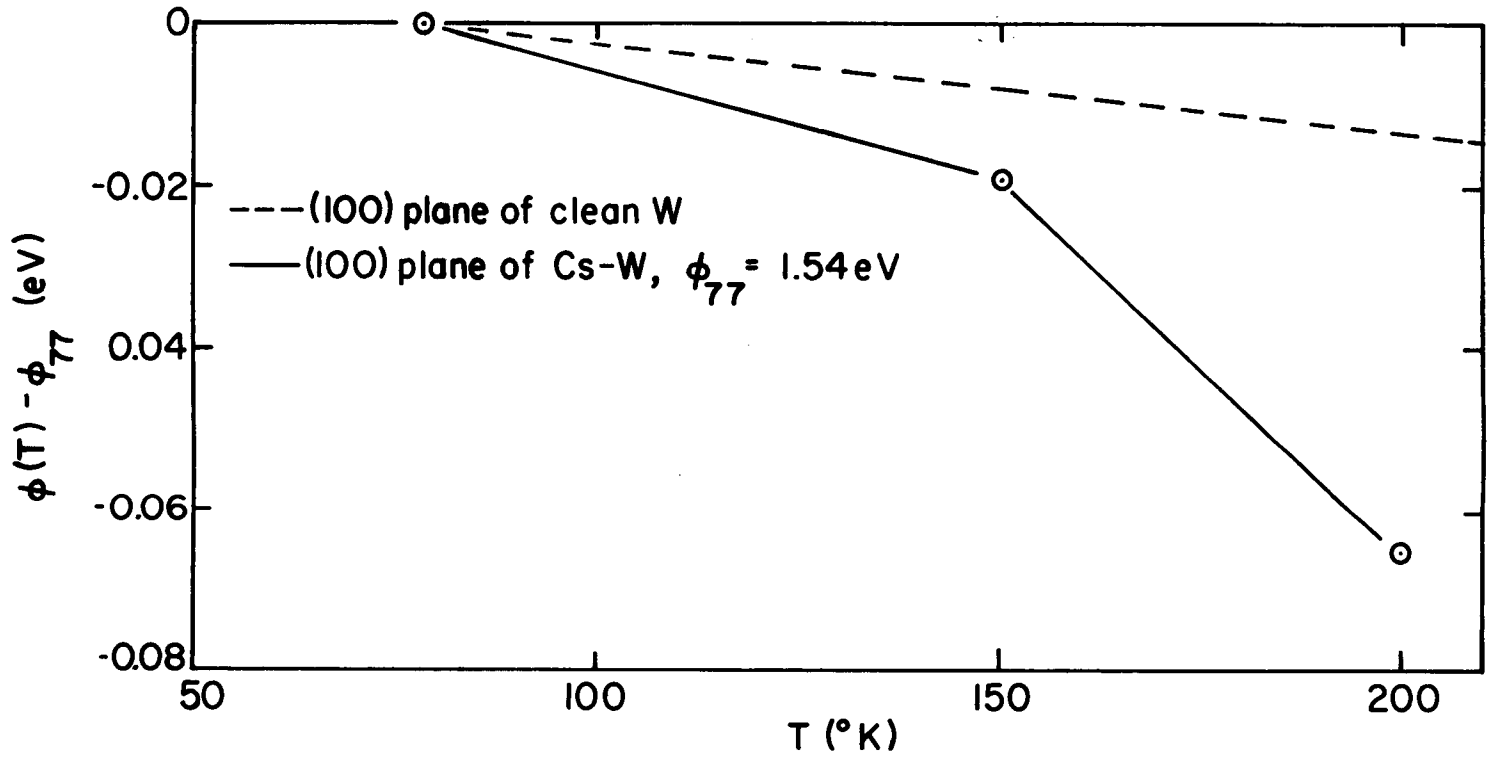

Figure 13. Plots show the variation of work function with temperature for the clean and Cs coated (100) plane of W. Average Cs coverage approximately $\sigma = 2.3 \times 10^{14}$ atoms/cm^2.

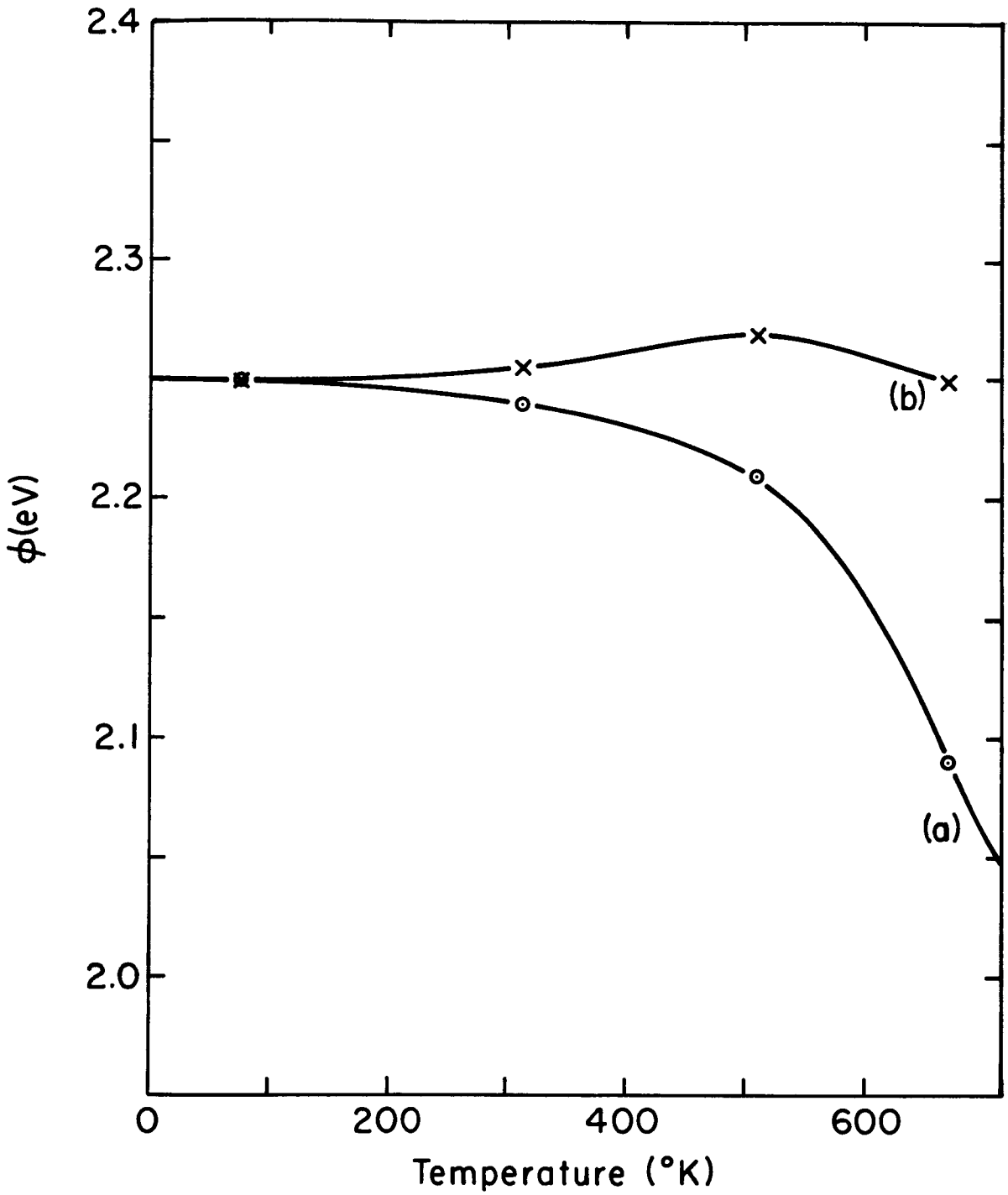

Figure 12. Curve (a) is the variation of the apparent work function of the (100) plane of a Zr/O coated tungsten emitter as determined by Equation (13). Curve (b) gives the curve (a) results corrected for the T-F contribution to the field emission current according to Equation (16).

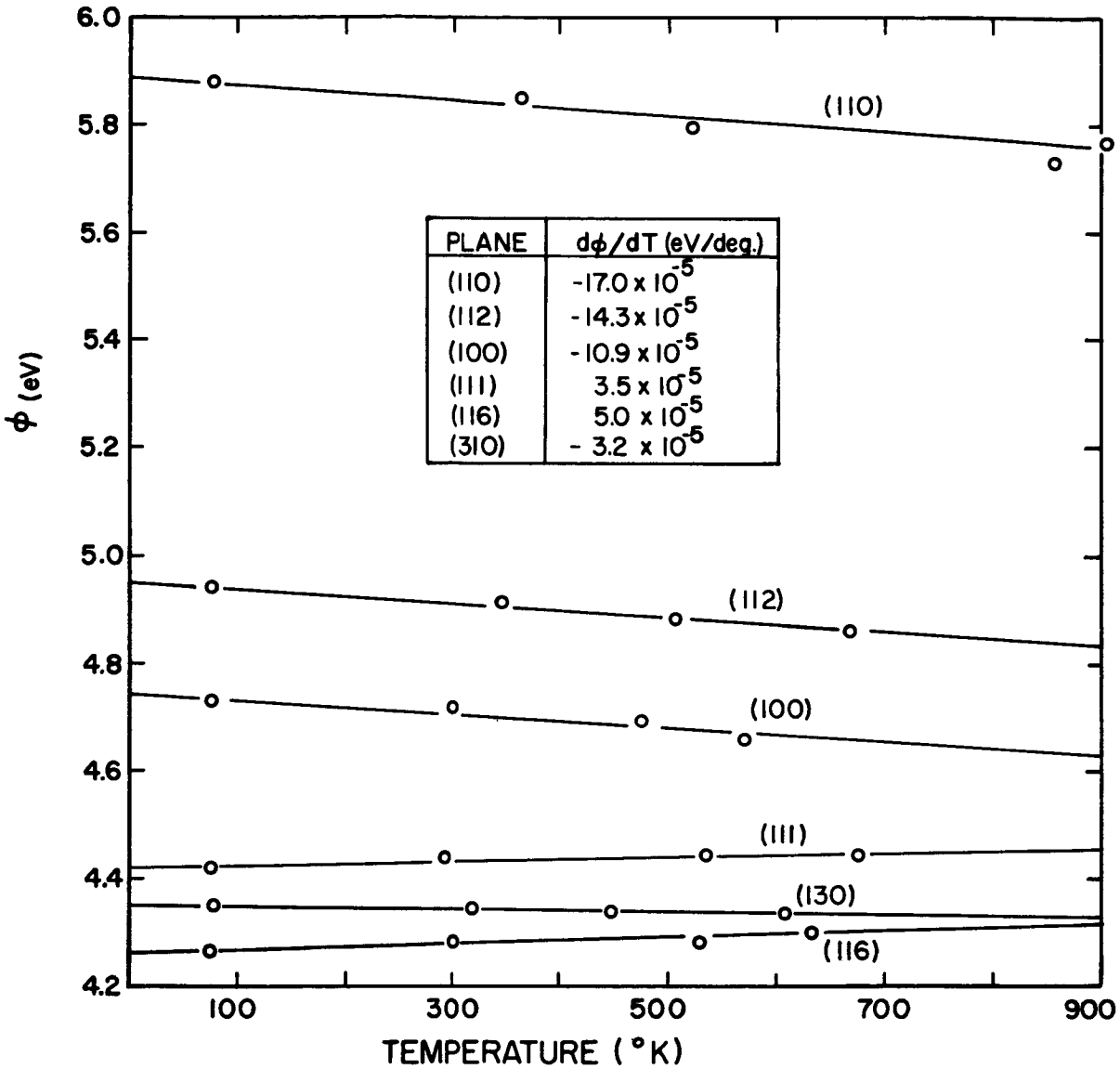

Figure 11. Temperature dependence of work function for various planes of a clean W substrate as determined from field electron emission data.

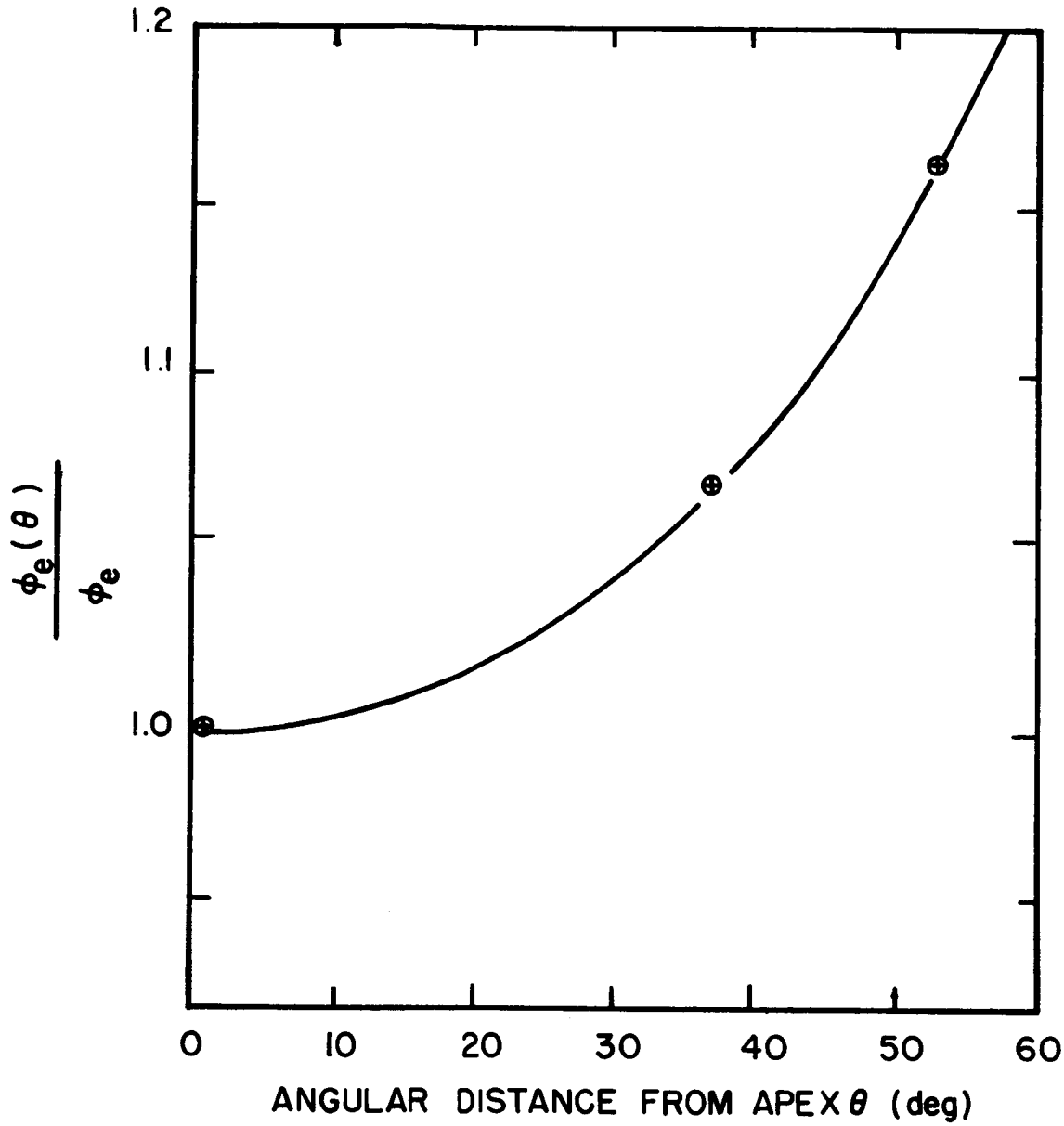

Figure 10. Relative variation of absolute work function [calculated by Equation (14)] with angular distance from apex for various {310} planes along the [100] zone line of a W emitter.

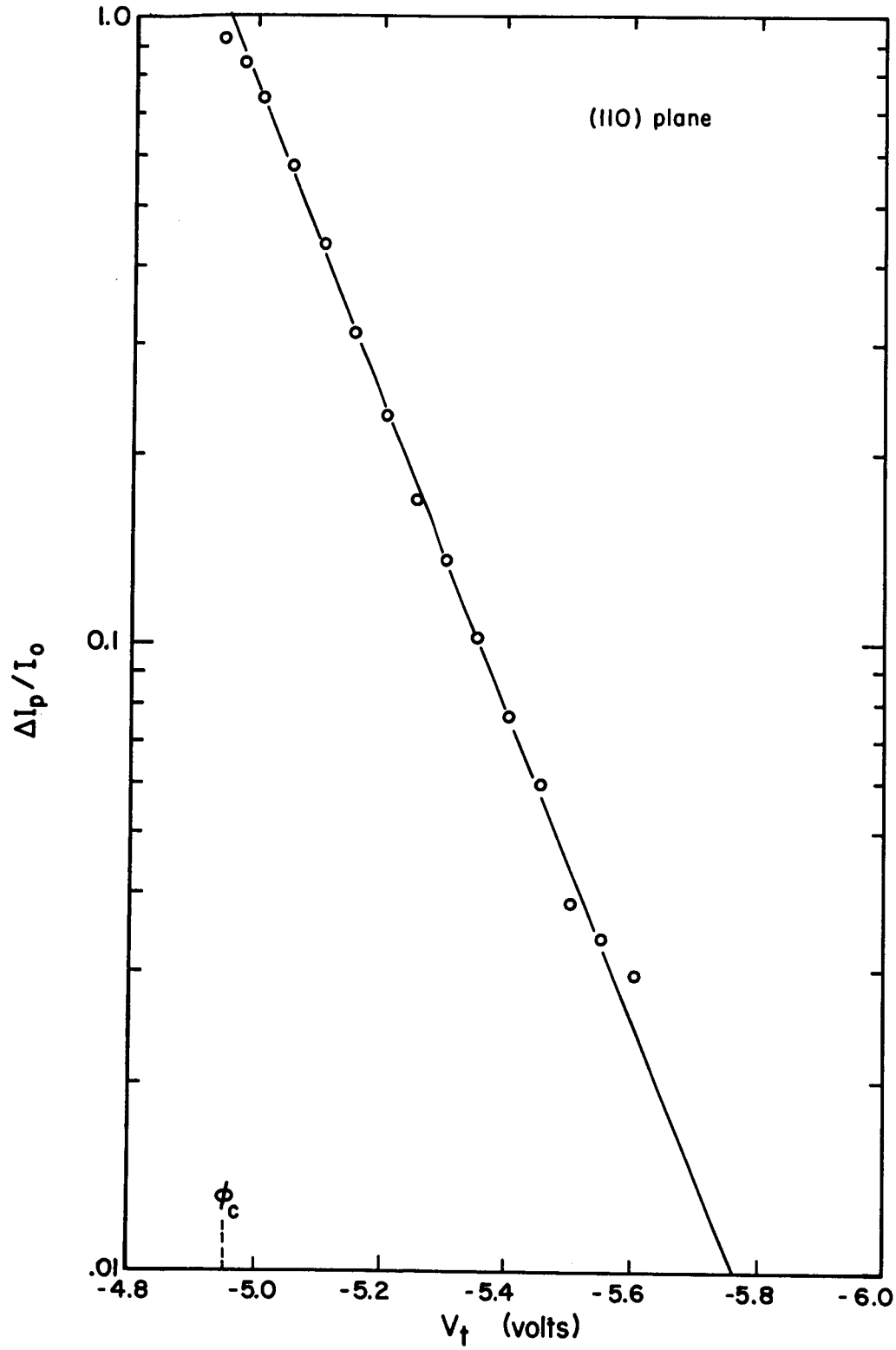

Figure 9. Integral emitted current from the <110> direction of an annealed W emitter plotted according to Equation (11). The anode voltage 1773 volts and d = 0.177 eV.

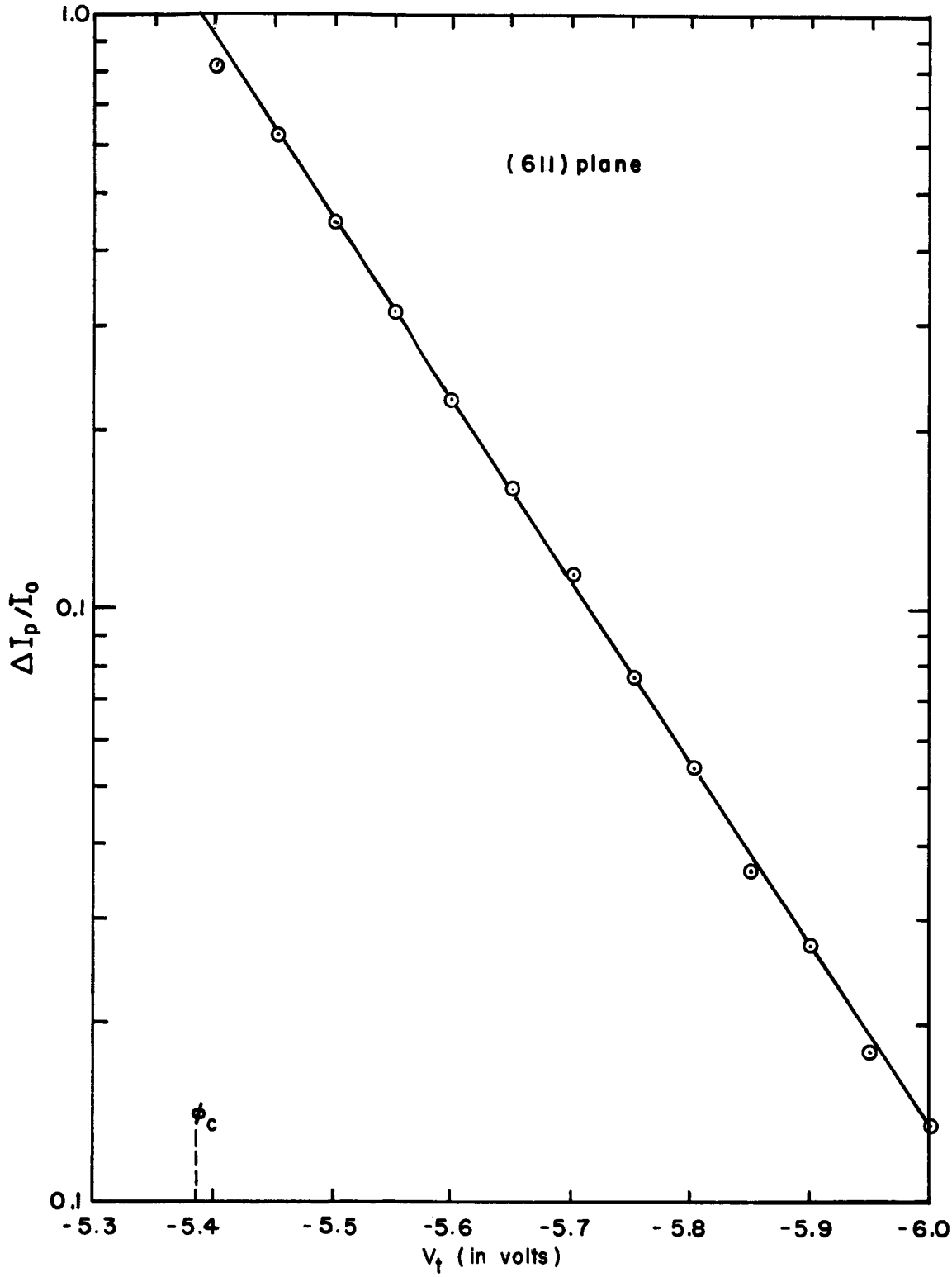

Figure 8. Integral emitted current from the <611> direction of an annealed W emitter plotted according to Equation (11). The anode voltage was 1461 V and d = 0.141 eV.

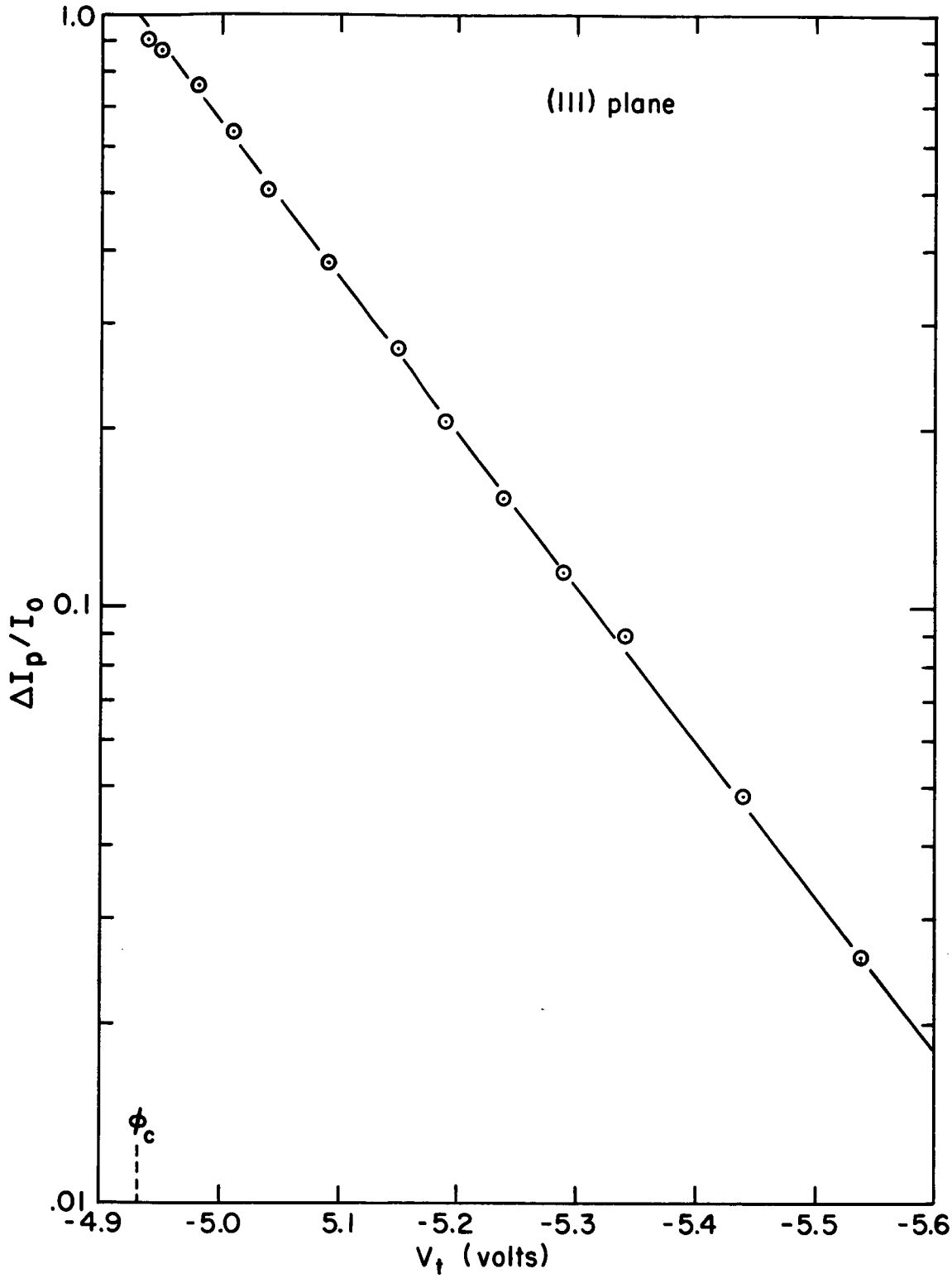

Figure 7. Integral emitted current from the <111> direction of an annealed W emitter plotted according to Equation (11). The anode voltage was 1306 V and d = 0.167 eV.

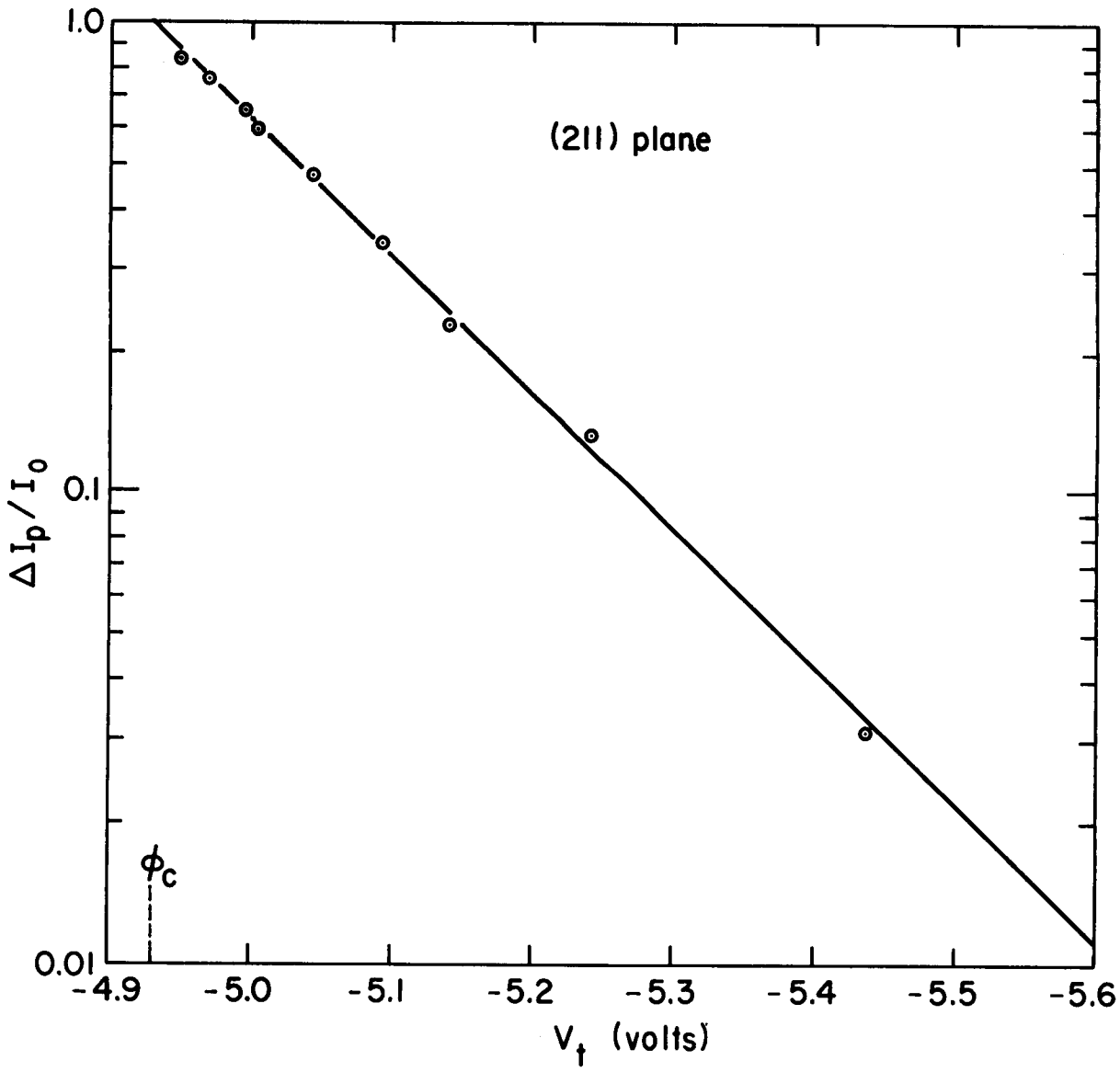

Figure 6. Integral emitted current from the <112> direction of a flash heated W emitter plotted according to Equation (11). The anode voltage was 1234 V and d = 0.146 eV.

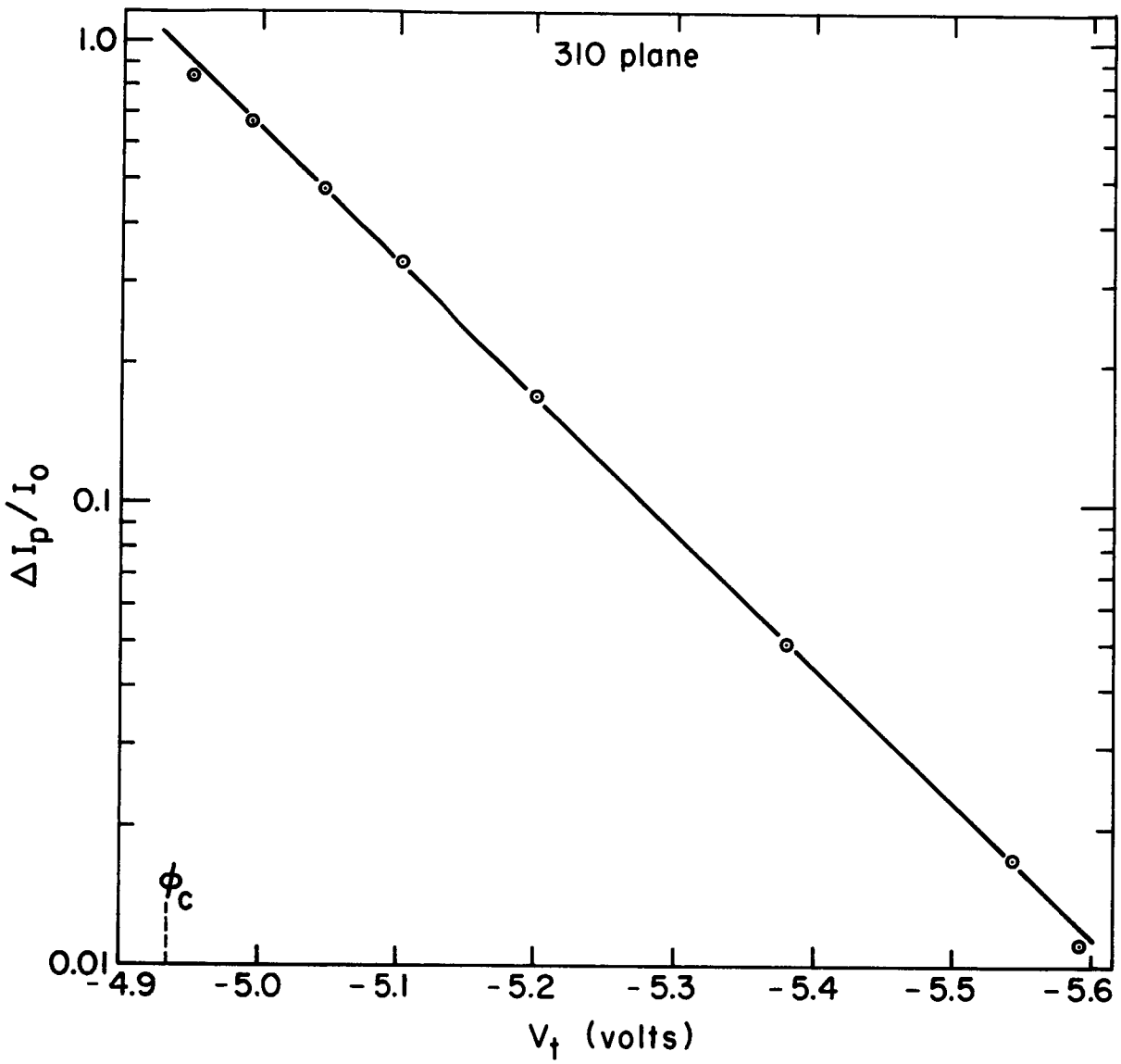

Figure 5. Integral emitted current from the <130> direction of a flash heated W emitter plotted according to Equation (11). The anode voltage was 1234 V and d = 0.149 eV.

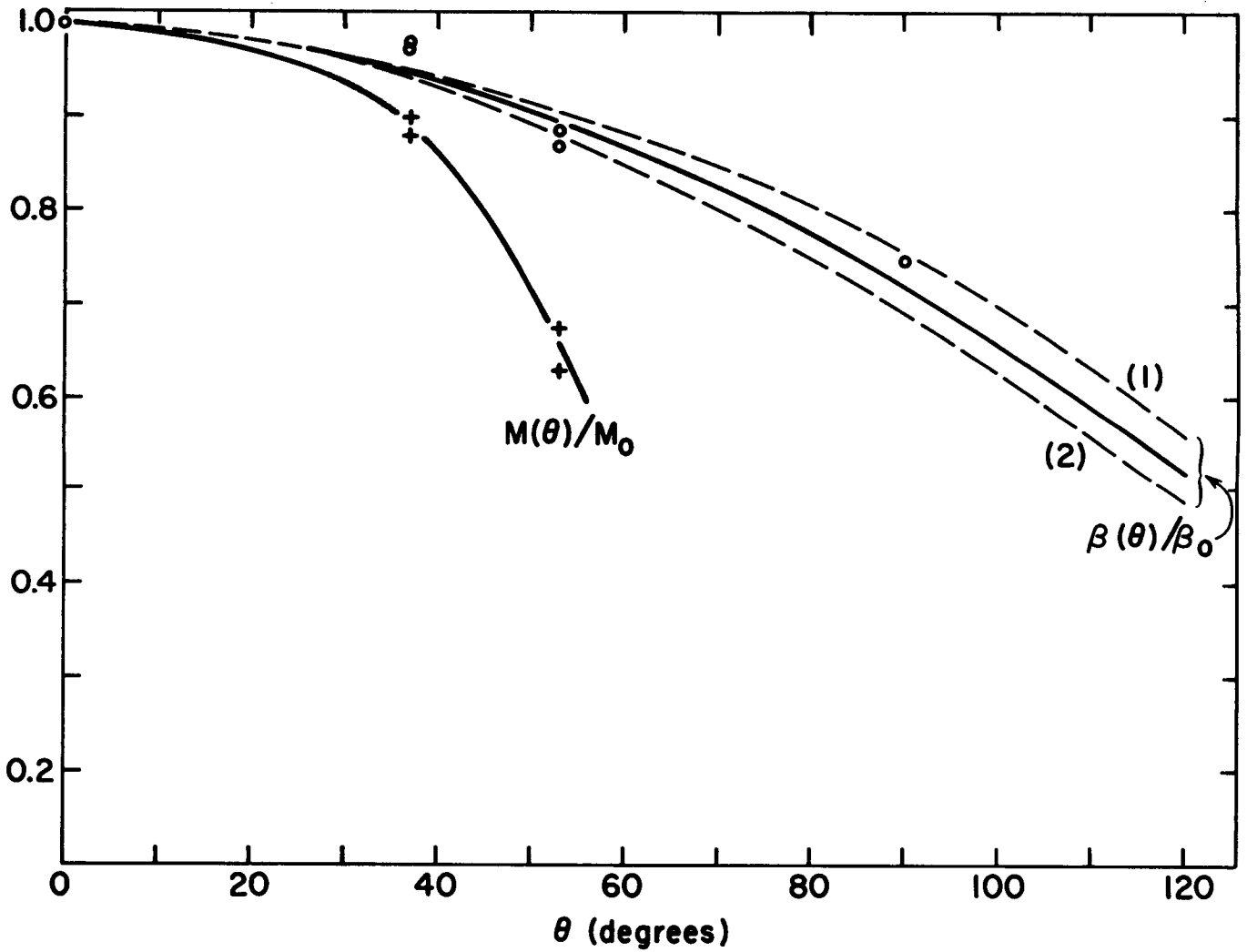

Figure 4. $\beta(\theta)/\beta_o$ is the relative variation of electric field with angular distance from emitter apex θ. Dashed curves: (1) emitter with pronounced constriction; (2) emitter with slight constriction; solid line for average emitter shape (see ref. 22). Experimental data for $\beta(\theta)/\beta_o$ given by circles. Lower curve gives the relative variation of magnification with θ; data points indicated by crosses.

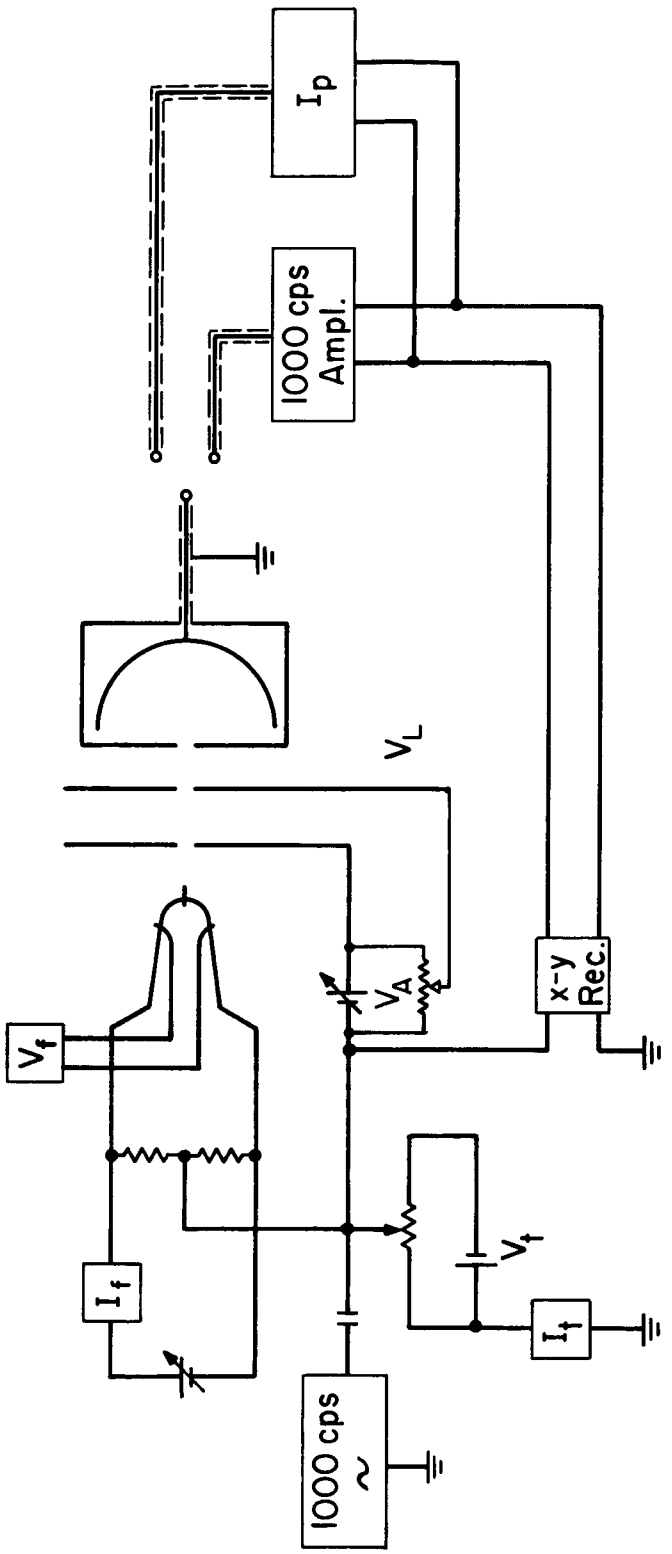

Figure 3. Circuit diagram for energy analyzer tube.

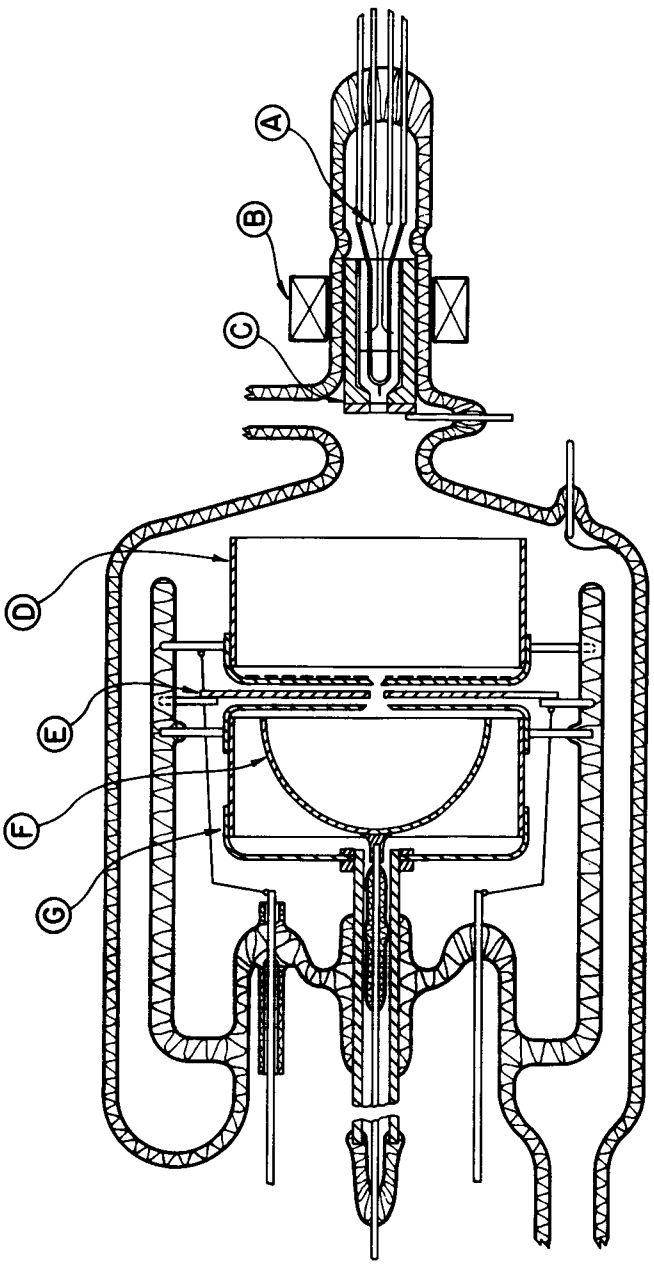

Figure 2. Diagram of energy analyzer tube utilized for measuring total energy distributions at various temperatures.

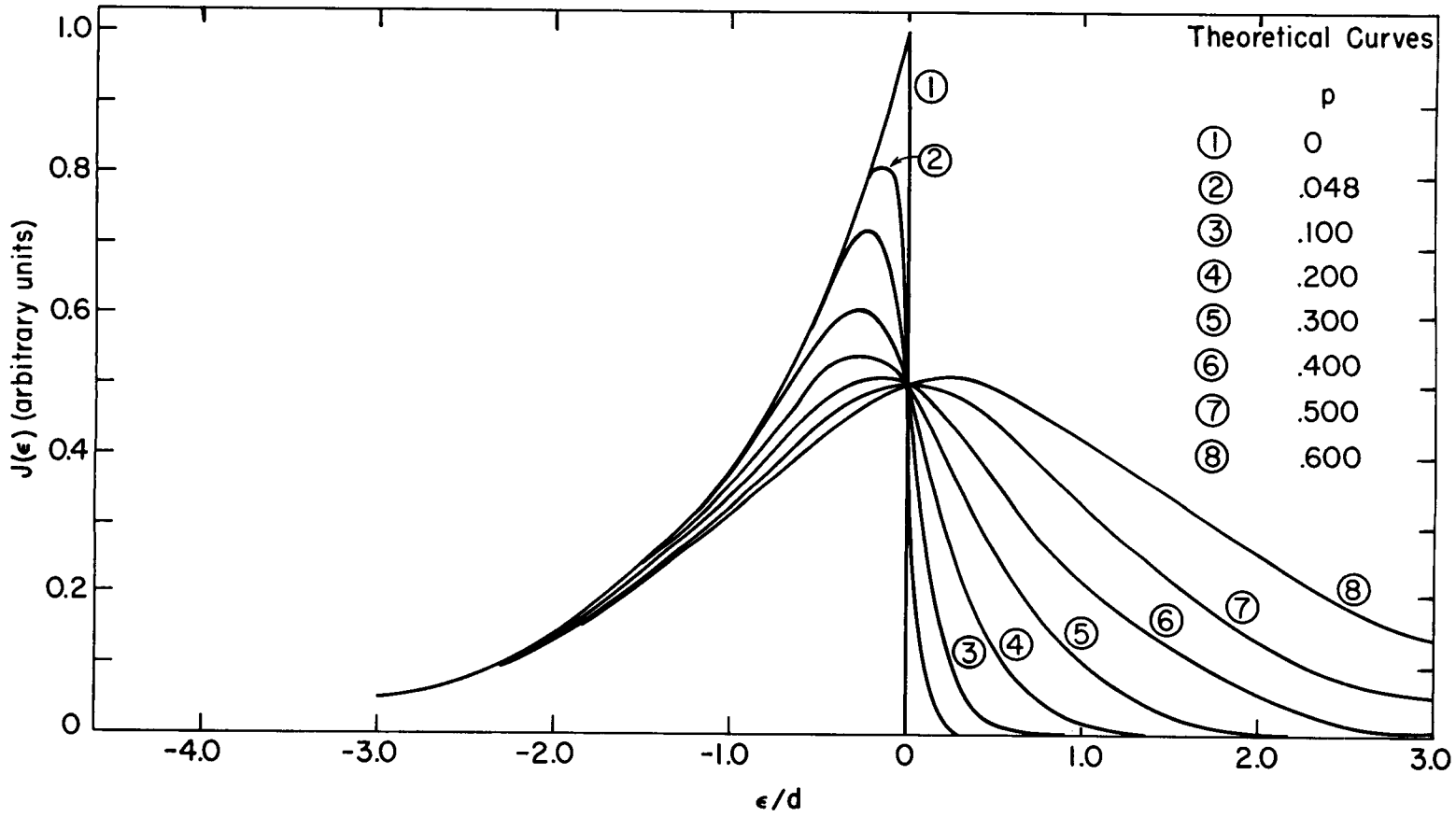

Figure 1. Theoretical total energy distribution plots based on the free electron model [Equation (5)] at various values of p.

21. E. W. Müller, J. Appl. Phys. 26, 732 (1955).

22. W. P. Dyke, et al., J. Appl. Phys. 24, 570 (1953).

23. D. W. Bassett, Proc. Roy. Soc. 286, 191 (1965).

24. P. C. Bettler and F. M. Charbonnier, Phys. Rev. 119, 85 (1960).

25. G. Erlich and F. G. Hudda, J. Chem. Phys. 44, 1039 (1966).

26. N. Sun and W. Band, Proc. Cambridge Phil. Soc. 42, 72 (1946).

27. L. F. Mattheiss, Phys. Rev. 139, 1893 (1965).

28. I. M. Dykman, Ukrain Fiz. Zhur. 1, 81 (1956).

29. L. W. Swanson, et al., Final Rept. NASA, CR-54106, (Field Emission Corp., McMinnville, Ore., 1964).

30. A. Gel'berg, et al., Radiotekn. i Electron 3, 1000 (1958).

31. R. C. Bosworth, Proc. Roy. Soc. A162, 32 (1937).

32. R. Gomer and L. W. Swanson, J. Chem. Phys. 38, 1613 (1963).

33. Final Rept., DA36-039, SC-90829 (Field Emission Corp., June 1964).

34. V. N. Shrednick, Soviet Phys. - Solid State 3, 1268 (1961).

35. E. Fawcett and D. Griffith, J. Phys. Chem. Solids 23, 1631 (1962).

36. E. Fawcett and W. A. Reed, Phys. Rev. 134, A723 (1964).

37. J. A. Rayne, Phys. Rev. 133, A1104 (1964).

38. G. B. Brandt and J. A. Rayne, Phys. Rev. 132, 1945 (1963).

39. W. M. Walsh, Jr. and C. C. Grimes, Phys. Rev. Letters 13, 523 (1964).

40. T. L. Loucks, Phys. Rev. 143, 506 (1966).

41. L. Bouckaret, R. Smoluckowski and E. Wigner, Phys. Rev. 50, 58 (1936).

REFERENCES

1. L. W. Nordheim, Proc. Roy. Soc. (London) A121, 626 (1928).

2. R. H. Fowler and L. W. Nordheim, Proc. Roy. Soc. (London) A119, 173 (1928).

3. A. Sommerfeld and H. Beth, Handbuch der Physik 24, 442 (1933).

4. E. Guth and C. J. Mullin, Phys. Rev. 61, 339 (1942).

5. W. W. Dolan and W. P. Dyke, Phys. Rev. 95, 327 (1954).

6. E. L. Murphy and R. H. Good, Jr., Phys. Rev. 102, 1464 (1956).

7. R. D. Young, Phys. Rev. 113, 110 (1959).

8. R. D. Young and E. W. Müller, Phys. Rev. 113, 115 (1959).

9. L. W. Swanson, L. C. Crouser and F. M. Charbonnier, Phys. Rev. 151, 327 (1966).

10. L. W. Swanson and L. C. Crouser, Phys. Rev. Letters 16, 389 (1966).

11. R. Stratton, Phys. Rev. 135, A794 (1964).

12. P. H. Cutler and D. Nagy, Surface Science 3, 71 (1964).

12a. R. H. Good and E. W. Müller, Handbuch der Physik 21, 176 (1956).

13. R. Fischer, Phys. Stat. Sol. 2, 1088, 1466 (1962).

14. R. D. Young and H. E. Clark, Appl. Phys. Letters 9, 265 (1966).

15. R. D. Young and H. E. Clark Phys. Rev. Letters 17, 351 (1966).

16. C. Herring and M. H. Nichols, Rev. Mod. Phys. 21, 185 (1949).

17. C. R. Crowell and R. A. Armstrong, Phys. Rev. 114, 1500 (1959).

18. A. van Oostrom, Phys. Letters 4, 34 (1963).

19. A. van Oostrom, Philips Res. Rept. Supplement, Netherlands, No. 11 102 (1966).

20. M. Drechsler and H. Liepack, Adsorption et Croissance Cristalline (CNRS, Paris, 1965) p. 1.

These expressions exhibit a striking similarity with those obtained for T-F emission and given by Equations (A14), and the same "mirror symmetry" is found which was noted by Young in the more limited case of thermionic and cold field emission, i.e., temperature and electric field play symmetrical roles, the transverse energy distribution is exponential in both cases, and the normal energy distribution in one case has the same form as the total energy distribution in the other. As in the case of T-F emission, Equations (A18) have a limited range of validity and obviously break down when $q > 1$, i.e., $c > kT$, in which case the applied field is so large that (near the top of the potential barrier) the supply function increases more rapidly than the transmission coefficient decreases with decreasing E_x, and the use of a limited expansion of $D(E_x)$ about its value at the top of the potential barrier is no longer justified since the energy distribution peak occurs below the top of potential barrier. The normal energy distribution is symmetrical with respect to the top of the potential barrier when $q = 1/2$, i.e., in this case exactly one half of the total emitted current is contributed by electrons escaping through the potential barrier by tunnel effect. Finally, the average values of the energy components for emission in the transition region may be derived from Equations (A18):

$$\overline{E_x} = W_o + kT\, f(q), \quad \overline{E_t} = kT, \quad \overline{E} = W_o + kT\left[1 + f(q)\right], \tag{A19}$$

where the function $f(q)$ is given by $f(q) = \pi q \cot \pi q$. Again, Equation (A19) is valid only when q is appreciably smaller than unity (i.e., approximately $q < 0.7$).

the potential barrier which corresponds to y = 1, v(y) = 0 and $D(W_o) = 0.5$. A somewhat lengthy derivation yields a satisfactory approximation for $D(E_x)$ near the top of the barrier:

$$D(E_x) \cong \frac{1}{1 + \exp\left(\frac{E_x - W_o}{c}\right)} \tag{A16}$$

with $$c = \frac{\hbar e^{1/4} F^{3/4}}{\pi m^{1/2}}$$

In the present case most of the emitted electrons have energies well above the Fermi energy, and one may again neglect the factor 1 in the denominator of the Fermi-Dirac distribution function. The total emitted current J_o and the energy distribution functions can be expressed in terms of the basic parameter:

$$q = \frac{c}{kT} \tag{A17}$$

and integration of Equations (A6) and (A7) yields the following expressions:

$$\left\{\begin{array}{ll}
J_o = \frac{4\pi me(kT)^2}{h^3} \exp\left(-\frac{\phi}{kT}\right) \exp\left(\sqrt{\frac{e^3 F}{kT}}\right) \frac{\pi q}{\sin\pi q} = J_{oS} \frac{\pi q}{\sin\pi q} & \text{(a)} \\
J(E_x)\, dE_x = J_o \frac{\sin\pi q}{\pi q} \frac{\exp\left(\frac{W_o - E_x}{kT}\right)}{1 + \exp\left(\frac{W_o - E_x}{c}\right)} d\left(\frac{E_x}{kT}\right) & \text{(b)} \\
J(E_t)\, dE_t = J_o \exp\left(-\frac{E_t}{kT}\right) d\left(\frac{E_t}{kT}\right) \quad \text{for } E_t \geq 0 & \text{(c)} \\
J(E)\, dE = J_o \frac{\sin\pi q}{\pi q} q \ln\left(1 + \exp\frac{E - W_o}{c}\right) \exp\left(\frac{W_o - E_o}{kT}\right) d\left(\frac{E}{kT}\right) & \text{(d)}
\end{array}\right. \tag{A18}$$

$E_x = E_f$, and the use of a limited expression of $D(E_x)$ about its value at the Fermi level is no longer justified since the peak of the normal energy distribution function occurs above the Fermi level. Comparison of the predictions with measured values of the emitted current indicates that Equations (A14) remain satisfactory approximations as long as p does not exceed about 0.7 provided the Sommerfield model is applicable.

Finally, the following expressions may be derived from Equations (A14) for the mean values of the energy components for T-F emitted electrons:

$$\overline{E}_x = E_f - d\left[1 + f(p)\right], \qquad \overline{E_t} = d, \quad \overline{E} = E_f - d f(p) \tag{A15}$$

with $f(p) = \pi p \cot \pi p$. The range of validity of Equations (A15) is the same as that of Equations (A14), i.e., approximately $0 < p \leqslant 0.7$.

Transition Region

There lies, between Schottky and T-F emission, a transition region in which electrons both above and below the top of the potential barrier contribute significantly to the total emitted current. If one approaches this region from the Schottky side, and gradually increases the applied field F, an increasingly large fraction of the emitted current arises from electrons escaping through the barrier by tunnel effect. As long as F is not too large the normal energy distribution has a peak at the top of the potential barrier, which suggests that the transmission coefficient $D(E_x)$ of Equation (A8) be expanded about its value at the top of

$$p = \frac{kT}{d} \tag{A13}$$

and integration of Equations (A6) and (A7) yields the expressions:

$$\left\{\begin{aligned}
&J_{TF} = \frac{4\pi me}{h^3} D_o d^2 \frac{\pi p}{\sin \pi p} = J_{oF} \frac{\pi p}{\sin \pi p} && \text{(a)}\\
&J(E_x)\, dE_x = J_{TF} \frac{\sin \pi p}{\pi p} \left[p \ln\left(1 + \exp\left(\frac{E_f - E_x}{kT}\right)\right)\right] \\
&\qquad \exp\left(\frac{E_x - E_f}{d}\right) d\left(\frac{E_x}{d}\right) && \text{(b)}\\
&J(E_t)\, dE_t = J_{TF} \exp\left(-\frac{E_t}{d}\right) d\left(\frac{E_t}{d}\right) \text{ for } E_t \geqslant 0 && \text{(c)}\\
&J(E)\, dE = J_{TF} \frac{\sin \pi p}{\pi p} \frac{\exp\left(\frac{E - E_f}{d}\right)}{1 + \exp\left(\frac{E - E_f}{kT}\right)} d\left(\frac{E}{d}\right) && \text{(d)}
\end{aligned}\right\} \tag{A14}$$

These expressions of course reduce to the $0^{\circ}K$ expressions Equations (A10) for $p = 0$. As p increases, an increasing number of electrons are emitted above the Fermi level, resulting in a broadening of the total and normal energy distributions, as illustrated in Figure 1 for the total energy. However, as indicated by Equations (A14), the transverse energy distribution remains unchanged. It should be noted that Equations (A14) have a limited range of validity, as they obviously break down for $p = 1$ (in which case the value of J_{TF} given by Equation (A14a) goes to infinity); the reason for this failure is that, for $p > 1$ (i.e., $kT > d$) the transmission coefficient $D(E_x)$ increases with E_x more rapidly than the supply function decreases near

$$\overline{E}_x = E_f - 2d, \quad \overline{E}_t = d, \qquad \overline{E} = E_f - d \tag{A 12}$$

The range of validity of the field emission theory is limited by the condition that the top of the potential barrier remain above the Fermi level, which requires that the applied field F be smaller than ϕ^2/e^3.

T-F Emission

T-F emission is defined as the electron emission from a heated metal under the influence of a strong applied electric field, when the relation between T and F is such that the major fraction of the emitted electrons escape by tunnel effect rather than over the barrier. T-F emission is related to cold field emission in a similar manner as Schottky emission is to thermionic emission. The addition of temperature in the former case and of an applied electric field in the latter case causes some enhancement of the emission, but does not fundamentally alter the emission characteristics. Thus in T-F emission the emitted electrons originate predominantly near the Fermi level, and the approximation of Equation (A9) is still used for the transmission coefficient. The main difference with the cold field emission case is that the Fermi-Dirac distribution function is now a continuous function, instead of the discontinuous function (with values 0 or 1) corresponding to cold field emission. The total emitted current J_{TF} and the energy distribution functions can be expressed in terms of a basic parameter

$$
\left\{
\begin{aligned}
&J_{oF} = \frac{4\pi me}{h^3} \; D_o d^2 && \text{(a)}\\
&J(E_x)dE_x = J_{oF}\left(\frac{E_x - E_f}{d}\right) \exp\left(\frac{E_x - E_f}{d}\right) d\left(\frac{E_x}{d}\right) \quad \text{for } E_x < E_f && \text{(b)}\\
&J(E_t)\, dE_t = J_{oF} \exp\left(-\frac{E_t}{d}\right) d\left(\frac{E_t}{d}\right) \quad \text{for } E_t \geqslant 0 && \text{(c)}\\
&J(E)\, dE = J_{oF} \exp\left(\frac{E - E_f}{d}\right) d\left(\frac{E}{d}\right) \quad \text{for } E < E_f. && \text{(d)}
\end{aligned}
\right\} \tag{A10}
$$

The distribution functions reduce to zero when E_x and E exceed E_f. As first noted by Young[7], there is an interesting "mirror" symmetry between the energy distribution functions for thermionic emission and cold field emission: the transverse energy distributions are both exponential, and the normal energy distribution in one case has the same form as the total energy distribution in the other case, with the energy d (proportional to F) playing for cold field emission the same role as the energy parameter kT for thermionic emission. Finally, the average values of the energy components for the emitted electrons are obtained from the standard expression:

$$
E_j = \frac{\int E_j \; J(E_j)\, dE_j}{\int J(E_j)\, dE_j} \tag{A11}
$$

which yields for the cold field emission case:

$$D(E_x) = \frac{1}{1 + \exp\left(\frac{4\sqrt{2m}\,|E_x|^{3}}{3\hbar_e F}\, v(y)\right)} , \qquad (A8)$$

Equation (A8) remains valid even if $|E_x|$ is appreciably greater than the heighth of the potential well W_o, i.e., for electrons having a normal energy greater than the top of the potential barrier.

This form of the transmission coefficient is too complex to allow integration of Equations (A6) and (A7). However, noting the rapid dependence of $D(E_x)$ on the normal energy, one would expect that only electrons with high value of normal energy will be emitted in appreciable number. Since the maximum possible value of E_x is E_f for a cold metal (T = 0), this suggests that the exponent in the transmission coefficient be expanded in Taylor series about the value $E_x = E_f$ and that only the two leading terms be retained; thus

$$D(E_x) \cong D_o \exp\left(\frac{E_x - E_f}{d}\right) , \qquad (A9)$$

where $D_o = D(E_f)$. In the case of cold field emission, the Fermi-Dirac distribution function is unity for $E < E_f$ and zero for $E > E_f$. Substituting into Equations (A6) and (A7), one readily obtains the cold field emission current J_{oF} and the energy distribution functions:

where $D(E_x)$ is the transmission coefficient; in the one-dimensional model considered here, the transmission coefficient depends only on the normal energy E_x.

The total energy distribution of the emitted electrons is obtained by integrating Equation(A7) over all possible values of E_x; the transverse energy distribution is obtained by integrating Equation (A6) over all possible values of E_x; the normal energy distribution is obtained by integrating either Equation (A6) over E_t or Equation (A7) over E. Finally, the total emitted current J is obtained by double integration of either equation over the appropriate range of the energy components.

Equations (A6) and (A7) apply in the general case of electron emission from a heated metal in the presence of an electric field F at the metal surface, which includes thermionic emission and cold field emission as particular cases (F = O and T = O respectively.) It is not possible to integrate Equations (A6) and (A7) in their general form; instead, several cases must be considered, depending on the relative values of temperature and field. For each case, the equations can be integrated after the Fermi-Dirac distribution function $\left[\exp\left(\frac{E - E_f}{kT} \right) + 1 \right]^{-1}$ and/or the transmission coefficient $D(E_x)$ are replaced by simpler approximations, which are sufficiently correct over the range of energies where electrons are emitted in appreciable quantity.

Cold Field Emission

A generalization of the WKB approximation yields [6] the following expression for the transmission coefficient:

$$\left\{ \begin{array}{l} E_t = \dfrac{p_y^2}{2m} + \dfrac{p_z^2}{2m} \\ \\ E_x = E - E_t = \dfrac{p_x^2}{2m} + V(x) \end{array} \right\} \qquad (A3)$$

The electron supply function can be rewritten in terms of any two of the energy variables E, E_x and E_t. In terms of normal and transverse energy components, the supply function (i.e., the number of electrons, with normal energy between E_x and $E_x + dE_x$ and with transverse energy between E_t and $E_t + dE_t$, which are incident per unit time on a unit area of the metal surface) is:

$$N(E_x, E_t)\, dE_x dE_t = \frac{4\pi m}{h^3 \left[\exp\left(\dfrac{E_x + E_t - E_f}{kT} \right) + 1 \right]} dE_x\, dE_t \qquad (A4)$$

In terms of total and normal energy, the supply function is:

$$N(E, E_x)\, dE\, dE_x = \frac{4\pi m}{h^3 \left[\exp\left(\dfrac{E - E_f}{kT} \right) + 1 \right]} dE\, dE_x \qquad (A5)$$

Finally, the energy distribution functions for the emitted electron current are:

$$J(E_x, E_t)\, dE_x dE_t = \frac{4\pi me\, D(E_x)}{h^3 \left[\exp\left(\dfrac{E_x + E_t - E_f}{kT} \right) + 1 \right]} dE_x\, dE_t \qquad (A6)$$

$$J(E, E_x)\, dE\, dE_x = \frac{4\pi me\, D(E_x)}{h^3 \left[\exp\left(\dfrac{E - E_f}{kT} \right) + 1 \right]} dE\, dE_x \qquad (A7)$$

APPENDIX

General Expressions for the Electron Energy Distribution Functions

According to the Fermi-Dirac statistics, the density (number per unit volume) of conduction electrons with momenta in the range $\vec{p}$, $\vec{p} + \vec{dp}$, is:

$$n(p_x, p_y, p_z)\, dp_x dp_y dp_z = \frac{2}{\hbar^3 \left[\exp\left(\frac{E - E_f}{kT}\right) + 1\right]}\, dp_x dp_y dp_z , \qquad (A1)$$

where T is the absolute temperature of the metal.

Let the metal surface be normal to the x axis of coordinates. The electron supply function, i.e., the number of electrons within the same momentum range incident per unit time upon unit surface area, is:

$$n(p_x, p_y, p_z)\, dp_x dp_y dp_z = v_x\, n(p_x p_y p_z)\, dp_x dp_y dp_z, \qquad (A2)$$

where v_x is the x component of electron velocity.

Since we are interested in energy distribution functions, it is convenient to rewrite the electron supply function in terms of energy rather than momentum components. Let E be the total energy of a given electron (which is a constant), and define the normal and transverse components of energy E_x and E_t by the expressions:

directions for which constant energy surfaces at or near E_f intersect broad partially-filled bands the Sommerfeld model is adequate as expected. On the other hand, those directions which possess narrow, nearly-filled d bands or bands that cross within a few times d below E_f are accordingly found to exhibit anomalies in their energy distribution results, as is the case shown in Figure 32 for the <110> and <100> directions of clean W. Thus, we conclude that total energy distribution measurements promise to provide an important tool for analyzing certain characteristics of energy surfaces near E_f for metals and semi-conductors.

with the smaller values of E_t for the hole surfaces at N for <110> direction emission, one expects a larger contribution to the emission from the former hole surface. Since along the <110> direction each of the two overlapping electron and hole bands contribute to the total emission, the larger value of Δ for emission from the nearly filled band at N may predominate in the observed exponential tail of the energy distribution to give the anomalously large values of Δ as shown in Figure 26 for the <110> direction.

CONCLUSION

We have shown that for those emission directions obeying Equation (5) measurement of the absolute value of ϕ, β , and M can be obtained, thereby providing important insight into the electronic and geometric nature of the surface. Also, the temperature dependence of ϕ is shown to vary both in sign and magnitude with crystal direction, thus providing an interesting basis for further theoretical study of the relative importance of thermal effects on the inner and outer part of the work function.

The total energy distribution results clearly indicate that the Sommerfeld model description of the field emission from W and conceivably other transition metals must be employed carefully since it is clearly inadequate for the <100> and possibly the <110> directions. We find that our energy distribution results are in good agreement with expectations based on theoretical band structure calculations for W by Mattheiss[27] and Loucks[40]; namely, along those

of the nearby physical surface on the inter-atomic potentials and, hence, on the band structure along a specific direction normal to the surface. The results with coadsorbed Zr/O provide evidence that the effect of adsorbed layers only affects the energy distribution curves through the variation of d as both work function and applied electric field are necessarily changed. If our interpretation is reasonably correct, we have evidence that small electron surfaces do exist approximately 0.4 eV below E_f along the <100> direction in accordance with predictions from bulk considerations.

A final comment should be made concerning the possible influence of the two hole surfaces -- a small ellipsoidal hole surface located at N and a large octahedral-shaped surface centered on H -- on the energy distribution results. Treating theoretically the emission from a valence band, Stratton[11] obtains a general expression for the energy distribution similar to that of conduction band emission, i.e., Equation (1). As in the case of conduction band emission the major contribution to $J(\epsilon)$ again comes from electrons with small values of E_m. Stratton also finds that values of Δ for valence band emission are larger than conduction band emission for corresponding values of p.

In the case of W one must consider the effect of the hole surfaces centered on the $\overline{\Gamma}\overline{N}$ and $\overline{\Gamma}\overline{H}$ axis on the electron emission along the <110> and <100> directions. Loucks[40] has concluded that relativistic corrections cause the hole surfaces at N to vanish, as shown in Figure 36, or to be greatly reduced in size. In view of the large E_t values associated with the hole surfaces on H for emission along the <100> direction when compared

If we take the hump in the 100 energy distribution to represent excess current, it is clear that E_m is zero or less than d near the Fermi surface, so that the band structure term vanishes, and then becomes larger than d in the region of excess current. Also implied in this interpretation is that the excess current must be caused by a small electron surface along the $\bar{\Gamma}\bar{H}$ direction, not in the center of the zone. In this way such an electron surface would not lead to emission in other directions because of the high tangential k values. Conceivably, these small energy surfaces occurring slightly below the Fermi level may be due to the small hump in the Δ_7 band shown in Figure 35 where spin-orbit coupling corrections have been taken into account. The apparent Sommerfeld behavior along the <100> direction with the low work function Zr/0 layer present demonstrates the fact that emission between $\epsilon \cong -0.35$ and the Fermi level arises from another energy surface with $E_m > d$ as expected from Figure 35 and the corresponding Fermi surface shown in Figure 36. It should be mentioned that this interpretation is different from one put forth earlier[10].

Additional confirmation that the energy surface producing the 100 anomaly is small, stems from the fact that the <116> directions, which are only 13° from the <100> direction, yield energy distributions in complete agreement with Equation (5).

It should be mentioned that the degree of correlation between the energy surface shapes inferred from bulk electronic measurements and theoretical considerations and from energy distribution results is not completely clear at this time. This uncertainty arises from the unknown influence

a smaller nearly-spherical hole surface is expected to occur along the <110> directions centered on symmetry points N. Cross sections of the Fermi surface of W without spin-orbit or relativistic corrections are reproduced in Figure 34. Relativistic or spin-orbit coupling corrections yield a band structure along the $\overline{\Gamma}\overline{H}$ direction as shown in Figure 35 and thereby alters the portion of Fermi surface given in Figure 34 to that shown in Figure 36 (these figures taken from Reference 40). The primary feature of spin-orbit and relativistic corrections[40] is the disappearance of the electron lens and a separation between the electron and hole surface along $\overline{\Gamma}\overline{H}$ and a disappearance of the hole surfaces at N.

The above mentioned anomaly in the experimental 100 energy distribution suggests the possibility of unusually small closed energy surfaces near E_f along the $\overline{\Gamma}\overline{H}$ direction. In order to provide a quantitative basis for this possibility, it is necessary to solve the integral in the band structure term

$$\left[1 - \frac{1}{2\pi}\int_0^{2\pi} \exp\left(-E_m/d\right)d\phi_p\right]$$

for the various constant energy surfaces contributing to the emission. At the present time the complexities of the proposed shapes of the energy surfaces and uncertainties as to the magnitude and variation of E_m with ϵ preclude quantitative evaluation of this term. However, certain qualitative features of the energy-surface structure can be ascertained from the variation of the band structure term and, more specifically, E_m, required to account for the results shown in Figure 20.

of the Fermi surface, i. e., the maximum value of E_t for a given range of ϕ_p and E along a particular direction, is sufficiently large that the band structure term of Equation (1) is unity. It is interesting to speculate that the hump occurring 0. 35 eV below the Fermi energy in the energy distribution curve along the <100> direction is due to band structure effects.

In order to examine the possibility of band structure effects on the clean W results it will be instructive to briefly review the current picture of the electronic structure of W. From a variety of electronic and solid state measurements[35 - 39] and theoretical analyses[27, 40] of group VI metals, and more particularly W, it is now apparent that free electron behavior is not manifested, nor expected. Figure 32 shows the expected band structure of W along several major crystallographic directions based on theoretical compilations by Mattheiss[27]. The notation of Bouckaret, Smoluchowski and Wigner[41] is employed and Figure 33 shows the first Brillouin zone of the bcc structure with the corresponding labeling scheme. The point at which the Fermi level intersects the bands along the various directions defines the Fermi surface in k-space. Several important features of the Fermi surface for W have now been established. Most interesting of these is an octahedral "jack-like" electron Fermi surface centered on the origin of the Brillouin zone. Γ, pointed along the six <100> directions (Γ H) and separated from a similarly-shaped hole octahedron at symmetry points H by small "ball-like" protrusions of electron surface also centered on the Γ H axis; depending on the degree of spin-orbit coupling the ball-like protrusions along Γ H may also contain smaller "lens-shaped" electron surfaces[27]. In addition,

values of ϕ_e = 2.28 eV and $\beta / \bar{\beta}$ (θ) = 0.72 were employed, a correct value of p = 0.48 occurs at the near symmetrical distribution, whereas the Fowler-Nordheim function ϕ_f = 2.84 eV with $\beta/\bar{\beta}$ = 1 yields p = 0.38. This internal self-consistency therefore lends support to the Table V values of ϕ_e and β obtained by the absolute method on the 100 plane coadsorbed with Zr/O

In order to further compare the energy distribution results with the theory, Figures 30 and 31 exhibit plots of Δ/d and ϵ_p/kT as a function of p. From the overall agreement of the data with theory for the respective curves one can conclude that the energy distribution theory based on Equation (5) is upheld along the <100> direction when a low work function adsorbate such as coadsorbed Zr/0 is present.

BAND STRUCTURE EFFECTS

The theoretical considerations of the total energy distribution of field-emitted electrons from metals given earlier suggests that, except for Fermi surfaces of small radii of curvature or small m_c/m in the case of spherical surfaces, free electron theory (i. e., Equation (5)) is adequate. The results reported here generally support this picture for clean W along the <116>, <112>, <111> and <130> directions. It should be emphasized, however, that agreement of the experimental energy distribution results with Equation (5) does not necessarily substantiate the Sommerfeld model for the metal. Agreement with theory basically implies that the radius of curvature

In spite of the large increase in M (compared with Table I results) upon Zr/O adsorption, the value of $\beta/\overline{\beta}(\theta)<1$ for the 100 suggests a faceted region. Examination of this system by field ion microscopy[34] has revealed a geometrical perturbation of the surface which increased the net plane step height and size in the 100 region. In the vicinals of the 100 a rapid change in the curviture occurs due to the termination of net plane edges. Since a local change in M arises from the integral effects of surface geometry, it is possible that the central regions of the 100 may possess an increased value of M as well as a lower than average β due to the large net planes on the 100. It also follows that proceeding from the <100> to the <310> direction should result in the observed increase in both β and M because of the rapid termination of net plane edges. Thus, we conclude that information concerning geometrical changes in the surface can be ascertained from probe work function and energy distribution measurements.

Because of the anomalous energy distribution from the <100> direction, one may question the validity of the 2.28 eV work function obtained from Equation (14) even though the fit of the data to Equation (11) is adequate. In an attempt to ascertain the correctness of this value of ϕ_e, the variation of the energy distribution with temperature was measured and plotted in Figure 29. The values of ϕ obtained both by Equations (13) and (14) were used to calculate p. Inasmuch as values of p = 0.5 according to theory should exhibit a symmetrical energy distribution, it was possible to determine the correct value of p and hence ϕ. Accordingly, as shown in Figure 29 where the lower

surface does not exhibit the anomalous hump shown in the clean W results. This is apparently due to the near zero value of $J(\epsilon)$ in the energy range where the anomaly occurs on clean W. Table V gives the values of ϕ_e, M and $\beta/\bar{\beta}$ (θ) obtained from the <100> and <310> directions. Figure 28 shows a plot of the $I_p(V_t)$ data from the low work function emitter according to Equation (11). The large increase in M from both the <310> and <100> directions upon co-adsorption of Zr/O is indicative of a significant rearrangement of the substrate geometry. The localization of the work function changed to the 100 plane upon adsorption is apparent by noting that its work function is decreased from its clean value by 2.4 eV whereas the 310 work function is diminished by only 0.34 eV. This large anisotropy in work function can lead to a large patch field correction which, according to Young's formulation[15], will significantly reduce ϕ_f and ϕ_e in Table V. In view of the large uncertainty in the size of the low work function region, no patch field correction has been attempted. However, the unusually low values of both ϕ_e and ϕ_f (considering that the ZrOW complex has already reduced the work function compared to the ZrW complex by $\sim$1 eV) makes the further reduction required by patch field corrections somewhat surprising.

TABLE V

Results From Zr/O Coated Tungsten Emitter (<310> Oriented)

Plane	ϕ_e(eV)	ϕ_f(eV)	$\bar{\phi}_f$(eV)	$\beta/\bar{\beta}$ (θ)	M x 10^{-5}	θ(deg)
100	2.28 + 0.03	2.84 + 0.03	3.00 + 0.05	0.72	6.2	18
310	3.63 + 0.04	3.62 + 0.13	3.12 + 0.05	1.00	18.2	0

free electron theory. In the case of the <100> direction the disagreement with theory is clearly due to the hump in the Figure 20 results occurring at 0.35 eV below E_f. For the 110 results the anomalously large value of Δ/d does not stem from a disagreement with the exponential decay law but rather from the unexpectedly large value of d, which was also responsible for the unusually large values of ϕ_e for the <110> direction noted in a previous section.

EFFECT OF COADSORBED ZIRCONIUM/OXYGEN ON THE EMISSION CHARACTERISTICS OF W

Investigation of the emission characteristics of Zr/O coadsorbed on a W emitter were performed by coating a <310> oriented emitter from a suitable source. The striking alteration of the emission distribution, as shown in Figure 7(c) of Section II has been discussed elsewhere[33]. The value of Δ at p = 0 can readily be obtained from Equation (5) and is given by

$$\Delta \cong 0.69d \,. \tag{31}$$

At a constant current density $\phi^{3/2}/F$ = const which when combined with Equation (31) yields

$$\Delta \cong \text{const}\ \phi \,. \tag{32}$$

Figure 27, showing the experimental energy distribution results obtained from the <100> direction of a clean and Zr/O coated W emitter, clearly indicate a reduction in Δ ; moreover, the energy distribution from the coated

agreement with theory for all crystallographic directions, including the <100>. The larger deviations from theory at the lowest values of p are due to the resolution limitations of the analyzer which become more apparent at low p, as expected. The good agreement at low values of p for the <100> direction are somewhat surprising in view of the obvious non-free electron behavior; however, since this data were obtained from a <100> oriented emitter the resolution of the analyzer should be best for the 100 data. These data suggest that the variations of h and ϵ_p with p for the <100> direction, which arise mainly from the Fermi-Dirac distribution term $\left[1 + \exp(\epsilon/pd)\right]^{-1}$ in Equation (5), are not affected by the inadequacies of the Sommerfeld model exhibited below the Fermi level.

Although the variation of Δ/d with p is in general agreement with Equation (5) for the <611>, <111>, <310> and <211> directions except at low values of p where the resolution limitations of the analyzer become more important, the absolute values of Δ appear to be consistently too large. This is most likely due to the electron optical effects which, as mentioned, tend to decrease the rate of diminution of the term $\exp(\epsilon/d)$ with $-\epsilon$ and, hence, increase the apparent value of Δ. At the largest values of p additional uncertainty occurs due to excessive flicker noise which made accurate differentiation of the I_p vs V_t curve somewhat difficult. We therefore view these results as confirming the expected variation of Δ/d with p within the overall uncertainty of the measurements.

On the other hand, the variation of Δ/d with p for the <100> and <110> directions and particularly their absolute values are clearly not in accord with

the apparent value of Δ will be increased in the lower temperature range where the sharp peaks in the energy distribution curves exceed the resolution limitations of the analyzer.

A cursory examination of the energy distribution curves of Figures 15 - 20 reveals general agreement with the theoretical expectations of Figure 1 for all but the 100 plane results. The latter results show an anomalous broad shoulder approximately 0.3 eV below E_f on the trailing edge of the distribution. This special behavior for the <100> direction has been observed on both <100> and <310> oriented emitters. In addition, two different collector electrode surfaces provided identical results for all directions including the <100> direction. Thus, electron optical effects, magnetic field interactions, and collector patch field effects may be discarded as possible artifacts leading to the observed 100 results. It should be mentioned that the direction of emission must coincide almost exactly with the <100> in order to observe the special distribution given in Figure 20. For example, Figure 17 shows nearly complete agreement with Equation (5) for the <611> direction which is only 13° from the <100> direction.

In order to illustrate more clearly some of the pertinent features of the energy distribution curves a comparison is made in Figures 21 through 26 between the variation of the peak height h, the position of the peak ϵ_p on the energy axis relative to the Fermi level and the value of Δ with the parameter p and the theoretical predictions of the free electron model depicted in Figure 1. The variables ϵ_p and Δ were made dimensionless by dividing by kT and d respectively. Notice that variations of ϵ_p/kT and h with p are in close

The normalization factor n was adjusted for each plane to cause the experimental peak heights to match theory at p = 0.25, and was further adjusted slightly with temperature to cause the trailing edges, i.e., at large $-\epsilon/d$, to coincide with the respective 77° curve. The latter adjustment was necessitated by the temperature dependence of work function which enters into the function $\exp \epsilon/d$, which in turn controls the decay of $J(\epsilon)$ with $-\epsilon$. The temperature range is given in terms of the non-dimensional parameter $p = kT/d$ and extends approximately from 77 to 900°K for each direction investigated. By plotting the abscissa as ϵ/d the shapes of the curves can be compared directly with the corresponding theoretical curves of Figure 1.

Because the energy distribution curves in Figures 15 - 20 were all obtained from a <100> oriented emitter, except for the 110 results, which were obtained from a <310> oriented emitter, the rather large angles of deflection required for the <112> and <111> directions resulted in values of ϕ_e that were much larger than the Table I results. Hence, the value of d was evaluated from Equation (3) using measured values of ϕ_f and $F = \bar{\beta}(\theta)V$. As mentioned previously, the electron optical effect caused by beam deflection increases the calculated value of ϕ_e due to a smaller measured value of m_e. The net effect of this artifact of the analyzer tube on the Figures 15 - 20 results is to cause a slight broadening of the exponential tail for negative ϵ/d; this in turn causes the half width measurement Δ of the energy distribution curves to exhibit a slightly larger value than if the same measurement were performed with the emission direction along the emitter axis. In addition,

CLEAN TUNGSTEN ENERGY DISTRIBUTION RESULTS

According to Equations (5) and (10), both the differential and integral forms of the current density vary exponentially with ϵ /d at low temperatures. We have shown that the variation of the integral field emitted current with ϵ obeys Equation (11) for five of the six crystallographic directions investigated. This is rather compelling, although not sufficient, evidence that the Sommerfeld model is adequate for describing the emission along these directions. Except for the <110> , the five crystal directions whose emission obeys Equation (11) all give reasonable values of ϕ_e, thus providing nearly unassailable proof for the adequacy of the Sommerfeld model for the <310>, <211> , <111> and <611> directions. In order to provide further experimental proof for these experimental conclusions and further insight concerning the discrepancies observed along the <100> and <110> directions, we have measured the total energy distribution for each of these planes as a function of temperature. Also, the determination of $d\phi/dT$ from the variation of total current with temperature, as described in the preceding section, hinges on the adequacy of the FN theory at elevated temperatures which can best be verified by total energy distribution measurements.

The total energy distribution curves for six major crystallographic directions of W shown in Figures 15 through 20 were obtained by graphical differentiation of the integral current as illustrated by the following relation

$$J(\epsilon) = -ndI_p/dV_t \qquad (30)$$

ad-atom system. For $I - \phi > 0$ (where I is the adsorbate ionization potential), as is the case for the coverage interval reported here, the desorption path ultimately leads to an atomic ground state for the desorbing ad-atom as $x \rightarrow \infty$. Hence, the electronic charge distribution must ultimately increase at the ad-atom as $x \rightarrow \infty$. However, as pointed out by Gomer and Swanson[32] (see Figure 3 of Reference 32) it may be possible in the case of metallic adsorption for the electronic charge distribution at the ad-atom to first decrease and then increase to that of the atomic state as $x \rightarrow \infty$. This situation results in an initial increase in the value of μ with temperature (or x) in accordance with observations.

On the basis that the temperature variation of ϕ is due to μ (T) one may rule out a surface field induced dipole moment (i.e., $\mu_{ind} = \alpha F_s$) as a major contribution to μ, since increasing x should result in lower values of F_s, and hence, μ_{ind}. Additional values of ϕ(T) on other crystal faces will be necessary to elucidate the detailed role of substrate structure and work function. The results presented here establish beyond reasonable doubt the existence of an enhanced lowering of the work function with temperature which is a genuine result of a temperature dependent dipole moment for the ad-atom.

The value of $d\phi_{100}/dT$ in the absence of Cs is approximately 1.1×10^{-4} eV/deg.

Bosworth postulates a temperature dependent increase in the ad-atom dipole moment μ (T) as the primary cause of the decrease in work function of alkali-coated W with temperature. In our results the temperature range of the work function measurements was such that ad-atoms were essentially localized, hence they support the conclusion of Bosworth.

TABLE IV

Work Function Change With Temperature for Cesium on Molybdenum

$\sigma \times 10^{-14}$ (atoms/cm^2)	$\bar{\phi}_{77}$	$T_2 - T_1$	$\Delta\phi$	$\Delta\phi/\Delta T \times 10^4$ (eV/deg)
0.24	3.49	152 - 77	-0.012	-1.59
1.20	1.96	270 - 77	-0.029	-1.49
1.25	1.91	270 - 77	-0.018	-0.86
1.30	1.87	162 - 77	-0.009	-1.03
1.30	1.87	209 - 77	-0.019	-1.46

It is therefore apparent that a temperature dependent decrease in the electronic charge density at the ad-atom and/or increase in the dipole length must be responsible for the observed values of $d\phi_{100}/dT$. An increase in the vibrational energy of the ad-atom with temperature will undoubtedly cause an increase in dipole length provided the dipole moment is not wholly contained in the ad-atom; however, to understand the variation of the ad-atom charge distribution with distance x from the surface necessitates knowledge of the relevant wave functions of the combined metal-

in magnitude with temperature. This is in contrast to CsF co-adsorbed on W which, as discussed in Section VI, exhibits a dipole complex which increases in magnitude with temperature. Because Zr and O relative to Cs and F are closer in atomic size it is possible that the surface field erected dipole model discussed in connection with the Cs/F results may be more applicable to the Zr/O system. According to Dykman[28] this model should exhibit a dipole moment which diminishes in strength with temperature as observed here for Zr/O co-adsorbed on the 100 plane of W.

In the present investigation the temperature dependence of ϕ_{100} for a cesiated tungsten emitter has also been established. The results of the variation of $\overline{\phi}$ with temperature for a cesiated molybdenum emitter obtained previously[29] is given in Table IV for comparison. After each measurement the 77°K work function was checked in order to ascertain whether any field induced adsorbate migration occurred during the higher temperature range investigated, no adsorbate rearrangement was detected and the values of $d\overline{\phi}/dT$ for Cs on Mo lie between 1 and 1.5 x 10^{-4} eV/deg. These values of $d\overline{\phi}/dT$ are at least an order of magnitude higher and of opposite sign to the values reported for clean Mo[30] in the same temperature range. Similar results to those reported here have also been obtained for sodium on W by Bosworth[31] employing contract potential methods.

The results of the temperature variation of ϕ_{100} both in the absence and presence of a Cs layer is shown graphically in Figure 13. It is apparent that, whereas the clean 100 work function decreases with temperature, the cesiated surface exhibits an enhanced lowering of the work function. The

Inasmuch as effects (1) through (3) are not expected to lead to an alteration in sign with crystal direction, one may interpret the appearance of both positive and negative values of $d\mu_T/dT$ as evidence for the importance of band structure effects manifested through Equations (28) and (29). For example, it is interesting to speculate that the negative $d\phi/dT$ values observed along the <100>, <112> and <110> directions may arise from nearly filled narrow d-bands along these directions. Examination of the postulated electronic structure of tungsten[27] suggests such possibilities exist along the <110> and <100> directions where nearly filled d-bands occur. Further theoretical study of the other terms, primarily those arising from lattice expansion as they relate to transition metals, will be needed in order to fully understand their relative importance to $d\phi/dT$.

One additional contribution to the temperature derivative of ϕ, considered by Herring to be only a fraction of k, is contained in Φ and represents the temperature variation of the surface double layer dD/dT. For metal surfaces coated with adsorbates which greatly alter D, the value of dD/dT is not negligible as shown later for Cs/F co-adsorbed on W and as shown in Figure 12 for Zr/O co-adsorbed on the 100 of W and in Figure 13 for Cs also adsorbed on the 100 plane of W. For such low ϕ surfaces the T-F correction to the apparent work function becomes more significant and amounts to ~ 0.2 eV at 650°K as shown in Figure 12. Inasmuch as the Zr/O layer nearly cancels out the clean W value of $d\phi/dT = -10.9 \times 10^{-5}$ eV/deg we conclude that the ad-layer possesses a dipole complex which diminishes

"free electron" contribution to the molar specific heat capacity C_v. According to Herring[16] the effect of electronic specific heat may contribute a term to $d\phi/dT$ of either sign. If the bulk electrons are treated as non-interacting and occupying a continuum of levels of density N(E) per unit energy, the levels being independent of temperature, the standard theory for a degenerate Fermi gas gives

$$\mu = \mu_o - \frac{(\pi kT)^2}{6}\left(\frac{d\left[\ln N(E)\right]}{dE}\right)_{\mu=\mu_o} + OT^4 , \qquad (26)$$

where μ_o is the zero temperature chemical potential; thus

$$\partial \mu_T / \partial T \cong \frac{-(\pi k)^2 T}{3}\left(\frac{d\left[\ln N(E)\right]}{dE}\right)_{\mu=\mu_o} . \qquad (27)$$

For free electrons (i.e., $N(E) \propto E^{1/2}$), Equation (27) becomes

$$\partial \mu_T / \partial T \cong -(\pi k)^2 T / 6\mu_o , \qquad (28)$$

which is ordinarily very small. However, the existence of narrow, partially filled d-bands in transition metals may greatly alter both the sign and magnitude of the derivative $d(\ln N[E])/dE$ in Equation (27). This can be illustrated for a nearly filled band[26] where

$$d\mu_T/dT = (\pi k)^2 T / 6(E_h - \mu_o) , \qquad (29)$$

and where E_h is the highest energy in the zone. In general, for metals with Fermi levels a few kT from the top or bottom of the band, as may be the case for narrow d-bands, N(E) can be expected to vary considerably from free electron theory due to non-parabolic E-k relationships.

where Φ is the electrostatic potential inside the metal and μ is the chemical potential or "inner" part of the work function. Inserting Equation (21) into the relation

$$d/dT = 3\alpha v(\partial/\partial v)_T + (\partial/\partial T)_v \qquad (22)$$

leads to mathematical formulation of the effects mentioned previously:

$$d\phi/dT = 3\alpha v\left[\partial(\Phi - \mu/e)/dv\right]_T + (\partial\Phi/\partial T)_v - (\partial\mu/e\partial T)_v. \qquad (23)$$

The term in brackets refers to effect (1), the second term refers to effect (2), and the last term contains both effects (3) and (4). For most refractory metals effect (1) is believed to be positive and the order of a few times k; effect (2) is negative and a rough estimate is given by[16]

$$\frac{\partial\Phi}{\partial T} = -\left[\frac{1.47 \times 10^8 Z}{MT_d^2 \Omega_o}\right] \cdot k, \qquad (24)$$

where M is the atomic mass, T_d the debye temperatue, Z the fraction of ionic charge at each lattice point and Ω_o the volume of a single unit cell in angstroms. Effect (2) is therefore negative and the order of a few k. On the other hand effect (3), given approximately by[16]

$$\partial\mu_v/\partial T = C_v(\partial T_d/\partial n)_{v,T}, \qquad (25)$$

is believed to be approximately -0.2k for W where $(\partial T_d/\partial n)_{v,T}$ represents the change in T_d when one electron per mole is added to the metal with a compensating imaginary positive charge. Effect (4) represents the normal

is an interesting exception in that it exhibits considerably more noise than other planes investigated. Excluding the latter exception, the data suggests that the thermal initiated atomic displacements in the central regions of net planes are diminished as the number of next-nearest-neighbors increase.

Flicker noise was greatly increased by the presence of a small amount of gas contamination and could be used as a criteria of the surface cleanliness. An interesting exception, however, was the presence of co-adsorbed Zr/O on the 100 plane of W which actually reduced flicker noise even though the work function was greatly reduced.

Temperature Coefficient of Single Plane Work Functions

Perhaps the most interesting feature of the temperature coefficient of work function as depicted in Figure 11 for clean W is its variation in both sign and magnitude with crystal direction. Over the temperature range investigated the temperature coefficient of work function $d\phi/dT$ appears reasonably constant. Herring[16] points out four major contributions to $d\phi/dT$ that must be considered:

(1) effects due to thermal expansions;

(2) effect of atomic vibrations on the internal electrostatic potential and

(3) chemical potential;

(4) the effect of electronic specific heat.

Taking the potential outside the metal surface to be zero the work function can be written as

$$\phi = \Phi - \mu/e \,, \tag{21}$$

TABLE III

Comparison of the Flicker Noise for Various Planes at ~500°K

Plane	Atom Density Atoms/cm^2	$\Delta I/I_p$
110	14.14	0
100	10.00	0.011
211	8.16	0.024
310	6.32	0.083
111	5.77	0.026
611	3.20	0.028
100 (with Zr/0)	- - -	0.006

lateral displacement of exposed surface atoms on a net plane occurs at temperatures as low as 300°K[25], gross surface geometric changes of a field evaporated end form only begin to occur at ~500°K[23]. For thermally annealed emitters employed here whose radii of curvature exceed 1500 Å, negligible irreversible or reversible surface geometric changes occurred in the temperature range 77 to 900°K. In fact below 500°K it can be assumed that the surface atoms within a net plane are essentially immobile and only exhibit thermal vebration about their lattice sites. This can be established by observing the onset of flicker noise in the probe current with increasing temperature as shown in Figure 14 for the < 100 > direction. Flicker noise, which is proportional to I_p, stems from fluctuations in the local surface potential due to thermal initiated atomic displacements which result in a low frequency modulation of I_p. We estimate that the probe hole accepts emission from ~30 surface atoms for the emitter size employed, hence statistical fluctuations involving relatively few atoms can lead to the noise shown in **Figure 14.**

As other planes were investigated it was observed that the onset of flicker noise generally occurred at higher temperatures for the more densely packed planes. By measuring the average amplitude ΔI of the flicker noise at some value of I_p one may use the ratio $\Delta I/I_p$ for various crystal directions at a specified temperature as a rough comparison of the ease of thermally exciting the surface atoms. The results shown in Table III indicate an inverse relationship between low frequency flicker noise (less than 10 cps for the recorder employed) and the atom density of the emitting plane. The 3 10

therefore disallows the calculation of ϕ_e, may also obviate the strict use of the Sommerfeld model along the<110>direction.

EFFECT OF TEMPERATURE ON EMISSION

The variation of ϕ_f with temperature for several major directions of clean and coated W has been performed according to the field emission methods described in an earlier section. The results, shown in Figure 11 for clean W and Figures 12 and 13 for W_{100} co-adsorbed with Zr/O and adsorbed with Cs respectively, have several surprising and interesting features. It must be emphasized before discussing these results that their validity is based on the applicability of the Sommerfeld model for describing field emission from W. As will be shown later, this model, while obviously inadequate for the <100> direction of clean W, appears to be adequate for all other major crystal directions investigated. To what extent the ϕ_f vs T results for the 100 plane might be affected by the inadequacy of the Sommerfeld model is not clear at this time. Before discussing the temperature coefficient of work function we shall mention briefly the observations of a related phenomena which caused some difficulty in obtaining energy distributions at elevated temperature.

Flicker Noise

The upper limit of the temperature range for work function and energy distribution measurements was kept below that required to cause thermodynamic motivated geometric changes[24] in the emitter surface. Although

is obtained for the 110 plane of the <110> oriented emitter; however, it is still anomalous in that $\beta_{110}/\bar{\beta}$ is expected to be less than unity for the faceted 110 direction. It should be pointed out that the two values of ϕ_e (110) listed in Table I were the lowest obtained for the 110 plane; other measurements of ϕ_e for the 110 were even larger and seemed to vary in an erratic fashion with the annealing history of the emitter.

As pointed out by Young[15], patch field corrections can be important even to field emission work functions on a plane possessing a large work function difference from its surroundings as in the case of the 110 of a bcc crystal. Unfortunately, the patch field correction, as outlined by Young, required to cause agreement between ϕ_e and ϕ_f leads to a 110 work function value in excess of 7 eV. In view of the fact that all other work function measurements of macroscopic 110 surfaces give values in the range of 5.0 to 5.3 eV, we find it difficult at this time to accept a value in excess of $\sim$6.0 eV, as normally given by ϕ_f measurements. The nearly 1 eV difference between field emission and non-field emission methods of measuring the 110 work function may be due to the more ideal surface obtained by field emission methods as dramatically established by field ion micrographs[23]. It is conceivable that patch field corrections enter more subtly than outlined by Young. For example, the large transverse fields arising from patch effects may affect the electron tunneling in a fashion not obvious from the usual one dimensional models. Also, as will be discussed more fully in a later section, band structure effects, which are manifest in the <100> direction and

As a further check on the free electron theory of field emission along the <310> direction, values of ϕ_e were determined according to Equation (14) for a range of anode voltages. The results, given in Table II, yield a value of $\phi_e = 4.40 \pm 0.13$ eV for the <310> direction compared to a value of $\phi_f = 4.32 \pm 0.05$ eV. The close agreement between values of ϕ_e evaluated at different anode voltages provides further support for the validity of the Sommerfeld model in describing emission along the <310> direction. Also, the close agreement between ϕ_e and ϕ_f suggests that at $\beta_{310} \cong \overline{\beta}$ for the 310 plane. The latter result is not unexpected since the 310 plane of W appears to be relatively small and free from faceting in its thermal end form[23].

TABLE II

Values of ϕ_e for 310 Plane as a Function of Anode Voltage Where $\phi_f = 4.32 \pm 0.05$ eV

V (volts)	ϕ_e(eV)
1461	4.42
1391	4.47
1299	4.32
1228	4.33
1158	4.42
1067	4.44

For the most part local variations in β with crystallographic direction do not follow the variations in M for clean annealed W. The large value of ϕ_e relative to ϕ_f given in Table I for the off-axis 110 plane leads a value of $\beta_{110}/\overline{\beta}$ which is unusually high in view of the low value of M and the well-known faceted end form of this plane. A closer agreement between ϕ_f and ϕ_e

non-<110> oriented emitters by magnetic deflection is somehow impossible. For the <110> oriented emitter the value of M is lowest for the center of the 110 plane and increases slightly toward the net plane edges as expected from the large faceted 110 plane.

Given in Column 2 of Table I are absolute work function values ϕ_e calculated according to Equation (14) employing slope values m_e from plots of $\Delta I_p/I_o$ as shown in Figures 5-9. The ratios of local β to average $\bar{\beta}$ were obtained from the ratios $(\phi_e/\phi_f)^{3/2}$. Values of ϕ_e and ϕ_f for the 211 agree within experimental error indicating no large discrepancy between β_{211} and $\bar{\beta}$ for both flashed and annealed end forms. The 310 results show a slight lowering of β_{310} and ϕ_e on annealing, the latter being contrary to the expectation that removal of quenched -in atomic disorder by annealing should lead to a higher value of absolute work function. Examination of thermally annealed patterns suggest that $\beta_{111}/\bar{\beta}$ should be less than unity, rather than larger by 11%. It is believed that electron optical effects due to the large magnetic field required for angular deflection of the beam may have increased the value of ϕ_e for the 111 plane. This belief was substantiated by noting that the value of ϕ_e calculated for various {310} planes increased with θ as shown in Figure 10. This apparently stems from the alteration of the electron optics of the analyzer with increasing beam deflection as mentioned earlier. The values of ϕ_e given in Table I have been corrected by assuming the apparent increase in ϕ_e with θ shown in Figure 10 for the {310} planes applies to others as well. Excluding the 111 results, this correction is less that 3% for all planes listed in Table I.

except for the higher relative value of M_{110} observed here. Inspection of thermally annealed field ion micrographs by Bassett[23] showed that the 110 and 211 planes possess equally large facets, yet both van Oostrom's and our results show $M_{211} > M_{110}$. This implies that local values of M are influenced by perturbations in the surrounding equipotential surface due to alterations in local geometry or by possible transverse electric fields due to patch effects. Somewhat surprising is the low relative value of M_{100}, since field ion micrographs indicate that 211 net planes are much larger than the 100 planes thereby suggesting $M_{100} > M_{211}$. As shown earlier[10] the Sommerfeld model upon which the FN theory is based does not hold for the <100> direction of clean W, hence, it is possible that the form of the FN equation preexponential, from which M_{100} is evaluated, is incorrect.

An interesting feature of the Table I results is the low value of the 110 work function for non-<110> oriented emitters; both <310> and <100> oriented emitters gave nearly identical values of $\phi_f \cong 5.0$ eV for the 110 plane rather than the customary ~6.0 eV value. On the other hand, the <110> oriented emitter gave the usual 5.8 eV value of ϕ_f for the 110 plane. This effect of emitter orientation on ϕ_f was confined to the 110 plane, since all other planes gave nearly identical values of ϕ_f independent of emitter orientation after corrections for the $\beta(\theta)$ variation were made. We have no clear-cut explanation for these orientational effects on the value of ϕ_f for the 110 plane, although in comparing the 110 results for the <310> oriented emitter with the 3^o off-axis results from the <110> oriented emitter, one observes similar values of M and ϕ_f. This suggests that proper allignment of the 110 plane for

TABLE I

Results From Clean Tungsten Substrates

< 310 > Oriented Emitter

Plane	ϕ_e(eV)	ϕ_f(eV)	$\beta/\bar{\beta}(\theta)$	$M \times 10^{-5}$	θ (deg)
211 (flashed)	4.84 ± 0.06	4.93 ± 0.01	0.97	2.1	25
211 (annealed)	5.05 ± 0.05	5.00 ± 0.02	1.01	2.7	25
310 (flashed)	4.34 ± 0.02	4.21 ± 0.01	1.05	3.6	0
310 (annealed)	4.16 ± 0.03	4.28 ± 0.01	0.96	3.4	0
111 (annealed)	4.80 ± 0.03	4.49 ± 0.02	1.11	1.6	43
110 (annealed)	6.20 ± 0.06	5.02 ± 0.03	1.37	2.2	26
100 (annealed)	- - - - -	4.59 ± 0.02	- - -	1.5	18
	< 100 > Oriented Emitter				
611 (annealed)	4.41 ± 0.04	4.32 ± 0.04	1.03	1.8	13
	< 110 > Oriented Emitter				
110 (annealed)	6.40 ± 0.09	5.79 ± 0.04	1.16	1.4	0
110 (off axis)	6.02 ± 0.06	5.16 ± 0.02	1.26	2.3	3

In order to make comparison of M values meaningful, the values given in Table I have been corrected for the variation in $\bar{\beta}$ as emitters of differing radii of curvature r were used. This was accomplished by assuming that $M \propto \bar{\beta} \propto 1/r$ so that uncorrected M values could be multiplied by $\bar{\beta}_o/\bar{\beta}$, where $\bar{\beta}_o$ was an arbitrarily chosen reference. From Table I we observe that the local value of M decreases in the order 310 > 211 > 611 > 111 > 100 > 110. This is nearly identical to the order observed in a similar study by van Oostrom[19]

The emitting area can be obtained directly from the experimental intercepts $B(\theta)$ of the FN plots by noting

$$B(\theta) = CA\beta^2/\phi , \tag{19}$$

where C is a constant. Whence, according to Equations (18) and (19) the value of M at an angle θ from the emitter apex relative to the magnification M_o along the emitter axis is given by

$$M(\theta)/M_o = \left[B_o/B(\theta)\right]^{1/2}\beta(\theta)/\beta. \tag{20}$$

The values of $M(\theta)/M_o$ decrease more rapidly with θ than $\beta(\theta)/\beta_o$ as expected from the enhanced beam compression caused by the emitter shank, although the exact functional form of the relation $M = f(\beta)$ cannot be established because of possible distortion of the beam by the deflecting magnetic field, particularly at large θ.

The values of work function ϕ_f given in Table I for various crystal faces were obtained from Equation (13) by using the average value $\overline{\phi}_o = \overline{\phi}_f = 4.52$ eV as the reference and making the appropriate corrections for variations in $\beta(\theta)$ as given in Figure 4. Prior to each measurement the emitter was either annealed for 300 seconds at 1000°K or flashed to 1800°K and quenched to 77°K at which temperature each of the measurements were made. The results show that the annealed values of ϕ_f for the 211 and 310 planes are slightly larger than those obtained by flashing and quenching due to alteration of the end form with temperature.

temperature, first noticed by Muller[21], is undoubtedly caused in part by temperature dependent local faceting.

To partially circumvent these problems we have established experimentally the variation in β with θ by measuring the relative variation in m_f for various $\{310\}$ planes along the $[100]$ zone line of a $<310>$ oriented emitter. If the reasonable assumption that each 310 plane exhibits identical values of ϕ is accepted, then the relative variation of m_f with θ is inversly proportional to β. The experimentally determined relative variation of β determined for the $<310>$, $<130>$, $<\bar{3}10>$, and $<\bar{1}30>$ directions is shown in Figure 4, where β_o refers to the on-axis value. The data points fall within the envelope established by a numerical calculation[22] of β/β_o for a sphere-on-orthagonal cone imitating an emitter with a slight and pronounced constriction. The deviation of the data from the solid curve representing an average emitter shape does not exceed 2%, which is within the accuracy of the FN plots. It is therefore concluded that the corrections to the probe FN work function calculations based on the average emitter shape curve of Figure 4 are reasonably accurate. Thus, one of the major uncertainties of the FN slope method of determining ϕ_f for various crystal faces is removed.

Also plotted in Figure 4 is the variation of linear magnification M vs θ which is related to the probe hole area A_p and the emitter area A "seen" by the probe hole as follows:

$$M = (A_p/A)^{1/2}. \tag{18}$$

In the present case the resolution for planes 13 to 26° off the emitter axis ranged from 30 to 40 mV with poorest resolution at the largest beam deflection as expected. For an on-axis direction the resolution was considerably better, but not as good as the 10 mV value claimed by van Oostrom. Resolution is defined here as the width of the theoretical energy distribution curve at the peak of the experimental curve, with the latter normalized such that the low energy tails coincide. Inasmuch as resolution is not critical except at low temperatures where sharp peaks occur, the resolution at maximum beam deflection was adequate to investigate the energy distribution shapes at elevated temperatures.

SINGLE PLANE WORK FUNCTIONS

The variation of β with angular separation θ from the emitter apex is one of the primary difficulties in utilizing Equation (13) to obtain meaningful relative work function variation with crystal direction. This variation in β is due to the increased shielding of the tip by the emitter shank with increasing θ. In addition, another variation in β occurs due to differing amounts of the thermodynamic motivated local faceting of certain crystal faces[20]. This local faceting varies in magnitude with the temperature at which the emitter was annealed prior to thermal quenching and is largest for the low index planes because of the lower surface energy. The slight variation in ϕ_f calculated by Equation (13) for a given plane with annealing

measurments were taken along a particular zone line at positions where the current went through either a maximum or minimum as a function of beam deflection. This allowed precise positioning of the desired crystal face on the aperture of the anode throughout the voltage range covered by the FN plot. The total current I_t was measured simultaneously with the probe current as shown schematically in Figure 3.

The resolution of this analyzer tube, estimated to be 10 mV by van Oostrom[19], is normally ascertained by comparison of the experimental and theoretical energy distribution curves. Unless rigorous analysis of all factors leading to the resolution limit can be made the latter must suffice as a means of estimating the resolution. Magnetic shielding around the tube reduced the earth magnetic field to zero, however, the magnetic field in the region of the collector was approximately 0.1 gauss at a beam deflection of 55^{o}. Although no quantitative calculations of the effect of magnetic field on the resolution have been performed, it is believed a field of 0.1 gauss will not appreciably reduce the resolution for this tube design. A more serious effect on the measured energy distribution in this analyzer design is caused by the alteration of the electron optics as the apparent electron source and, hence, position of the crossover changes with beam deflection. The seriousness of this effect will be discussed later in connection with the results. In order to minimize magnetic deflection, emitter orientation was varied by fabricating emitters from zone refined oriented W wires produced in this laboratory. For this study <310>, <110> and <100> emitter orientations were employed.

potential analyzers the energy sorting is accomplished by the work function barrier of the collector, so that it was necessary to first lower the tip potential to approximately $-\phi_c$ (the work function of the collector) before a measurable current could be detected. The width of the energy distribution curves are such that the total curve can be measured within a ~ 1 V range. In order to electronically differentiate the integral curves, I_p was modulated by a 15mV, 1000 cps signal superimposed on the emitter bias voltage and detected with a narrow band 1000 cps amplifier. The magnitude of the 1000 cps signal in the collector circuit was proportional to the first derivative of I_p with respect to V_t and was also plotted on an xy recorder as a function of V_t.

A small, rotatable external electromagnet B and internal concentrator C shown in Figure 2 were used to deflect the beam in order to position the emission from the desired crystallographic plane onto the aperture of the anode electrode. The internal concentrator could be tied electrically to the anode potential by allowing it to rest on a small platinum ring. With this arrangement the tube could be used to measure both energy distribution and work function from various single crystal faces. The I(V) data for work function measurements were obtained with the tip at -8 V and a constant ratio of V_L/V_A in order that the electron trajectories through the lens would be constant over the voltage range. During the I(V) measurements with magnetic deflection, compensation of the magnetic current must be performed in order to maintain a constant position of the desired crystal face on the aperture over the anode voltage range. Work function and energy distribution

by varying the cathode potential approximately 1.5 V. The ratio of V_L to V_A is a critical quantity and for this particular lens system best results were obtained with $V_L/V_A = 0.003$.

The emitter assembly A consisted of a field emission tip spot welded to a 10 mil tungsten filament with 3 mil potential leads utilized to sample the potential V_f and, hence, resistance change across a small length of filament in order to accurately measure the emitter temperature. The temperature of the emitter was controlled by resistive heating of the emitter support filament with an isolated dc supply as shown in the diagram of Figure 3. Care was taken to insure that I_fR drops across the filament during heating would not alter the tip bias voltage by applying V_t at the center of a 50 Ω resistor symmetrically placed in the circuit.

The aperturing of the primary beam by the 1 mm probe hole was sufficient to cause a ratio of the collected to the total emitted current of $\sim 10^{-3}$ when probing the emission from a low work function region of the emitter. This corresponds to a tip area "seen" by the probe hole of approximately 3 x 10^{-14} cm^2 for the emitter sizes employed in this investigation. The collector current I_p, which ranged from 10^{-9} to 10^{-14} A was measured by a Cary vibrating reed electrometer with an xy recorder readout. In order to minimize the electrical noise pickup by the collector lead as it emerged from the tube, the lead was enclosed in a molybdenum cylinder which connected directly to the shield of the coaxial cable leading to the electrometer. The energy distribution curves were obtained by graphical or electronic differentiation of the collector current I_p versus tip bias voltage V_t curves. In retarding

potential and acts as a shielding electrode for the hemispherical collector (also operating near ground potential) and accordingly reduces the effect of undesirable reflection inherent in most retarding potential analyzers. It should be noted that an electron passing through the cross over formed near the center of the hemispherical collector will have nearly normal incidence on the collector surface so that the total energy of the emitted electrons will be analyzed.

The tube, constructed of aluminosilicate glass, contained molybdenum electrodes and a collector consisting of a hot spun molybdenum hemispherical cup (radius of curvature of 15 mm) exhibiting surface roughness less than 1 micron. The electrode apertures were 1, 2 and 4 mm, increasing in size toward the collector. A thin willemite screen on the anode allowed pattern viewing. Deposition of coadsorbed zirconium-oxygen was accomplished by resistively heating a poorly outgassed 10 mil zirconium wire contained in the tubulation opposite the emitter. After evacuation the tube was sealed off and placed in a liquid nitrogen cryostat where the measurements were performed. The insertion in liquid nitrogen greatly increased the vacuum stability, reduced tip contamination from the screen to a negligible amount during the emission of high total currents (2μA) and extended the lower limit of the temperature range to 78^{o}K.

In practice, the anode potential V_A was constant and the focal length adjusted by varying the potential of the lens electrode V_L (See Figure 3). The total energy distribution curves were taken for fixed values of V_L and V_A

When the correction term $\delta = V(1 - \pi p \cot \pi p)/2.3$ cannot be neglected the work function at temperature T becomes

$$\phi(T) = \phi_o \left(\frac{m_f + \delta}{m_{fo}} \right)^{2/3} \left(\frac{\beta(T)}{\beta_o} \right)^{2/3}, \qquad (16)$$

where the subscript o refers to the low temperature values, and $\beta(T)$ corrects for the thermal expansion of the emitter of radius r and is approximately given by

$$\beta(T) = \beta_o(1 - \Delta r/r). \qquad (17)$$

Thus, field electron I(V) data can be utilized to evaluate the temperature coefficient of work function over the temperature range of validity for Equation (7). In practice the upper limit of temperature is determined by the field induced rearrangement of the emitter geometry due to surface migration. The value of V mid-range in the FN plot is the appropriate value to use in the correction term δ.

EXPERIMENTAL TECHNIQUES AND PROCEDURES

The energy analyzer tube utilized in this investigation was based on a design by van Oostrom of the Phillips Laboratory[19] and is depicted in Figure 2. Briefly, the tube is designed in such a way that electrons passing through the lens system are focused near the center of the spherical collector F. The electrode system of the analyzer consists of an anode D, a focusing electrode E and a Faraday cage G. The latter electrode is operated near ground

Recent anomalous values of ϕ_e calculated by the absolute method has led to a reexamination[15] of Equation (14) and the inclusion of surface patch field effects. This consideration led to a correction term which multiplies the right hand sign of Equations (13) and (14) by a factor $(\pm F_o/\beta V + 1)^{4/3}$ and $(\pm F_o/\beta V + 1)$ respectively where F_o, the net strength of the patch field, is positive for a high ϕ plane and negative for a low ϕ plane relative to the surrounding planes. It was shown, however, that for crystal planes greater than 100Å in diameter a work function difference between it and the surrounding planes of at least 1 eV is necessary to cause an appreciable patch field correction to either Equations (13) or (14). The significance of patch field corrections will be discussed in a later section.

Temperature Dependence of Work Function

In order to assess the effect of temperature on the energy distribution results it is necessary to evaluate and understand the variation of the local work function with temperature. A thorough review of the theoretically expected contributions to the temperature coefficient of the work function has been given by Herring and Nichols[16] and experimentally confirmed by both contact potential[17] and field electron emission[18] methods. Using field electron emission van Oostrom[18] measured values of $d\phi/dT$ by monitoring the change in field electron current at constant voltage between 78° and 293°K. A more accurate and less restrictive method described here involves obtaining FN plots at each temperature. Using the more general T-F formulation given in Equation (7), the 0°K expression for m_f given in Equation (12) becomes

$$m_f = V(1-\pi p\cot\pi p)/2.3 - 2.96 \times 10^7 \phi^{3/2} s(y)/\beta. \qquad (15)$$

it is observed that the value of d and ϕ_c can be obtained from the slope m_e and intercept respectively of a plot of $\log (I_o - I)/I_o$ versus V_t. The value of d so obtained can be compared with expectation in order to provide a rough check on the energy distribution theory.

It is further observed from Equation (2) that a "Fowler-Nordheim plot" of $\log I_o/V^2$ versus $1/V$ yields a slope m_f which is related to ϕ and the geometric factor $\beta = F/V$ as follows:

$$m_f = -2.96 \times 10^7 \phi_f^{3/2} s(y)/\beta, \tag{12}$$

where s(y) is a slowly varying tabulated function[12a] arising from the image potential. The values of ϕ_f relative to a reference value ϕ_o can readily be established as shown by rewriting Equation (12) as follows:

$$\phi_f = \phi_o (m_f/m_{fo})^{2/3}, \tag{13}$$

where m_{fo} is the FN plot slope for the reference surface and the value β is assumed unchanged. Because of the difficulty in determining accurate values of β Equation (12) cannot be employed for accurate absolute work function calculation. However, as pointed out by Young[14], Equations (11) and (12) can be combined to give the following expression for ϕ

$$\phi_e = -3m_e t(y)/2m_f V s(y), \tag{14}$$

where V is the anode voltage. Accordingly, an absolute value of work function can be ascertained from combined energy distribution and FN plots via Equation (14).

that electrons emitting from a certain crystal direction are largely confined to a small solid angle in the bulk.

Absolute Work Function Measurements

In addition to providing interesting and informative data concerning fundamental mechanisms of electron emission from the metal surfaces, energy distribution measurements when combined with current voltage I(V) data can also yield absolute work functions of single crystal faces. The ability to perform such an analysis depends on the validity of the total energy distribution expression Equation (5). For retarding potential energy analyzers the total energy of the emitted electrons E collected at a metal surface of work function ϕ_c must exceed

$$E > \phi_c + E_f - V_t, \tag{9}$$

where V_t is the emitter to collector bias potential. Increasing V_t allows all electrons emitted down to a certain energy level $-\epsilon$ to be collected; also at $0^{\circ}K$ the condition $V_t = \phi_c$ represents the current cut-off since population of electronic states above E_f is zero. The collected integral current I_p at a specified value of ϵ when $p = 0$ is given by:

$$I_p = \frac{I_o}{d} \int_o^{\epsilon} e^{\epsilon/d}\, d\epsilon = I_o(1 - e^{-\epsilon/d}), \tag{10}$$

where I_o is the maximum field electron current. By rewriting Equation (10) in the working form

$$\log (I_o - I)/I_o = -\phi_c/2.3d + V_t/2.3d \tag{11}$$

Integration of Equation (5) over ϵ yields the well-known expression for thermal-field emission J_{TF}

$$J_{TF} = J_o \int_{-\infty}^{\infty} e^{\epsilon/d} \left[1 + e^{\epsilon/d}\right]^{-1} \frac{d\epsilon}{d} = J_o \pi p/\sin\pi p, \qquad (7)$$

which is valid in the range $0 \geqslant p > 0.7$. For small values of T, we note $\pi p/\sin\pi p \cong 1$ and the $0^{\circ}K$ approximation $J = J_o$ is obtained as given in Equation (2).

For the sake of completeness the general expressions for the energy distribution of the total, normal and transverse components of the emitted electrons from a Sommerfeld metal are given in the appendix for various ranges of field and temperature. It is important to note that according to Equations (A10c) and (A14c) the transverse energy distribution for both $0^{\circ}K$ and TF emission is independent of T and E and has an average value of d. It is of interest whether the angular distribution of emitted electrons within the bulk vary significantly with E. Considering a typical situation where $\phi = 4.5$ eV and $F = 4 \times 10^7$ V/cm we obtain $E_t \cong 0.18$ eV, and by assuming the bottom of the conduction band is -10.8 eV a typical value of E is ~ 6 eV. One can readily deduce that the expression for the average angle $<\theta>$ at which electrons impinge on the surface potential barrier perpendicular to the emission direction is:

$$\tan^2 <\theta> = E_t/E \qquad (8)$$

hence, for the preceding typical field emission case $<\theta> \cong 10^{\circ}$. It is clear that $<\theta>$ is essentially unchanged since only a $\sim 10\%$ variation is required in E to sweep over the total energy distribution. These considerations indicate

The specific effect of band structure occurs in Equations (1) and (4) only through the term in brackets and can be neglected when $E_m/d>1$. Under usual field electron emission conditions $d \cong 0.15$ to 0.25 eV and it is therefore reasonable to believe that E_m is sufficiently large for most degenerate metals exhibiting large Fermi energies that the band structure term in Equations (1) and (4) is negligible; however, for transition metals with partially filled narrow d bands, the value of E_m may be sufficiently small to perturb $J(\epsilon)$ through the band structure term.

The original derivation of $J(\epsilon)$ by Young[7] based on the Sommerfeld free electron model is a special case of Equation (1) when the Fermi-Dirac distribution of $f(\epsilon)$ is assumed and the band structure term is neglected. With these considerations one obtains:

$$J(\epsilon) = J_o e^{\epsilon/d} \Big/ (1 + e^{\epsilon p/d})d, \tag{5}$$

where $p = kT/d$ is a dimensionless parameter. The mathamatical derivation of Equation (5) breaks down for $p>1$ and becomes unreliable when p exceeds about 0.7. A graphical representation of $J(\epsilon)$ versus ϵ/d yields a set of curves whose shape depends only on the dimensionless parameter p as shown in Figure 1. For the value of $p = 0.5$ an exactly symetrical distribution of the emitted electrons about E_f is obtained as shown in Figure 1; the condition $p = 0.5$ can be restated in terms of an "inversion temperature" T^*:

$$T^* = d/2k = 5.67 \times 10^{-5} F/\phi^{1/2} t(y). \tag{6}$$

Total Energy Distribution

An expression for the current density per unit total energy $J(\epsilon)$ (relative to the Fermi level $\epsilon = E - E_f$) was derived by Stratton[11] for a degenerate metal of arbitrary band structure and electron distribution $f(\epsilon)$. Employing the WKB approximation for the transmission coefficient, expanding in the usual fashion about E_f and neglecting quadratic and higher order terms, Stratton obtains:

$$J(\epsilon) = J_o f(\epsilon) e^{\epsilon/d} \left[1 - \frac{1}{2\pi} \int_o^{2\pi} e^{-E_m/d} d\phi_p \right] \Big/ d, \qquad (1)$$

where J_o denotes the total current density (integrated over all ϵ) at $0^\circ K$, which is given by

$$J_o = \frac{e^3 F^2}{8\pi \phi t^2(y)} \exp \left[-4(2m\phi^3)^{1/2} v(y) / 3\hbar eF \right]$$

$$= \frac{1.54 \times 10^6 F^2}{\phi t^2(y)} \exp \left[-6.83 \times 10^7 \phi^{3/2} v(y)/F \right] \ A/cm^2, \qquad (2)$$

and where E_m is the maximum value of the transverse energy E_t for a specified energy surface ϵ and polar angle ϕ_p in the plane perpendicular to the emission direction. The value of d is given by:

$$d = \hbar eF/2(2m\phi)^{1/2} t(y) = 9.76 \times 10^{-9} F/\phi^{1/2} t(y) \ eV, \qquad (3)$$

where the electric field F is in V/cm and the work function ϕ in eV. The image correction terms t(y) and v(y) are slowly varying tabulated functions[12a] of the auxilliary variable $y = (e^3 F)^{1/2}/\phi$. As first shown by Fischer[13] in the case of spherical energy surfaces with a positive Fermi energy and an effective mass $m_c = r_c m$, so that $E_m(\epsilon, \phi_p) = r_c E$, Equation (1) becomes:

$$J(\epsilon) = J_o f(\epsilon) e^{\epsilon/d} \left[1 - e^{-r_c E_m/d} \right] \Big/ d. \qquad (4)$$

single face work function values and the experimentally determined variations of the local electric field strength with angular separation from the emitter apex from 0 to 90°. The temperature coefficient of the various single face work functions are discussed in connection with a presentation of the total energy distribution results from several major directions of a clean W crystal. Next we deal with the resultant effect of a coadsorbed zirconium-oxygen layer on the energy distributions and work functions of the various crystal faces of a W emitter. In the last section we discuss the applicability of the FN theory to metal substrates in light of these results along with some speculation of the band structure effects noted along the <100> direction.

THEORETICAL CONSIDERATIONS

Since the original derivation of the FN equation several theoretical works have expanded the original theory to include a broader range of temperatures[6], normal and total energy distributions[7] and, more recently, quantum mechanical corrections to the one-dimensional image force model have appeared[12]. Because of the possibility of band structure effects in our results, we shall consider the derivation of the total energy distribution from the standpoint of Stratton[11] whose derivation was based on a metal of arbitrary band structure. The inclusion of the temperature dependence of the total energy distribution requires a careful look at the temperature dependence of the work function. Thus a short description of the analysis of the temperature dependence of work function by field electron techniques is given.

Thus, no serious experimental challenge of the adequacy of the original FN model as it applies to the metal-vacuum interface--a Fermi-Dirac distribution of free electrons and the classical image force barrier at the surface--has been made. Recently, however, an investigation[9] of the energy exchange accompanying field electron emission over a wide temperature and field range revealed a significant departure from the predictions based on the Sommerfeld model, particularly at elevated temperatures. These results could be explained either by a departure of the total energy distribution from theoretical expectations or a large temperature coefficient of the average energy of the charge carriers in the bulk. In order to distinguish between these two possibilities a detailed study of the total energy distribution of field emitted electrons from various crystallographic directions of a W emitter as a function of temperature and in the presence of a coadsorbed zirconium-oxygen layer has been performed. Although definite departures from the Sommerfeld free electron model have been discovered along the <100> direction[10], the results along other directions generally confirmed the expected temperature and field dependence of the total energy distribution up to approximately 900°K.

The derivation of the total energy distribution expression according to Stratton[11], who included band structure effects, and the expected temperature and field effects are given in the following section. Also discussed are the means by which absolute single crystal face work functions can be determined from the energy distribution measurements. Experimental methods and procedures are discussed in a later section followed by the calculated

III TOTAL ENERGY DISTRIBUTION OF FIELD EMITTED ELECTRONS FROM TUNGSTEN AND SINGLE PLANE WORK FUNCTIONS

INTRODUCTION

The field electron emission process between a metal-vacuum interface was given theoretical foundation in 1928 by Fowler and Nordheim[1,2] who based their calculations on a one-dimensional Sommerfeld free electron model at $0^{\circ}K$. The resultant Fowler-Nordheim (FN) equation has since been found adequate for describing field electron emission from clean and adsorbate coated metals in the applicable temperature range. A modification of the FN equation to include temperature effects was later treated quantitatively by several authors[3-6]. Although total emission measurements generally confirmed the expected temperature and field dependence of the emitted electrons, a more rigorous test of the theory was performed by Young and Muller who determined both theoretically[7] and experimentally[8] the total energy distribution of emitted electrons from a tungsten substrate in the temperature range 77 to $300^{\circ}K$. Experimental attempts to measure the energy distribution of field emitted electrons prior to the work of Young and Muller were clouded by the erroneous belief that normal distributions were obtained from point-to-plane electrode geometries.

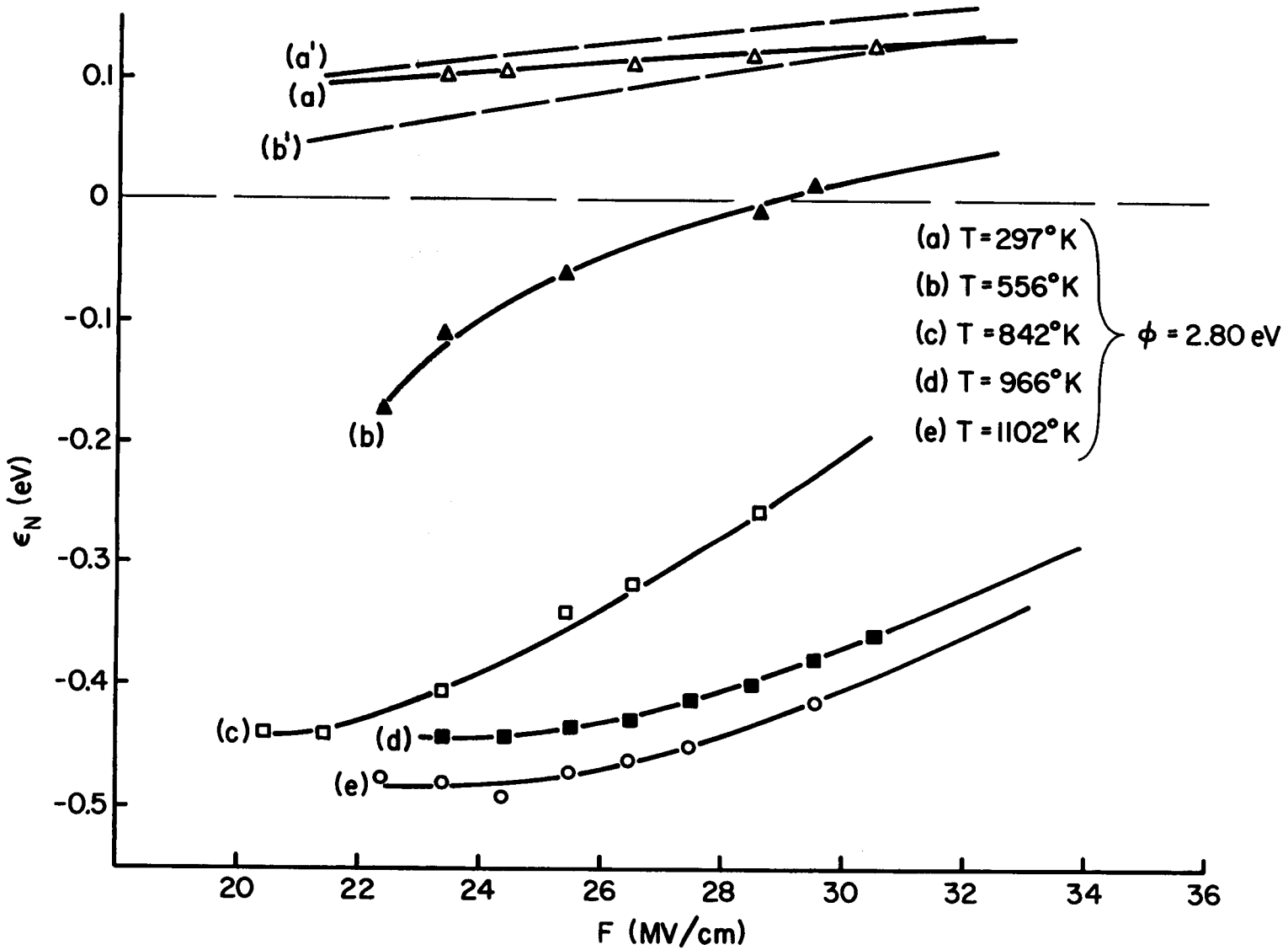

Figure 14. Solid curves represent the experimentally determined energy exchange per electron ϵ_N with the lattice as a function of applied electric field F at the indicated temperatures for zirconium-oxygen coated tungsten. Dashed curves are corresponding ones calculated according to Equation (15). Negative values of ϵ_N indicate emission cooling.

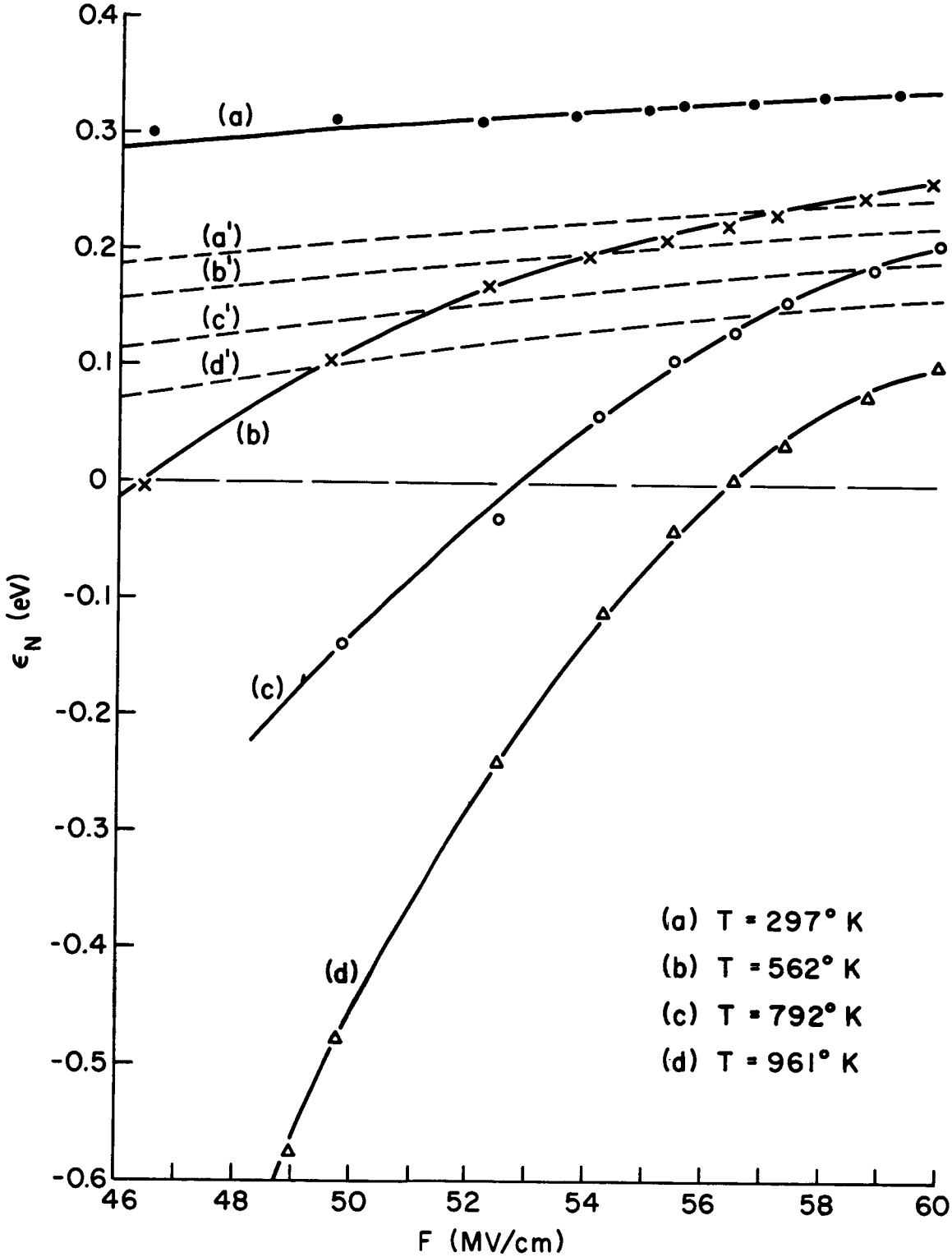

Figure 13. Solid curves represent the experimentally determined energy exchange per electron ϵ_N with the tungsten lattice as a function of applied electric field F at the indicated temperatures for clean tungsten. Dashed curves are corresponding ones calculated according to Equation (15). Negative values of ϵ_N indicate emission cooling.

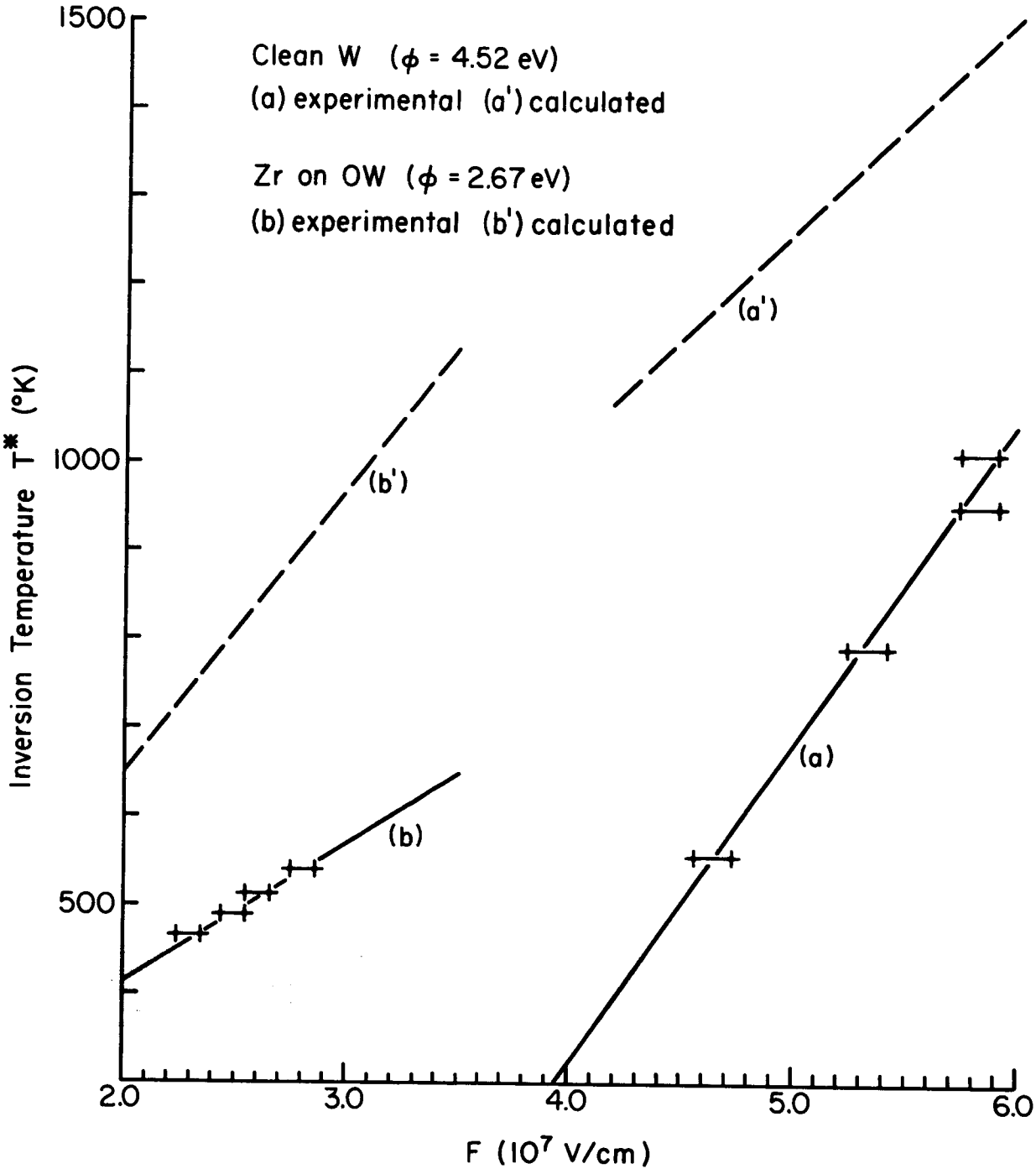

Figure 12. Experimentally determined inversion temperatures T^* for a clean and zirconium-coated tungsten emitter as a function of applied electric field. Dashed curves are the respective calculated inversion temperatures according to Equation (12).

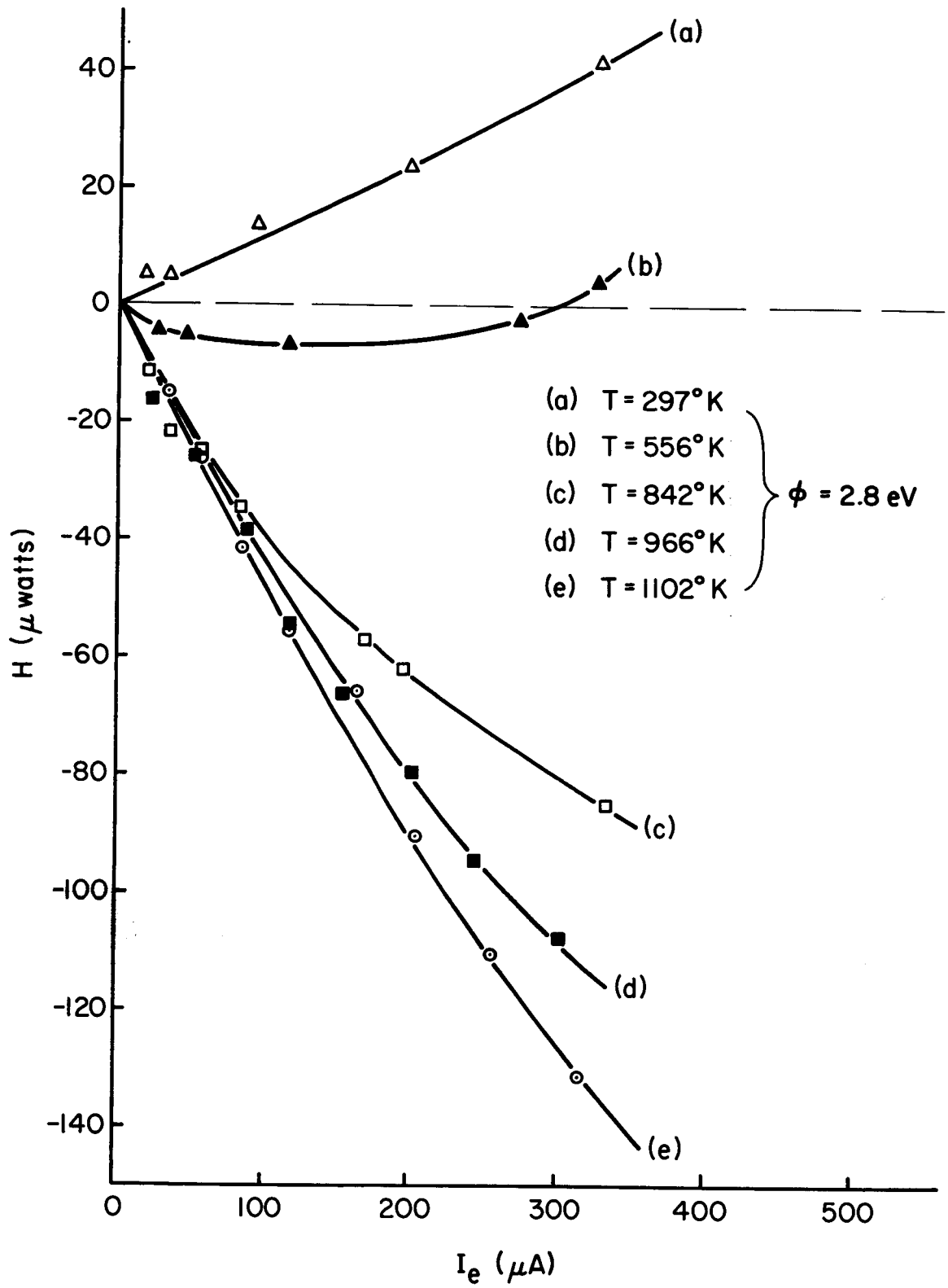

Figure 11. Experimentally determined power exchange H at a tungsten emitter coated with zirconium-oxygen as a function of field emission current I_e. Negative values of H indicate emission cooling.

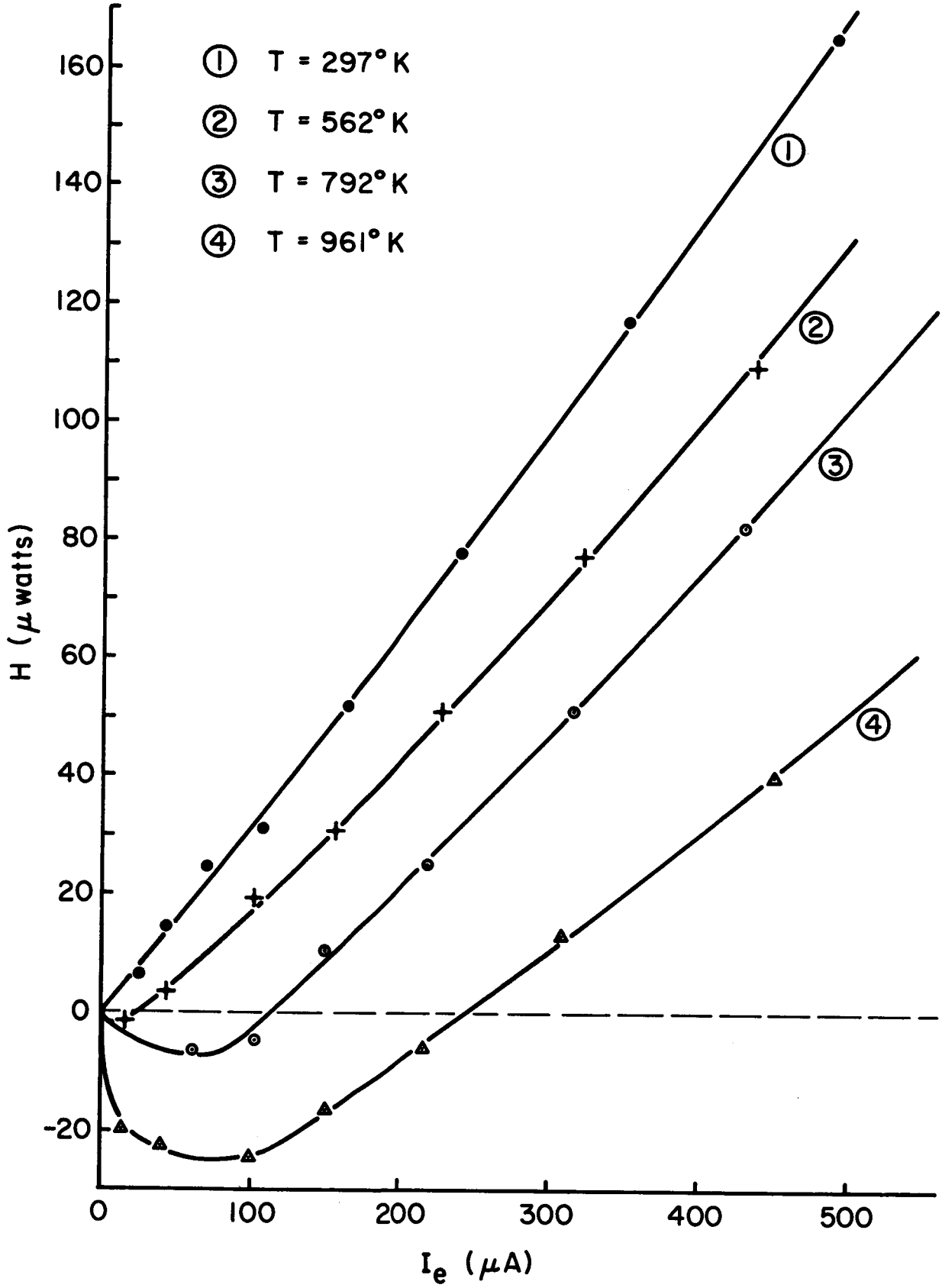

Figure 10. Experimentally determined power exchange H at the emitter as a function of field emitted current I_e at the indicated temperatures for clean tungsten where ϕ = 4.52 eV. Negative values of H indicate emission cooling.

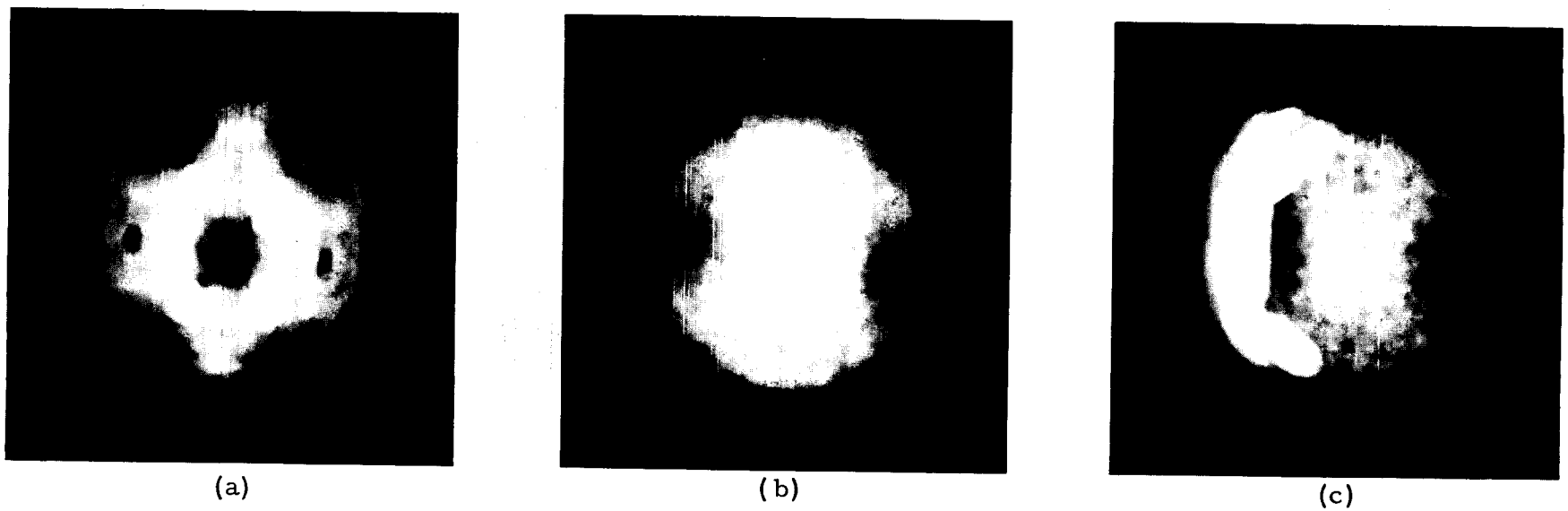

Figure 9. (a) Pulse field electron pattern of a tungsten tip with cesium coverage in excess of one monolayer. The average work function of the covered surface is 1.78 eV.

(b) Pattern of same tip but after emitting a peak pulse current of 53 mA (1μsec pulses at 100 pps) for 300 sec; the coverage in the emitting region has decreased to approximately 0.5 monolayer, as determined by the work function change to 2.1 eV.

(c) Evidence of cesium migration from the heavily covered shank to the tip, produced by heating pattern (b) to 173°K for only 300 sec.

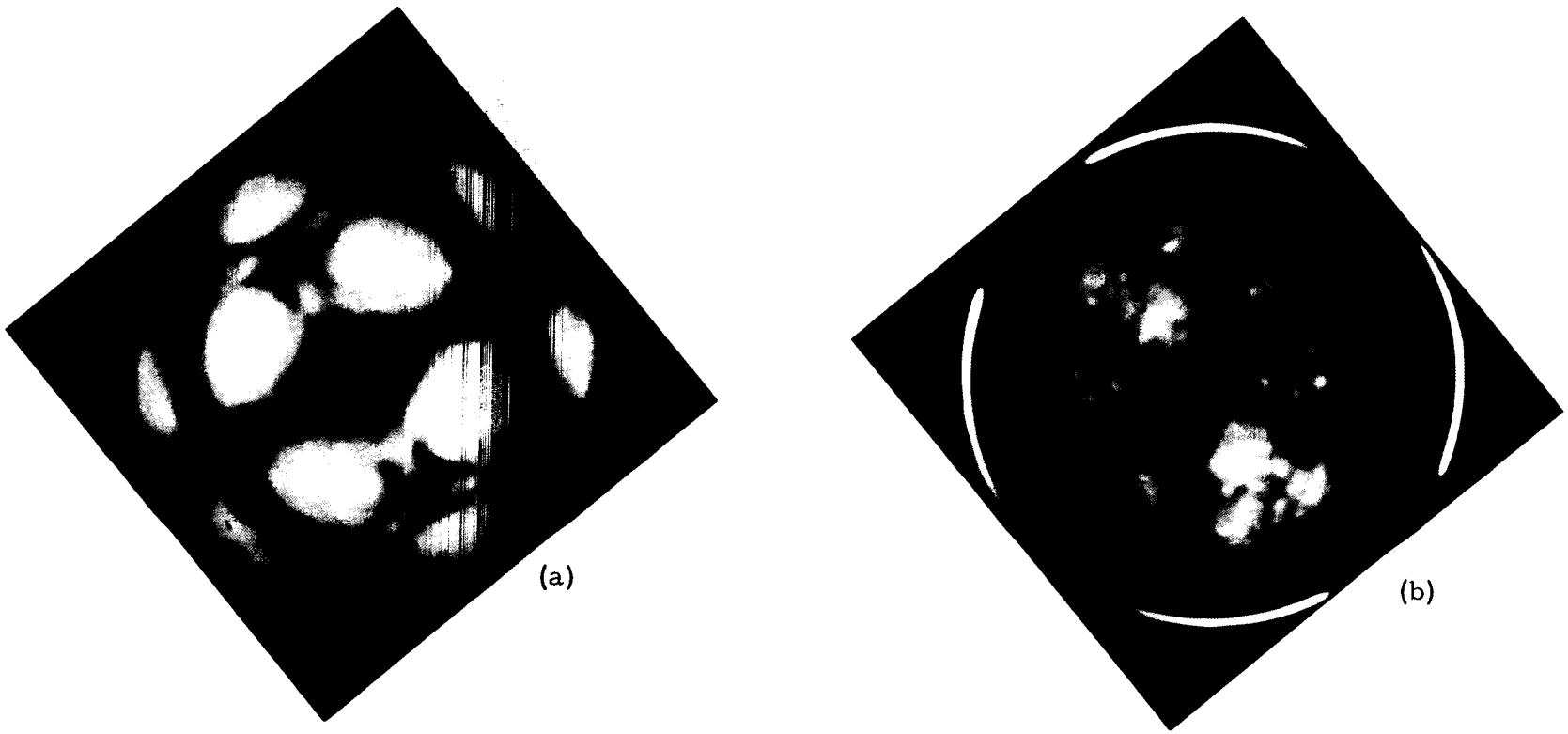

Figure 8. (a) Pulse field electron pattern of a near monolayer coverage of barium on tungsten exhibiting an average work function of 2.0 eV. Picture taken at 3.4 kV.

(b) Same as pattern (a) but after emitting 84 mA of peak pulse electron current at a duty factor of 10^{-4} for 300 sec. Picture taken at 7.8 kV.

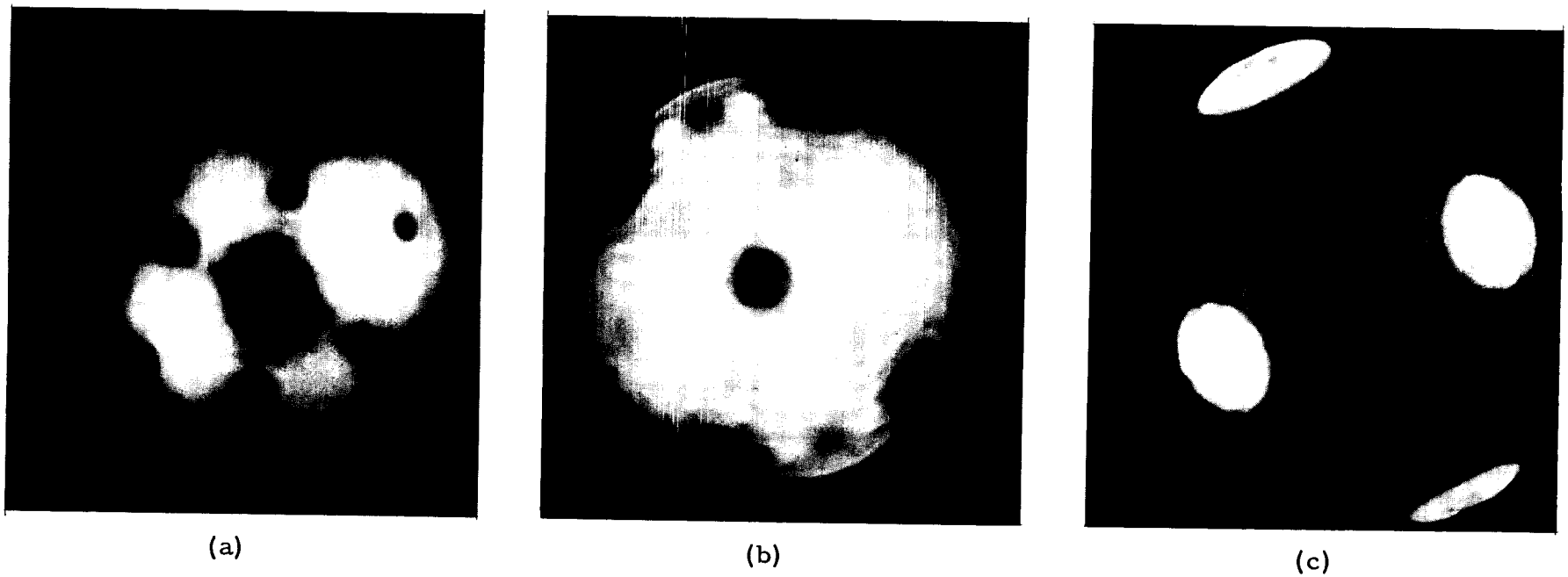

Figure 7. (a) Typical field electron pattern of clean and smooth $\bar{1}10$ oriented tungsten emitter.

(b) Pattern of the same emitter, showing cumulative disruption of the clean tungsten surface (just prior to vacuum arc) resulting from emission of a peak pulse current of 57 mA at 15.3 KV (ϕ = 4.52 eV) with a duty factor of 10^{-4}.

(c) Pattern of the same emitter with a co-adsorbed zirconium-oxygen layer and emitting stably a peak pulse current of 102 mA at 14.8 kV (ϕ = 2.8 eV for the brightly emitting areas).

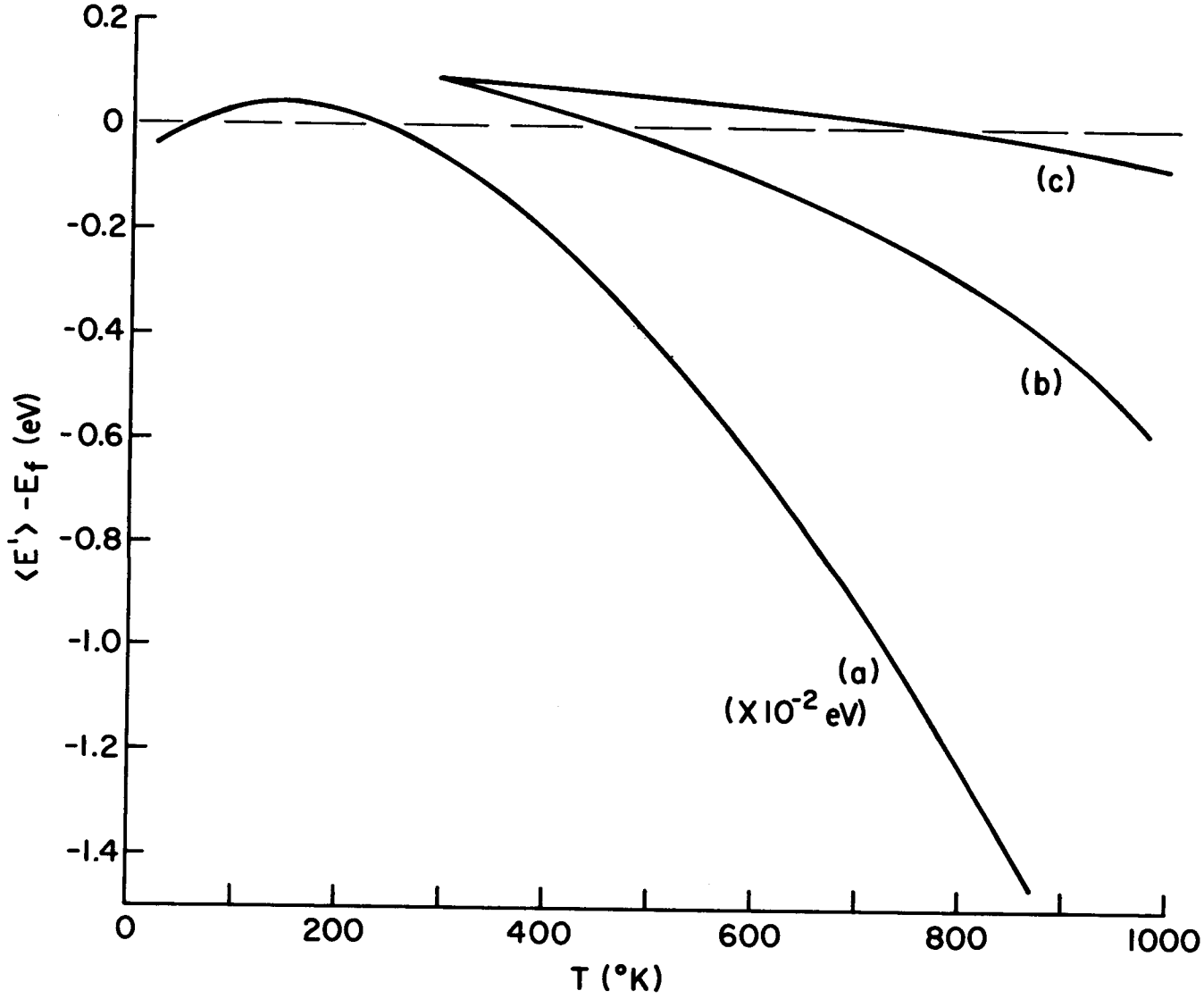

Figure 6. Curve (a) shows the expected variation of $\langle E' \rangle - E_f$ according to Equation (19) and based on Potter's [22] thermoelectric data for tungsten. Curves (b) and (c) give the predicted variation of $\langle E' \rangle - E_f$ based on a comparison between the experimental and theoretical results of Figure 13 at F = 6.0 and 5.0 x 10^7 V/cm respectively.

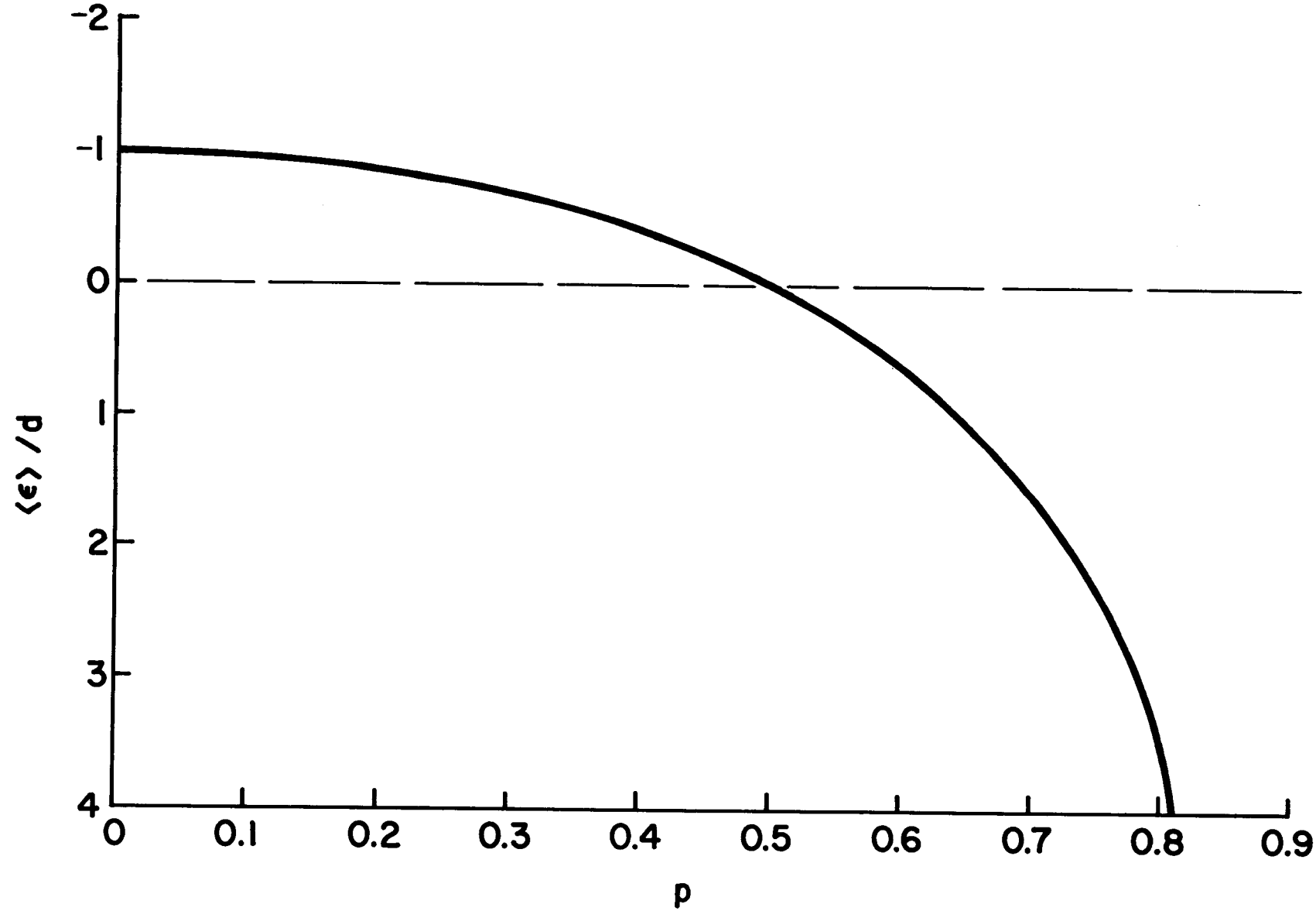

Figure 5. A plot of ⟨ϵ⟩/d vs p according to Equation (15).

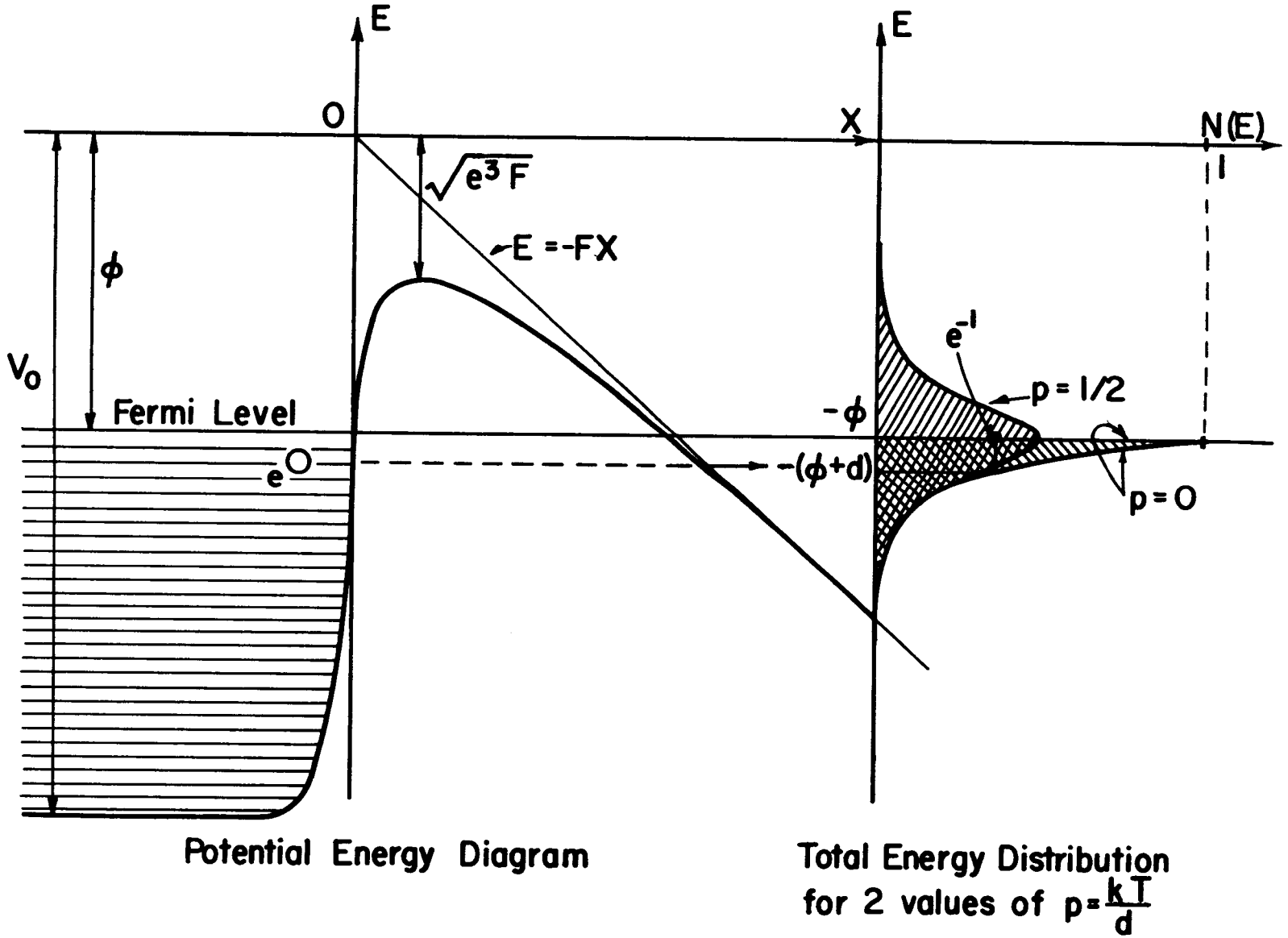

Figure 4. Potential energy diagram and total energy distribution for field and T-F emitted electrons.

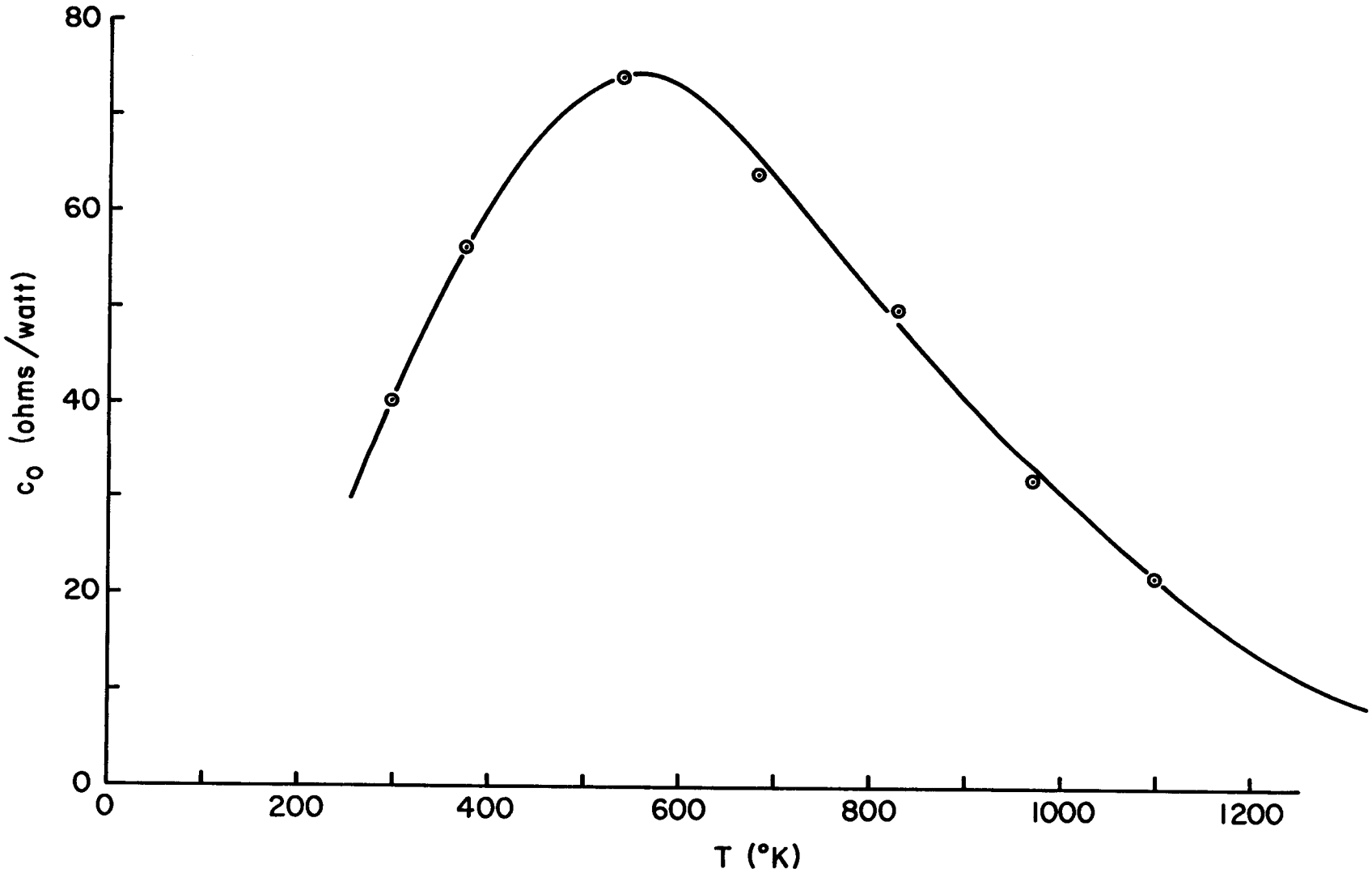

Figure 3. Plot of experimentally determined conversion factor (for converting ΔR changes to H) as a function of emitter temperature.

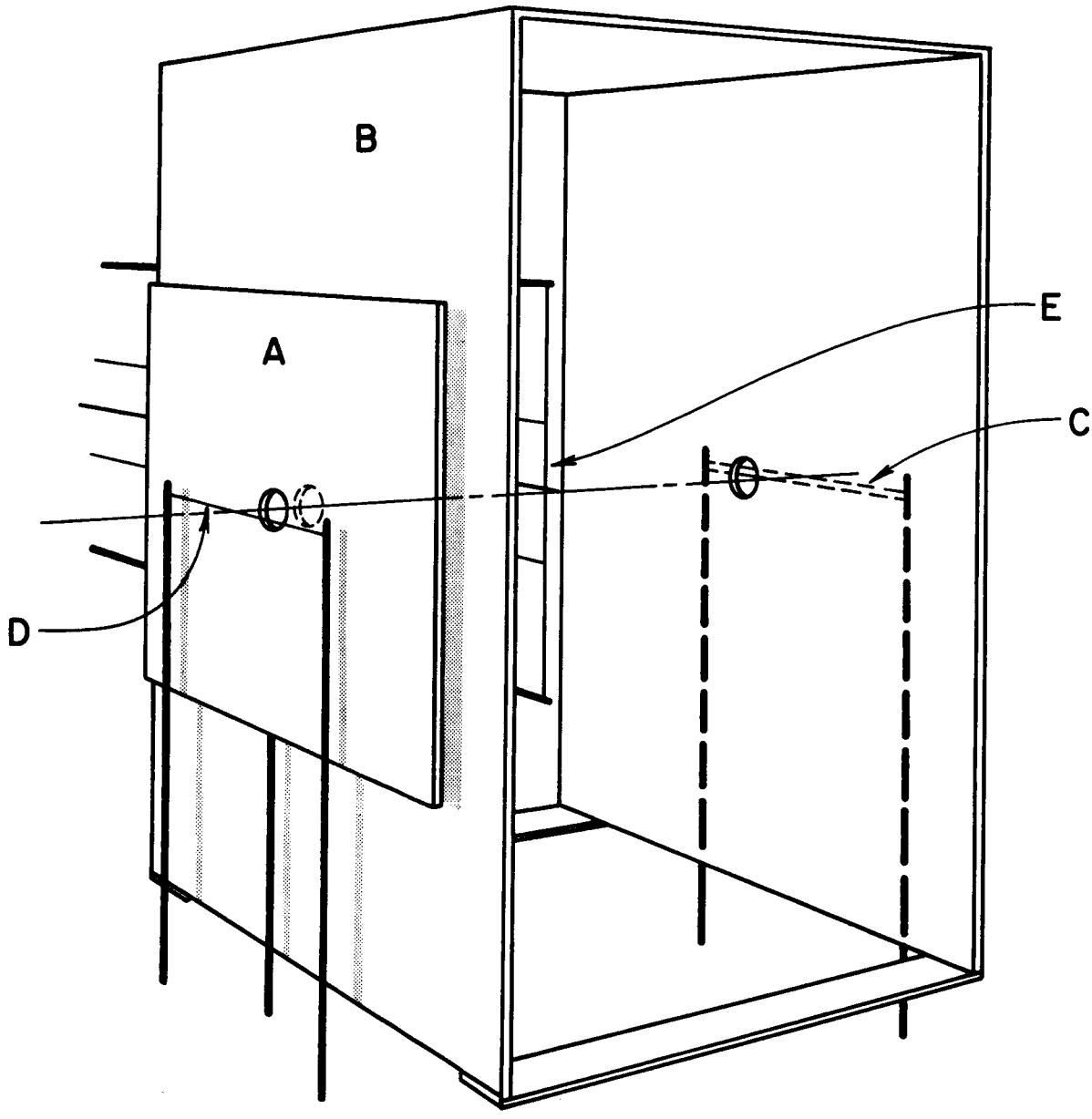

Figure 2. Diagram showing tip assembly, associated filaments and electrodes for quantitative study of emission heating and cooling.

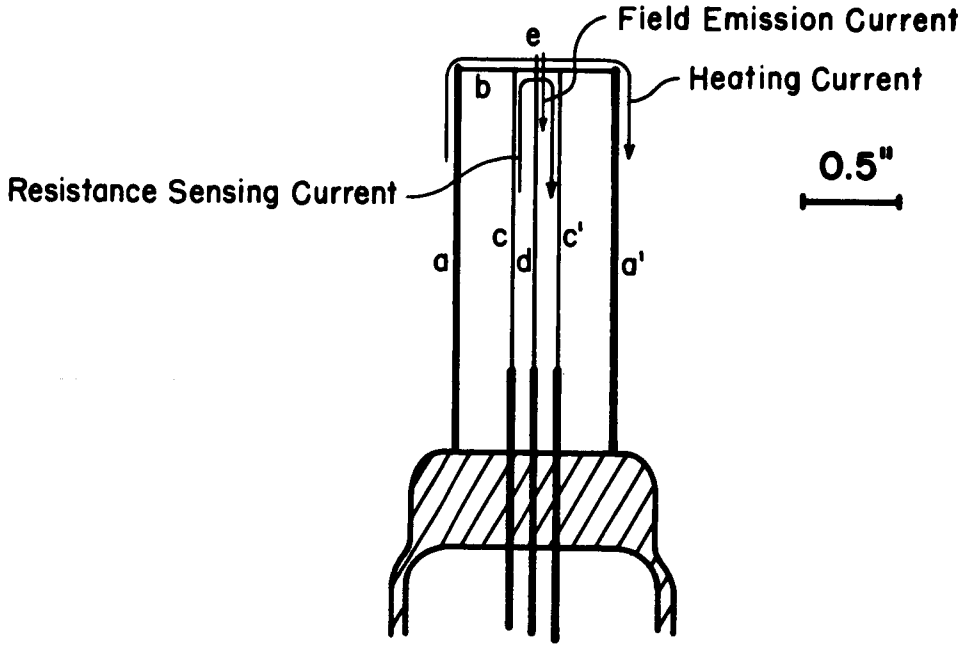

Figure 1. Diagram of tip assembly used in tube for studying emission heating and cooling. Field emitter is formed at end of central lead.

17. R. D. Young, Phys. Rev. 113, 110 (1959).

18. I. Brodie, International Journal of Electronics 18N, 223 (1965).

19. D. Alpert and D. A. Lee (Private Communication).

20. N. F. Mott and E. H. Jones "The Theory of the Properties of Metals and Alloys" (Oxford University Press, London, 1936) p. 305-314.

21. F. Seitz, "Theory of Solids" (McGraw-Hill Book Co., Inc., New York, 1940) p. 178.

22. H. H. Potter, Proc. Phys. Soc. (London) 53, 695 (1941).

23. J. Houston (Private Communication).

24. P. A. Redhead, Can. J. Phys. 42, 886 (1964).

25. R. D. Young (Private Communication).

26. E. Fawcett and W. A. Reed, Phys. Rev. 134, A 723 (1964).

27. E. Fawcett, Phys. Rev. 128, 154 (1962).

28. E. Fawcett and D. Griffiths, J. Phys. Chem. Solids 23, 1631 (1962).

REFERENCES

1. W. P. Dyke, J. K. Trolan, E. E. Martin and J. P. Barbour, Phys. Rev. 91, 1043 (1953).

2. W. W. Dolan, W. P. Dyke and J. K. Trolan, Phys. Rev. 91, 1054 (1953).

3. E. E. Martin, J. K. Trolan and W. P. Dyke, J. Appl. Phys. 31, 782 (1960).

4. O. A. Richardson, Phil. Trans. Roy. Soc. London A201, 497 (1903).

5. W. B. Nottingham, Phys. Rev. 59, 907 (1941).

6. J. E. Henderson and G. M. Fleming, Phys. Rev. 48, 486 (1935); 54, 241 (1938); 58, 908 (1941).

7. F. M. Charbonnier, R. W. Strayer, L. W. Swanson and E. E. Martin, Phys. Rev. Letters 13, 397 (1964).

8. F. M. Charbonnier, Wright Air Development Division Technical Report No. 59-20 (AD-272760) January 1960 (unpublished).

9. F. M. Charbonnier, in Ninth Field Emission Symposium, Notre Dame University, June 1962 (unpublished).

10. P. H. Levine, J. Appl. Phys. 33, 582 (1962).

11. M. Drechsler, in Eighth Field Emission Symposium, Williams College, September 1961 (unpublished); Tenth Field Emission Symposium, Berea College, September 1963 (unpublished).

12. M. Drechsler, Z. Naturforsch. 18a 1376 (1963).

13. L. W. Swanson, R. W. Strayer and F. M. Charbonnier, Surface Science 2, 177 (1964).

14. R. Stratton, Phys. Rev. 135, A794 (1964).

15. R. H. Good and E. W. Müller, Handbuch der Physik 21, 176 (1956).

16. L. W. Swanson and L. C. Crouser, Phys. Rev. Letters 16, 389 (1966).

between experiment and theory is lacking, and the departures cannot be explained by experimental uncertainties. An anomalously low inversion temperature is obtained for both clean and zirconium-oxygen coated tungsten and the values of the average energy exchange per electron is both above (at low temperatures) and below (at high temperatures) the values expected from theory.

The underlying cause of the disagreement between experiment and theory does not seem attributable to a deviation from theory in the total energy distribution of the emitted electrons, but rather to a variation of the average energy, relative to the Fermi level, of the conducting carriers with temperature and field. Further investigation of the Nottingham Effect, in other cathode materials which are nearly free-electron in character, and further theoretical study of the conduction processes and the electron-lattice interactions at elevated temperatures, should contribute a more detailed understanding of the Nottingham Effect.

ACKNOWLEDGMENTS

The authors wish to acknowledge the support of part of this work by the National Aeronautics and Space Administration, Washington, D. C. We also wish to express our gratitude to J. K. Trolan, R. W. Strayer, and E. E. Martin for stimulating discussions and for assisting in the experimental work, and to W. P. Dyke for his interest and support.

is worth pointing out one interesting resemblance, that is, all three curves predict a value of $< E' > - E_f$ whose sign varies from positive to negative as the temperature increases. While this does not provide a quantitative explanation for the disagreement with theory in the Figures 13 and 14 results, the qualitative evidence is substantial enough to require further theoretical and experimental investigation of the connection between the thermoelectric effect and $< E' > - E_f$. In particular, theoretical examination of bulk conduction processes of tungsten, the mechanism of the energy exchange between the conducting charge carriers and the lattice, and the respective influence of temperature and electric field, is needed to further the understanding of the Nottingham Effect.

CONCLUSIONS

The results presented in this paper provide conclusive evidence for an energy exchange that accompanies field electron emission and which is localized to an area not appreciably greater than the emitting area of the cathode. Energy exchanges which lead to both heating and cooling of the emitter have been predicted and observed over a wide range of temperature, work function and applied field strength. The gross trends in the variation of the energy exchange and the inversion temperature with field, temperature, and work function can be described by free-electron theory based on bulk conduction at the Fermi level. However, detailed quantitative agreement

the replacement electrons is equal to the Fermi energy.

Investigations of the magneto-resistance[26,27] and surface conductance[28] of tungsten have provided evidence that electrical conduction in tungsten involves nearly equal numbers of positive and negative charged carriers. If the holes of a nearly filled d-band take part in the conduction, one may expect, according to the discussion following Equation (18), a negative value of $d\langle E' \rangle/dT$. Furthermore, if the hole band possesses a low degeneracy temperature T_d, the contribution to Equation (18) of the neglected higher order terms becomes significant as $T \rightarrow T_d$; a conduction mechanism of this nature, which causes $\langle E' \rangle$ to decrease with increasing temperature, can readily account for the unusually low observed inversion temperatures.

A variation of $\langle E' \rangle$ with temperature should result in a uniform displacement of the experimental curves of $\epsilon_N(F)$, at various temperatures, from their theoretical values. As shown in Figure 13, this is confirmed for the 297°K results, but the direction of the shift requires a positive $\langle E' \rangle - E_f$. In contrast, the higher temperature results of both Figures 13 and 14 exhibit a deviation from theory which requires a value of $\langle E' \rangle - E_f$ whose magnitude and sign varies with field.

Curves (b) and (c) of Figure 6 show the required variation in $\langle E' \rangle - E_f$ necessary to account for the discrepancy between the experimental and theoretical results of Figure 13 at F = 6.0 and 5.0×10^7 V/cm respectively. Although the magnitudes of the calculated curves (b) and (c) of Figure 6 are in wide disagreement with curve (a) (based on the thermoelectric data), it

does Equation (11) adequately describe the total energy distribution over the temperature and field range investigated? We recall that Equation (11) is valid for both a free-electron model and a nonfree-electron model provided the band structure term is negligible, i.e., $E_m/d >> 1$. Measurements of the total energy distribution performed in the temperature range 77-300°K on tungsten have generally supported Equation (11) and therefore, the contemporary field emission theory upon which Equations (11) and (15) are based. In order to obtain a completely rigorous check of the applicability of Equation (11) to tungsten, it is necessary to measure the total energy distribution over a wider range of temperatures and for emission through a variety of crystal planes. These measurements, reported in preliminary fashion[16], generally confirm the validity of Equation (11) and yield the predicted symmetrical energy distribution at p = 0.5, with two exceptions: the first is a markedly different shape of the energy distribution for electrons emitted along the <100> direction[16] which suggests that some refinements are necessary in the basic model upon which field emission theory is based; the second is a distribution agreeing in shape but appreciably wider than predicted for emission in the <110> direction[25].

Although measurements of the total energy distribution are not a stringent test of the free-electron nature of bulk conduction of electrons, they do provide sufficient evidence that the anomalies in the Nottingham Effect cannot be attributed entirely to discrepancies in the energy distribution of the emitted electrons. This suggests an examination of the second basic premise of the Nottingham Effect, namely that the average energy of

experimental values of ϵ_N given in Figure 13 for clean tungsten at 297°K are larger than theory, while at higher temperatures the experimental values of ϵ_N are considerably less than expected from theory particularly at low values of F. Hence, at a fixed field ϵ_N decreases with emitter temperature much more rapidly than predicted by theory, particularly at low values of F.

Similarly, the experimental values of ϵ_N for the zirconium-oxygen coated tungsten results given in Figure 14 show reasonable agreement with theory for the 297°K results, while the results above 556°K show deviations from theory similar to those noted for the clean tungsten results. No attempt was made to calculate ϵ_N at the higher emitter temperatures (experimental curves c, d, and e) since the corresponding values of p exceed 0.7 and, therefore, the theory becomes seriously inaccurate. The accuracy and precision of the experimental data above 840°K, while not easily specified, is somewhat less than that of the lower temperature data because of the occurence of some thermal-field induced rearrangement of the adsorbate. Nevertheless, both the clean tungsten and zirconium-oxygen coated tungsten results provide clear evidence of a significant departure of the Nottingham Effect from the theory based on the assumption $\langle E' \rangle \cong E_f$. As discussed in a previous section, the two most likely sources of possible experimental errors are in a direction to diminish the cooling effect and hence, to further increase the observed discrepancy between experiment and theoretical expectations.

In an attempt to explain the observed anomalies in the Nottingham Effect, one is led to examine the two basic premises of the theory. First,

zirconium-oxygen coated tungsten. Unfortunately, experimental inversion temperatures for a specified surface can only be obtained over a moderate range of emitted currents I_e, hence over a small range of fields F since I_e is an exponential function of F. The experimental and calculated values of the inversion temperature are compared in Figure 12 for the clean and low work function zirconium-oxygen coated tungsten surfaces. In both cases the experimental inversion temperatures vary linearly with field, but are substantially below the predictions of Equation (12). For example, at $F = 4.6 \times 10^7$ V/cm the experimental value of T^* for clean tungsten is 550°K as compared to the predicted value of 1165°K. Similarly, for the low work function zirconium-oxygen coated surface at $F = 2.4 \times 10^7$ V/cm the experimental value of T^* is 475°K as compared to the predicted value of 775°K. An earlier study of the Nottingham Effect by Drechsler [12] also reveals an anomalously low value of T^* for tungsten.

The above mention discrepancies are significant since emission cooling of tungsten field emitters appears to occur at lower temperatures and to be much more important than predicted by the Sommerfeld model. This is further illustrated by the second method of comparing the experimental results with theory, as shown in Figures 13 and 14 where the average energy exchange per electron ($\epsilon_N = H/I_e$), as obtained experimentally and also theoretically from Equation (15), are plotted as a function of F. The values of F are obtained from the I_e - V characteristics plotted according to Equation (10) in the form $\log I_e/V^2$ vs $1/V$; the slope of the latter plot yields the average value of $\beta = F/V$ provided a value for ϕ is assumed. The

cooling to heating occurs at a current which increases with emitter temperature. The results of Figure 10 are in qualitative agreement with these predictions of Equations (12) and (28).

Effect of adsorbed layers. - Similar results are given in Figure 11 for a low work function surface consisting of a tungsten emitter coated with coadsorbed zirconium-oxygen. The extreme stability of zirconium-oxygen coatings with respect to surface migration and thermal desorption makes such coatings uniquely suited for the investigation of the Nottingham Effect over a wide range of emitter temperatures. It is observed that emission cooling, i.e., $T < T^*$, occurs throughout most of the experimental temperature range except for temperatures below $550^{\circ}K$.

The wider occurence of emission cooling is due to the lowering of the surface work function since, in view of Equation (26), the inversion temperature is proportional to work function. Thus, at a given emitted current emission cooling will begin at a lower emitter temperature and will be larger at a given temperature; conversely, greater currents can be drawn before the emitter temperature becomes excessive due to Joule heating.

COMPARISON WITH THEORY

The experimental results can be compared quantitatively with theory in two ways. First, the inversion temperatures given theoretically by Equation (12) can be compared with those obtained experimentally for clean and

Three general observations can be obtained from the data given in Figure 10:

(1) H increases nearly linearly with I_e at low temperatures;

(2) It appears that the amount of heating at a specified I_e decreases with increasing temperature;

(3) The Nottingham inversion (i.e., H = 0) occurs at increasingly higher values of I_e (or F) as the emitter temperature increases.

The first two observations are in qualitative agreement with the predictions of Equation (23) since the Joule heating term is negligibly small in the present experiments. Recalling that the inversion temperature T^* corresponds to p = 1/2, it follows that $p = \frac{T}{2T^*}$ and Equation (23) can be rewritten (neglecting the Joule heating term):

$$H \cong H_N = \pi k T I_e \cot(\pi T/2T^*). \tag{28}$$

At low temperatures or large electric fields the term $\cot(\pi T/2T^*)$ is insensitive to F, thereby causing H to vary in a near linear fashion with I_e; also, as T increases the $T \cot(\pi T/2T^*)$ term decreases, thereby causing H to decrease. As T approaches T^*, H is no longer proportional to I_e, but instead depends more sensitively on the variation of T^* with F and, hence, I_e. When the condition $T = T^*$ is attained, then H = 0. At higher temperatures Nottingham cooling is observed at low currents. However, as the emitted current is increased (at fixed emitter temperature) T^* increases according to Equation (12) and the transition from Nottingham

observed to decrease rapidly as a result of erosion of the adsorbed coating by impinging ions.

Clean tungsten results.- Figure 10 shows the measured power exchange H at a clean tungsten emitter as a function of I_e for various temperatures. The data were reproducible to within $\pm$ 5%. Similar data, taken from another tube whose emitter was blunter, were not as reproducible and gave values of H approximately 25% larger because of the larger power dissipation within the tube; however, the data confirmed the functional trends shown in Figure 10. The field electron pattern and I_e - V characteristic were checked throughout the run to insure that contamination or geometrical rearrangement of the emitter surface remained at a negligible level.

The corrections to the emitter temperature due to the emission heating (or cooling) were small even at the highest value of I_e and could be neglected. This can be shown by rewriting Equation (24) as follows:

$$T_o - T_1 = \frac{1}{K \pi \alpha r} \left[H - \frac{H_r}{2} \right]. \qquad (27)$$

For a typical emitter where $r = 1.3 \times 10^{-5}$ cm and $\alpha = 0.157$ radians, Equation (22) gives $H_r = 1.4\mu W$ at $T = 1000^{\circ}K$ and $I_e = 600\ \mu A$. Thus, throughout the range of I_e and T investigated, H_r can be neglected. At the highest value of H investigated, e.g., $H = 160\ \mu W$ at $T = 297^{\circ}K$, Equation (27) gives a value of $6^{\circ}K$ for $T_o - T_1$, using the previously mentioned values of r and α; the maximum correction to T is therefore 2% and can be neglected, since it is comparable with the accuracy of the temperature measurement.

field emission current, the beam voltage and power are roughly proportional to the tip radius. To minimize heating of the collector plates B of Figure 2, measurements of ΔR at a given I_e were taken as rapidly as possible. This problem was not as serious for the low work function surfaces where field emission voltages and, hence, maximum power dissipation required for a given I_e were reduced by the ratio of the work function change to the 3/2 power.

Another important experimental problem was the impingement on the emitter support structure of high energy ions formed at the anode. Relatively few ions can cause serious errors in the power input since the ions carry energies of hundreds to thousands of eV, as opposed to a fraction of one eV for the emitted electrons. Such ions can only be formed by electron induced desorption processes, since temperature changes at the anode were not sufficient to cause thermal desorption of contaminants, and the tube vacuum was sufficiently good to minimize formation of ions from the residual gas. Recent investigations[24] of electron induced desorption suggest that the number of ions formed per electron, particularly at voltages in excess of a few hundred volts, is less than 10^{-7} ions/electron; thus, an electron current of 500 μA at 4 kV should correspond to an ion power input of less than 0.2 μW, which is below the sensitivity of the measurements. It is interesting to note that an ion current as low as 10^{-13} amperes, though it produces negligible input power, can produce readily detected effects on the emitter surface. This was observed in the case of zirconium-oxygen coated tungsten emitters where the field electron current at high I_e was

(2) Adsorbates which are thermally desorbed by emission heating provide evidence that the energy exchanges are strongly localized to an area not much greater than the emitting area;

(3) Peak tip temperature estimates derived from the observed adsorbate removal cannot be accounted for by resistive heating alone and are in reasonable agreement with the much larger values predicted by the Nottingham Effect theory.

Direct Measurement of the Energy Exchange

Emission heating and cooling results were obtained on clean and zirconium-oxygen coated tungsten cathodes by emitting a specified field electron current and measuring the change in filament resistance ΔR which could, using the conversion factors given in Figure 3, then be converted to a power exchange H at the emitter. The upper limit of emitter temperature at which such measurements could be performed was determined by the onset of field-temperature induced deformation of the emitter tip in the case of uncoated emitters and by rearrangement of adsorbed layers in the case of zirconium-oxygen coated emitters.

Since the measured power exchanges range from 0 to 150 microwatts, it is important that the field emitted electron beam power dissipated in the tube be as small as possible in order to eliminate ambient temperature variations. Sharp emitter tips are therefore advantageous since, at a given

Using prior measurements of the temperature required to desorb cesium to various residual coverages the peak emitter tip temperature at the end of each pulse could be estimated by methods described in an earlier section. This experimentally determined temperature rise could then be compared with the temperature change due to both resistive ΔT_r and Nottingham heating ΔT_N, calculated according to Equation (24). The comparison is illustrated in Table I at three different levels of emitted current. In each case the resistive heating contributes less than 6% to the total ΔT, illustrating

TABLE I

Tip temperature due to emission heating as inferred from cesium coverage change

I_e(mA)	ϕ(eV)	ΔT_r(^oK)	$\Delta T_r + \Delta T_N$(^oK)	ΔT(obs) (^oK)
43	1.58	18	368	338
48	1.68	26	438	347
36	2.16	12	505	743

the dominant role of Nottingham heating at low temperatures. The agreement between experiment and theory is considered satisfactory in view of the problems involved in evaluating ΔT (obs).

The investigation of the behavior of various adsorbates at very high pulsed currents has therefore established the following:

(1) Strongly bound low work function adsorbates (e.g., zirconium-oxygen on tungsten) allow larger current densities of emitted current than the corresponding clean substrates because of the enhanced emission cooling associated with reduced work function;

the pattern shows that barium was removed only from the very tip of the emitter, indicating that emission heating is highly localized. From an estimate of the work function in the interior of Pattern 8(b) and knowledge of the decrease in field with increasing angle from the emitter apex, one can estimate that barium was removed back from the apex an angular distance of $\sim 120^{\circ}$, which is only about twice the angular distance of the electron emitting area in Pattern 8(a).

Further evidence of the extreme localization of the Nottingham heating was obtained from a similar experiment using a cesium layer. Figure 9(a) shows a tungsten emitter with a cesium coverage in excess of a monolayer; Figure 9(b) is the same surface after subjecting the emitter to a peak pulse current of 53 mA for 300 sec. The cesium coverage was reduced to approximately 0.5 monolayer coverage by thermal desorption. In contrast to the barium on tungsten sequence, no bright ring of emission was observed because of the heavier cesium coverage and lower binding energy of cesium, which caused cesium evaporation to extend further down the emitter shank. However, on heating to a temperature sufficient to cause mobility of the adsorbed cesium, a sharp boundary migrated across the tip (see Figure 9(c) indicating migration of the cesium from the heavily covered emitter shank to the depleted emitter tip. It could be estimated from the time and temperature required for the boundary to appear that the low coverage cesium region extended less than a few tenths of a tip radii beyond the field of view, in general agreement with the barium results.

These observations are consistent with the foregoing theory of the Nottingham Effect. Equation (10) shows that a constant current density J requires

$$\frac{\phi^{3/2}}{F} \cong \text{const.} = C. \tag{25}$$

Combining Equations (25) and (12) gives the following expression for the inversion temperature at a constant J:

$$T^* \cong \frac{5.67 \times 10^{-5}\, \phi}{t(y)\, C}, \tag{26}$$

for ϕ in eV. Thus, a lower T^* (or larger cooling effect) is obtained at a constant J as ϕ decreases, the inversion temperature being roughly proportional to work function. Alternatively, for a given allowed tip temperature a larger J can be obtained as ϕ decreases.

From the behavior of other adsorbates a qualitative estimate of the magnitude and location of the heating effects was obtained. Figure 8(a) shows the pulse field electron pattern of a tungsten emitter with near monolayer coverage of barium sufficient to cause a lowering of the work function from 4.5 to 2.0 eV; Figure 8(b) shows the same pattern after emitting a pulse field electron peak current (duty factor about 10^{-4}) of approximately 80 mA for 300 sec. The pattern shows a large decrease in barium coverage at the tip, to only a few tenths monolayer, due to emission induced heating and consequent evaporation of barium. However, the bright ring surrounding

RESULTS

Temperature Sensitive Coatings

As mentioned previously, the observed temperature stability of field emitters at high current density levels, where Joule heating by itself should cause strong instability, provided initial evidence of the Nottingham Effect. It was subsequently observed that strongly bound adsorbed layers on tungsten, such as zirconium-oxygen layers, which lowered the work function, also reduced the emitter temperature and allowed even greater emitted current densities before the onset of excessive tip heating. In one experiment illustrated in the photos of Figure 7 a peak pulse current (duty factor approximately 10^{-4}) of 57 mA was obtained from a clean $\langle 110 \rangle$ oriented tungsten emitter before the onset of instabilities due to Joule heating. This current caused sufficient heating to activate diffusion phenomena, producing slip planes and roughening of the tungsten surface. After annealing the emitter to restore a smooth surface and applying a zirconium coating to the emitter a pulse emission current of greater than 102 mA was obtained. This results from the increased emission cooling characteristics of the lower work function (ϕ = 2.8 eV) surface. Thus, the tip temperature was substantially less than for the clean emitter at half the current. As shown in Figure 7(c), the lowering of the work function due to zirconium adsorption occurs selectively in the $\{100\}$ regions, while the remaining surface exhibits nearly clean tungsten characteristics and the emitted current density in the zirconium-coated regions of pattern 7(c) is approximately 4 times that of the clean tungsten surface in pattern 7(b).

where $\rho(T)$ is the bulk resistivity at the temperature T. The complete expression for H obtained from Equations (15), (21) and (22) is

$$H = \pi k T I_e \cot \pi p + \frac{\rho(T) I_e^2}{\pi a r} . \qquad (23)$$

An analytical expression for the temperature T_o at the emitter apex compared to the temperature T_1 at the emitter base (assumed fixed) can be obtained[8] for a truncated conical shaped emitter of radius r_o at the point of truncation; neglecting radiation losses and assuming $r_o = r$ the expression takes the form:

$$T_o - T_1 = \frac{kT \cot \pi p}{K} \left(\frac{I_e}{ar}\right) + \frac{\rho(T)}{2K\pi^2}\left(\frac{I_e}{ar}\right)^2 , \qquad (24)$$

where K is the thermal conductivity. The first term in Equation (24) is due to the Nottingham Effect whereas the second term is caused by Joule heating. It has been found by Houston[23] that approximately the same value of T_o is obtained for a conical emitter if one considers the variable resistivity at various points or if one uses for simplicity a constant value of $\rho(T)$ corresponding to an "effective" temperature $T = 0.8T_o$, i.e., $\rho(T) = \rho(0.8T_o)$. The neglect of radiation losses means the emitter tip is slightly cooler than that calculated by Equation (24), but in the case of emitter sizes utilized in this study the radiative correction to the tip temperature is less than 0.5% at 1000°K and therefore can be neglected.

expected to occur within a fraction of an emitter tip diameter (approximately 10^{-5} cm) in view of the extremely short mean free path of conduction electrons near the Fermi energy with respect to electron-phonon and electron-electron interactions. The details of the energy exchange between those electrons taking part in the conduction current and those taking part in the emission current is a matter which requires further theoretical studies; its calculation is obviously more complex for nonfree-electron metals where the functional dependence of $\langle E' \rangle$ on temperature may differ appreciably from a simple free-electron model.

Assuming for the remaining part of this discussion that the Nottingham energy exchange with the lattice is $\epsilon_N = \langle \epsilon \rangle$, i.e., that $\langle E' \rangle = E_f$, then one obtains for the total power input H to the lattice

$$H = \langle \epsilon \rangle I_e + H_r, \tag{21}$$

where I_e is the total emitted current. H_r is the power input due to Joule heating, and positive values of H refer to a net power input to the lattice.

Next, we consider the energy input due to the Joule heating term H_r. An approximate expression for the resistive power exchange for a conical emitter of radius r and cone half-angle α is given by the following expression:

$$H_r \cong \frac{\rho(T) I_e^2}{\pi \alpha r}, \tag{22}$$

principles through Equation (18). This can be accomplished as pointed out by Seitz[21], by expressing $\langle E' \rangle$ in terms of the thermoelectric power S as follows:

$$\langle E' \rangle = E_f - eTS, \tag{19}$$

where

$$S = \int_0^T \frac{\mu}{T} \, dT, \tag{20}$$

and μ is the Thompson coefficient of the metal. The quantity eTS represents the reversible heat carried by the current whose direction of flow, relative to the current flow and temperature gradient, depends on the sign of μ. In keeping with the usual convention a positive μ signifies the evolution of heat as electrons go to places of higher temperature and according to Equation (19), a lowering of the average energy of the charge carriers.

Based on Potter's[22] values of S for tungsten, one finds that $\langle E' \rangle - E_f$ varies with T as shown in curve (a) of Figure 6. On this basis one can expect a small decrease in $\langle E' \rangle - E_f$ with increasing temperature (e.g., 0.015 eV at 900°K).

Emitter Temperature

Both Nottingham and Joule heating must be considered in determining the temperature change produced by the energy exchange processes accompanying field electron emission. In the case of the Nottingham Effect, the energy exchange between the conduction electrons and the lattice is

The final form of the expression to the first order in kT/E_f is

$$\langle E' \rangle \cong E_f + \frac{(\pi kT)^2}{3} \left[\frac{1}{E_f} + \frac{\lambda' (E_f, T)}{\lambda (E_f, T)} \right], \tag{18}$$

where $\lambda' (E_f, T)$ is the value of the first derivative of λ with respect to E at the Fermi level. The function $\lambda (E_f, T)$ is undetermined by the Sommerfeld-Lorentz theory and must be calculated from more detailed quantum mechanical approaches. The direction and magnitude of the variation of $\langle E' \rangle$ with T is ultimately governed by the function $\lambda (E_f, T)$.

Upon examining the expectation regarding the direction of the variation of $\langle E' \rangle$ with T for a more general model, Mott and Jones [20] concluded that $d\langle E' \rangle /dT$ should be positive for metals possessing partially filled bands and negative for those possessing nearly filled bands. They further concluded that transition metals with overlapping s and d bands, in which the main resistance producing factor is s→d transitions, should exhibit a positive $d\langle E' \rangle /dT$ for a nearly filled d band, whereas for a partially filled d band the sign of $d\langle E' \rangle /dT$ will depend on the $E(k)$ and $\lambda(E, T)$ relationships near the top of the Fermi distribution. As expected, both positive and negative $d\langle E' \rangle /dT$ have been measured for the transition metals and, for many, both the magnitude and sign of $d\langle E' \rangle /dT$ vary with temperature.

In view of the limited knowledge of the $E(k)$ and $\lambda(E, T)$ relationships for most transition metals, it is more fruitful to estimate the variation of $\langle E' \rangle$ with T from experimental values of $\langle E' \rangle$ vs T rather than from first

energy. This is not the case since the field emitted electrons carry a substantial average transverse energy and the inversion temperature (no energy exchange) occurs when the average total energy of the emitted electrons is equal to the Fermi energy, the average normal energy being then substantially smaller.

An approximate expression for the average normal energy $\langle \epsilon_n \rangle = \langle E_n \rangle - E_f$ is readily obtained with our model, yielding:

$$\langle \epsilon_n \rangle \cong -d \left[1 + f(p)\right] = -d \left[1 + \pi p \cot \pi p\right]. \tag{16}$$

Brodie's temperature T_n^* corresponds to $\langle \epsilon_n \rangle = 0$; therefore $f(p) = -1$ and $p = 0.65$ in fiew of Figure 5. This can be contrasted with the conditions $f(p) = 0$ and $p = 0.50$ for $\langle \epsilon \rangle = 0$. Since $p = kT/d$ is directly proportional to temperature, it follows that

$$\frac{T_n^*}{T^*} = \frac{0.65}{0.50} = 1.3, \tag{17}$$

which accounts for the difference between Brodie's values and those predicted by Equation (12). Recently corrected computer calculations by Lee and Alpert,[19] yet unpublished, confirm that, when p approaches unity and the approximation for $D(E_x)$ breaks down. Also Equations(12) and (15) are essentially correct and negligible error is made up to $p = 0.7$ by omitting the quadratic and higher order terms in Equation (6) for $D(E_x)$.

Though the average normal and total energy increase with field emitter temperature, comparison of Equations (15) and (16) shows that the

average transverse energy of the field emitted elctrons is equal to d and independent of temperature, at least within the range of validity of the foregoing calculations.

Average Energy of the Conduction Electrons

For a Fermi gas at temperature T, conduction involves only those electron states for which the derivative of the Fermi function $df(E)/dE$ is finite. Since the derivative of the Fermi function is appreciable only in a range of a few kT about E_f, it is clear that conduction is limited to states near the Fermi surface at low temperatures. In our experiments, the values of kT ranged from 0.02 to 0.07 eV, while experimental values of ϵ_N ranged from -0.60 to + 0.30 eV; hence, near the inversion condition ($\epsilon_N = 0$) a variation of $\langle E' \rangle$ by a few hundreths of an eV may cause the inversion temperature to depart significantly from the predicted value based on Nottingham's assumption that $\langle E' \rangle = E_f$. It is therefore instructive to obtain the expression for the average energy of the charge carriers in a conductor possessing a temperature gradient and internal electric field.

An expression for $\langle E' \rangle$ has been given by Mott and Jones [20] for a conductor in which the electron energy E is an arbitrary function of the wave vector k. A slightly different expression for $\langle E' \rangle$ has been derived by Seitz [21] by considering the Sommerfeld-Lorentz solution of the Boltzmann transport equation. In the latter case the interaction of the electrons (viewed as a degenerate Fermi gas) with the lattice is contained in a function $\lambda(E,T)$ representing the mean free path of the conducting electrons.

An analytical expression for $\langle \epsilon \rangle$ can be obtained from Equation (11) by performing the following integration:

$$\langle \epsilon \rangle = \frac{\int_{-\infty}^{\infty} \epsilon\, J(\epsilon)\, d\epsilon}{\int_{-\infty}^{\infty} J(\epsilon)\, d\epsilon} = -df(p). \tag{14}$$

For the cases depicted in Figure 4 the function f(p) is unity for p = 0 and zero for p = 0.5; thus, for field emitted electrons at T = 0, $\langle \epsilon \rangle = -d$ and at $T = T^*$, $\langle \epsilon \rangle = 0$. Levine[10] has shown that $f(p) \tilde{=} \pi p/\tan \pi p$ so that Equation (14) may be written in an alternative form

$$\langle \epsilon \rangle = -\pi p d \cot \pi p. \tag{15}$$

The form of Equation (15) predicts $\langle \epsilon \rangle/d$ to be a function of p only, as shown graphically in Figure 5. In order to obtain simple and useful analytical expressions for $\langle \epsilon \rangle$ and T^* [Equations (12) and (15)], the foregoing derivation uses some customary approximations, particularly the limitation of the tunneling probability $D(E_x)$ to the first two terms of a series expansion [see Equation (6)]. Using computer techniques, this approximation can be avoided and more precise numerical values can be obtained. In a recent computer calculation for tungsten, Brodie[18] reported values approximately 30% higher for the inversion temperature, attributing the difference to the approximation in $D(E_x)$ used to derive Equations (12) and (15) above. Further study shows that Brodie erroneously used the normal energy distribution of the field emitted electrons and obtained a faulty inversion temperature T_n^* by requiring that the average <u>normal</u> energy $\langle E_n \rangle$ be equal to the Fermi

exactly symmetrical distribution of the emitted electrons about E_f, and leads to $\langle \epsilon \rangle = 0$. This condition, p = 1/2, provides a simple expression for the "inversion temperature":

$$T^* = \frac{d}{2k} = \frac{5.67 \times 10^{-5} F}{\phi^{1/2} t(y)} \quad (^oK), \tag{12}$$

If, as suggested in the introductory remarks, the average energy of the conduction carriers is near E_f no net energy exchange occurs at T^*, and the significance of T^* is that is separates emission heating (for $T < T^*$) and cooling (for $T > T^*$).

The integration of Equation (11) over ϵ leads to the well-known expression for the current density J_{TF}:

$$J_{TF} = J_o \int_{-\infty}^{\infty} e^{\epsilon/d} \left[1 + e^{\epsilon/pd}\right]^{-1} \frac{d\epsilon}{d} = J_o \frac{\pi p}{\sin \pi p}, \tag{13}$$

which holds almost exactly in the region $0 \geq p > 0.7$. Using the lower limit of $-\infty$ in place of the correct value of $-E_f$ in order to facilitate integration does not greatly alter the result because of the exponential decrease of $J(\epsilon)$ for $\epsilon < 0$. For small values of p (i.e., low T or high F) $\pi p / \sin \pi p \simeq 1$ and the 0^oK approximation of the Fowler-Nordheim equation $J = J_o$ is obtained as given in Equation (10).

where J_o denotes the total current density (integrated over all energies) at 0°K, which is given by:

$$J_o = \frac{e^3 F^2}{8\pi \phi t^2(y)} e^{-b} = \frac{1.54 \times 10^{-6} F^2}{\phi t^2(y)} e^{-6.83 \times 10^7 \phi^{3/2} v(y)/F} \quad (A/cm^2), \tag{10}$$

and where E_m is the maximum value of $E_\perp$ for a specified energy surface ϵ and polar angle ϕ_p in the yz plane. The specific effect of band structure occurs only through the integral of Equation (9) and can be neglected when $E_m/d \gg 1$. Under normal field electron emission conditions $d \cong 0.15$ to 0.25 eV, and it is reasonable to believe that E_m is sufficiently large, for most degenerate metals exhibiting large Fermi energies, that band structure effects are negligible; however, for transition metals with partially filled narrow d bands, Fermi surface shapes along certain crystallographic directions may be sufficiently small to perturb $J(\epsilon)$ through the band structure term. This possibility and its experimental observation for the case of tungsten are discussed in a recent paper.[16]

Neglecting band structure effects and inserting the Fermi-Dirac distribution $f(\epsilon)$ into Equation (9) gives

$$J(\epsilon) = \frac{J_o}{d} \left[\frac{e^{\epsilon/d}}{1 + e^{\epsilon/pd}} \right], \tag{11}$$

where $p = KT/d$ is a dimensionless parameter. The mathematical derivation of Equation (11) breaks down for $p \geq 1$ and becomes unreliable when p exceeds about 0.7. Equation (11) is identical to the original derivation of $J(\epsilon)$ by Young[17] based on the Sommerfeld free-electron model and is plotted in Figure 4 for $p = 0$ and $p = 0.5$. The latter value of p has an

the emission direction. Assuming specular transmission (i.e., no discontinuity in $E_\perp$ at the emitting surface) the WKB approximation for the transmission coefficient is

$$D(E_x) = e^{-B(E_x)}. \tag{5}$$

Expanding the exponential in a Taylor series about E_f, one obtains $D(E_x)$ in the well known form

$$D(E_x) \cong e^{-b + (E_x - E_f)/d - \cdots\cdots}, \tag{6}$$

where

$$b = \frac{4}{3}\frac{(2m\phi^3)^{1/2}}{\hbar eF}\, v(y) = 6.83 \times 10^7 \phi^{3/2}\, v(y)/F, \tag{7}$$

and

$$d = \frac{\hbar eF}{2(2m\phi)^{1/2} t(y)} = \frac{9.76 \times 10^{-9}}{\phi^{1/2} t(y)}\, F \ (eV), \tag{8}$$

if F is in V/cm and ϕ in eV. The correction terms t(y) and v(y), which are due to the image potential, are tabulated[15] slowly varying functions of the auxiliary variable $y = \sqrt{e^3F}/\phi$. Combining Equations (3) and (6), retaining only the first two terms in the exponential of Equation (6), introducing polar coordinates $E_\perp$ and ϕ_p, and integrating $E_\perp$ from 0 to E_m leads to the following form of the total energy distribution $J(\epsilon)$ of the emitted current density:

$$J(\epsilon) = \frac{J_o\, f(\epsilon)\, e^{\epsilon/d}}{d}\left[1 - \frac{1}{2\pi}\int_0^{2\pi} e^{-E_m/d}\, d\phi_p\right], \tag{9}$$

Average Total Energy of the Emitted Electrons

An expression for the average total energy $\langle \epsilon \rangle$ (relative to the Fermi level, i.e., $\langle \epsilon \rangle = \langle E \rangle - E_f$) of the field emitted electrons can be obtained directly from the expression for the total energy distribution of field emitted electrons. The situation is depicted in Figure 4 which gives a one dimensional potential plot of the surface of a metal (Sommerfeld free-electron model assumed) with work function ϕ and externally applied field F. At $T = 0^{\circ}K$ all electron levels of the metal above the Fermi level E_f are empty and emitted electrons must necessarily originate from below E_f. The total energy distribution depicted in Figure 4 is an exponential curve with maximum at E_f for $T = 0^{\circ}K$, then changes shape and becomes symmetrical about E_f at a certain temperature T^*, which depends on field and work function. $\langle \epsilon \rangle$ is negative below T^* and positive above T^*.

An expression for the current density per unit total energy (relative to E_f) $J(\epsilon)$ was derived recently be Stratton [14] for a degenerate metal of arbitrary band structure. This can be written as

$$J(\epsilon) = \frac{2\, ef(\epsilon)}{h^3} \iint D(E - E_\perp)\, dp_y\, dp_z, \tag{3}$$

where $f(\epsilon)$ is the electron distribution function and

$$E_\perp = (p_y^2 + p_z^2)/2m \tag{4}$$

is the energy transverse to the emission direction.

The integration over the transverse momenta must be carried over all values of p_y and p_z which, for a particular constant energy surface ϵ, are inside the shadow of the energy surface projected on a plane perpendicular to

THEORETICAL CONSIDERATIONS

A theoretical expression for the energy exchange between the field emitted electron current and the lattice is necessary for comparison with experimental results. Although such a calculation, based on a free-electron model, was previously published by Levine,[10] it will be instructive to consider the structure of the calculation in order to delineate clearly the limitations and applicability of the model and the resulting analytical expressions.

We consider first a cathode field emitting electrons with an average electron energy $\langle E \rangle$, which are collected at the anode and subsequently conducted back to the cathode through a conductor at temperature T. Letting $\langle E' \rangle$ be the average energy of the conduction electrons in the emitter, then a net energy exchange of an amount

$$\epsilon N = \langle E \rangle - \langle E' \rangle \qquad (1)$$

is released to the lattice at the cathode. As pointed out originally by Nottingham,[5] for the case $T = 0^{\circ}K$ conduction in the external circuit occurs at the Fermi level (except through the batteries) and

$$\epsilon N = \langle E \rangle - E_f^o, \qquad (2)$$

where E_f^o is the $0^{\circ}K$ Fermi energy. It is convenient to proceed by first deriving the expression for $\langle E \rangle$ in terms of the electric field and surface work function and then examining the variation of $\langle E' \rangle$ with temperature.

was sufficiently low that, at low emission levels, contamination of the emitter surface remained negligible several hours after initial cleaning.

During the investigation of emission heating field electron currents up to 500 μA were drawn from the emitter. In order to minimize contamination of the tip at the maximum current level, a magnetic field was applied in a direction such that the emitted current was collected on the anode plates B of Figure 2, which had previously been well outgassed by electron bombardment during the tube evacuation and could therefore dissipate appreciable power without significant release of contaminants.

Resistivity changes developed across the emitter support filament, due to emitter temperature variations caused by either emission heating or electron bombardment during calibration, were measured by a Keithley Model 660 differential voltmeter which was capable of measuring voltage changes due to ΔR with a precision of approximately 1 part in 5,000. The current passing through the emitter support filament was adjusted to the value necessary to give the required tip temperature (as determined by a previous calibration curve of filament resistance vs temperature) and was also measured by monitoring the voltage drop across a standard 1-ohm resistor through which the filament current flowed.

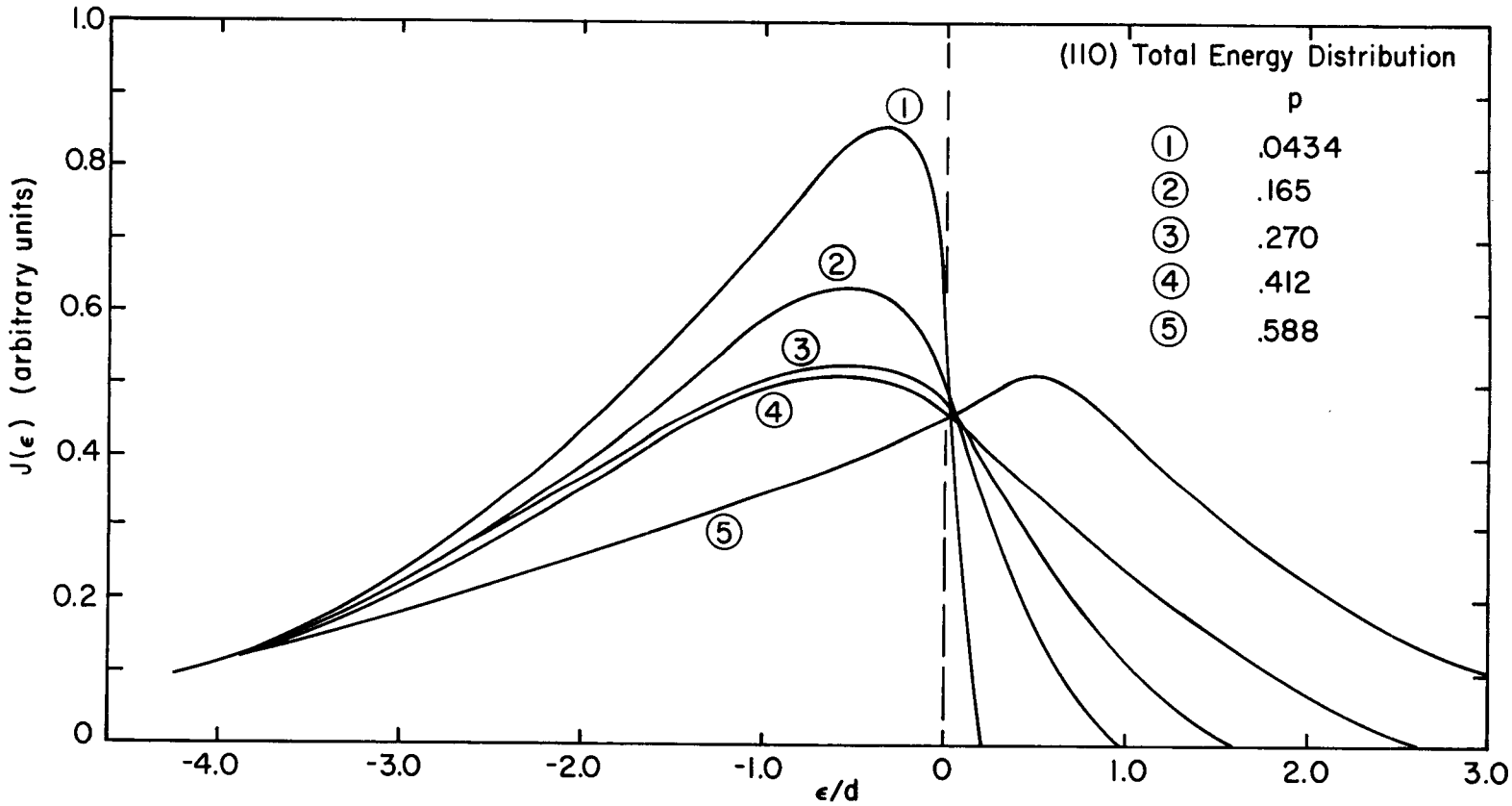

Figure 19. Experimental total energy distribution plots along the <110> direction of a W emitter as a function of p, where d = 0.153 eV and F = 3.70 x 10^7 V/cm.

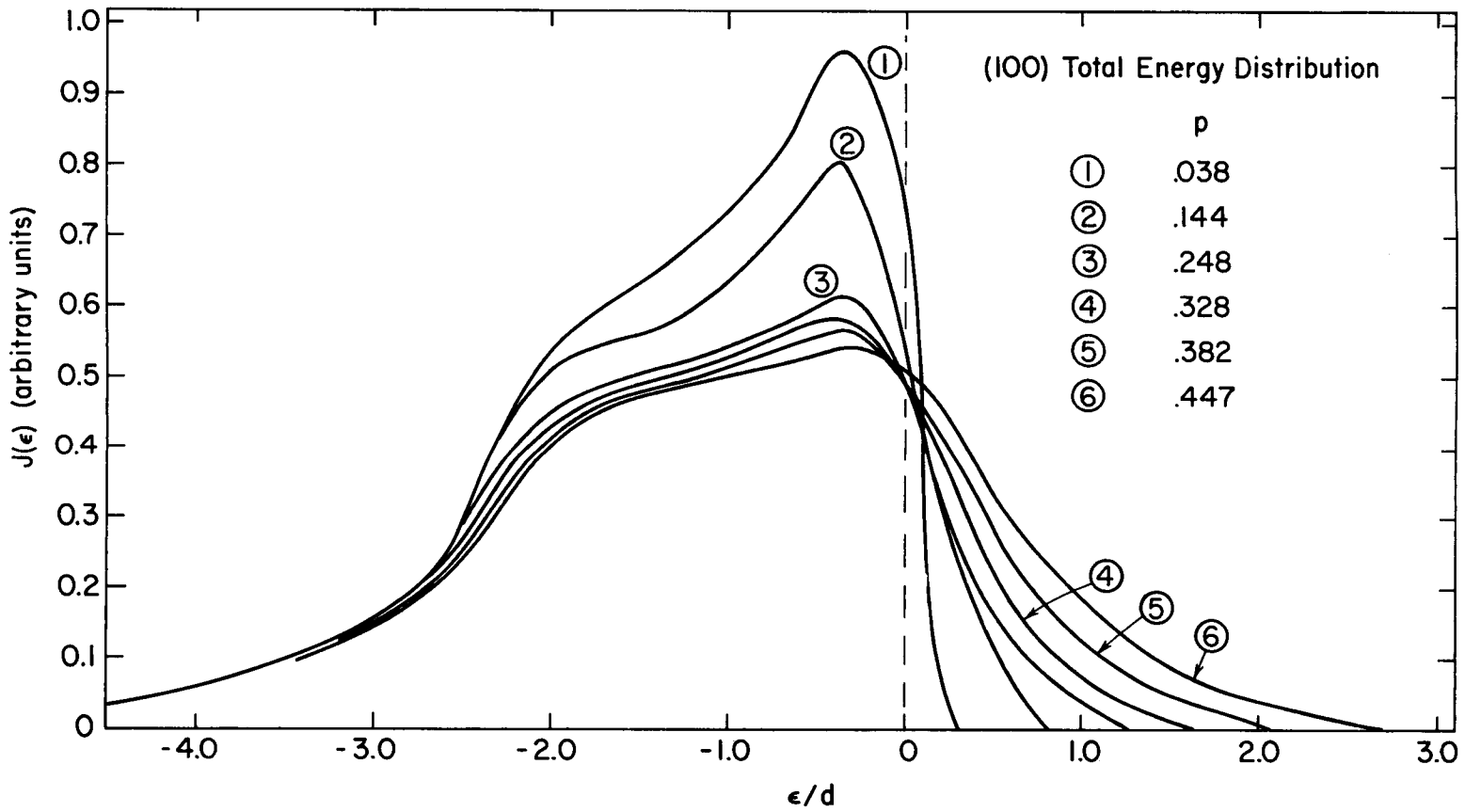

Figure 20. Experimental total energy distribution plots along the ⟨100⟩ direction of a W emitter as a function of p, where d = 0.174 eV and F = 4.08 x 10^7 V/cm.

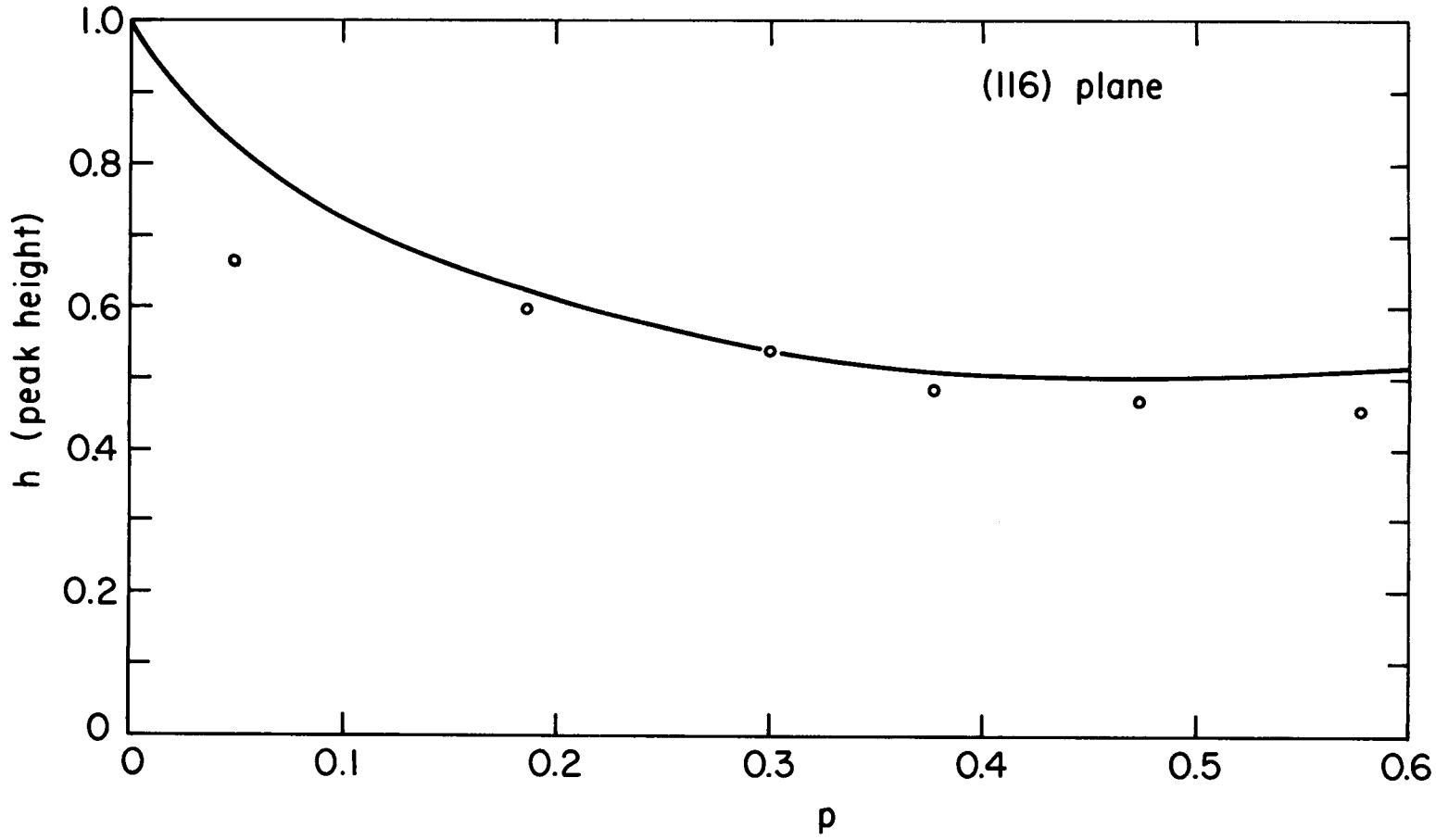

Figure 21. Variation of relative peak height h of the experimental energy distribution curves as a function of p. Solid line based on free electron model [Equation (5)]

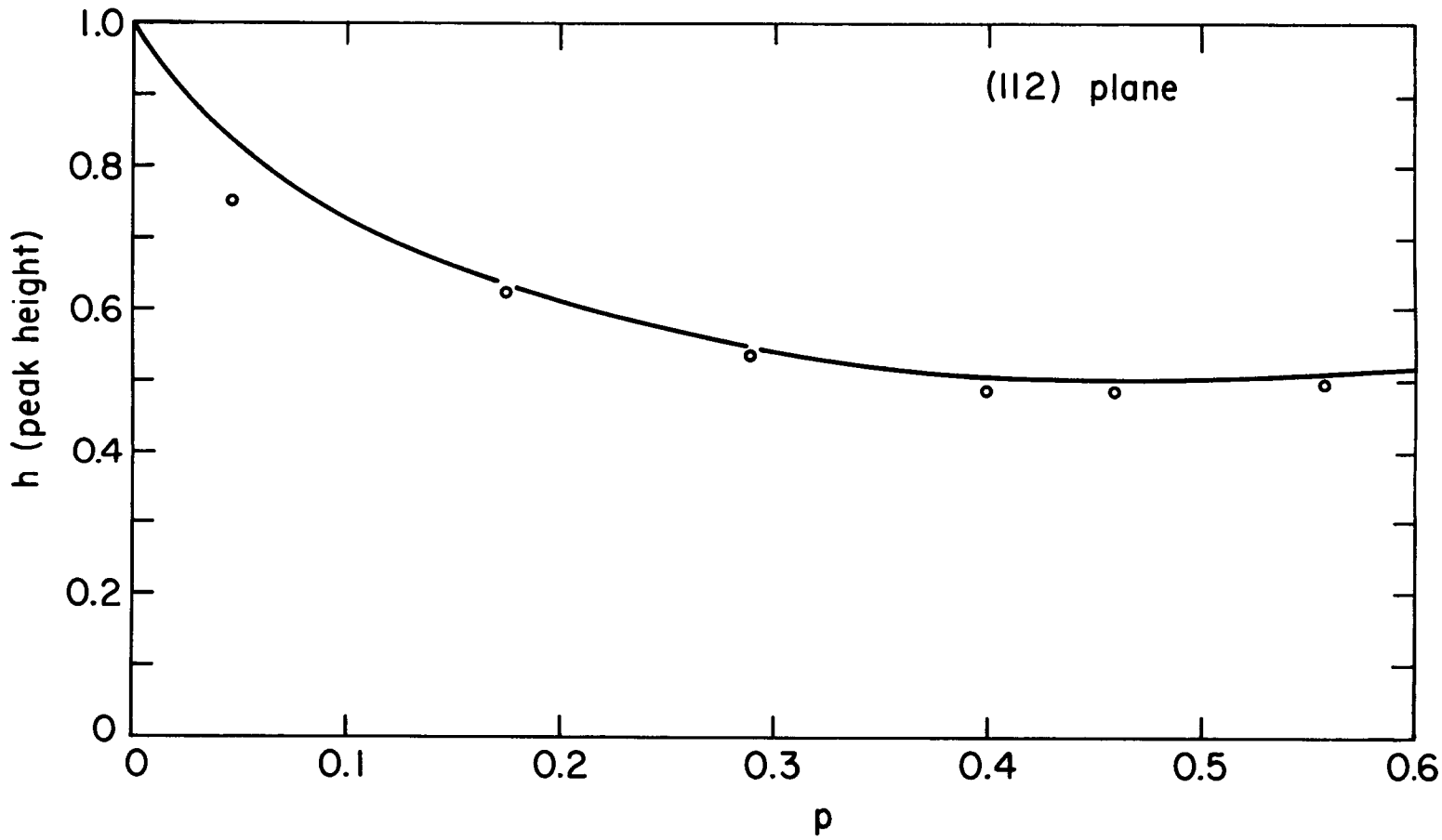

Figure 21. (Cont'd)

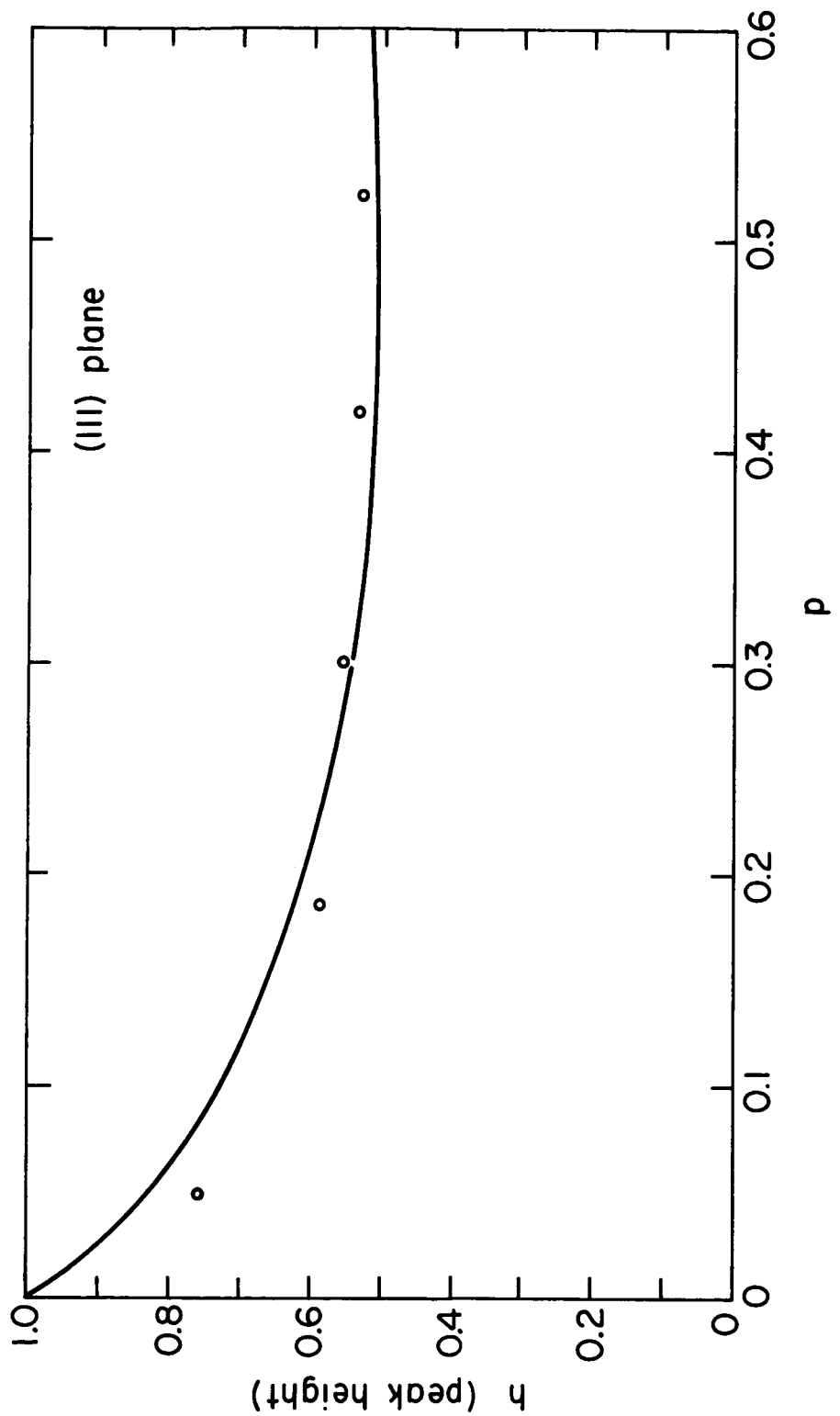

Figure 21. (Cont'd)

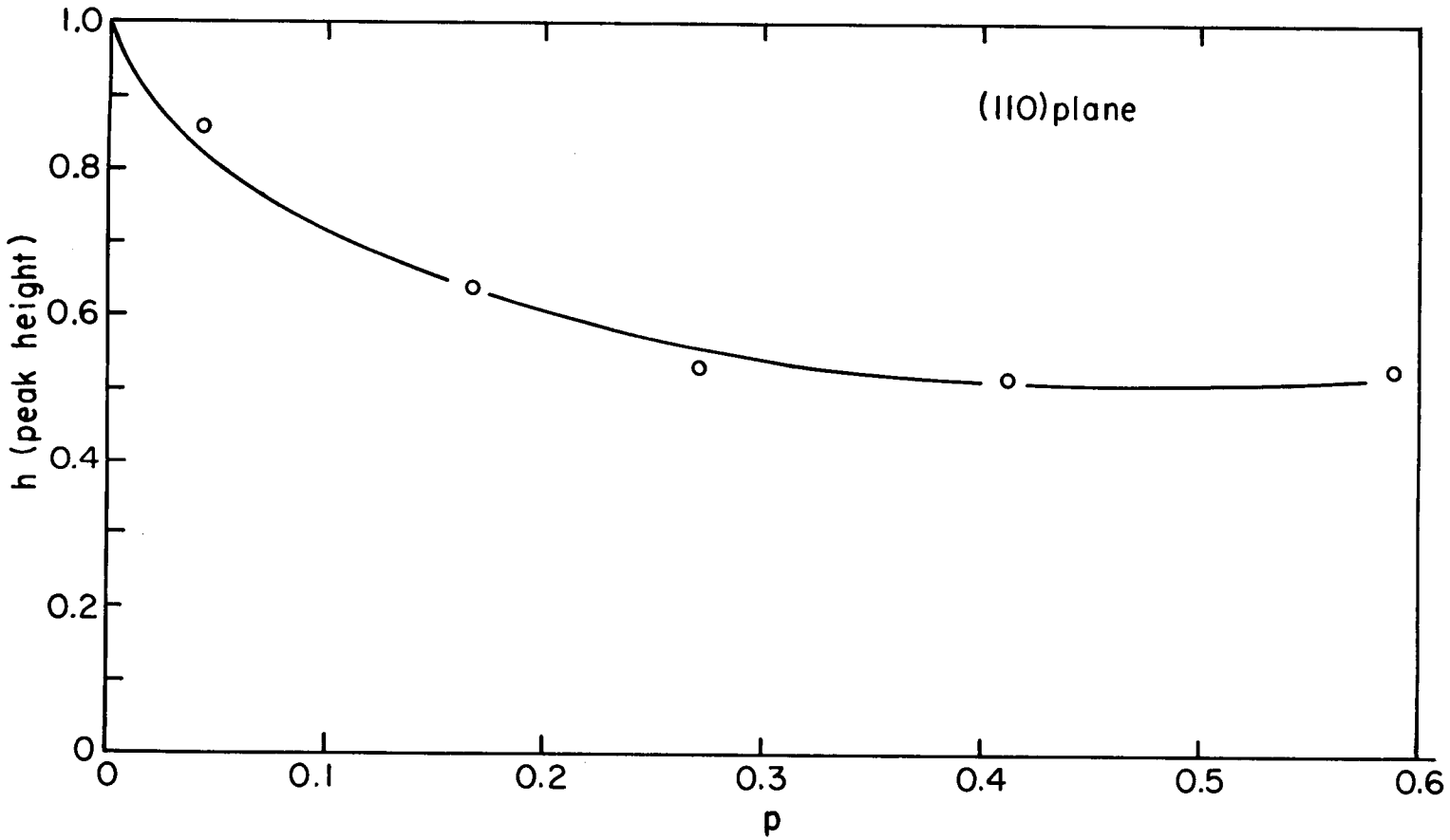

Figure 22. Variation of relative peak height h of the experimental energy distribution curves as a function of p. Solid line based on free electron model [Equation (5)] .

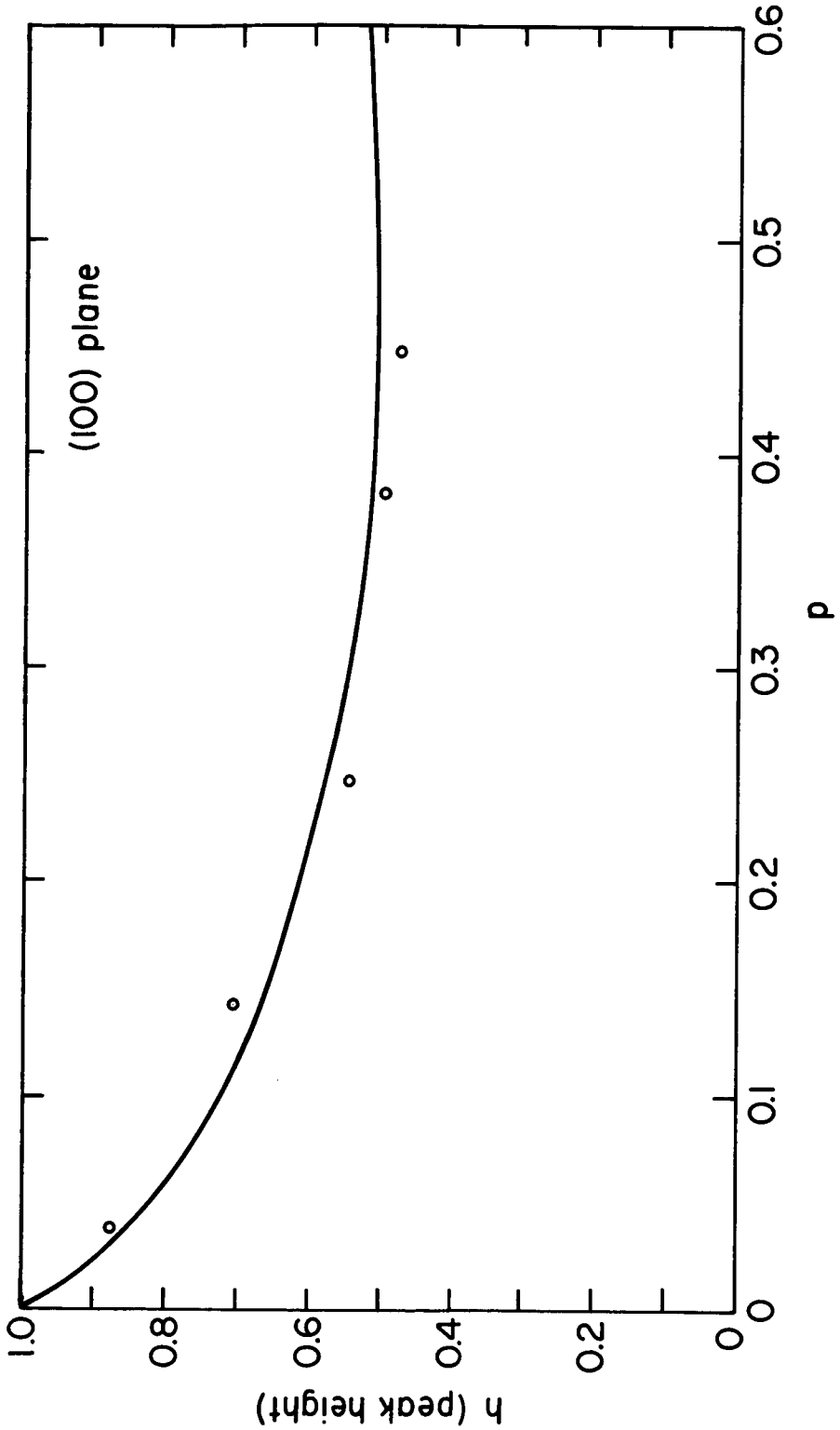

Figure 22. (Cont'd)

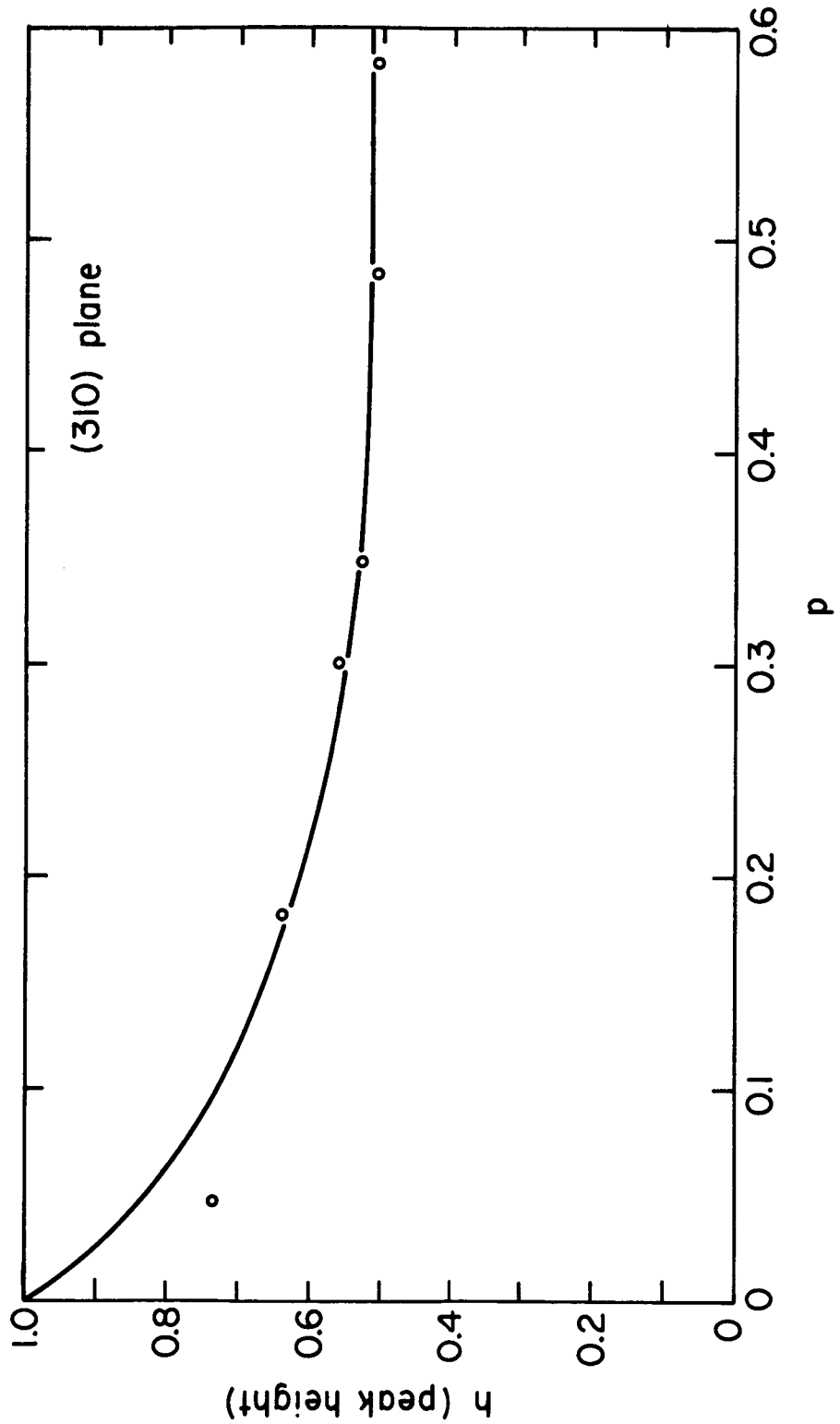

Figure 22. (Cont'd)

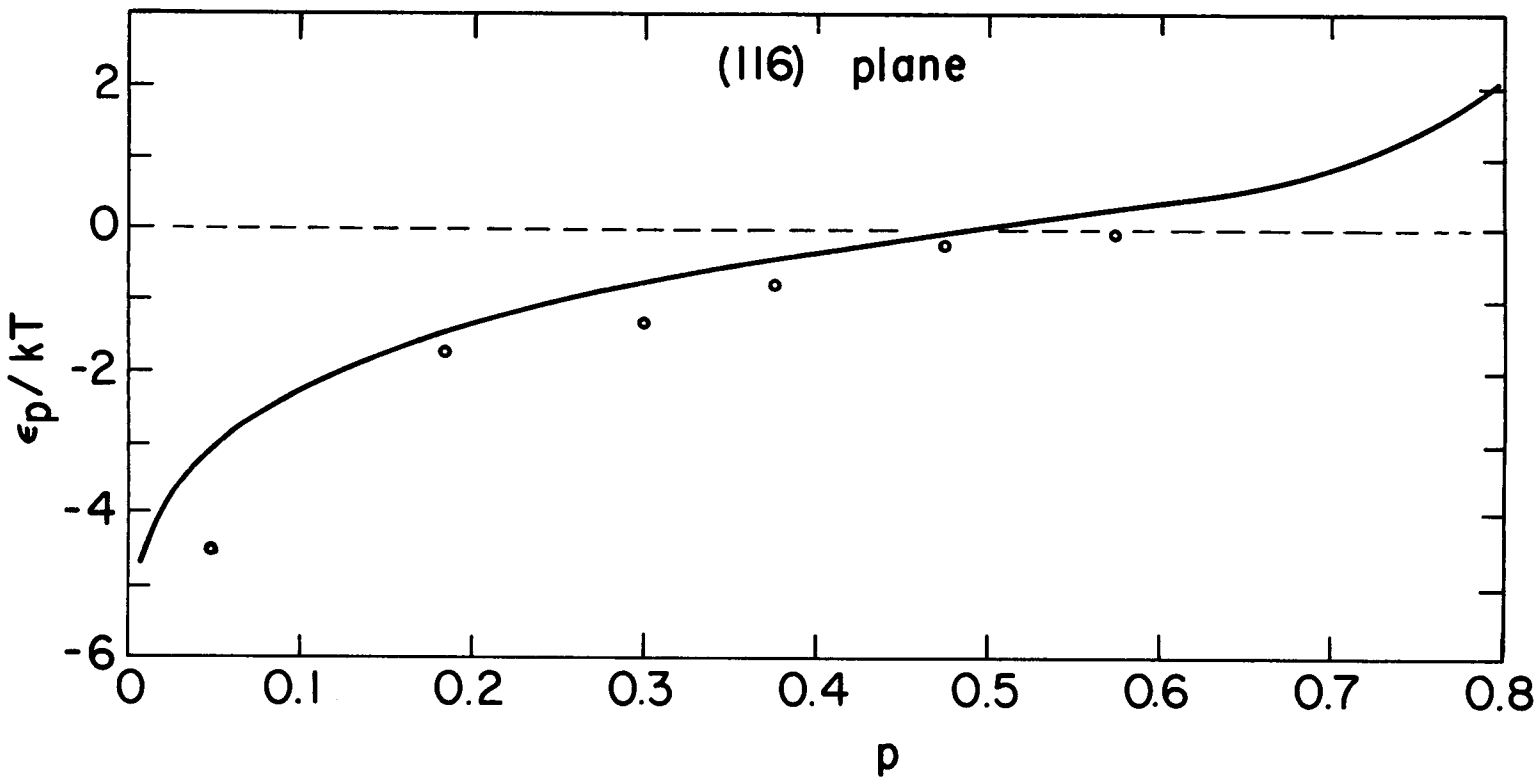

Figure 23. Experimentally observed variation of the position of the energy distribution peak relative to the Fermi level ϵ_p as a function of p. Solid line based on free electron model [Equation (5)].

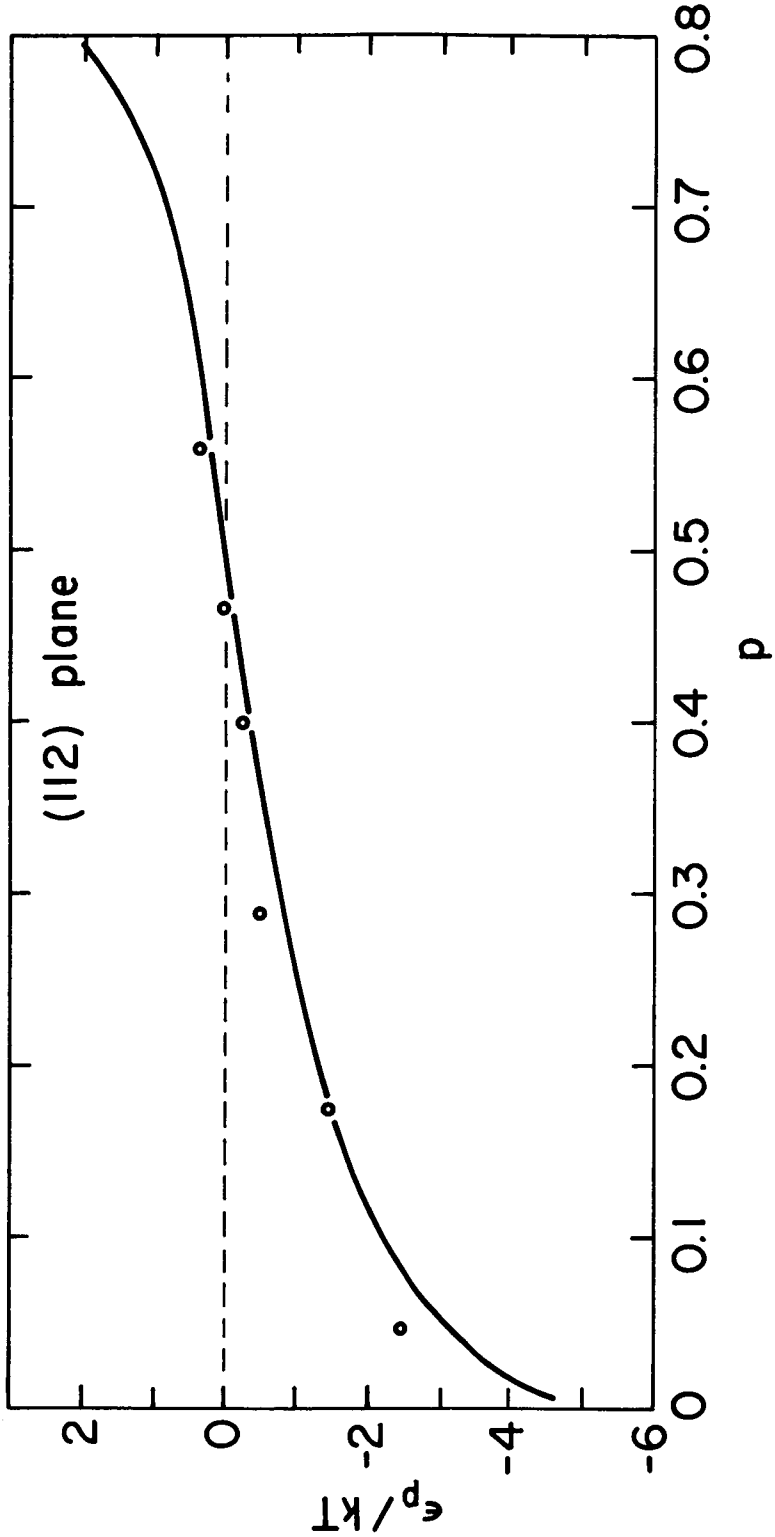

Figure 23. (Cont'd)

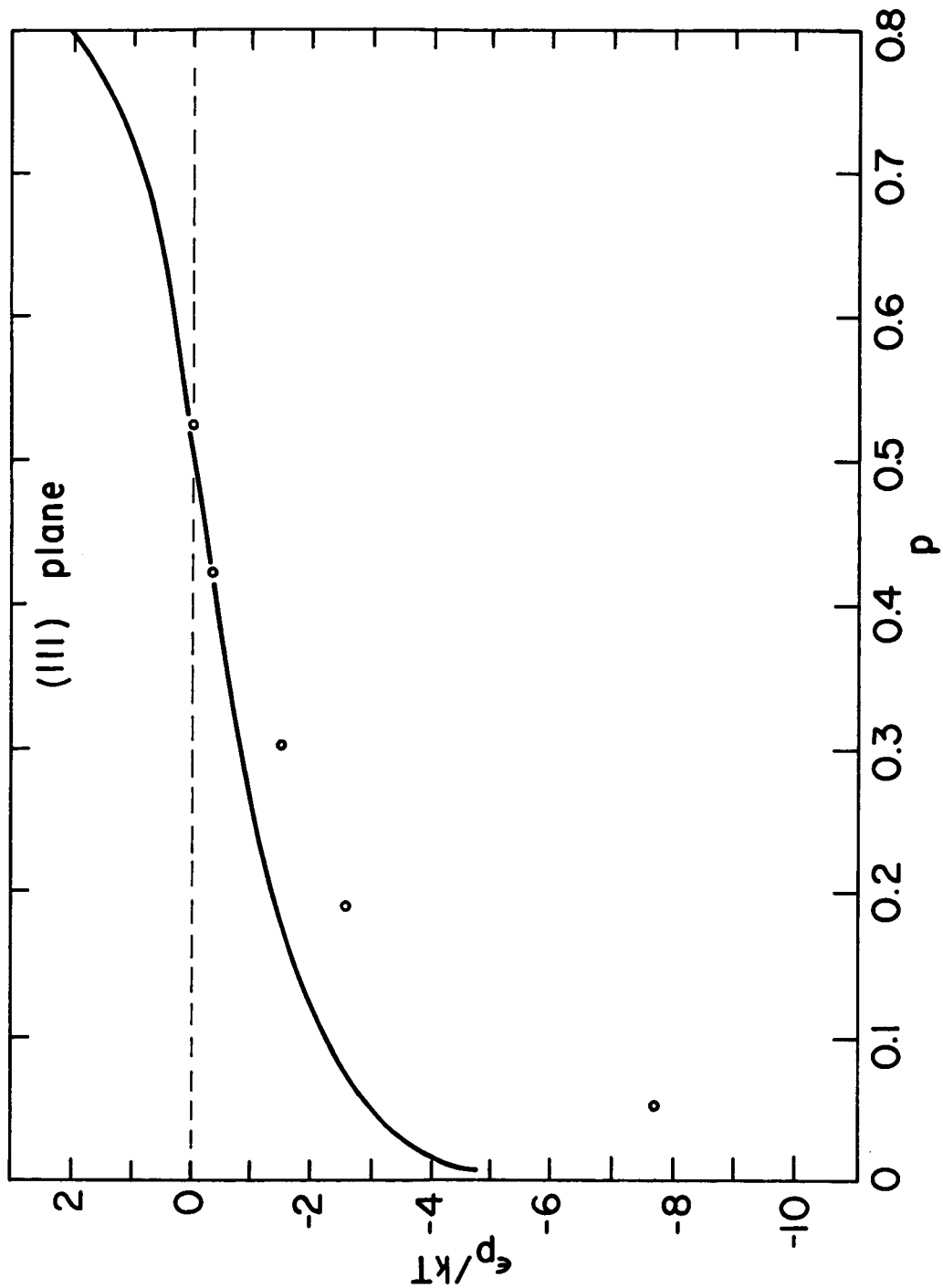

Figure 23. (Cont'd)

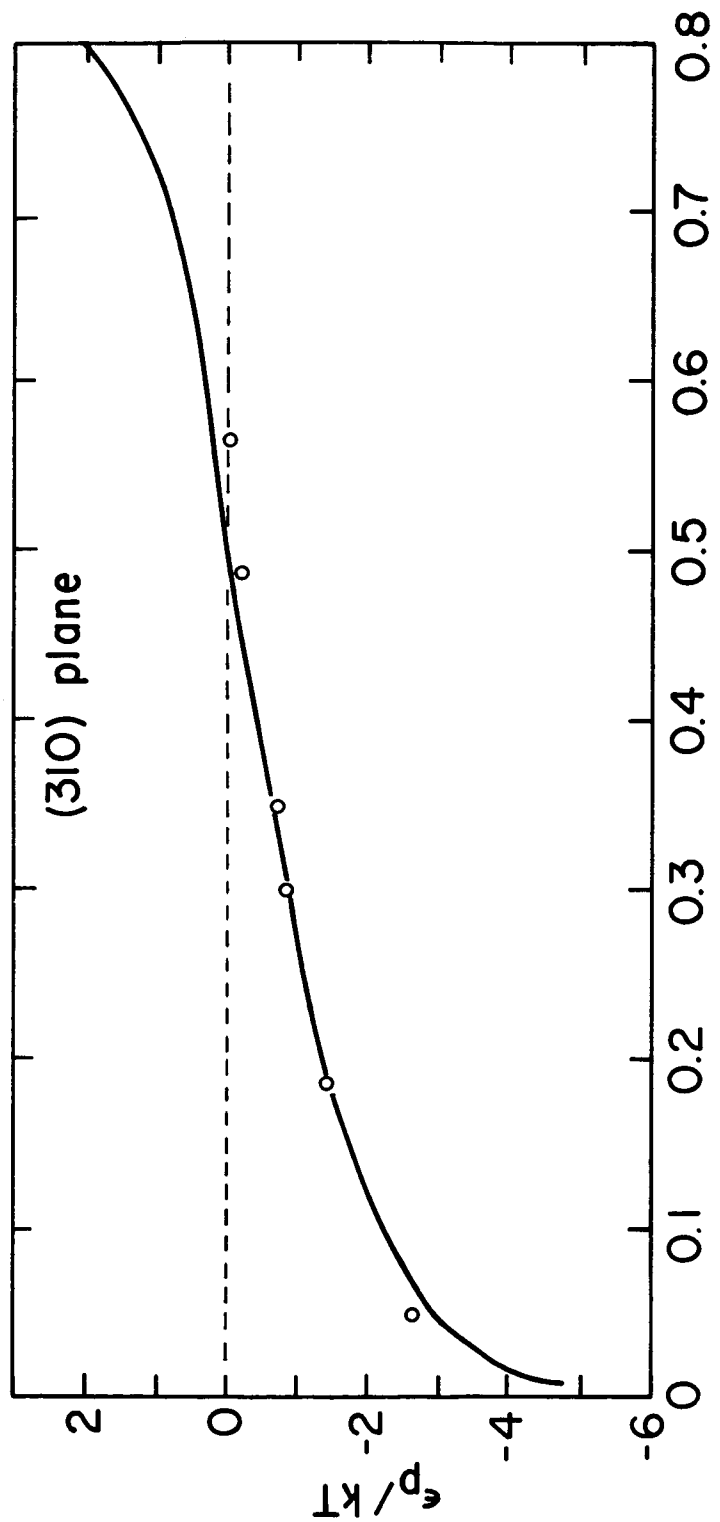

Figure 24. Experimentally observed variation of the position of the energy distribution peak relative to the Fermi level ϵ_p as a function of p. Solid line based on free electron model [Equation (5)].

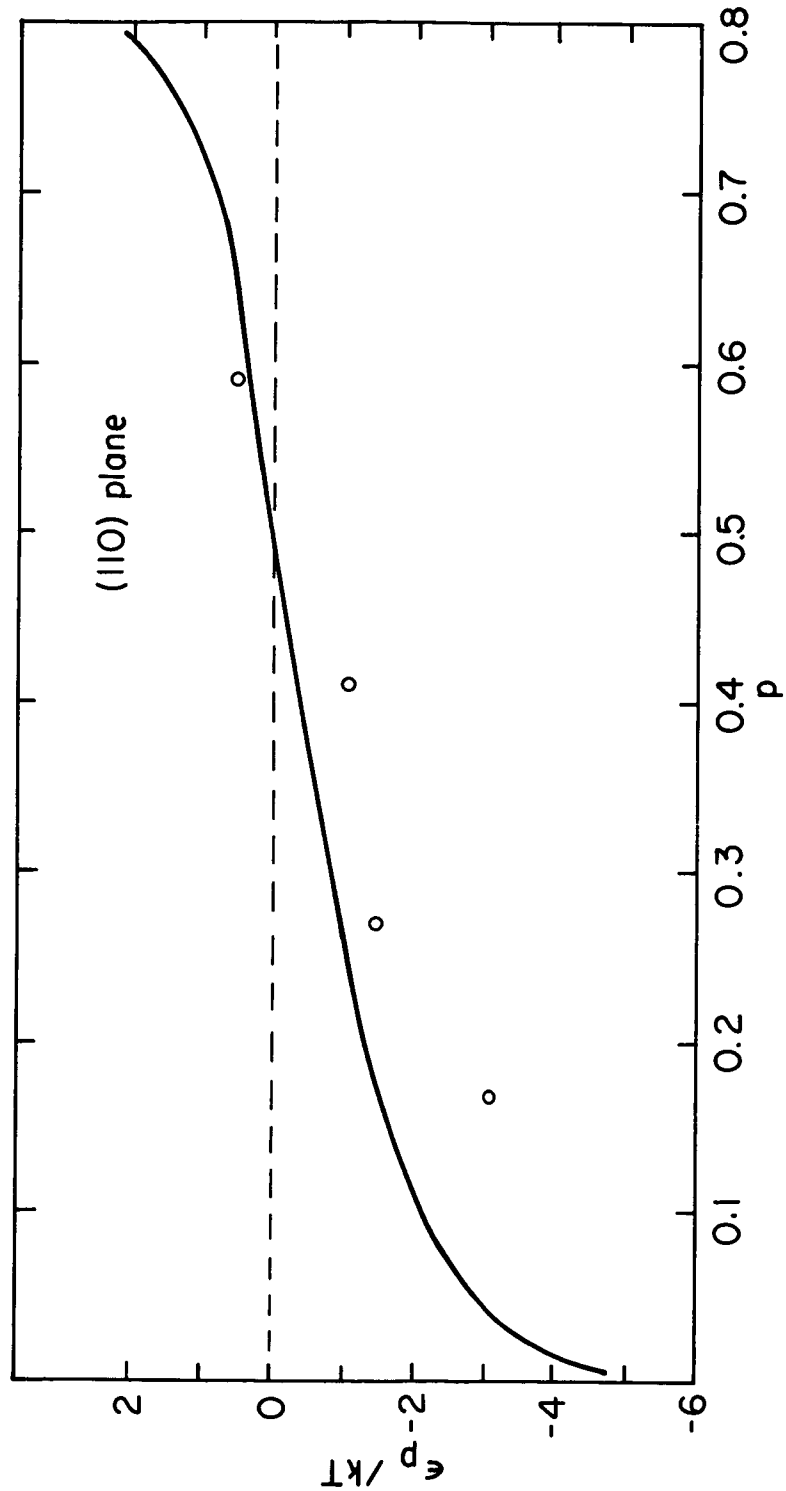

Figure 24. (Cont'd)

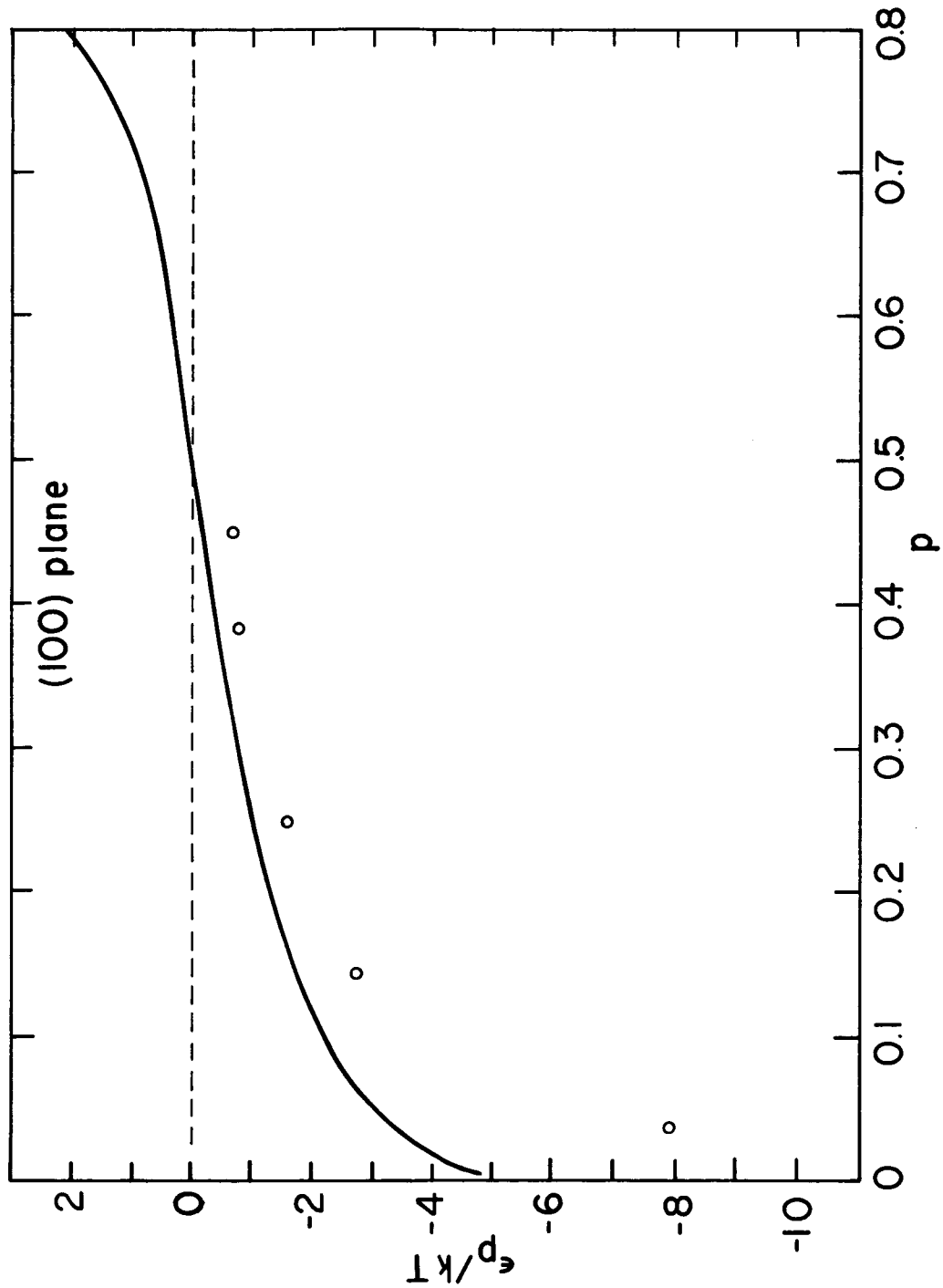

Figure 24. (Cont'd)

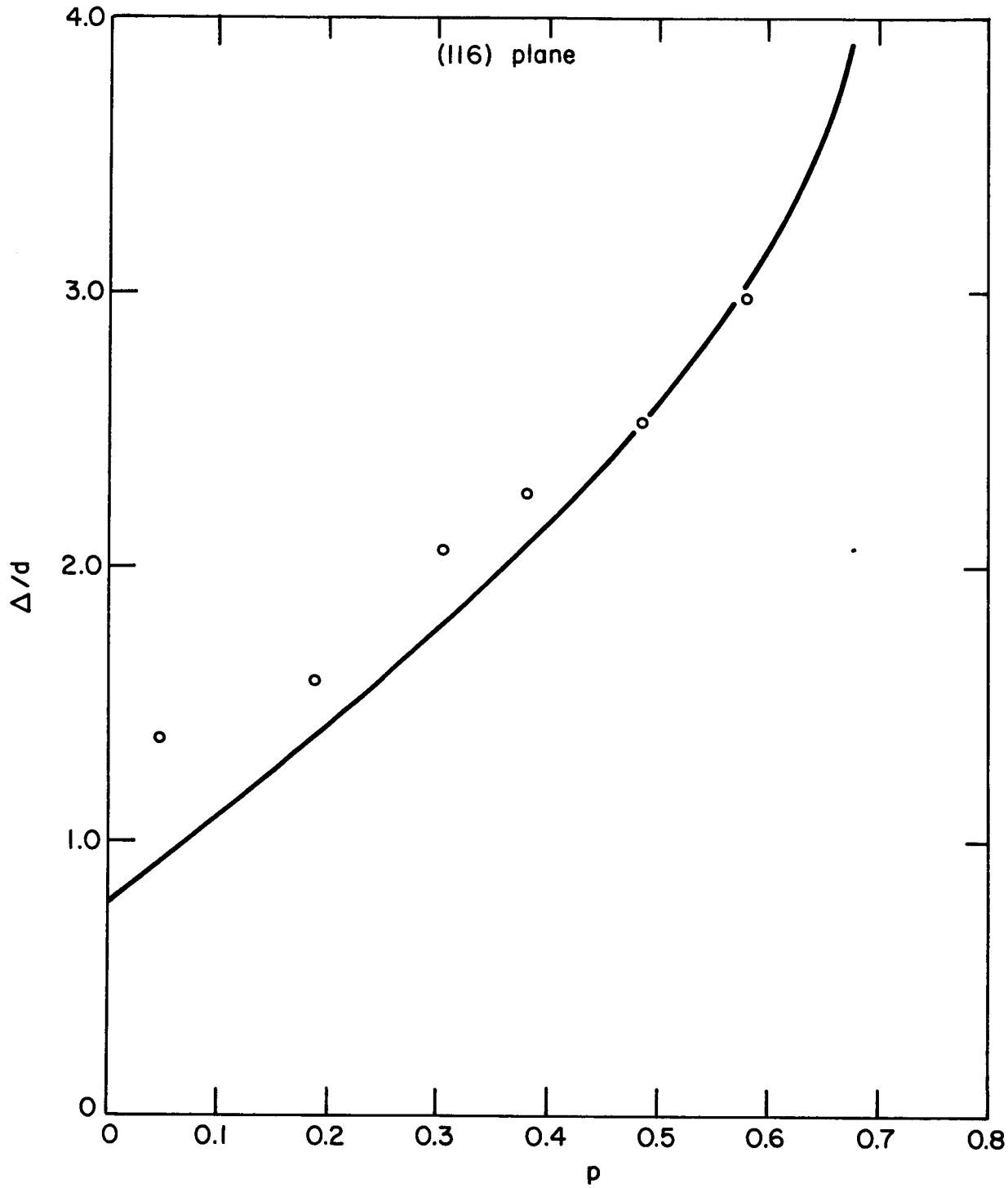

Figure 25.

Experimental normalized half-widths Δ/d of the total energy distribution curves plotted as a function of p. Solid line based on free electron model [Equation (5)] .

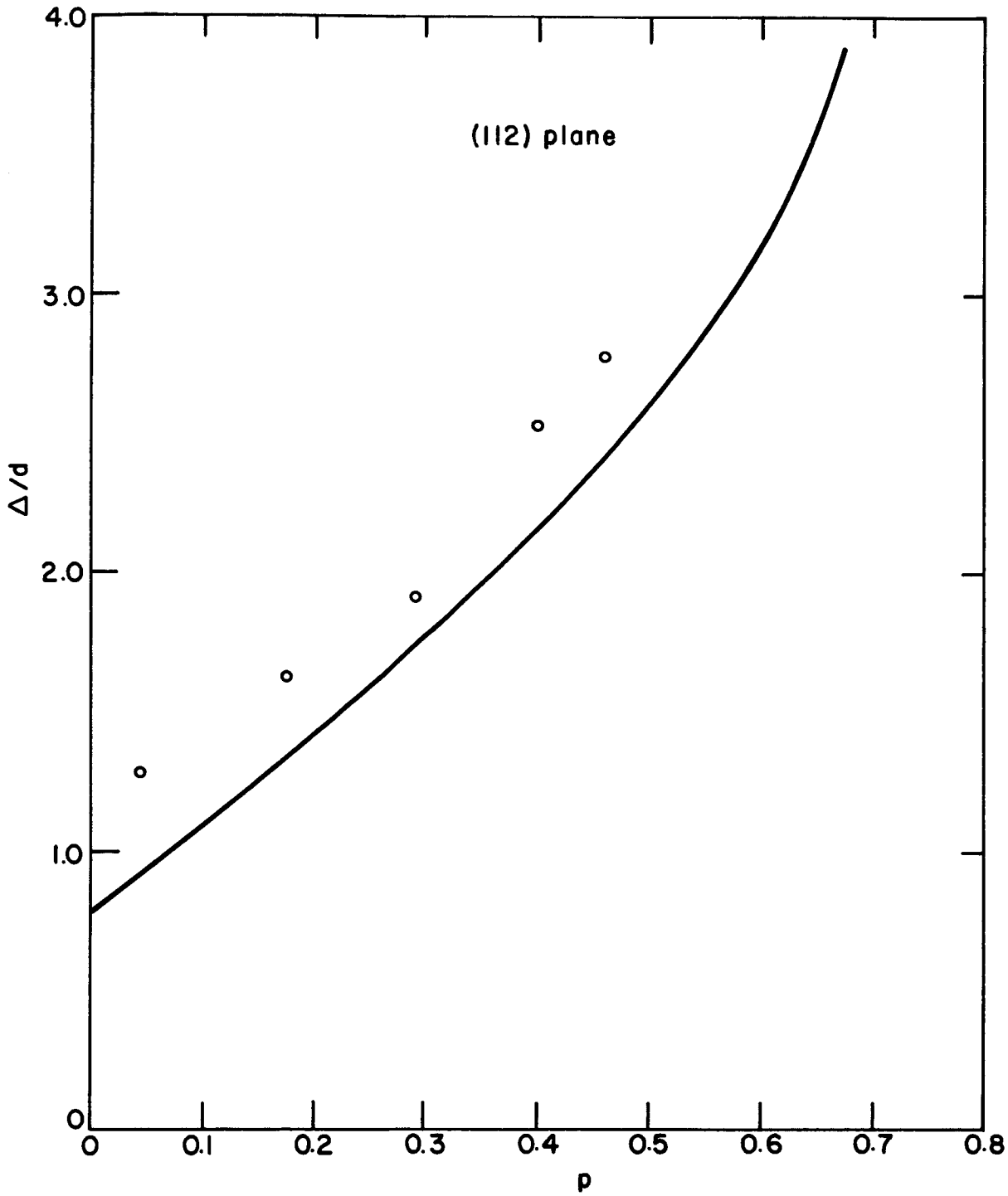

Figure 25. (Cont'd)

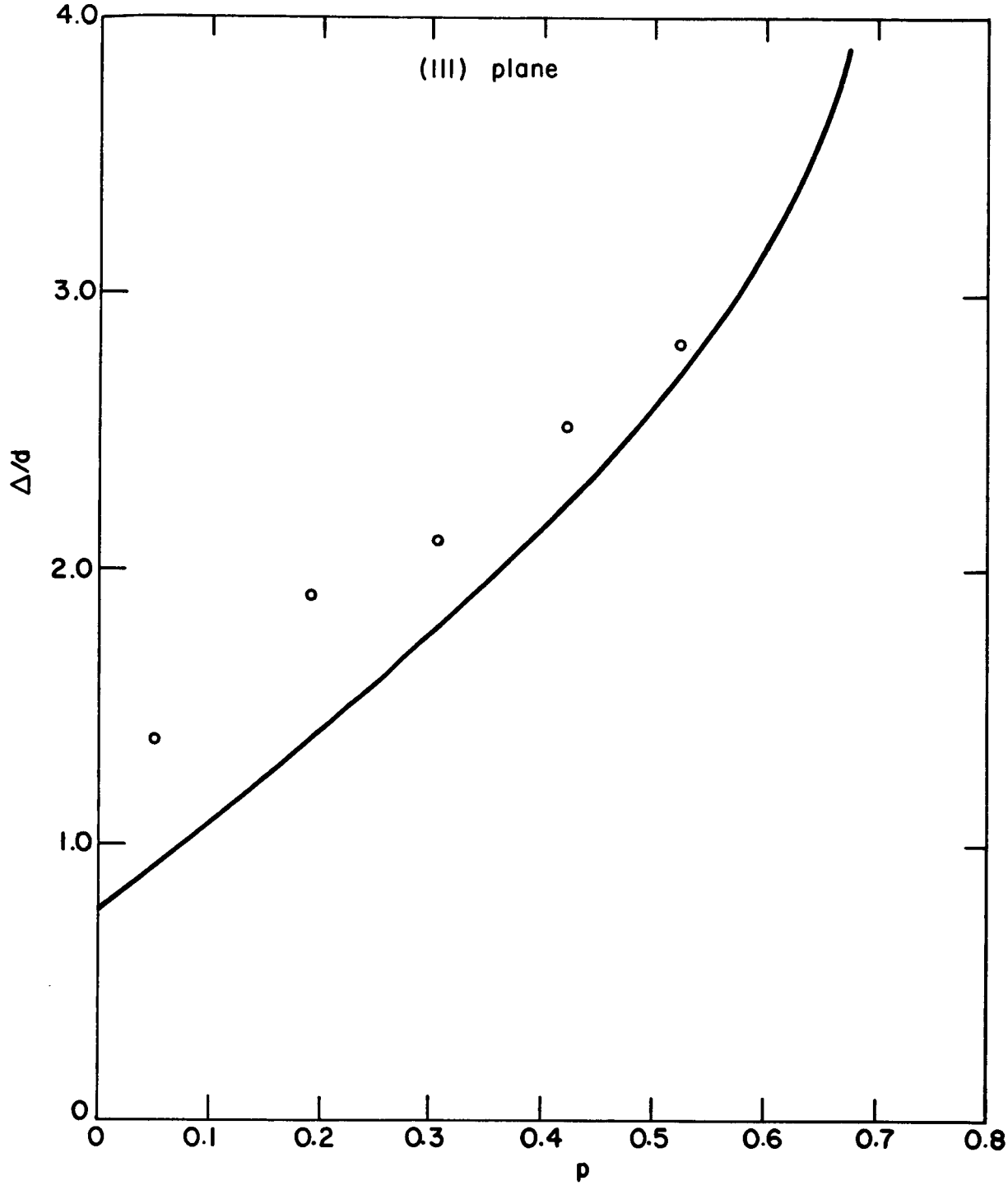

Figure 25. (Cont'd)

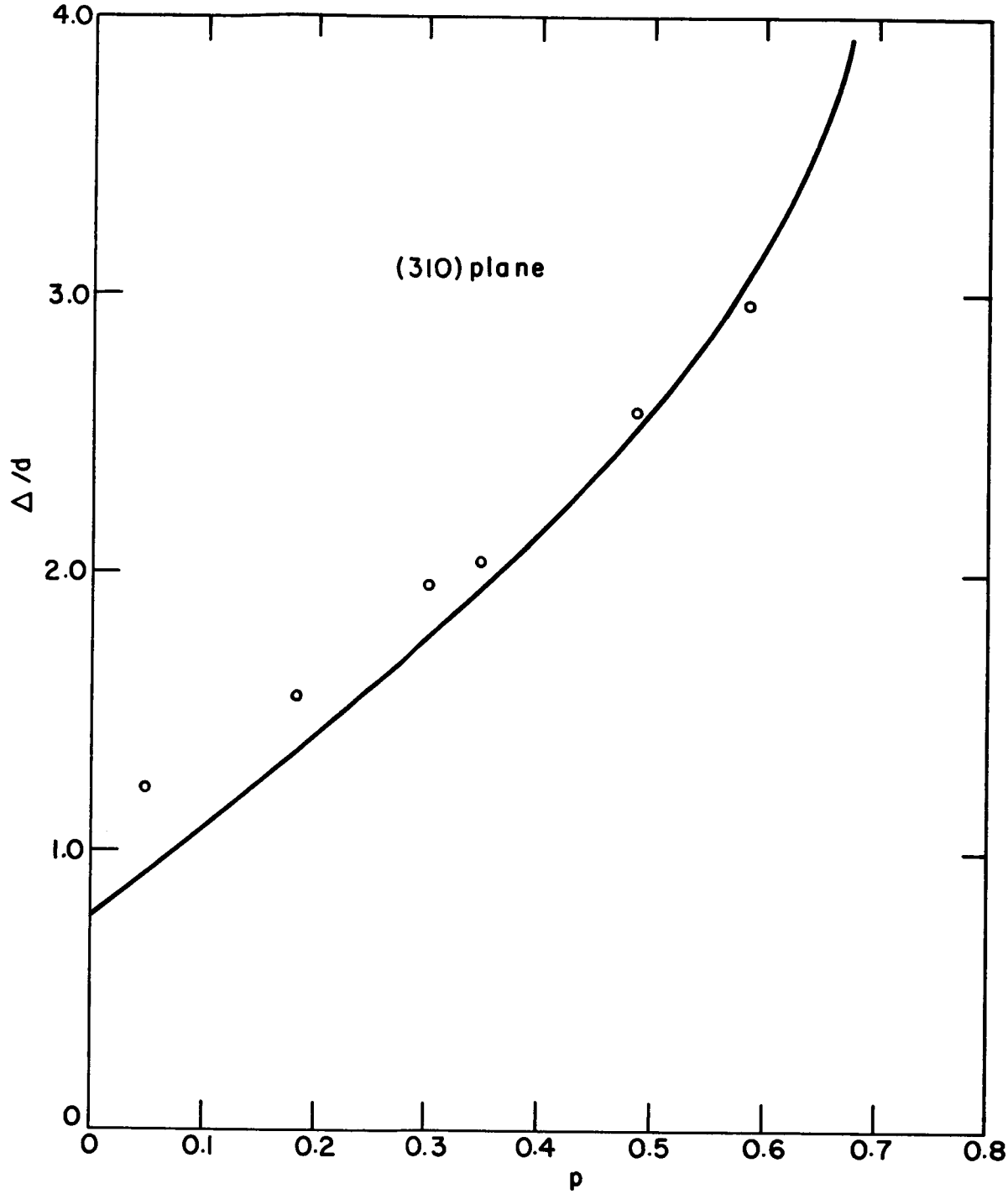

Figure 26. Experimental normalized half-widths Δ/d of the total energy distribution curves plotted as a function of p. Solid line based on free electron model [Equation (5)].

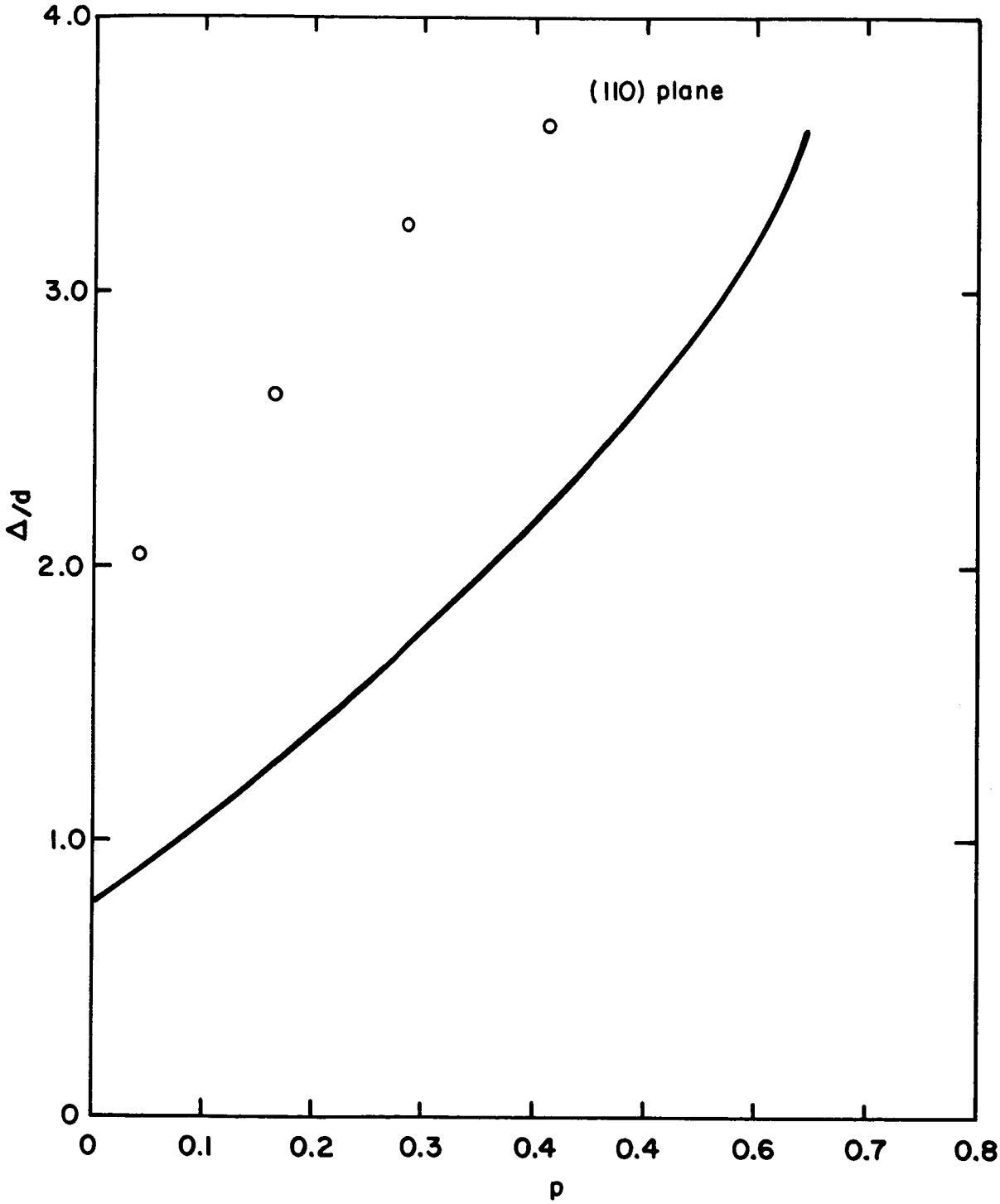

Figure 26. (Cont'd)

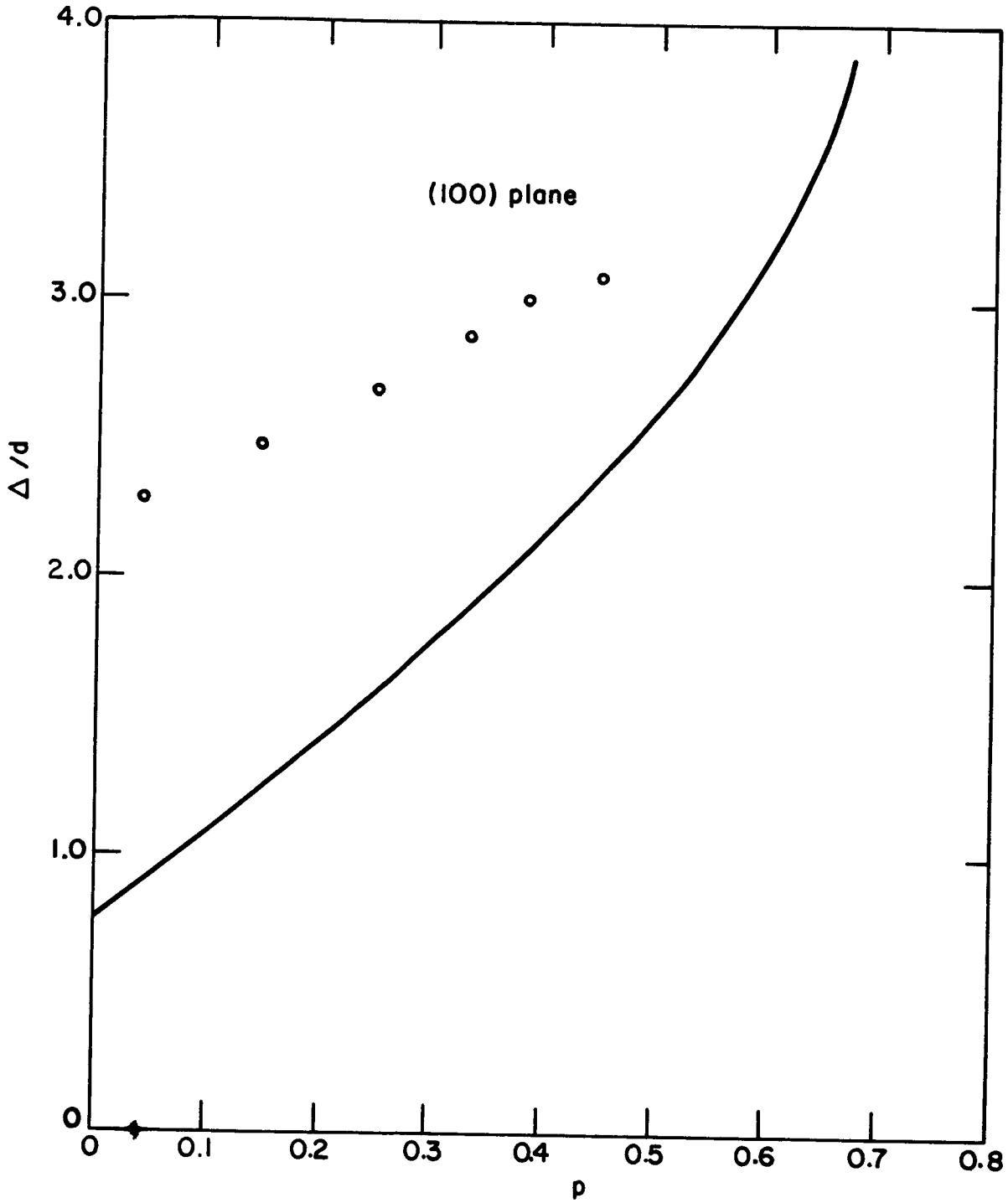

Figure 26. (Cont'd)

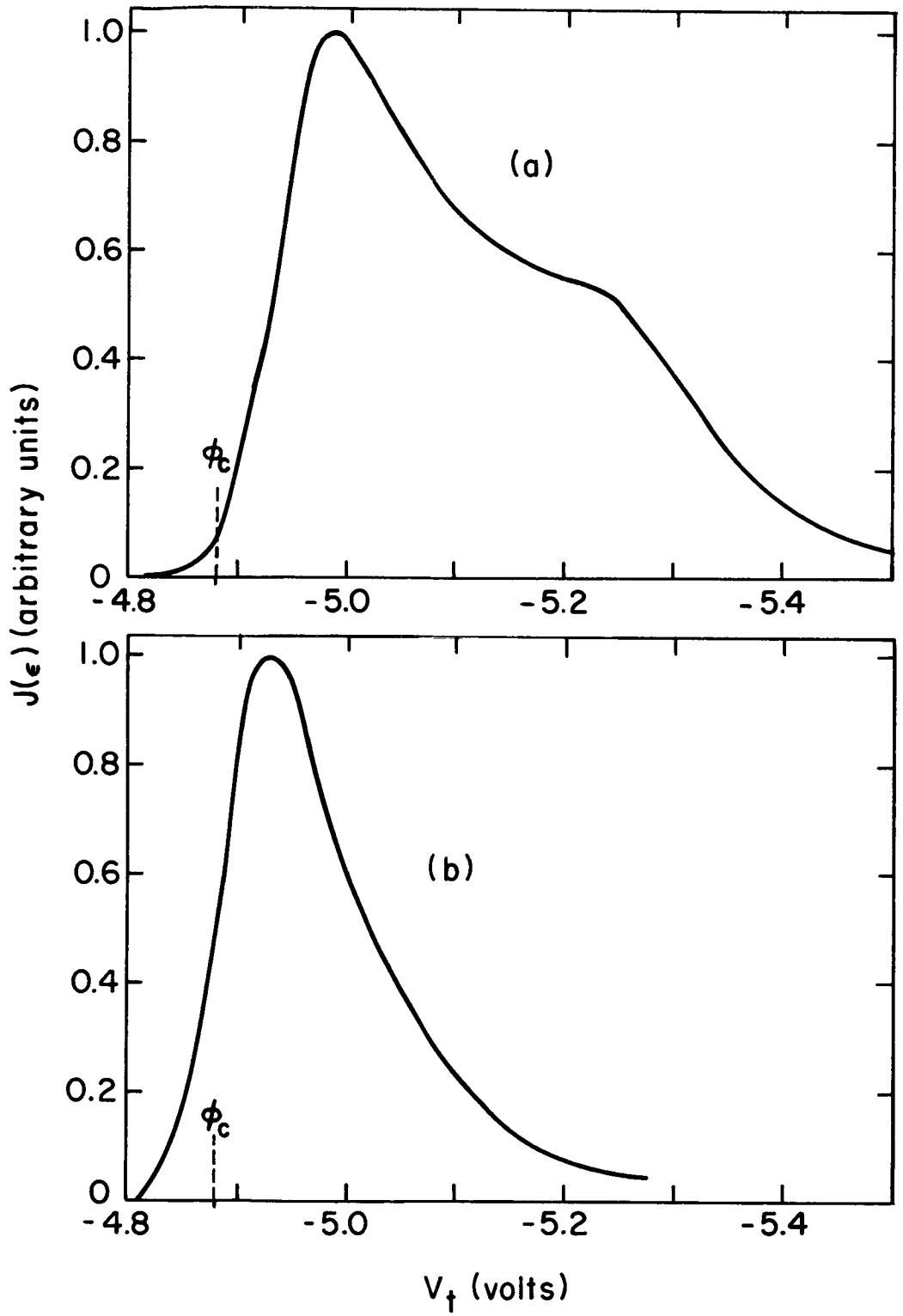

Figure 27 (a) Curve shows the total energy distribution from the ⟨100⟩ direction of a W emitter where d = 0. 140 eV and the anode voltage is 1235 V. (b) Curve shows the total energy distribution from the ⟨100⟩ direction of a Zr/O coated W emitter where d = 0. 091 eV and the anode voltage is 767V.

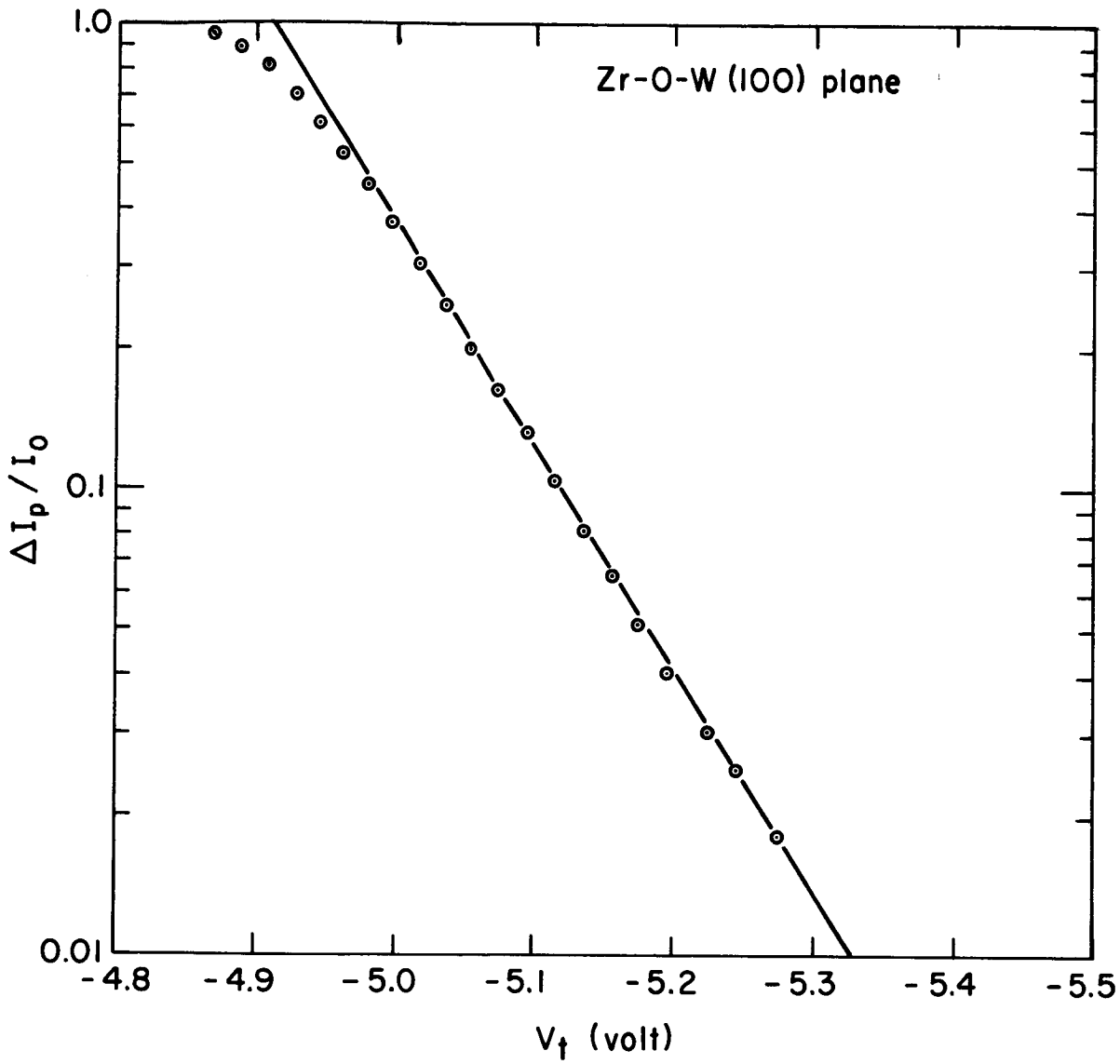

Figure 28. Integral emitted current from the<100>direction of a zirconium-oxygen coated W emitter plotted according to Equation (11). The anode voltage was 767 V and d = 0.091 eV.

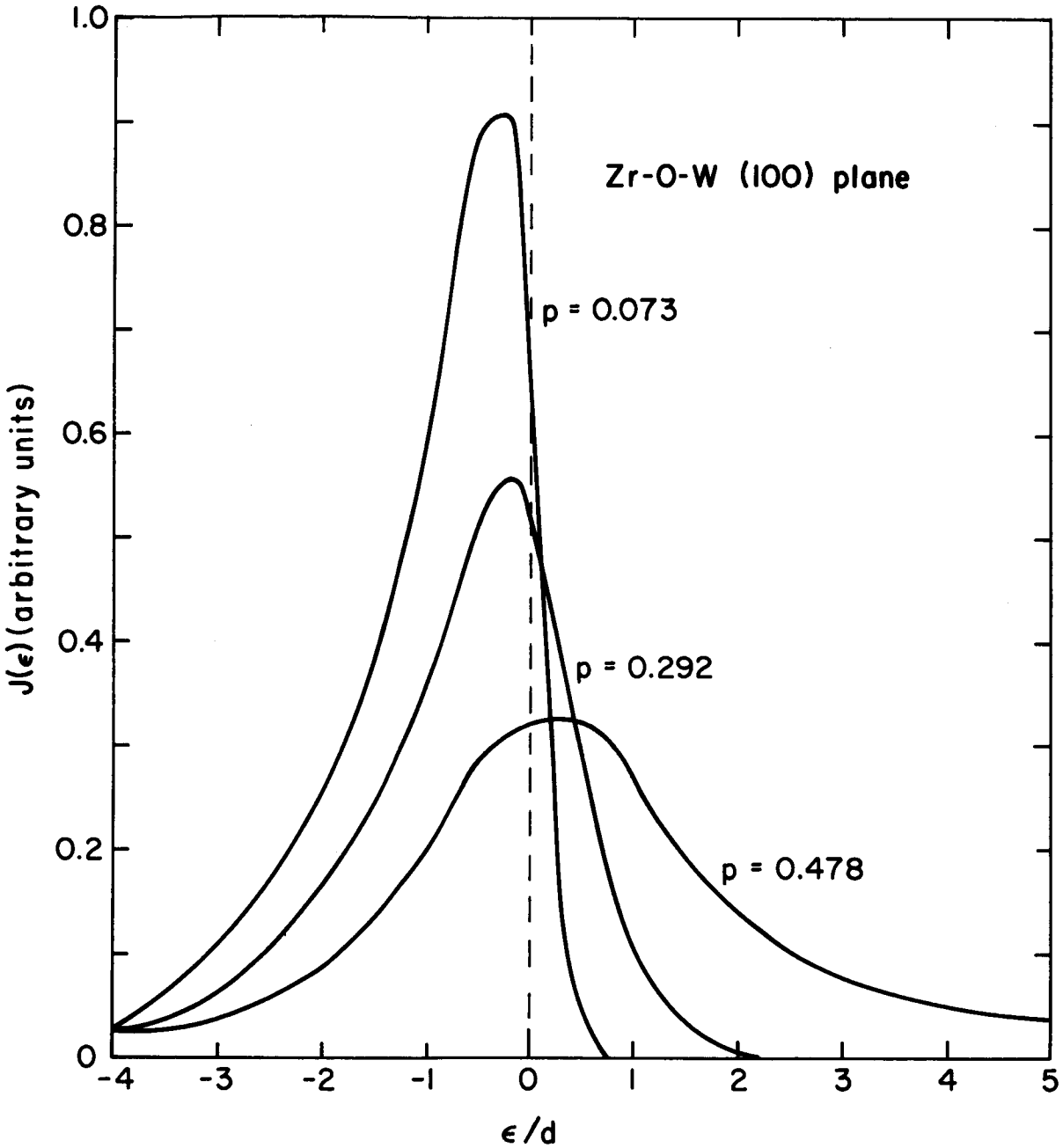

Figure 29. Curves show the total energy distribution from the ⟨100⟩ direction of a Zr/O coated W emitter at the indicated values of p. The anode voltage was 767 V and d = 0.091 eV.

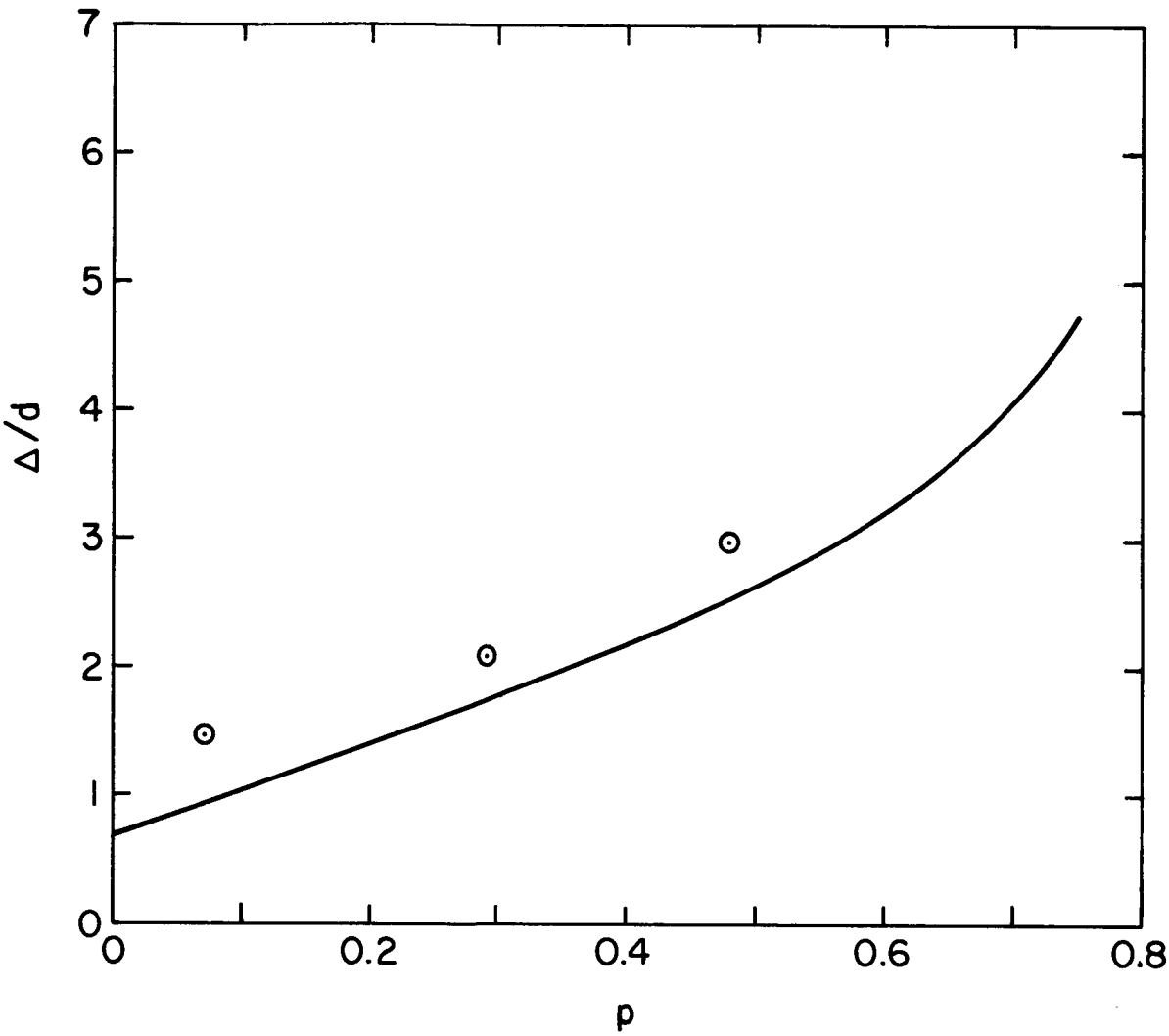

Figure 30. Data points show the variation of the normalized half width of the total energy distribution with p for the ⟨100⟩ direction of a Zr/O coated W emitter, where d = 0.091 eV. Solid line is the theoretical curve based on a free-electron model [Equation (5)].

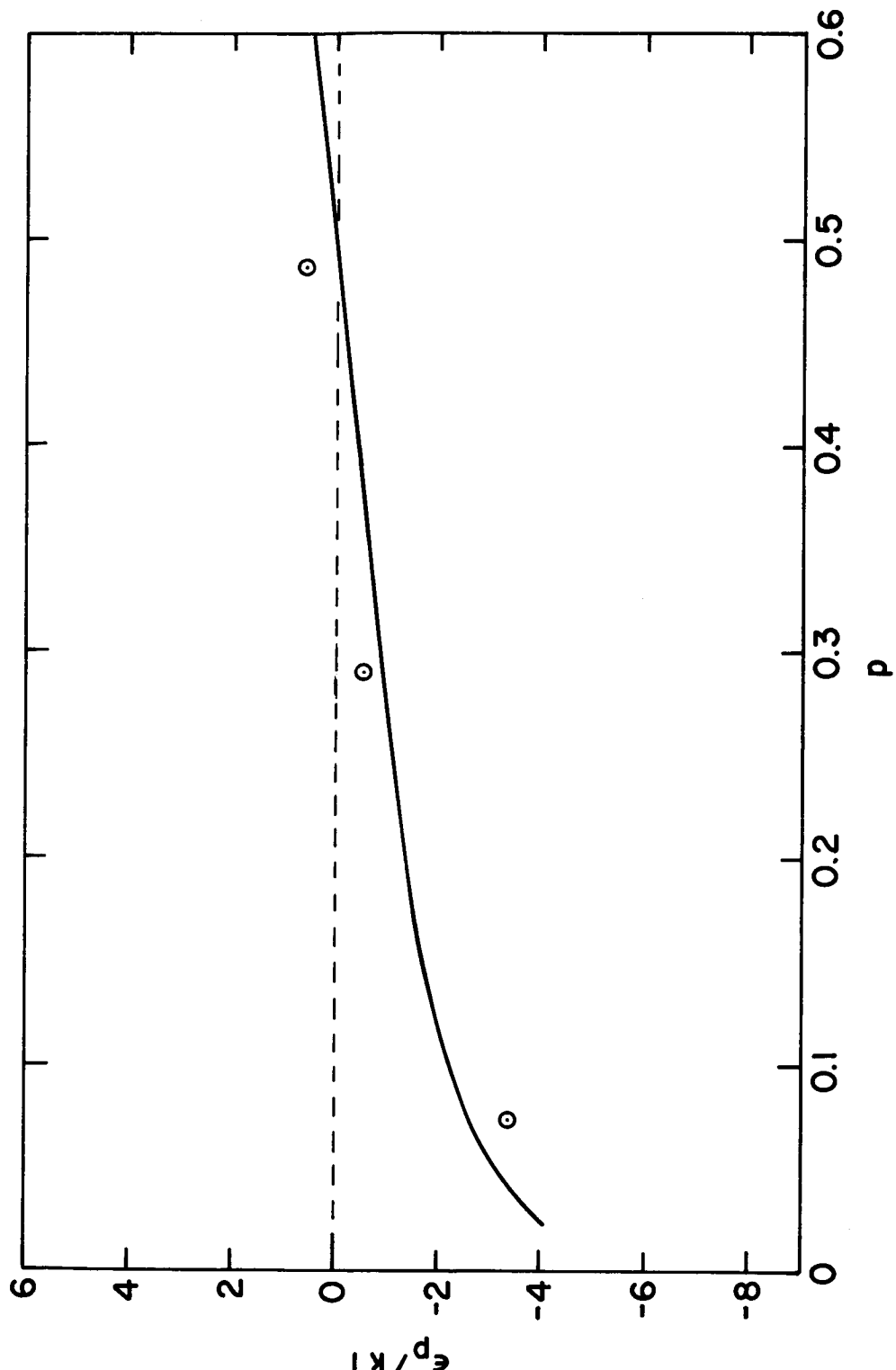

Figure 31. Data points show the variation of the position of the energy distribution peak relative to the Fermi level ϵ_p with p for the ⟨100⟩ direction of a Zr/O coated W emitter, where d = 0.091 eV. Solid line is the theoretical curve based on a free-electron model [Equation (5)].

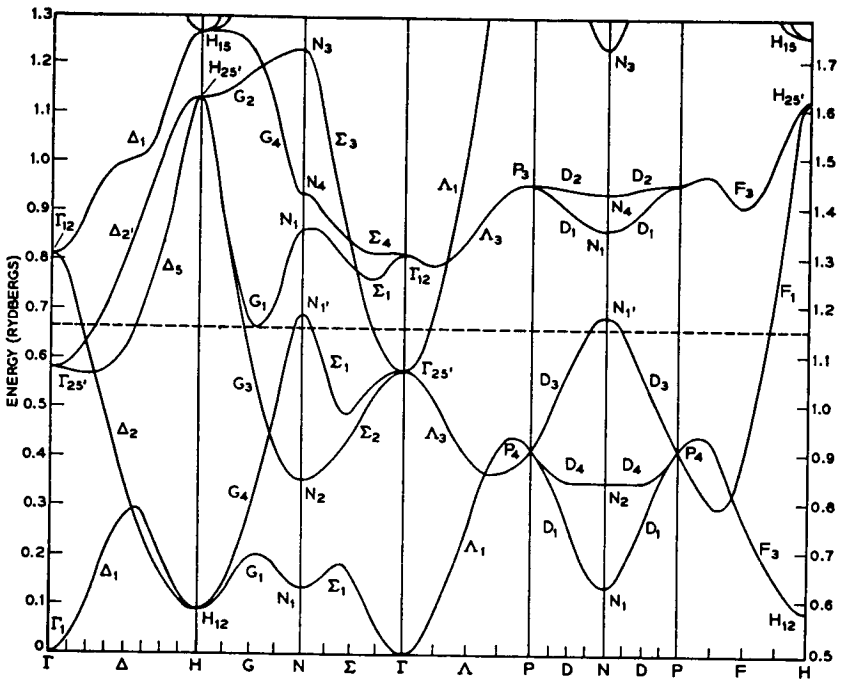

Figure 32. Energy bands E(k) along symmetry directions in the Brillouin zone for tungsten.

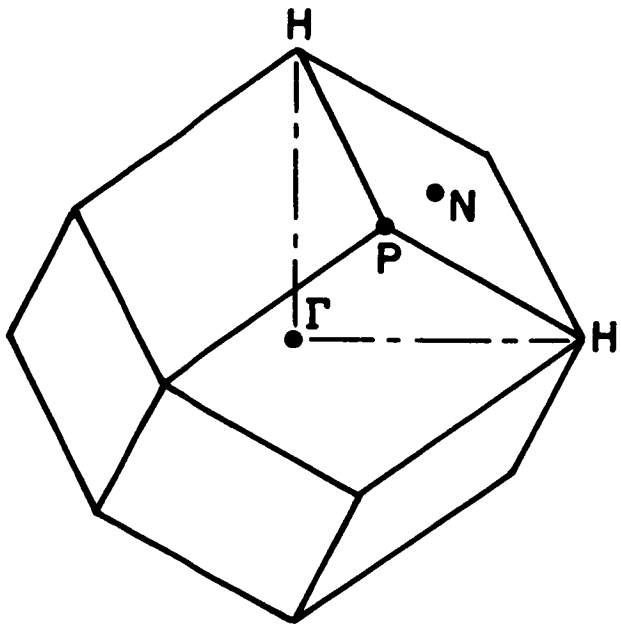

Figure 33. First Brillouin zone of a body-centered cubic structure. Letters indicate directions of reciprocal lattice space used in Figure 32.

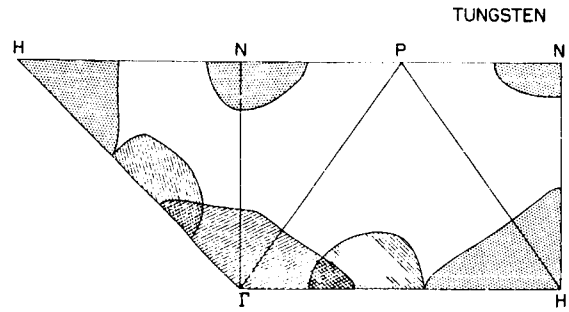

Figure 34. Nonrelativistic Fermi surface of tungsten.

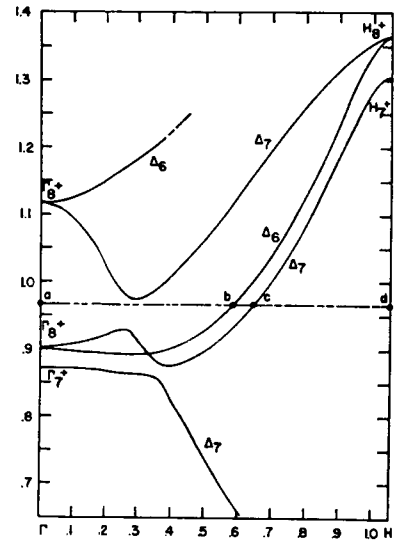

Figure 35. Relativistic energy bands for tungsten.

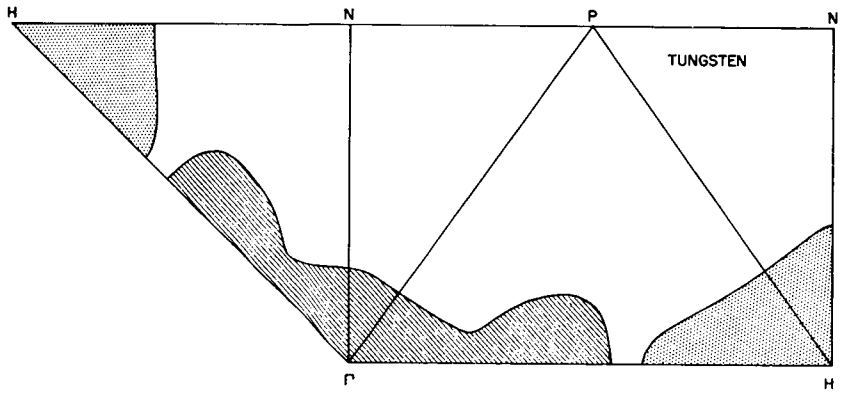

Figure 36. Relativistic Fermi surface of tungsten.

IV SINGLE PLANE STUDIES OF OXYGEN ON TUNGSTEN

INTRODUCTION

In the study of low work function adsorbates, the favorable properties of the alkali metals and alkaline earths have long been recognized. For Cs adsorbed on W, work function decreases of approximately three volts have been obtained and even greater decreases were obtained when Cs was deposited on top of a chemisorbed layer of O[1, 2].

Field emission studies of the Cs/W and Cs/O/W system are especially interesting since marked anisotropies in work function occur[3] and these are readily detected in the field electron patterns. The anisotropies yield information about dipole moments of the adsorbed complex on different planes if assumptions about the adsorbate coverages on these regions can be made.

When Cs is adsorbed on a W field emitter[1], the 110 planes preferentially adsorb Cs under equilibrium conditions to such an extent that these planes, although initially of very high work function, become the predominant electron emission areas until a coverage of 1.45×10^{14} atoms/cm^2 is reached at which point the (211) planes are equally bright. Deposition of Cs

on top of a chemisorbed layer of O, however, not only results in a lower minimum work function but alters electron emission anisotropy so that the 211 regions are the predominant electron emission regions when the Cs coverage is kept below that required to reach the work function minimum[2].

The presence of chemisorbed O apparently lowers the work function of the Cs/W adsorption complex by enhancing its dipole moment. A detailed field emission study of the effect of preadsorbed O on the properties of Cs monolayers indicates:

(1) a low work function of 1.15 eV can be attained if the emitter is initially dosed with approximately a monolayer of O ($\Delta\phi$ = 1.25 eV), heated to ~500°K, dosed heavily with Cs and then heated to ~350°K for 60 seconds.

(2) The stability of the Cs layer is appreciably enhanced by the presence of an underlying O layer.

(3) The temperature required to spread Cs over the substrate is sharply increased by underlying O at Cs coverages of approximately a monolayer.

(4) Although the 110 plane emits preferentially over the 100 and 211 planes in the case of Cs on clean W, the reverse apparently is true for Cs adsorbed on oxygenated W if insufficient Cs is present to allow attainment of the work function minimum.

Recent studies[4] of alkali metal adsorption on W using field emission probe techniques indicate that a considerable anisotropy in surface coverage of Cs exists on the various planes of a W field emitter when the adsorbate layer of moderate coverage is heated to equilibrate. In view of the remarkable effects of preadsorbed O on Cs layer properties, a probe field emission study of the Cs/O/W system would be of great interest. As a preliminary to this study an investigation of the O/W system has been carried out. The apparatus used in this study will now be described.

EXPERIMENTAL

Experimental Techniques

The tube is suitable both for work function and energy distribution measurements on any plane; moreover it contains both a Cs and an O source so that the above measurements may be carried out on single or coadsorbed layers of the above adsorbates.

A diagram of the tube is shown in Figure 1. The electron collector design is based on a design of Dr. van Oostrom of the Phillips Laboratory[5], Eindhoven. It differs from earlier probe tube designs by Müller[6], et al., in that it contains a lens electrode E. Electrons passing through the lens are focused near the center of the spherical collector F, and subsequently travel to the spherical electron collector along radius vector paths. This feature of the design enables the tube to be used successfully in total energy

analyzing experiments. The envelope construction enables the main electrode assembly to be removed for inspection or alteration simply by making one crack in the aluminosilicate glass which is conductivized on the inside only in the vicinity of the anode D. In order to minimize the electrical noise pickup by the electron collector lead as it emerges from the tube, the lead is enclosed by a molybdenum cylinder which connects directly to the shield of the coaxial cable leading to the electrometer.

The O and Cs sources are arranged perpendicular to each other and to the emitter axis and each supplies the emitter with adsorbates along a very small glass constriction which points toward the tip. Deflection of the field emission electron beam is effected magnetically.

A mechanical method of deflecting the electron beam current was also considered; however, a simple method of deflecting the emitter is unsatisfactory because unless the emitter is swiveled about its apex, the electron beam will not enter the electrode assembly perpendicular to the anode face. Failure to do so would result in erroneous work function data. Mechanical arrangements that orient the emitter about its apex are quite complicated although such a beam deflection arrangement may be superior in energy distribution analyses since possible disturbing magnetic fields may be removed during measurements.

The deflection method employs a small quadruple electromagnet constructed to fit snugly against the constricted part of the emitter glass envelope so that the horizontal axis through two opposite pole faces bisects that of the other pair at the emitter apex. The electromagnets have carefully

annealed armco cores while all other parts of the magnet assembly are constructed of nonmagnetic material. It is hoped that this will result in the absence of residual magnetic fields so that the probe beam will always be derived from the same crystallographic region of the emitter when the electromagnet current is switched off. In this and an earlier magnetic deflection probe tube, it was found necessary to compensate for the beam deflection resulting from alteration of the anode voltage which takes place during I, V data collection. This deflection is a consequence of the fact that electron deflection by a magnetic field is proportional to electron velocity which in the field emission tube depends upon anode accelerating voltage.

Procedures for measuring and calculating energy distributions are described in Section III of this report.

Emitter temperatures are derived from an accurate measurement of the resistance of a small section of the emitter's supporting filament C; this makes use of the fact that the resistivity of W is a well-known, monotonic, and nearly linear function of temperature over the range of interest. The resistance of a segment of the loop was determined by passing an accurately known dc current through it and measuring the potential difference across it by means of two small leads attached to the filament. The resistance was calibrated by measuring it at several well-determined temperatures. A servomechanism developed by Gomer and Zimmerman[7] was used to ensure constancy of emitter resistance and hence temperature.

Experimental Procedure

The tube was evacuated and processed by standard UHV procedures and sealed off from the vacuum system at $\sim 10^{-9}$ torr. Flashing of the Mo getter with the tube submersed in liquid nitrogen resulted in a final residual pressure of chemically active gases below $\sim 10^{-11}$ torr as judged by contamination rates of the cleaned field emitter.

Dosing of the emitter with O was effected by heating a platinum bucket containing CuO at a constant current for a standard time. The CuO had been prepared by heating the platinum bucket containing small pieces of well outgassed copper in a low pressure ~ 15 torr of spectroscopically pure O. Although the O beam was directed from one side, the emitter was uniformly dosed with O even when only partial monolayers of O were deposited at 78°K. At 20°K, O deposits[8] unilaterally on a field emitter owing to the fact that its sticking probability on pyrex and metal is unity at 20°K; at 80°K, however, the sticking probability on glass, if not on W, is obviously less than unity so that a dose of O from the source bounces around inside of the tube many times before being removed by the getter. During this time, the side of the emitter away from the source is subject to impingement by O; and even for deposits of less than a monolayer, the adsorbate will be distributed evenly over the emitter. Before dosing, the getter was activated in order to remove excess O from the tube.

Work function measurements may be made in two ways: attention can be focused on a particular plane in which case regular Fowler-Nordheim data

is obtained for a range of voltages and currents, the process being repeated for other planes of interest; alternatively, the field electron beam may be linearly deflected so that the tube collector continuously samples current from the crystal planes along a zone line. If the process is repeated at several different voltages, work function determinations of any plane along the zone line may be made. Correction must be made for the fact that the electron beam from a particular plane will be deflected by an amount which depends on the beam accelerating voltage. The latter technique for determining single plane work functions has been employed by Schmidt[9] who used it to investigate the system W/Ba. In the work reported here we have used the former technique to study the 110, 211, 100 and 111 planes of a 110 oriented W emitter.

RESULTS AND DISCUSSION

Results

Figure 2 depicts the change in work function which occurred when the emitter was saturated with O at 78°K and subsequently heated to various temperatures for 60 second intervals. Beyond 1500°K, the heating time was reduced to 15 seconds in order to minimize possible current changes arising from emitter dulling or from contamination from gas thermally desorbed from the glass wall surrounding the emitter.

The work function desorption curves indicate a grouping into two types of behavior in which the work function either goes through a maximum on heating as on the densely packed 110 and 211 planes or declines monotonically on heating as on the 100 and 111 planes. Although the maximum value for the oxygenated 110 plane work function is shown as 7.75 eV in Figure 2, values as high as 8 eV have been determined in other runs[10].

Figure 3 shows the work function change, $\Delta\phi$, and the change of preexponential $\Delta \log \frac{A_o}{A} = B$ for the 110 plane as the fully covered oxygenated emitter was heated in steps to ~2000°K. The initial work function change was 1.0 eV and climbed slowly to 1.1 eV at 400°K; beyond that it rose rapidly to a maximum of 1.9 eV at 800°K. Heating the emitter above 800°K, resulted in a continuous decline in work function until at 1800°K, the clean value was regained. The accompanying preexponential change behavior was markedly different. A drop of 50% in B occurred on heating to only 200°K and a gradual decline to a minimum at 800°K then took place. From 800°K to 1600°K, B rose to a sharp high maximum greater than the original 78°K value and from 1600°K declined to essentially the clean value at 2200°K. The most notable among these features are (i) the high 800°K maximum in $\Delta\phi$, (ii) the sharp initial decline in B and (iii) the interesting maximum in B occurring at 1600°K.

In Figure 4 are shown the $\Delta\phi$ and B values for the oxygenated 211 plane. From an initial value of 1.3 eV at 78°K, $\Delta\phi$ rose steadily to a maximum of 2.3 eV at 800°K, then, after remaining on a lower plateau until 1500°K, dropped sharply and approached the zero clean value at 2100°K. Unlike the B

values for the 110 plane, those for the 211 plane did not begin to drop sharply until the emitter was heated above 400°K. At 800°K, the value of B corresponding to the work function maximum had declined to zero although it rose again to nearly the 78°K value at 1400°K. No high temperature peak in the B versus T curve is observable in the high temperature range and the final values of B did not return to the clean values at 2000°K indicating some retention of O by the 211 plane.

A plot of $\Delta\phi$ versus temperature for the 111 plane (Figure 5) exhibits no maximum to correspond with those for the 110 and 211 planes; instead $\Delta\phi$ drops monotonically from a high of 1.8 eV at 78°K to 1.6 eV at 1200°K. This plateau is terminated by a decrease to 0.4 eV at 1400°K after which $\Delta\phi$ becomes slightly negative at 1750°K and then returns to the clean value at 2000°K. The preexponential B declines continuously from the 78°K value to a minimum at 1200°K. A maximum in the B versus temperature curve is apparent at 1700°K and a final decline to a value slightly less than the clean value takes place at 2000°K.

The 100 plane results (Figure 6) present similar features to those of the 111 plane; thus the work function declines slowly from a high initial value of 1.5 eV at 78°K to a minimum of -0.75 at 1700°K. At 2000°K, $\Delta\phi$ is back to the clean 100 value of zero. A broad minimum close to zero and 200°K wide characterizes the behavior of the B versus temperature curve which thereafter rises to a maximum at 1700°K before returning to the clean zero value at 2000°K.

Figure 7 collects together the results from the previous four curves. Comparison of the B curves shows that the initial decline in B begins at progressively higher temperatures along the series 110 < 211 < 100 < 111. Thus the closer packed planes register the initial decline at lower temperatures than the more open packed ones. Initial 78°K values of B are very close together and have a value of B = 1.9 ± 0.1 while initial values of $\Delta\phi$ increase in the order 110 < 211 < 100 < 111.

Figure 8 illustrates the results obtained by dosing the emitter with partial monolayers of O at 78°K. The O results indicate little or no change for the 110 plane in the low temperature range and perhaps a slight adsorption of O leading to a small increase in $\Delta\phi$ and B in the higher temperature range. Initial values of $\Delta\phi$ for the 110, 100 and 211 are respectively 0.15, 0.35 and 0.65 eV and hence increase markedly as the atom density of the substrate decreases. A maximum in the curve of $\Delta\phi$ versus temperature is just apparent for the 211 plane at 1000°K while a broad minimum appears for the 100 plane at 1400°K -- approximately 350°K lower than for the monolayer case. The B versus temperature curves differ from their monolayer analogues in the low temperature range; thus the 110 and 211 values increase on heating from 78°K to 600°K while the 100 plane values increase after an initial drop. In the high temperature range the B versus T curves more nearly resemble the monolayer ones. The 211 plane curve exhibits a well-defined maximum at 1500°K while the 100 curve has a truncated maximum at the same temperature.

Discussion

The most outstanding features of the results obtained below 1000°K for the monolayer are the maximum which occurs in the $\Delta\phi$ versus T curves for the 110 and 211 planes, the initial 78°K values of $\Delta\phi$ which increased for the various planes in the order 110<211<100<111, the initial decline in B which set in at temperatures which increased in the same order and the fact that initial 78°K values of B were nearly identical.

Changes in B which arise as a result of adsorption may be accounted for by a simple polarization model in which the high applied field induces a dipole moment in the adsorbate-substrate that contributes a small field dependent increment to the work function.

As shown by Schmidt and Gomer[11] for an induced dipole contained solely in the adsorbate we have

$$\phi(F) = \phi(0) + 4\pi\sigma a F_{eff} \tag{1}$$

$$= \phi(0) + \frac{4\pi\sigma a F}{1 + 9a\sigma^{3/2}} \tag{2}$$

where $\phi(0)$ is the work function at zero applied field, a is the polarizability, σ is the adsorbate surface density, F the applied field. The effective field F_{eff} is related to the applied field F by the Topping[12] depolarization equation. Using the Fowler-Nordheim equation

$$i = c\,\frac{(E_F/\phi)^{1/2}}{(E_F + \phi)t^2(y)}\exp - \frac{0.68\left[\phi(F)\right]^{3/2} v(y)}{F} \tag{3}$$

where E_F is the Fermi energy, t and v functions of y and $y = \frac{14.4F}{\phi^2}$; v(y) is a nearly linear function of y and may be written[13]

$$v(y) = \bar{v} + v'y \tag{4}$$

Substituting Equation (2) and (4) in Equation (3) and taking only the first term in the expansion of $\phi(F)^{3/2}$ we have

$$B = \log \left(\frac{E_F + \phi_o}{E_F + \phi}\right) \left(\frac{\phi_o}{\phi}\right)^{1/2} + \log t_o^2/t^2 + 0.98 \left[v'\phi^{-1/2} - v'_o\phi_o^{-1/2}\right] - \frac{5.6[\phi(0)]^{1/2} v\sigma a}{1 + 9a\sigma^{3/2}} \tag{5}$$

The subscripts refer to the adsorbate free substrate. Using E_F = 8 eV, a surface atom density of 10^{15} atoms of O per cm^2 for all planes and a value of the polarizability of 3 $\mathring{A}^2$ for the oxide ion $O^=$ we can calculate B values which vary from plane to plane by an amount which depends only on the first and third terms of Equation (5). However, only the first and last terms contribute significantly to B and the first term is much smaller than the last so that only a very slight dependence of B on substrate orientation emerges from Equation (5). This is in agreement with the experimental values of B for a saturated monolayer which within the limits of experimental error are identical for all four planes (See Table I).

Changes that may occur on a particular plane as a result of heating a low temperature deposited layer of adsorbate may be divided into the following possibilities:

(1) Migration of adsorbate in or out of the plane

(2) Change in binding mode of the adsorbate

(3) Desorption of adsorbate

(4) Rearrangement of substrate

All of these possibilities probably occur on some of the planes when the emitter is heated, although not all of them could be responsible for a work function increase and a simultaneous decrease in B. Changes in B that arise as a result of adsorption appear to be accounted for satisfactorily by the simple polarization model discussed above in which B is very nearly proportional to the product of polarizability and surface coverage. The low temperature decline in B is unlikely to be a consequence of substrate rearrangement alone since this would probably not affect the polarizability unless the O became buried completely under a W layer. It seems likely that the polarizability would be only slightly dependent on bond type and that it would slightly decrease as bond strength increased. Gomer and Bell[14] have found for CO deposited at 20° K on W that the slope of B versus coverage is independent of bond type. Thus the slope at high coverages where only physical adsorption was occurring was identical with that at low coverages where CO was chemisorbed. If we assume change in polarizability to be negligible then the low temperature decline in B must be mostly attributed to O desorption and the rise in $\Delta\phi$ to a changing of bonding mode of the remaining O so that the average negative dipole moment is greatly increased. It is suggested that for those situations where the preexponential declines rapidly and the work function rises slowly, desorption of a weakly-bound, slightly electropositive

adsorbate is taking place and that at the higher temperature where a rapid work function increase is accompanied by only a small further decline in B, conversion of the remaining adsorbate to a higher dipole moment layer takes place together with only a slight amount of further desorption.

TABLE I

Plane	B Calculated	B Experimental
110	-1.90	-2.08
211	-1.81	-1.70
100	-1.82	-1.85
111	-1.77	-1.95
$a = 3\ \mathring{A}^3$ for $O^=$ $\sigma \sim 10^{15}$ atoms/cm^2 $E_f \sim 8$ eV		

Comparison of calculated values of the preexponential with experimental values for O adsorbed on the 110, 211 and 100 planes of a W field emitter.

The fact that both B and $\Delta\phi$ show only a slight decrease up to 700°K for the 100 plane suggests that little or no change in either O concentration or bonding mode takes place on this plane up to 700°K; yet at 800°K B has

declined to nearly zero, although $\Delta\phi$ has only just begun its return to zero. A process of desorption and concomitant change of bonding mode which was invoked to explain the behavior of $\Delta\phi$ and B on the 110 and 211 plane may be responsible for the latter effects on the 100 plane. However, a decrease in polarizability must also take place since B declined to zero when $\Delta\phi$ indicated that considerable O was still present on the 100 plane. Except for the small drop in $\Delta\phi$ and slight decrease in B for the 111 plane at $T \leq 300^{\circ}K$, which is suggestive of slight O desorption, the constancy of $\Delta\phi$ and gradual decline in B for this plane up to $1200^{\circ}K$, suggest that some further desorption is taking place accompanied by rearrangement of the remaining adsorbate.

The interesting peaks occurring in the B versus temperature curves in the temperature range $1600\text{-}1800^{\circ}K$ are probably the result of rearrangement of substrate in which the surface transforms into a set of sharp ridges from which electron emission is greatly enhanced. This would lead to a sharp drop in effective emitting area and hence a significant increase in B. Accompanying the increase in B for the 111 and 100 planes is an apparent decline of $\Delta\phi$ to negative values. Real values for $\Delta\phi$ can be related to the apparent ones by the following procedure:

$$m_f = b\phi^{3/2}/\beta \tag{6}$$

where m_f is the Fowler-Nordheim slope, b is a constant and β the geometry dependent field factor. Hence the true work function ϕ_T is related to the clean ϕ_C by

$$\phi_T^{3/2} = m_T \beta_T \phi_C^{3/2} / m_C \beta_C \tag{7}$$

and the apparent one by:

$$\phi_A^{3/2} = m_A \phi_C^{3/2}/m_C \tag{8}$$

Since for the apparent case we assume β unchanged by adsorption. The relation between the true and apparent work function is then:

$$\phi_T^{3/2} = \phi_A^{3/2} \beta_T/\beta_C \tag{9}$$

since $m_A = m_T$. Now $\beta_T \quad \beta_C$ so that $\phi_T \quad \phi_A$. By using $\phi_T = \phi_A + \delta$ and expanding in power series we have as a first order correction to ϕ_A:

$$\delta = 0.67 \phi_A \left(\beta_T/\beta_C\right)^{-1} \tag{10}$$

In order to result in a 1 eV correction β_T must be ~30% greater than β_C.

The initial 78°K values of $\Delta\phi$ decrease in the order of increasing substrate work function. Whether or not the differences are due to dipole moment variations or to coverage variations is not known; the similar values of B obtained for each plane at 78°K on saturating the emitter with O indicate similar coverages on all planes in which case, $\Delta\phi$ would be a reliable indicator of relative dipole moment strength at monolayer coverage.

Gurney[15] has pointed out that if the ionization potential of an adsorbate element is comparable with the work function of a metal then the valence level of an adsorbate atom will become broadened as it approaches the metal and that the charge residing on the adatom will depend on the extent of broadening of the valence level and where its midpoint lies with respect to the metal Fermi level. O has an ionization potential of 13.6 V

which is considerably greater than the work function of any metal. Hence no broadening of the O valence level will occur on adsorption. An O atom can, however, accept a supernumerary electron in a stably bound state which is considerably higher than the valence level and may perhaps interact with the metal to form a broadened band. It is possible to explain on this basis the correlation between the O-W dipole moment and substrate work function alluded to above. As the substrate work function decreases, the center of the broadened adsorbate band falls further below the metal Fermi level resulting in a progressively increasing negative charge on the adsorbate which of course results in a higher dipole moment for the O-W complex.

The fact that the initial value of $\Delta\phi$ for the 211 plane partial monolayer is considerably larger than the values for the 100 and 110 planes is surprising. The monolayer results suggest that the dipole moment of the adsorbed O increases in the order 110<211<100. If this holds at partial monolayer coverages, then the initial coverage of O on the 211 plane when $\theta < 1$ appears to be greater than that on the other planes. This may be a consequence of a higher heat of adsorption for O on the 211 plane which may reflect in a higher initial sticking coefficient of O on W at 78°K. That the $\Delta\phi$ and B curves for O on the 211 plane of W did not return to their clean values at 2000°K either for the monolayer or for the partial monolayer also indicates a higher heat of binding of O on the W (211) plane than on the other planes investigated. Above 1000°K, the partial monolayer curves begin to resemble their monolayer analogues. This is to be expected since in this temperature region the surface coverages of O are likely to be closer to one another for

the two sets of curves than in the low temperature region. A notable difference between the partial and monolayer preexponential curves is to be found in the low temperature range; the sharp dips exhibited by the monolayer curves are absent in the partial monolayer ones. This may be cited as further evidence for the idea that at high coverages, the first change which takes place in the adsorbate layer on heating is due to desorption of weakly bound adsorbate state which probably only adsorbs to any appreciable extent when the O layer is nearly complete.

REFERENCES

1. Final Report, Contract NAS3-2596, Field Emission Corp., June 1964 p. 18.

2. Ibid. p. 22.

3. Ibid. p. 11 - 24.

4. Final Report, Contract NAS3-5902, Field Emission Corp., February 1966, p. 43.

5. A. van Oostrom, Philips Res. Rep. Supplement, Netherlands, No. 11, 102, (1966).

6. E. Müller and R. Young, J. App. Phys. 33, 91 (1962).

7. R. Gomer and D. Zimmerman, Rev. Sci. Instr. 36, 1046 (1965).

8. R. Gomer and J. Hulm, J. Chem. Phys. 27, 1363 (1957).

9. L. Schmidt, 13th Field Emission Symposium, Cornell University September (1966).

10. Report No. 7, Contract NASW-1082, Field Emission Corp., McMinnville, Oregon (1966).

11. L. Schmidt and R. Gomer, J. Chem. Phys. 42, 3573 (1965).

12. J. Topping, Proc. Roy. Soc. (London) A114, 67 (1927).

13. F. Charbonnier and E. Martin, J. App. Phys. 33, 1897 (1962).

14. A. Bell and R. Gomer, J. Chem. Phys. 44, 1065 (1966).

15. R. Gurney, Phys. Rev. 47, 479 (1935).

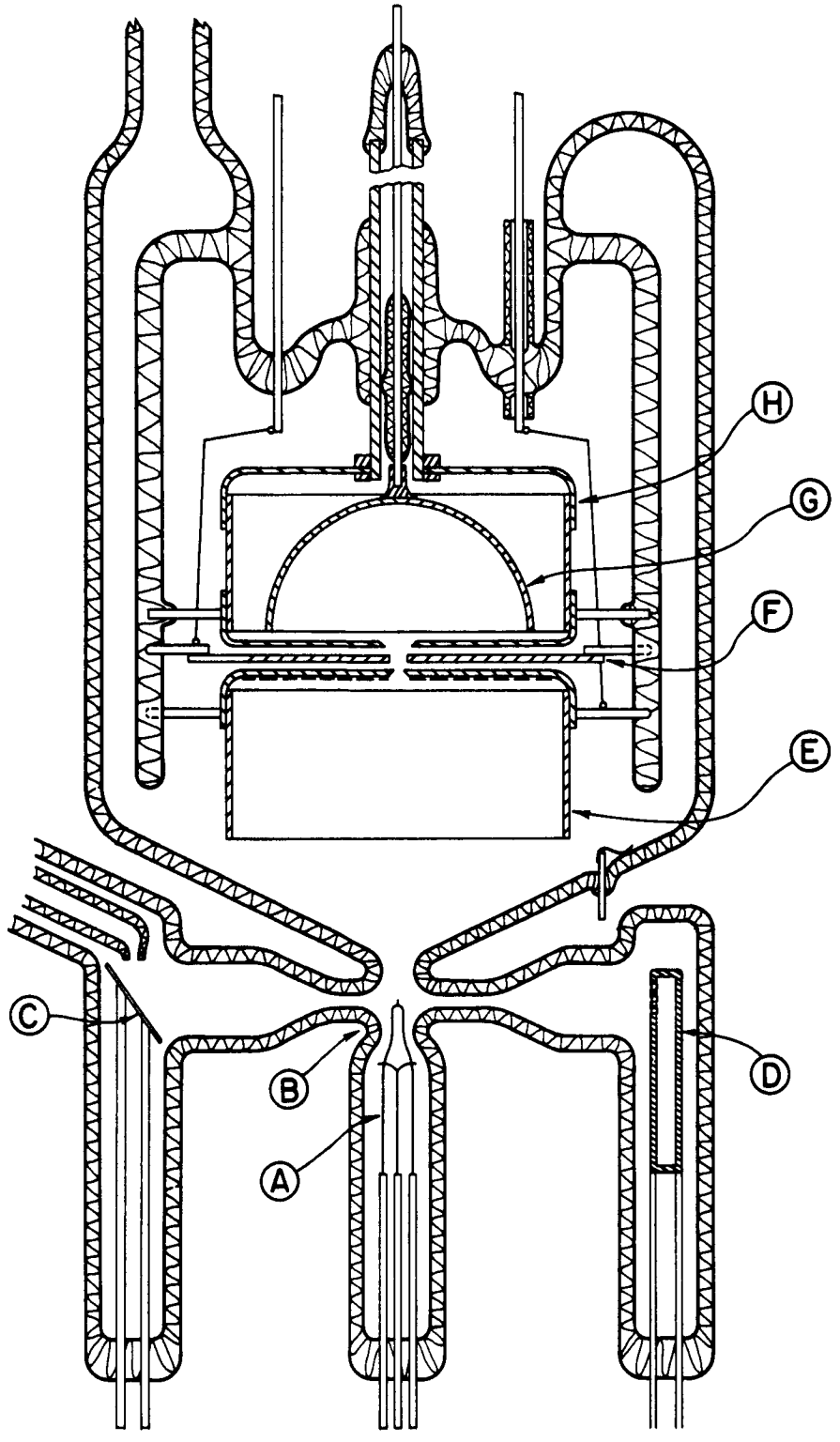

Figure 1. Diagram of coadsorption magnetic deflection probe tube. Tube contains following components:

(A) emitter assembly
(B) space for electromagnet
(C) cesium source platform
(D) oxygen source
(E) anode
(F) lens electrode
(G) spherical collector
(H) Faraday cage

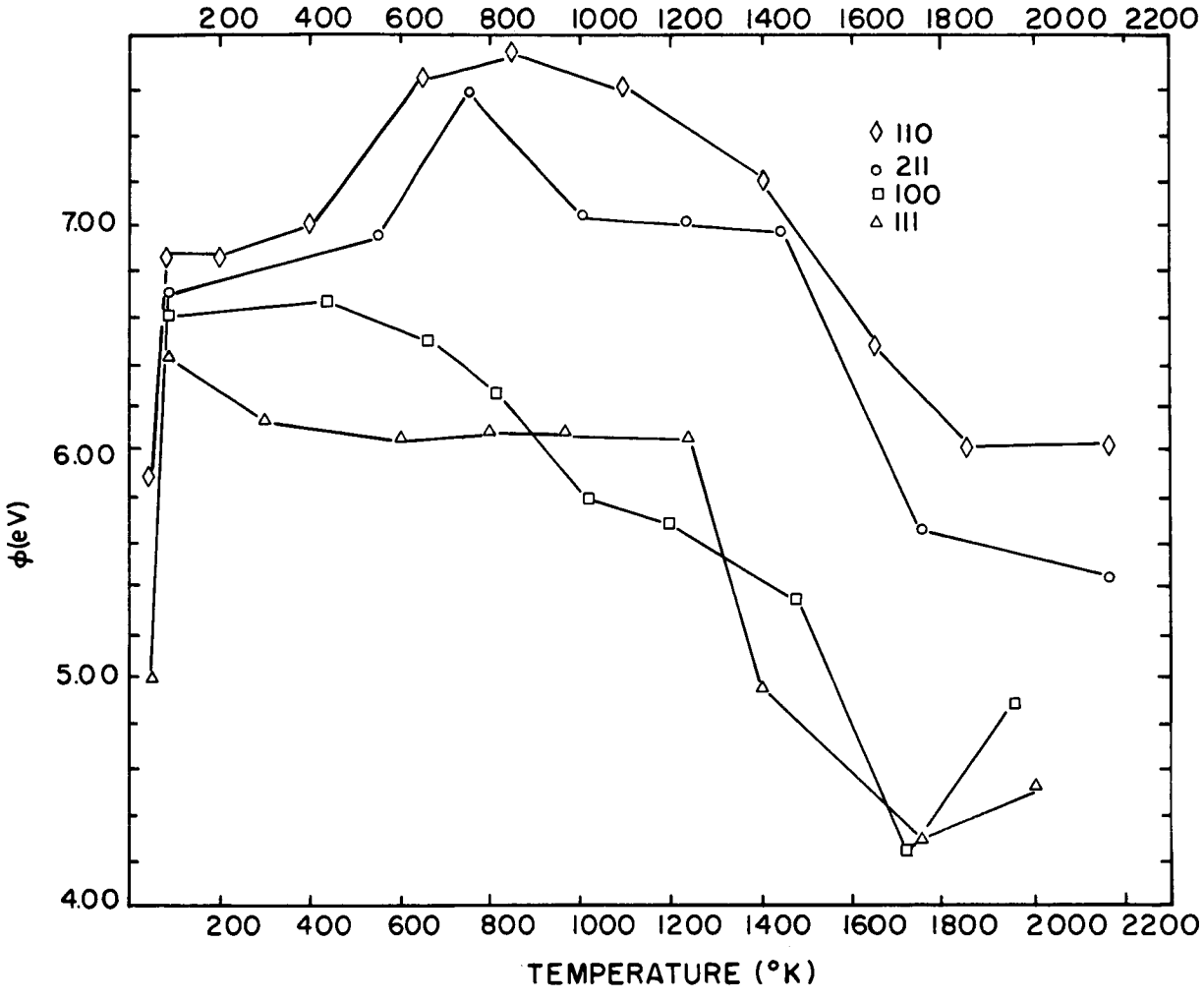

Figure 2. Work function versus 60 second heating temperatures for oxygen adsorbed on various planes of a tungsten field emitter.

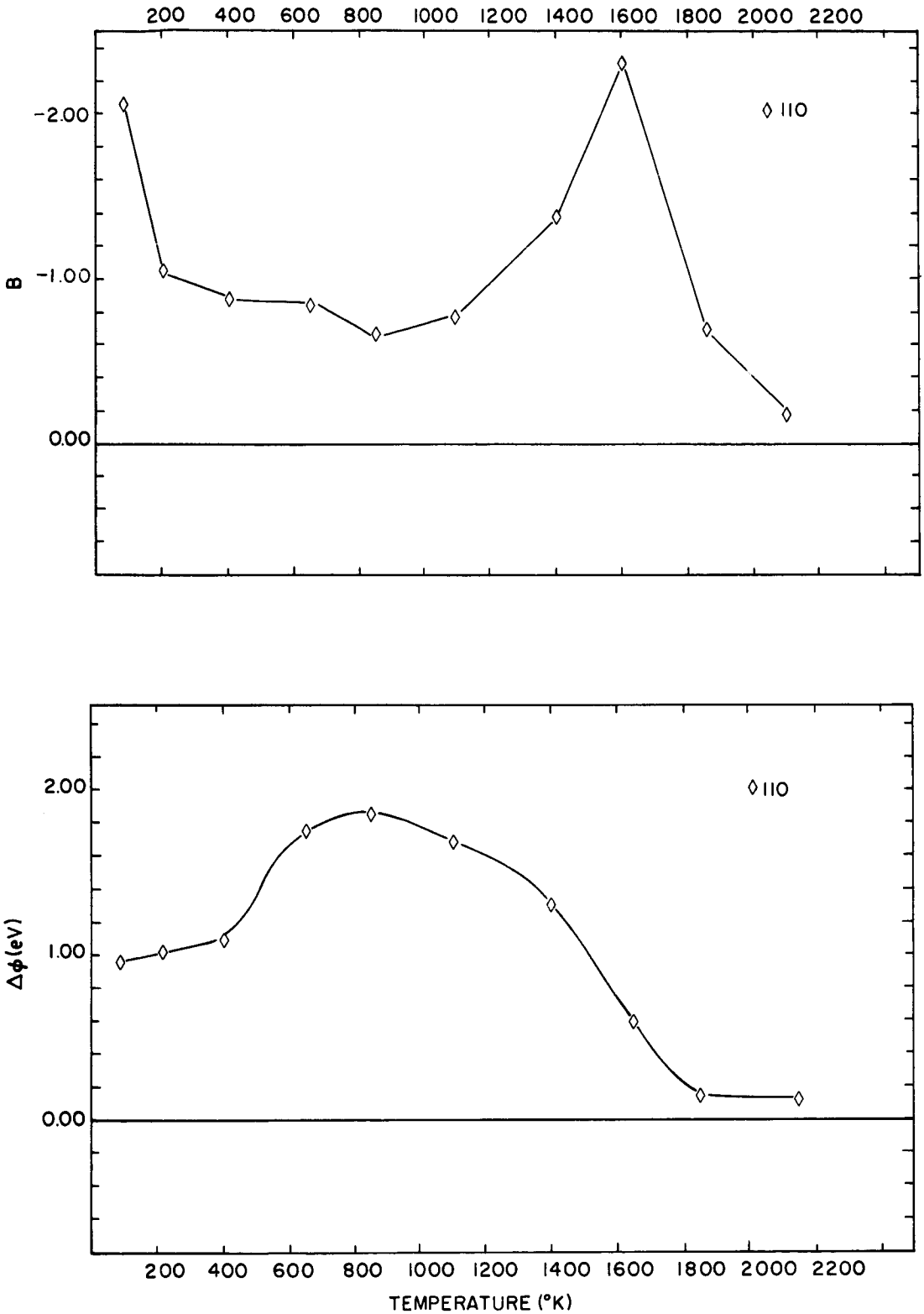

Figure 3. Dependence of work function change ($\Delta\phi$) and preexponential change (B) on 60 second heating temperature for oxygen adsorbed on 110 plane of tungsten.

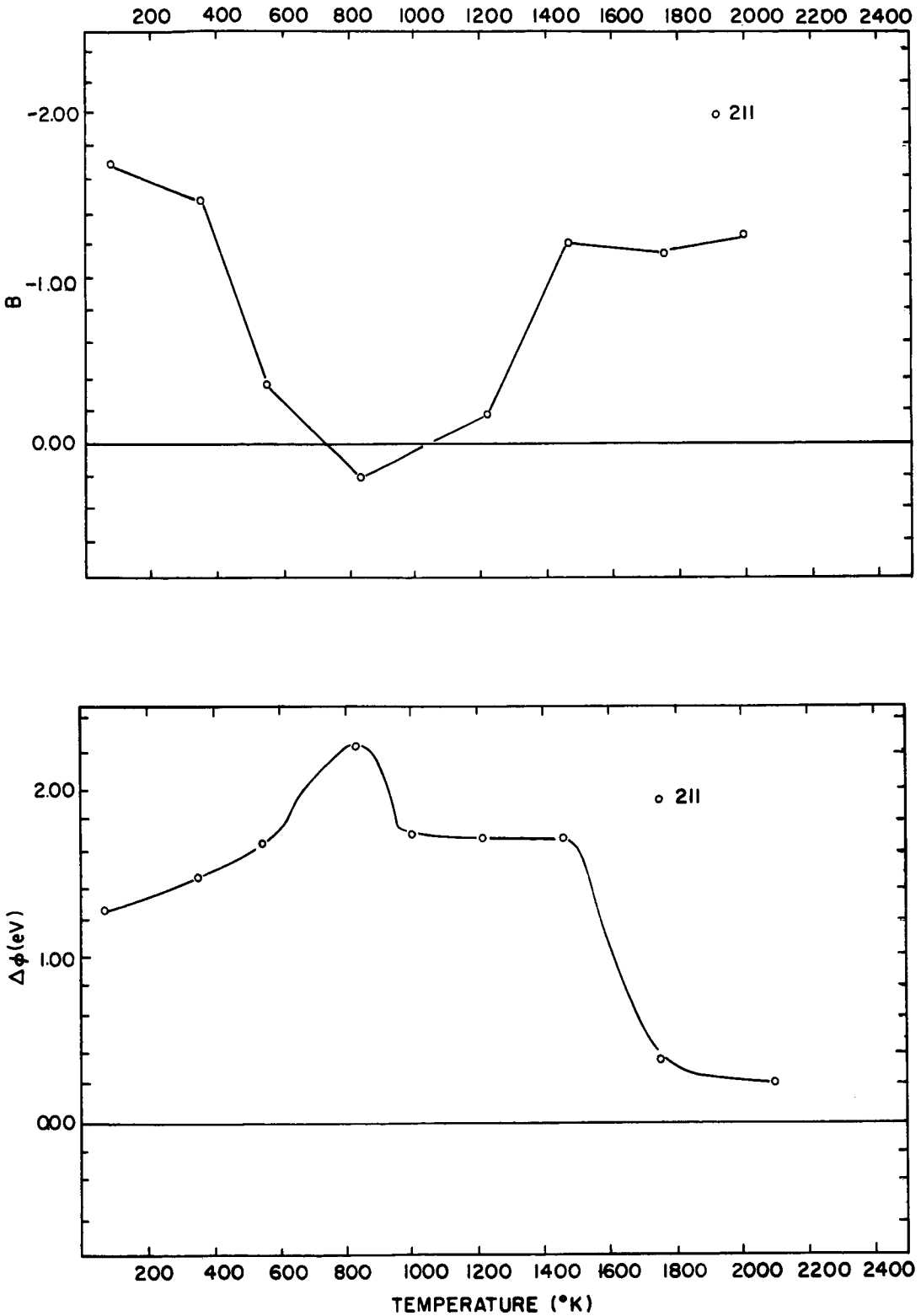

Figure 4. Dependence of work function change ($\Delta\emptyset$) and preexponential change (B) on 60 second heating temperature for oxygen adsorbed on 211 plane of tungsten.

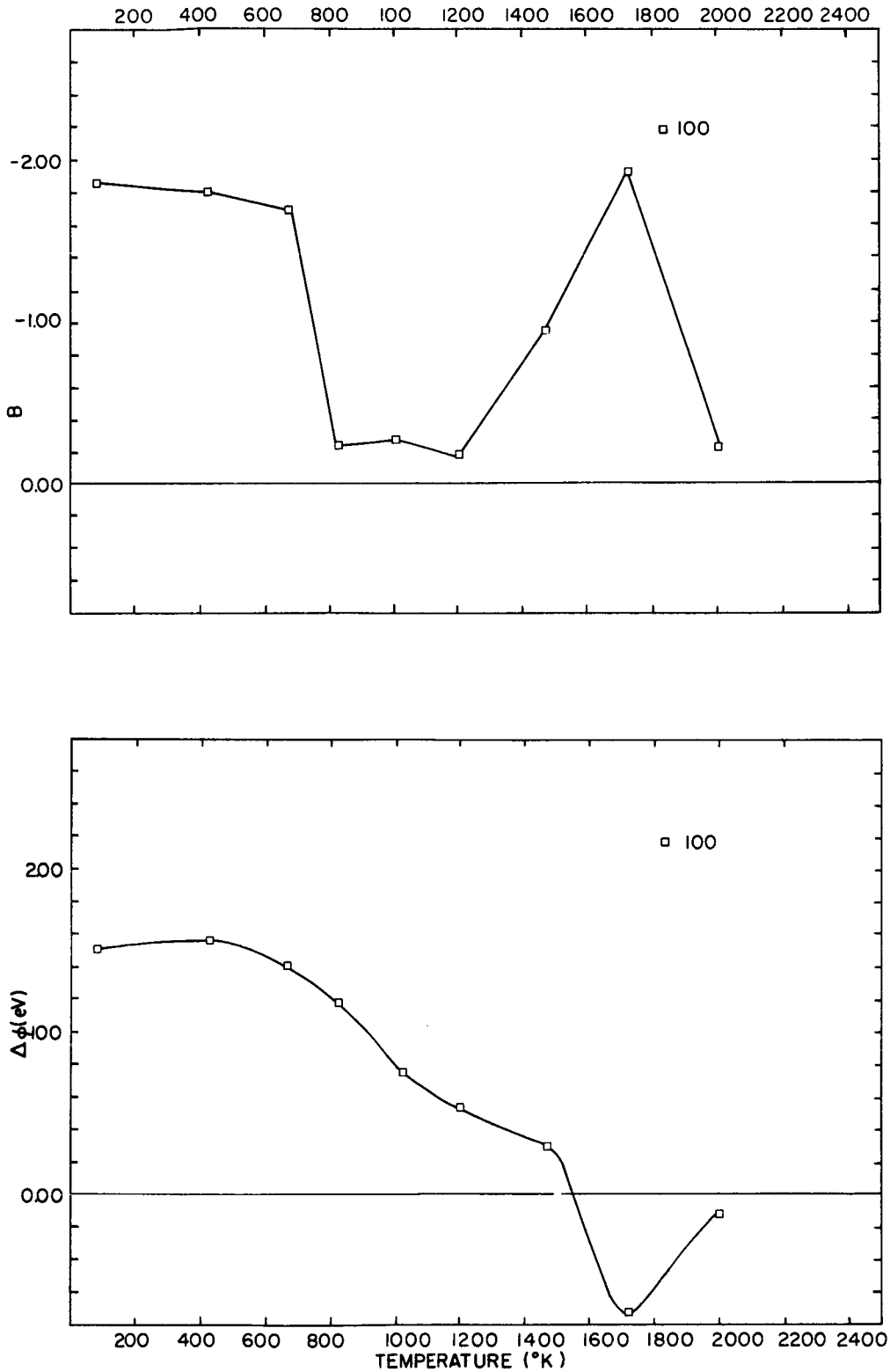

Figure 5. Dependence of work function change ($\Delta\emptyset$) and preexponential change (B) on 60 second heating temperature for oxygen adsorbed on 100 plane of tungsten.

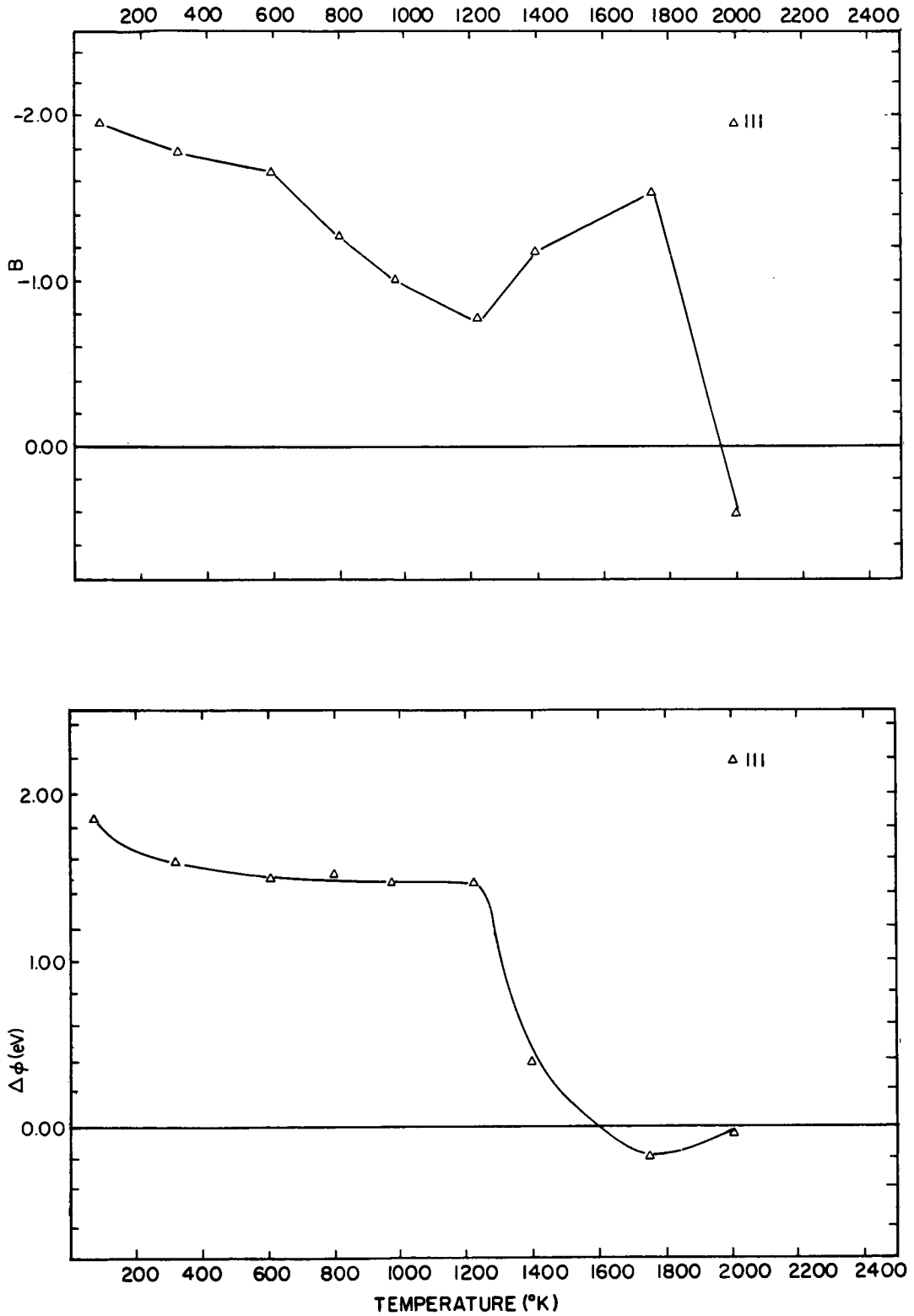

Figure 6. Dependence of work function change ($\Delta\phi$) and preexponential change (B) on 60 second heating temperature for oxygen adsorbed on 111 plane of tungsten.

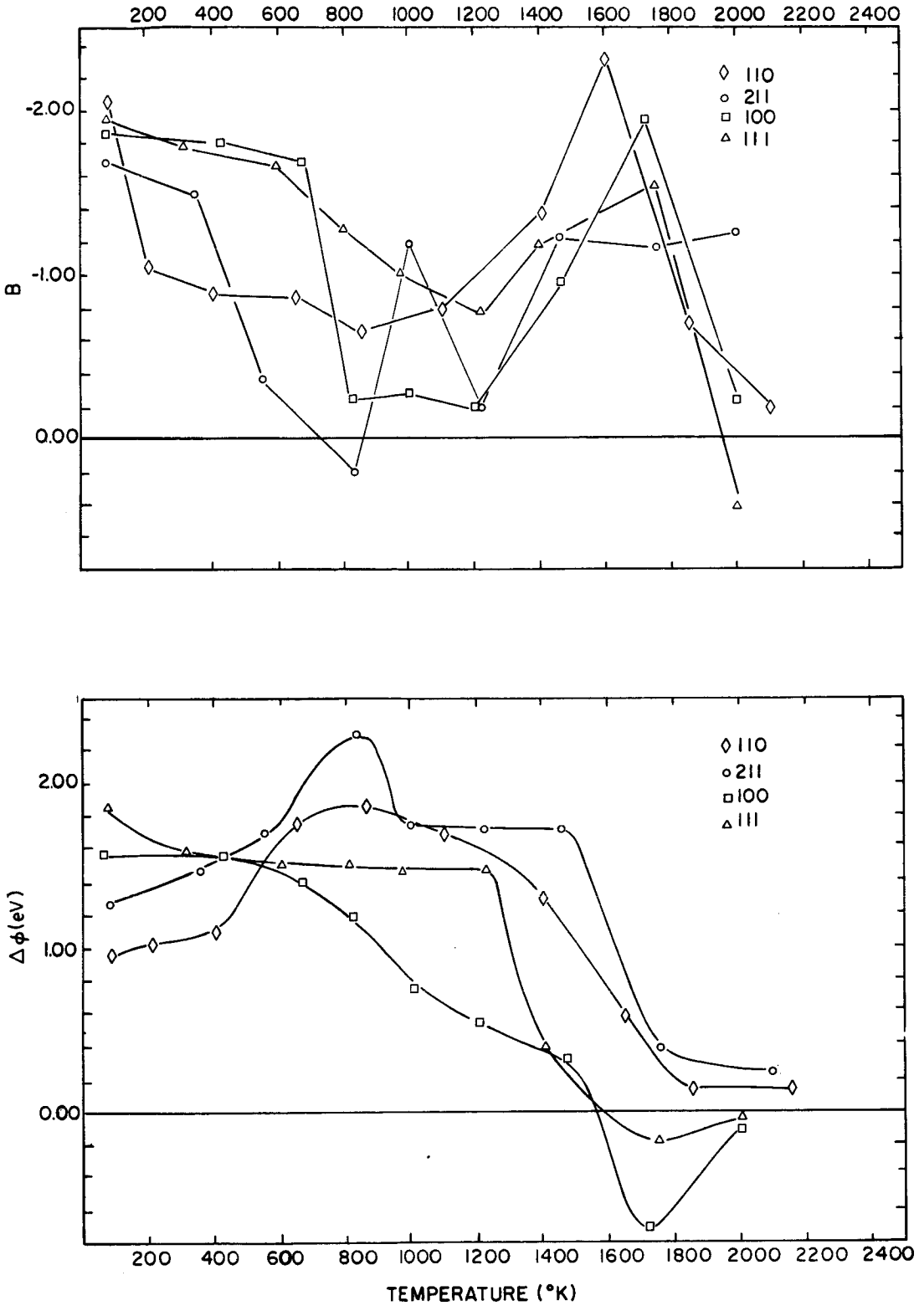

Figure 7. Dependence of work function change ($\Delta\phi$) and preexponential change (B) on 60 second heating temperature for oxygen adsorbed on 110, 211, 100 and 111 planes of tungsten.

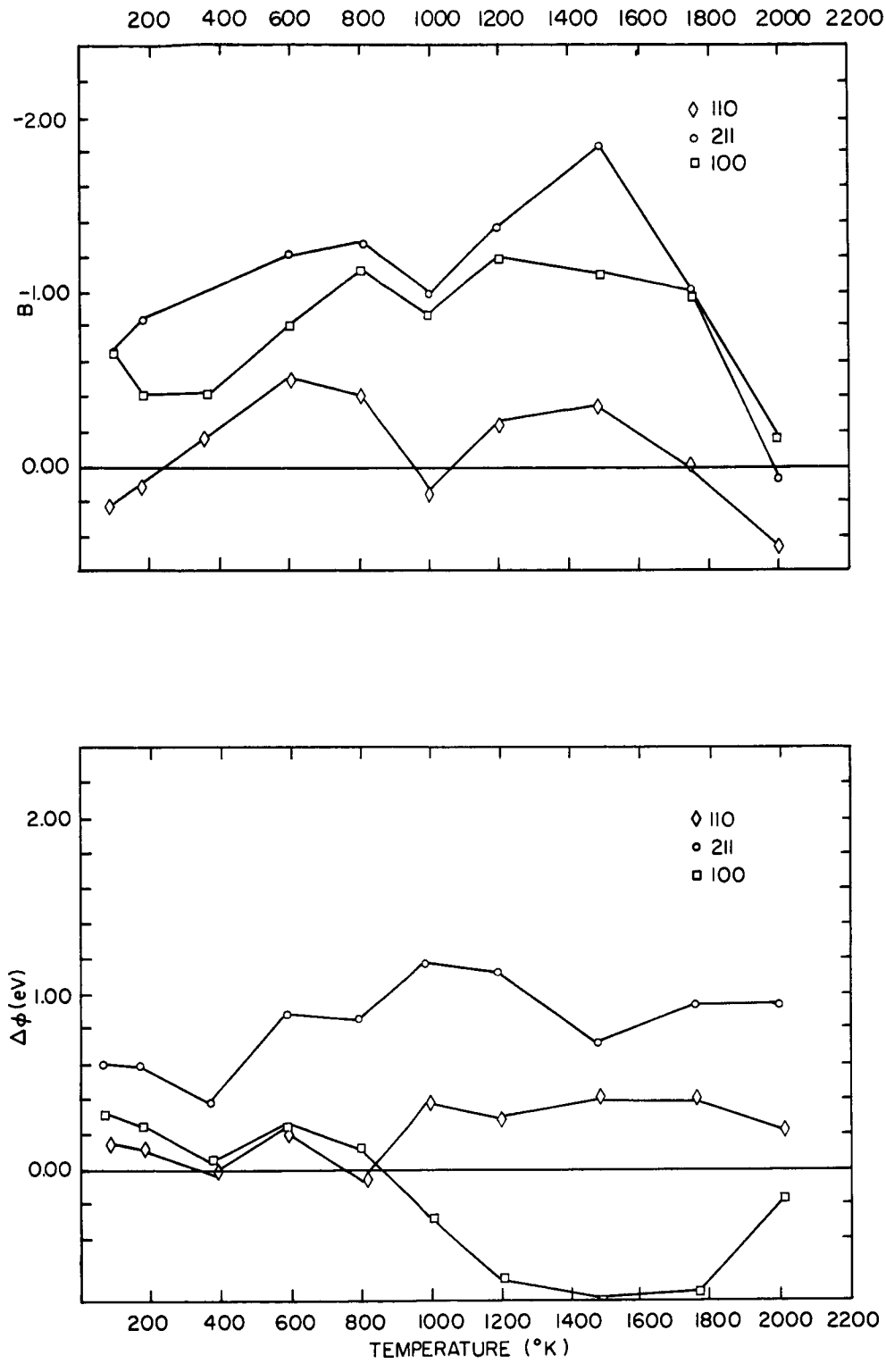

Figure 8. Dependence of work function change ($\Delta\phi$) and preexponential change (B) on 60 second heating temperature for the 110, 211, and 100 planes for the case of a partial monolayer of oxygen adsorbed on tungsten.

V THE EFFECT OF ELECTRIC FIELD ON THE DESORPTION RATES AND DISTRIBUTION OF CESIUM ON TUNGSTEN

INTRODUCTION

Although field emission has been extensively used as a tool for the investigation of the properties of adsorbed layers of cesium and other adsorbates, the employment of high fields in field emission subjects the interpretation of the results obtained to some uncertainty. For this reason it is desirable to investigate the various effects that arise from application of high fields. Two of these: field induced coverage changes of Cs on W and field desorption have been studied in this work. Provided that the Cs is sufficiently mobile, the application of a high field to the field emitter will, depending on the polarity of the field employed, either increase or diminish the concentration of Cs in the high field region. Field desorption, however, is a phenomena of wider occurence. Thus it may be applied to the desorption of electronegative and electropositive adsorbates; moreover, positive or negative ions may be desorbed if the appropriate polarity field is employed. Positive ion desorption is favored, from high work function surfaces, and negative ion desorption from low work function surfaces. Evidence for negative ion desorption of F^- will be presented in the next section. Field

desorption occurs when the applied field is high enough so that the potential energy curve for ionic desorption intersects the potential energy curve for neutral desorption close to the bottom of the neutral one. In this case ionic desorption may take place with a diminished activation energy when the bound atom receives an amount of thermal energy sufficient to excite it beyond the intersection of the ionic and neutral curves. The diminished activation energy is a function of field and its determination enables the zero field energy of desorption to be measured; additionally the shape of part of the potential energy curve for the interaction of neutral atoms with the substrate may be calculated.

FIELD EFFECT ON COVERAGE

The field effect phenomenon which was discovered[1] during measurements of the variation with temperature of the work function of Cs covered W and Mo emitters arises from the electrostatic interaction between the applied field and the dipole moment of the adsorbed Cs. This interaction alters the chemical potential, μ , of the adsorbed Cs, some of which then migrate either to or from the tip, until μ (tip) = μ (shank) once more. Average coverages in the above work were obtained from work functions derived from total field emission current measurements made with the tip at 78°K. Field dependent coverage changes were effected by heating the Cs covered emitter until the Cs became mobile at which point the emitter was subjected to an electric field

until Cs migration had ceased. The new equilibrium coverage was then frozen in by cooling the tip to 78°K with the field on. Although the coverage change is temperature dependent, the time constant for the establishment of surface equilibrium is long compared to the emitter time of cooling from 200-300°K to 78°K so that the coverage determined at 78°K should be close to that existing prior to quenching.

A procedure similar to that described above has been employed to obtain the effect of field on coverage for Cs adsorbed on the (100) plane of W. The data that has been collected so far was obtained by measuring the coverage change (as determined by the work function change) as a function of both positive and negative fields at 300°K. As in the case of the previous work, positive fields (tip positive with respect to screen) were limited to those which did not induce field desorption while negative fields were kept below those which produced excessive electron emission. Cs surface coverages, σ, were obtained from work function measurements by using a previously established σ versus ϕ relationship. A plot of ϕ versus electric field, F, is shown in Figure 1 and suggests a linear variation of σ with F, in which positive fields (tip positive) give rise to increased Cs concentrations. This last result agrees with earlier work concerning changes in average emitter surface concentration with field. Over the field range investigated the total change in $\Delta\phi$ as determined by Fowler-Nordheim plots was approximately 0.075 eV, although the large deviation of individual values of ϕ render this value subject to considerable error.

until Cs migration had ceased. The new equilibrium coverage was then frozen in by cooling the tip to 78°K with the field on. Although the coverage change is temperature dependent, the time constant for the establishment of surface equilibrium is long compared to the emitter time of cooling from 200-300°K to 78°K so that the coverage determined at 78°K should be close to that existing prior to quenching.

A procedure similar to that described above has been employed to obtain the effect of field on coverage for Cs adsorbed on the (100) plane of W. The data that has been collected so far was obtained by measuring the coverage change (as determined by the work function change) as a function of both positive and negative fields at 300°K. As in the case of the previous work, positive fields (tip positive with respect to screen) were limited to those which did not induce field desorption while negative fields were kept below those which produced excessive electron emission. Cs surface coverages, σ, were obtained from work function measurements by using a previously established σ versus ϕ relationship. A plot of ϕ versus electric field, F, is shown in Figure 1 and suggests a linear variation of σ with F, in which positive fields (tip positive) give rise to increased Cs concentrations. This last result agrees with earlier work concerning changes in average emitter surface concentration with field. Over the field range investigated the total change in $\Delta\phi$ as determined by Fowler-Nordheim plots was approximately 0.075 eV, although the large deviation of individual values of ϕ render this value subject to considerable error.

The field induced change $\Delta \phi = 0.08$ eV corresponds to $\Delta\sigma = 0.16 \times 10^{14}$ atoms/cm^2 so that σ varied from 1.82 to 1.98 x 10^{14} atoms/cm^2 under the influence of a field change of 48 MV/cm.

The physical basis for the field effect which was indicated in the preamble to this section has been discussed more fully in a previous report[1] in which the following equation was derived:

$$kT \ln \frac{\sigma_t(\sigma_o - \sigma_s)}{\sigma_s(\sigma_o - \sigma_t)} = E_a^o(\sigma_t) - E_a^o(\sigma_s) + \frac{\alpha F^2}{2} + |\mu| F, \qquad (1)$$

where $E_a^o(\sigma_t)$ and $E_a^o(\sigma_s)$ should be approximately equal to the coverage dependent zero field adsorption energies, σ_t and σ_s are the surface coverages of Cs on the tip and shank respectively and σ_o is the surface monolayer density; α is the polarizability of the adsorbed Cs and $|\mu|$ is the magnitude of the dipole moment of the adatom. The fact that the sign of the field effect varies with field is evidence that the $|\mu| F$ term is one of the important terms in Equation (1). If we let

$$R = \frac{\sigma_t(\sigma_o - \sigma_s)}{\sigma_s(\sigma_o - \sigma_t)},$$

and consider the change in each quantity, Equation (1) becomes

$$kT \, \Delta \ln R = \Delta E_a^o + |\mu| \Delta F, \qquad (2)$$

where $\Delta E_a^o = E_a^o(\sigma_s)$ and ΔF is the field change corresponding to the coverage change $\Delta\sigma_t$. Provided $\alpha \sim 0$ and the assumptions underlying the derivation of Equation (1) are correct μ may be derived from

$$\mu = \frac{kT \Delta \ln R - \Delta E_a^o}{\Delta F}. \qquad (3)$$

The coverage change was estimated by inspecting a curve of $\Delta\phi$ versus σ obtained[2] for Cs on the 100 plane of W and noting the change in σ corresponding to $\Delta\phi = 0.08$ eV at $\phi = 1.75$ eV. The slope of the ϕ versus σ curve at this point is 0.49×10^{-14} (eV - cm^2/atoms) so that a $\Delta\phi$ of 0.08 eV corresponds to a coverage change of 0.16×10^{14} atoms/cm^2. Earlier data[2] indicates that for average heats of adsorption of Cs on a W field emitter, a coverage change of 0.16×10^{14} atoms/cms^2 at $\phi = 1.75$ eV corresponds to a value of $\Delta E_a^o \sim 0.1$ eV. Work of Schmidt and Gomer[3] indicates that the heats of adsorption of K on different planes of W converge to that of the average heat of adsorption at high coverages so that there is some justification for our use of the average value in Equation (3). Substituting $T = 300^oK$, $\Delta F = 1.6 \times 10^5$ esu/cm, $\Delta E_a^o = 0.1$ eV and $R = 1.2$ in Equation (3) we find that $\mu = 1.05$ Debye, and that the term $kT\Delta \ln R$ makes a contribution of only 0.05 Debye to μ.

The dipole moment may also be estimated from the Helmholtz equation, $\Delta\phi = 4\pi\mu\sigma$ which gives a value of $\mu = 4.5$ Debye. The field effect value estimated above is significantly smaller than this; moreover it is smaller than the values (3.7 - 4.3 Debye) estimated in earlier field effect work dealing with average emitter coverage changes. Two experimental uncertainties may combine to produce the low estimate of μ from the field effect work. These are: the uncertainty about the value of the coverage change induced by the field and the uncertainty about the value of ΔE_a^o to be used in Equation (3). An error in the estimate of the coverage change may easily have arisen because of the proximity of the working range of coverage to that which

corresponds to a minimum in the value of the work function. Close to this minimum, the slope of $\Delta\phi$ versus σ varies rapidly so that small errors either in the determination of ϕ or in the establishment of the ϕ versus curve would result in large errors in estimates of the slope of the ϕ versus σ curve and hence in a large error in the estimate of the coverage change corresponding to the measured work function changes. In addition, the actual value of F interacting with μ may be reduced by an effective dielectric constant of the adsorbed layer. This correction which has not been considered, would result in larger calculated values of μ from the field effect on coverage.

In view of the above uncertainties, the order of magnitude agreement between the values of μ calculated above is reasonable.

FIELD DESORPTION

Field desorption experiments have been attempted at three Cs coverages $\sigma = 2.5 \times 10^{14}$, $\sigma = 1.5 \times 10^{14}$ and $\sigma \lesssim 0.1 \times 10^{14}$ atoms/cm^2 on the 100 plane of W. For a particular temperature and field the time was measured for the collector current to change from one value to another at a fixed tip voltage using the same initial and end point field emission currents. Such measurements were taken at each desorbing field over a temperature range large enough to allow construction of a reliable Arrhenius plot. It was hoped that a series of such plots could be obtained for different fields

in each coverage interval. At the highest Cs coverage five such plots were obtained corresponding to activation energies of desorption, E_p^F, of from 0.16 to 0.56 eV; the lowest energies being associated with the highest fields. A plot of E_p^F against field is shown in Figure 2 and is similar to that described in earlier work[2] in which total field emission currents were used for end points. A plot (Figure 2a) of field against the temperature required to complete the desorption run in 100 seconds, in which the temperature values obtained would be proportional to E_p^F if the preexponential for field desorption does not vary much with field, exhibits a minimum at 55 MV/cm^2. A similar though less well defined minimum is discernable at the same field in the E_p^F versus F curve.

Field desorption carried out in a coverage range just below that corresponding to the minimum value of $\emptyset$ was found to be severely regenerative. Once initiated the desorption proceeded very rapidly so that the total change in the (100) work function occurred only in the last 2 or 3 seconds of a run of 60 - 1000 seconds duration. Moreover the desorption frequently resulted in all of the Cs on the front of the emitter being desorbed so that the final field emission pattern contained only a bright ring on the rim of the anode screen which was caused by emission of electrons from the Cs remaining on the low field region of the emitter shank. Because of the lack of reproducibility in the desorption times, attempts to obtain Arrhenius plots in this coverage range were abandoned; instead the field required to cause desorption in 10 seconds or less was determined at different temperatures for

the same initial Cs coverage. The plot of field against temperature is linear (Figure 3) and is thus markedly different from the plot of field against temperature which was obtained in the high coverage range; also the field range is much smaller in the former case.

Field desorption runs were also obtained at very low Cs coverages and Figure 4 illustrates the variation of probe current at fixed field with desorption in this coverage range is seen to be initially very rapid and finally very slow. This behavior resembles that of Cs field desorption in the high coverage range ($2.2 \times 10^{14} < \sigma < 2.4 \times 10^{14}$ atoms/cm^2). Wide differences in the final probe current values were obtained from different runs even though they were characterized by similar initial current values. Consequently no attempt was made to obtain activation energy data because such uncertainties in end point probe currents corresponded to even greater uncertainties in desorption times. An interesting feature of all the final probe currents is that they are still higher by about 50 percent than that corresponding to the clean (100) plane.

DISCUSSION

The rate of field desorption is given by:

$$\frac{-d \ln \theta}{dt} = \nu \exp\left[\frac{-E_P^F}{kT}\right], \qquad (4)$$

where θ is the relative coverage of Cs on the emitter, ν is the preexponential factor and E_P^F is the field dependent desorption energy. Integration of this equation leads to:

$$-\ln\left(\frac{\theta_i}{\theta_f}\right) = \nu \exp\left[\frac{E_P^F}{kT}\right] t, \tag{5}$$

where θ_i and θ_f are the initial and final end points. This equation predicts that E_P^F will be proportional to T if θ_i, θ_f and t are maintained constant. An estimate of may be obtained from the last equation:

$$\ln\left[\ln\left(\frac{\theta_i}{\theta_f}\right)\right] = \ln\nu \frac{-E_P^F}{kT} + \ln t. \tag{6}$$

Since $\theta_i \sim \theta_f$ we may approximate:

$$\ln\left(\frac{\delta}{\theta_f}\right) = \ln\nu \frac{-E_P^F}{kT} + \ln t, \tag{7}$$

where $\theta_i = \theta_f + \delta$ · δ was estimated to be 0.13 for the field desorption carried out in the coverage range about $\sigma = 2.4 \times 10^{14}$ atoms/cm^2. From the smooth curves (a) and (b) in Figure 2 together with the time of 10 seconds and the value of $\delta \sim 0.13$, the curve of log ν versus electric field in Figure 5(a) was constructed. Preexponential values obtained in an earlier investigation of field desorption using total emission currents for end points were essentially constant throughout the field range. If this value of log ν = 13 is inserted in Equation (7) together with values of T obtained from Figure 2(a), then new values of E_P^F may be obtained. These are represented in Figure 5(b) by circles. Interesting features about curves 2(a), 2(b) and 5(b) are that they all indicate a

minimum in the relationship between E_P^F and F. Moreover the derived curve, 5(b), has a minimum value of E_P^F very close to that observed in the earlier work referred to above; in addition, the minima in both of these investigations occur at very nearly the same value of F.

A first order approximation to the relation between the field desorption energy E_P^F has been derived[2]:

$$E_P^F = E_a^o + I - \phi - e^{3/2} F^{1/2} + \mu F + 1/2 (\alpha_a - \alpha_i) F^2 + \Delta\phi^F, \qquad (8)$$

where E_a^o is the zero field heat of desorption, I is the adsorbate ionization potential, $\Delta\phi^F$ is the field induced contribution to the work function and α_a and α_i are the polarizabilities of the adsorbate atoms and ions respectively. The existence of a maximum in the curve of E_P^F versus is adequately explained by this equation which is of the form:

$$E_P^F = A - BF^{1/2} + CF + DF^2. \qquad (9)$$

If Equation (9) is differentiated with respect to F and the position of the calculated minimum is compared with the experimental value, then a relationship between B, C and D is obtained. The constant B should be universal and if its value is assumed to be known, then C may be expressed in terms of D. Possible pairs of values for C and D are given in TABLE I. By inserting the coordinates of the minimum of curve 5(b) in Equation (9) a value of A may be found for each pair of values of C and D. From A, E_a^o may be obtained since $A = I - \phi + E_a^o$; however only a narrow range of values of C and D about the values of $C = 2.08 \times 10^{-3}$ and $D = 1.92 \times 10^{-4}$ was consistent

with both a positive value of E_a^o and a value of C corresponding to a dipole moment of no less than 1 Debye. The above values of C and D corresponded to μ = 1 Debye, α = 55 $\mathring{A}^3$ and E_a^o = 0.2 eV, a value which is smaller than that measured in earlier work[2]. If the earlier value of E_a^o = 0.8 eV is assumed correct, then Equation (7) will only describe the main features of Figure 5(b) if $B > e^{3/2}$, where e is the electronic charge. Sets of values of α, μ and B consistent with Figure 5(b) and E_a^o = 0.8 eV are given in TABLE I. The solid line in Figure 5(b) was calculated from Equation (9) by using B = 0.46, E_a^o = 0.8 and C and D values corresponding to α = 55 $\mathring{A}^3$ and μ = 1 Debye, a value calculated from the field effect described in the first part of this section of the report.

Whether or not the field desorption data can be analyzed in terms of Equation (8) or the more generalized form (9) depends upon the validity of the model used to derive Equation (8). The model assumes that ionization of the adsorbate atom takes place before the adsorbate particle passes over a Schottky hump at a distance from the surface of $x_s = e^{1/2}/2F^{1/2}$. Values of x_s less than the atomic radius of Cs are predicted so that the above model may not be a realistic one. However the clear existence of the minimum in the curve of E_P^F versus F indicates the necessity of including terms such as CF and DF^2 in the expression for E_P^F.

The regenerative nature of field desorption which is initiated at a coverage below that (σ_{min}) corresponding to the work function minimum is due to the fact that ϕ increases faster than E_a^o as σ declines except for $\sigma < 0.2 \times 10^{14}$ atoms/cm^2. Gomer and Swanson[4] have presented an analysis of a

first-order desorption which proceeds with a coverage dependent activation energy of desorption. Thus if $|\eta|/kT \gg \theta^{-1}$, throughout the interval, where $\eta \sim (\partial E_a^o / \partial \theta - \partial \phi / \partial \theta)$ and provided that $\exp |(\theta_f - \theta_i)g/kT| \gg 1$, the rate constant for field desorption devolves into the following relations:

$$k_i = \nu \exp \left[- E_P^F / kT \right] = (kT/\theta_i |\eta|)/t \qquad (10)$$

$$k_f = \nu \exp \left[- E_P^F / kT \right] = (kT/\theta_f |\eta|)/t \qquad (11)$$

where θ_i is the initial coverage and θ_f the final one. The first relation holds if η is positive and the second one if η is negative. Since $\partial \phi / \partial \theta$ is negative and exceeds $\partial E_a^o / \partial \theta$, the first relation applies and we have:

$$\log \nu = E_P^F / 2.30\ kT - \log t + \log (kT/\theta_i \eta) \qquad (12)$$

Using a value of $\log \nu = 13$, $t = 10$ seconds, $\theta_i = 0.5$ and $\eta = 4.4$ eV/unit coverage, the lowest temperature used, $T = 78^oK$ corresponds to $E_P^F = 0.29$ eV while the highest corresponds to $E_P^F = 0.74$ eV. These values are plotted in Figure 5 (squares) and straddle the curve calculated from the field desorption data presented above.

REFERENCES

1. L. W. Swanson, R. W. Strayer and F. M. Charbonnier, Surface Science 2, 177 (1964).

2. L. W. Swanson et al., Final Report Contract NAS3-2596 Field Emission Corp., McMinnville, Oregon, June 1964.

3. L. D. Schmidt and R. Gomer, J. Chem. Phys. 45, 1605 (1966).

4. L. W. Swanson and R. G. Gomer, J. Chem. Phys. 39, 2813 (1963).

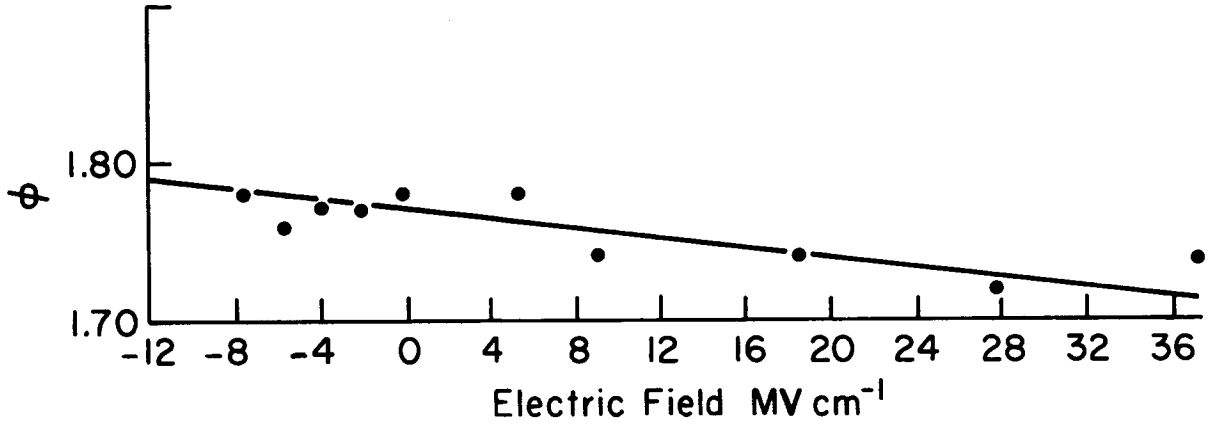

Figure 1. Curve illustrating decline of ϕ with field for Cs on the 100 plane of W.

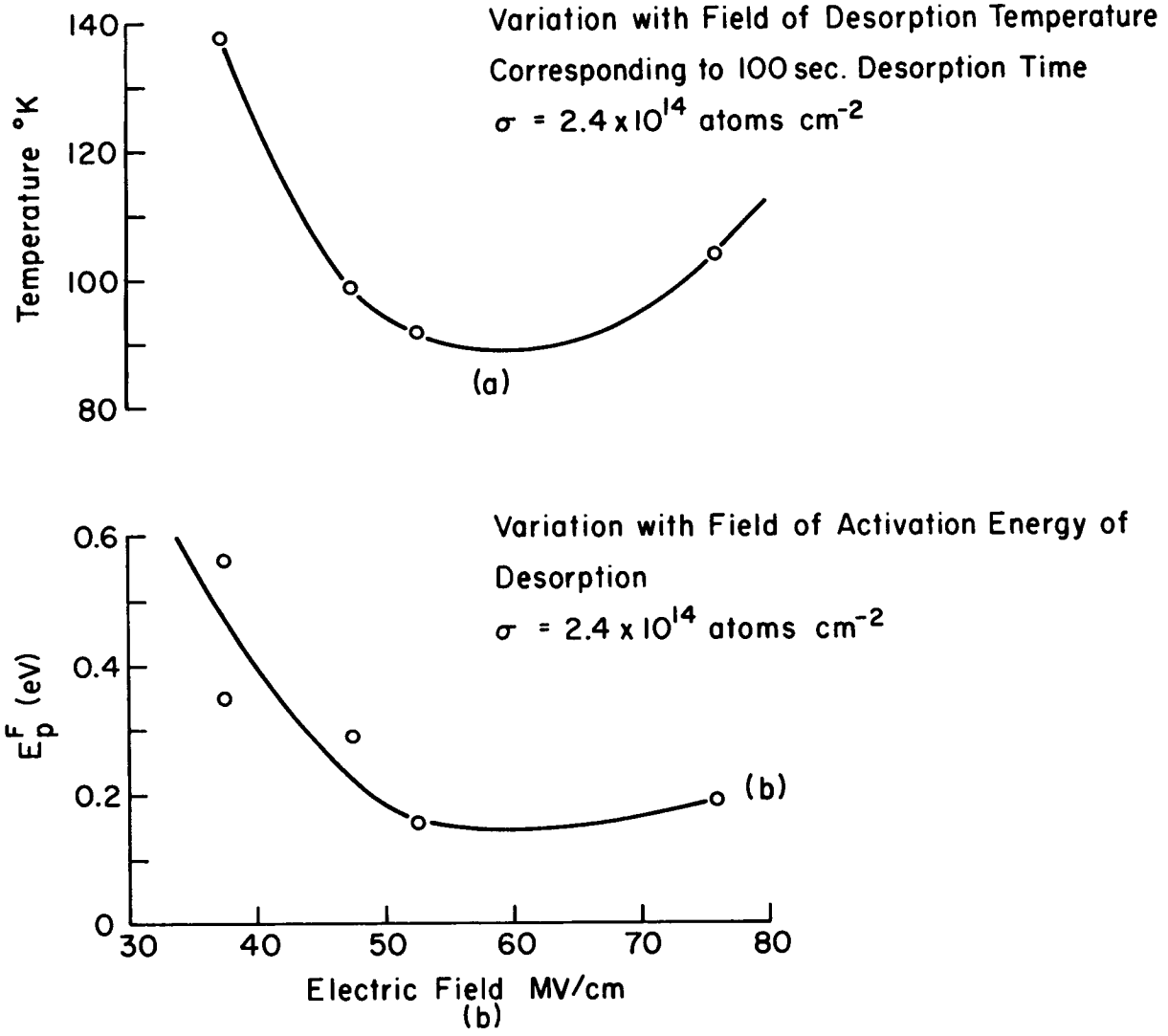

Figure 2. Curves illustrating (a) variation with field of desorption temperature corresponding to 100 second desorption time ($\sigma = 2.4 \times 10^{14}$ atoms/cm^2) and (b) variation with field of activation energy of desorption ($\sigma = 2.4 \times 10^{14}$ atoms/cm^2), each referring to the 100 plane of W.

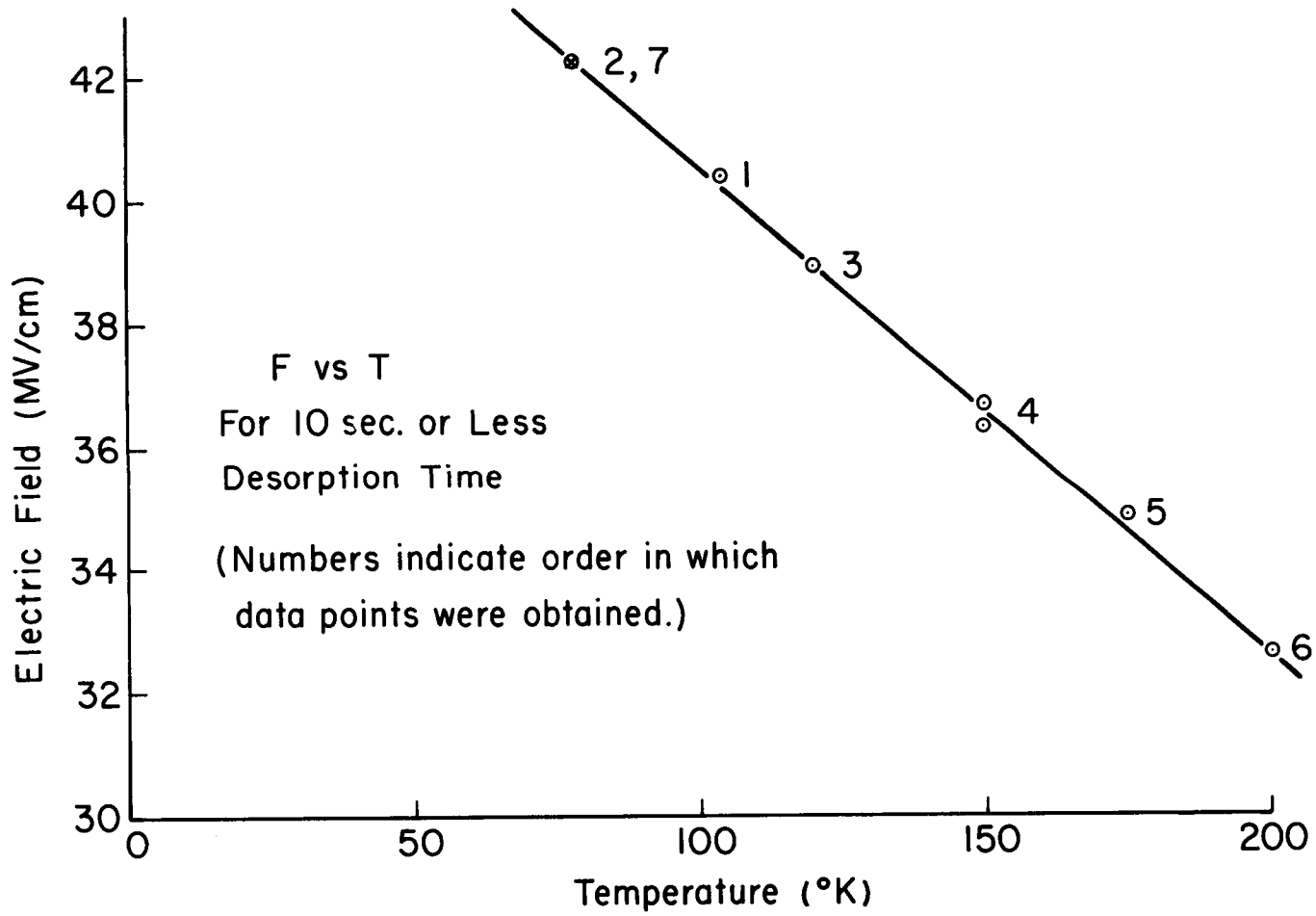

Figure 3. Plot of field desorption of Cs from W(100) against temperature for a desorption time of 10 seconds or less at ϕ = 2.1 eV and σ = 1.5 x 10^{14} atoms/cm^2. (Numbers indicate order in which data points were obtained.)

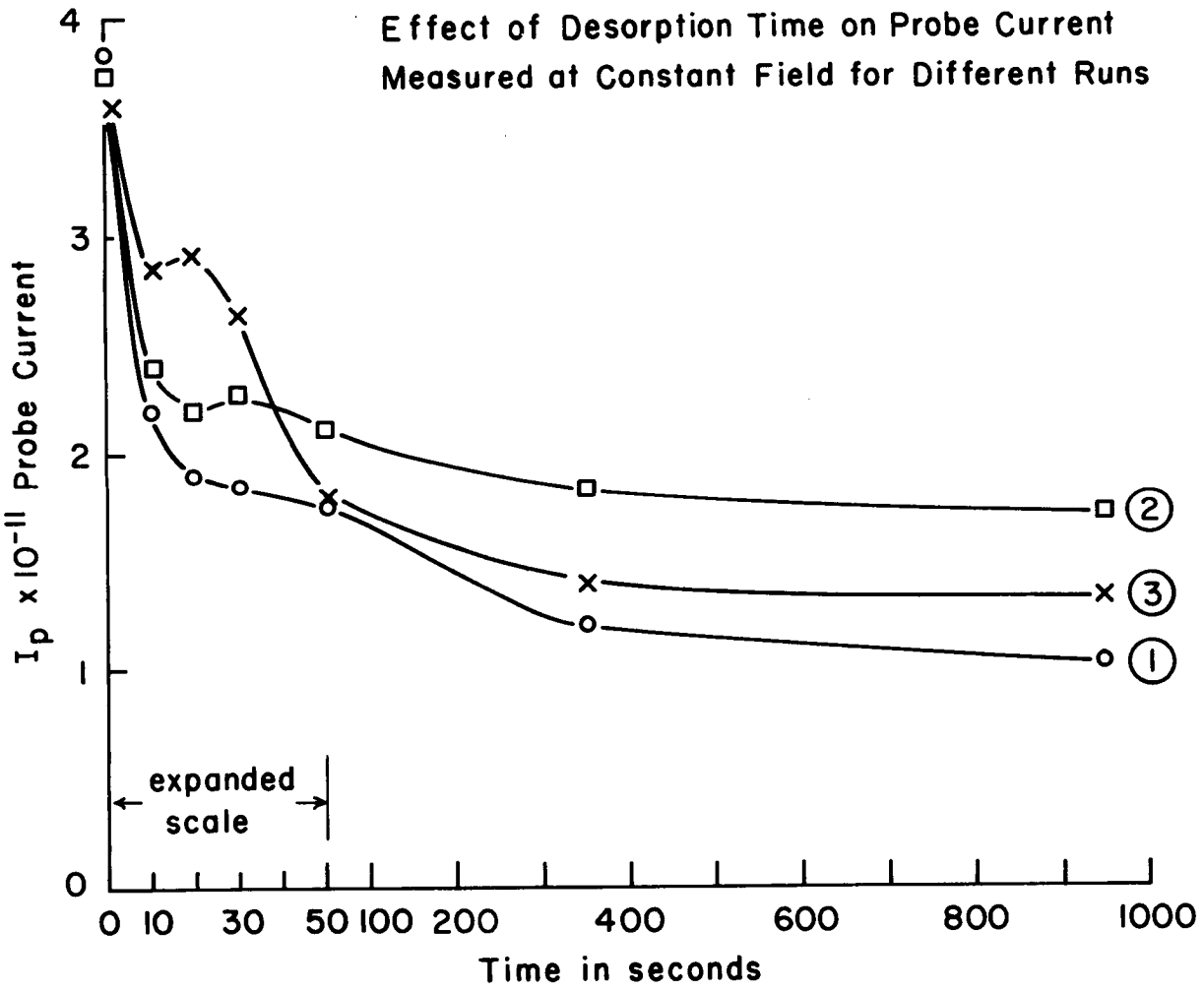

Figure 4. Effect of field desorption time on the 100 plane probe current measured at constant field for different runs which are numbered at end of various curves. (Field = 38 mV/cm and $\sigma \cong 0.1 \times 10^{14}$ atoms/cm^2) Temperature was 78°K.

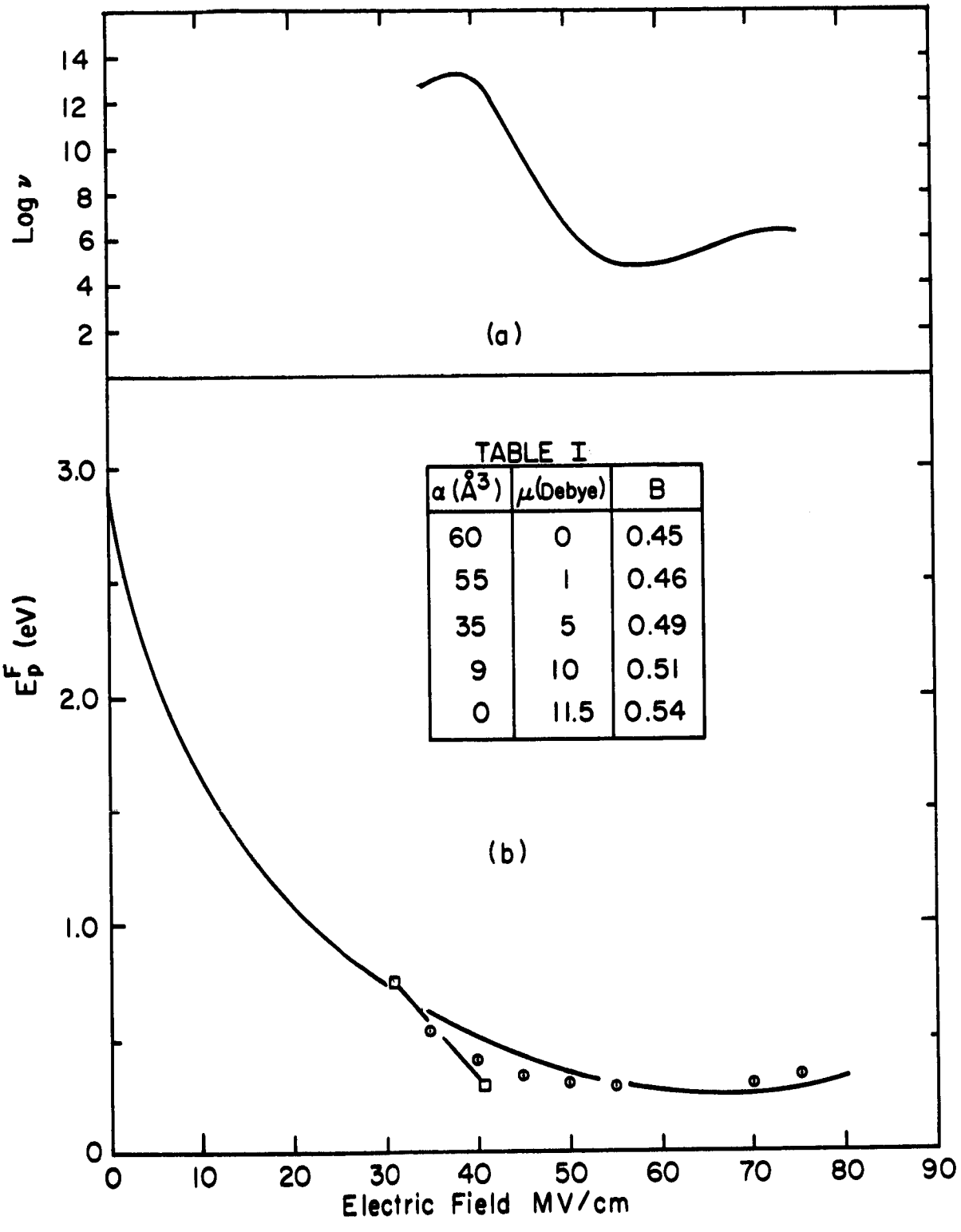

Figure 5. Curve (a) is a plot of logν versus F. The solid line in (b) is a plot against F of E_p^F calculated from Equation (9). Shown also are values of (⊙) E_p^F calculated from the T/F data of Figure 2(a) by assuming logν = 13. The square symbols represent values of E_p^F obtained from Equation (12).

VI ADSORPTION OF CESIUM FLUORIDE ON TUNGSTEN

INTRODUCTION

In the study of low work function adsorbates the favorable properties of the alkali and alkaline earth metals have long been recognized. For cesium adsorbed on tungsten, work function decreases of approximately three volts have been obtained and even greater decreases were obtained when Cs was deposited on top of a chemisorbed layer of oxygen[1,2]. In addition, an increase in binding of the Cs to the substrate is effected by the presence of O. In view of the enhanced work function lowering $\Delta\phi$ of coadsorbed systems involving highly electropositive and electronegative adsorbates it is of interest to examine the most extreme example of electropositive and electronegative adsorbates, namely the CsFW system. Some of the pertinent physical properties of O and F are summarized in Table I.

TABLE I

Physical Properties of Oxygen and Fluorine

	Ionization Potential (Volts)	Atomic Radius (A)	Electronegativity (Pauling Scale)	Electron Affinity (Volts)
O	13.55	0.60	3.5	1.46
F	17.34	0.50	4.0	3.45

An earlier field emission study of the CsFW system by Wolf[3] has shown remarkable similarities to the CsOW system. For example, deposition of CsF on W was observed to yield a work function as low as 1.1 eV. The field emission pattern yielding this low ϕ in the CsFW system is characterized by bright 211 planes. A similar bright 211 pattern has been observed in the CsOW system yielding a work function of 1.61 eV. Since work functions as low as 1.13 eV have been measured in this lab for the CsOW system, one might expect even lower work functions in the analogous system CsFW. Unfortunately, Wolf employed a CsF source which automatically forced him to work, at least after the initial deposition, with the stoichiometric ratio of Cs/F. Because gaseous fluorine is awkward to handle in vacuum systems we also employed a source of CsF from which both CsF and F could be deposited onto the emitter. As in the case of the CsOW system, the Cs can be removed from a CsFW layer by thermal heating leaving a layer of chemisorbed F. In this way desired amounts of F up to a F-W layer work function of 5.1 eV could be attained. In order to allow greater flexability in the ratio of Cs/F a separate source of Cs was also incorporated into the tube; in this way the variation of ϕ with Cs coverage for various underlying F coverages could be investigated in a fashion similar to the CsOW system.

EXPERIMENTAL

It was first hoped that a chemical source could be obtained which would yield a flux of F molecules when heated in vacuum. Such sources have

been successfully employed for the production in situ of O and H. Cobalt trifluoride was finally considered for trial and a source receptacle consisting of a platinum bucket supported by nichrome heating leads was filled with the finely powdered compound and sealed into a standard field emission tube. After the tube had been processed by the usual evacuation and baking procedures, the platinum bucket was raised to a dull red heat and maintained at this temperature for several hours. The relatively high thermal capacity of the source bucket and its contents allowed the nichrome heating leads to be momentarily outgassed at bright red heat. In spite of these precautions taken to ensure outgassing of the source material, copious amounts of carbon monoxide were liberated when an attempt was made to dose the emitter with F. Continued heating of the source tended to deplete the supply but remaining uncertainties about the nature of the adsorbate - was it carbon monoxide, fluorine, a cobalt fluoride or a mixture of any or all of these - led to the abandonment of this approach to F preparation.

Other potential F sources have been considered and one of them has now been successfully used. These methods involve a binary F compound which was deposited onto the emitter and the F left behind upon heating the emitter. The compound finally decided upon was CsF which is sufficiently volatile to be deposited by heating a platinum bucket containing it to a dull red heat. The amount of F deposited in a single dosing sequence is probably determined by the size of the Cs atoms of which about one Cs atom to every four W atoms is enough to constitute a monolayer of adsorbate. A greater

concentration of F than one to every four surface W atoms can be achieved by removing the Cs from the first dose and redepositing more CsF and then heating the adsorbate layer to $\sim 1000^{\circ}K$. Because of the need to heat to this temperature it is likely that the resultant F layer will be incomplete.

The construction of the field emission microscope for the coadsorption study shown in Figure 1 was standard except for provisions made to measure and control the emitter temperature[4]. Pattern viewing was accomplished by pulse techniques to eliminate any field effects due to viewing voltage. The tip temperature is derived from an accurate measurement of the resistance of a small section of the emitter's supporting filament C as described in Section IV. This makes use of the fact that the resistivity of W is a well-known, monotonic, and nearly linear function of temperature over the range of interest. The resistance of a segment of the loop was determined by passing an accurately known dc current through it and measuring the potential difference across it by means of two small leads attached to the filament. The resistance was calibrated by measuring it at several well-determined temperatures. The tube shown in Figure 1 contains a Cs source consisting of a platinum disc onto which Cs was condensed and subsequently sublimed onto the tip by controlled resistive heating of the disc. The CsF source consisted of optical grade crystals which were thoroughly outgassed during tube evacuation by placing them in a resistively heated platinum bucket. After seal off the tube was placed in a liquid N_2 cryostat; CsF could be deposited onto the emitter in pure form by heating the platinum bucket to $\sim 900^{\circ}K$.

The application of the field emission microscope to an investigation of the work function change of various substrates on adsorption is made possible by the well-known and experimentally confirmed Fowler-Nordheim law of field emission. This law may be expressed in terms of the directly measurable field emission current I and applied field F_a as

$$I = \frac{BF_a^2}{\phi t^2(\phi, F_a)} \exp\left[-\frac{b\phi^{3/2} v(\phi, F_a)}{F_a}\right], \quad (1)$$

where $t(\phi, F)$ and $v(\phi, F)$ are tabulated nondimensional functions[5] which take into account the image correction, B is proportional to emitting area, and $b = 6.8 \times 10^7$ where F_a is in V/cm, and ϕ in eV. Although Equation (1) is the zero-degree approximation, it holds reasonably well at higher temperatures provided ϕ is sufficiently large. By defining the field factor $\beta = F_a/V$ where V is the applied voltage, Equation (1) may also be written as:

$$\ln I/V^2 = \ln A + m/V, \quad (2)$$

where A is the intercept and m is the slope of a "Fowler-Nordheim" plot of the I(V) data plotted in the form $\ln I/V^2$ vs I/V. The slope m may be written as follows:

$$m = \frac{b\phi^{3/2} s(\phi, F_a)}{\beta}, \quad (3)$$

where $s(\phi, F_a)$ is another tabulated function[5]. In the range of F_a and ϕ, encountered in this investigation Equations (1) and (3) may be simplified by the following close approximation:

$$v(\phi, F_a) = 0.943 - 0.146 \times 10^{-6} F/\phi^2 \quad (4)$$

from which it can be easily shown that $s(\phi, F) = 0.943$. Using the known work function ϕ_s of the clean surface as a reference, and assuming β to be unchanged by adsorption, the work function ϕ at the surface when coated with an adsorbate can then be determined from Equation (3) written as follows:

$$\phi = \phi_s \left[\frac{m\, s(\phi, F_a)}{m_s\, s(\phi_s, F_a)} \right]^{2/3}, \tag{5}$$

where m_s and m are the slopes of the corresponding Fowler-Nordheim plots.

THE GENERAL BEHAVIOR OF CsF ON W

Migration

A deposit of CsF, considerably less than a monolayer, was unilaterally deposited onto the emitter at 77°K. The emitter was then heated for 60 second intervals at increasing temperatures and the pattern sequence of Figure 2 obtained. At temperatures below 142°K the original deposit transformed into what appeared to be a two phase system corresponding to a two dimensional dilute and condensed phase system shown in pattern (b). As the emitter temperature is raised to 160°K the high concentration phase recedes and the dilute phase migrates across the emitter giving typical Cs on W patterns. It should be mentioned that similar evidence of two dimensional phase separation was also observed for the CsW and CsOW systems[1, 2].

Consistent with the observations of Cs on clean W, the migration of Cs is complete at ~250°K and no further pattern change occurs until T ≅ 384°K at which temperature the overall pattern begins to attain a symmetrical distribution as seen in pattern (f) and, in addition, the overall work function lowers somewhat.

The above behavior can be explained by dissociative adsorption of the CsF and differential migration rates of the Cs and F. Apparently the Cs migrates in the usual temperature range of 150 - 250°K while the F migrates at a higher temperature range of 380 - 500°K. On the basis that CsF completely dissociates on adsorption one can consider the enthalpy H of the reaction

$$CsF\ (g) \xrightarrow{H} Cs\ (a) + F\ (a)\,, \tag{6}$$

where (g) and (a) refer to gas phase and adsorbed phase respectively. One can readily show from the thermochemical cycle that

$$H = H_{CsF} - H_{Cs\,-\,W} - H_{F\,-\,W}\,, \tag{7}$$

where H_{CsF} is the heat of dissociation of CsF and H_{Cs-W} and H_{F-W} the heat of adsorption of Cs and F respectively. Using Wolf's[3] value of $H_{F-W} = 6.38$, $H_{CsW} = 3.00$ and $H_{CsF} = 5.7$ eV, one obtains H = -3.68 eV. Thus, in view of the highly exothermic nature of Equation (6) it is not surprising to observe the complete dissociation of CsF upon adsorption.

Fluorine Adsorption - Desorption on Tungsten

By impinging a flux of CsF molecules on a W emitter held at 1200°K, Wolf showed that a F-W layer exhibiting a maximum value of ϕ_{FW} = 5.8 eV could be obtained. As will be shown later, above ~1000°K Cs is completely desorbed leaving a FW layer. Figure 3 shows plots of the value of ϕ_{FW} and $\ell n A$ [i.e., the preexponential term of Equation (2)] vs relative amount of CsF impinged on the emitter held at T = 1090°K. The accompanying patterns, which are indicated in Figure 3, are given in Figure 4; it was also found that upon termination of the CsF impingement and heating to higher temperatures, the F coverage gradually reduced to zero at T → 1800°K; also, the pattern sequence for desorption was identical to the adsorption sequence indicating reversibility. One of the interesting contrasts between the behavior of F and Cℓ or O on W is that, whereas complete thermal desorption of the latter two adsorbates lead to blunting of the emitter due to removal of $WC\ell_6^6$ or WO,[7] repeated desorptions of F from W do not cause significant changes in the emitter geometry.

A major discrepancy between our work and that of Wolf[3] is the much lower maximum value of ϕ_{FW} which in our case was only 5.16 eV as compared to 5.83 eV. Notice, however, that due to a decrease in $\ell n A$ a larger than expected decrease in emission occurs as F is added. Upon comparing our patterns with those published by Wolf, we find complete agreement; thus, assuming Wolf used the slope method of Equation (5) to obtain ϕ_{FW}, we have no explanation for the lower value of maximum ϕ_{FW} found in the present work. The near linear decrease in $\ell n A$ with F coverage may be

attributed to either a decrease in emitting area and/or the field induce dipole effect discussed in the O on W results (Section IV). There it was shown that $-\ell n A \propto \sigma_{FW}\, a$, where σ_{FW} is the F coverage and a its polarizability. In view of the much larger electron affinity of F relative to O one intuitively expects the maximum value of ϕ_{FW} to be at least as large as ϕ_{OW} (which is $\sim$6.2 eV). Thus, it appears that further studies of the FW system are warranted.

Adsorption of Cesium on a FW Layer

Figure 5 shows the ϕ vs relative Cs coverage relationship on a FW layer whose initial ϕ_{FW} = 4.97 eV. The data points were obtained by successive depositions of Cs, each one being followed by thermal equilibration. The shape of the curve is very similar to those observed on the OW surfaces except for the fact that a lower minimum work function value ϕ_m = 0.97 eV is obtained compared to a value of ϕ_m = 1.15 eV for a value of ϕ_{OW} = 5.65 eV. The value of $\ell n A$, after going through a minimum value at low coverage, exhibits a maximum at the coverage corresponding to ϕ_m. In other words the variation of $\ell n A$ with Cs coverage tends to enhance the effect of the work function lowering on maximizing the emission. Because of the possibility of variations in the effective emitting area with Cs coverage, which appears in the $\ell n A$ term, it is not warranted to pursue a calculation of the induced dipole effect as discussed in Section IV in connection with the single face studies of O on W.

The major changes in the emission distribution corresponding to the Figure 5 curve are shown in Figure 6. In contrast to the CsOW system

no enhanced emission is observed from the 112 planes at low Cs coverages. On the other hand, at Cs coverages approaching the coverage corresponding to ϕ_m strong emission from the 112 occurs in agreement with the CsOW system. Also in agreement with the CsOW system at ϕ_m the emission becomes rather uniform over the emitting area and at slightly higher Cs coverages the psuedo clean W emission distribution is observed in pattern (f) (compare with (a) of Figure 3). The latter also occurs at Cs coverages slightly greater than ϕ_m for both CsW and CsOW systems.

In order to gain further insight into the specific interactions involved in this composite system further studies of this nature in which the underlying F coverage is varied will be performed; also single face probe field emission investigations will provide more meaningful work function data to compare with theoretical models. Clearly F, like O, greatly enhances the work function lowering of Cs on W. For example, $\phi_m = 1.60$ eV for the CsW system whereas $\phi_m \cong 1.0$ eV for the CsF and CsOW systems. In the case of the CsOW system dipole moment calculation indicates that the underlying O enhances the transfer of electronic charge to the substrate, thereby greatly increasing the dipole moment formed by the positively charged adsorbed Cs and its image. Apparently, the same is true of the CsFW system even to a larger degree.

Desorption of Cesium from a FW Layer

The fact that a chemisorbed layer of O on W not only enhances the work function lowering the Cs, but also enhances the binding of Cs to the substrate was established earlier. As shown in Figure 7(a) chemisorbed layer

of F produces the same effect. At ϕ_m, for example, thermal desorption of Cs is effected at 530°K for an underlying chemisorbed layer of F, such that ϕ_{FW} = 4.98 eV, whereas for the CsW system a temperature of only 350°K is required. Also the temperature required to completely remove Cs from the FW layer in 60 seconds is ~1100°K, while for the clean W case only ~920°K is required. It should be pointed out that our study of desorption thus far pertains to atomic Cs. This was assured by properly biasing the emitter so as to return ionic Cs. Thus, the thermal stability of the composite system at ϕ_m is markedly increased by addition of F. As the temperature is increased above ~1300°K the F begins to desorb and the work function approaches the clean value of 4.52 eV.

By forming the FW surface in the manner described, we observe that Cs adsorption and desorption is completely reversible throughout the coverage range. This can be noted by the similarity in patterns whether obtained by adsorption or desorption; also, the variation of $\ell n A$ shown in the desorption sequence of Figure 7 is nearly identical to that observed in the adsorption sequence of Figure 5.

Temperature Dependence of ϕ for a CsFW Surface

The calculation of the work function at elevated temperatures by field emission techniques is given in Section III. For the CsW system the value of the temperature coefficient for the work function was $\Delta\phi/\Delta T \cong -1 \times 10^{-4}$ eV/deg. We have made a similar measurement for the CsFW layer at a coverage where $\phi \cong 1.72$ eV at T=77°K. As shown in Figure 8, the value of ϕ

decreases nearly linearly with T in the range 90 to 180°K. This temperature dependence of ϕ was completely reversible indicating the unlikelihood of desorption or migration of Cs. The value of the temperature coefficient of the CsFW system determined from Figure 8 is $\Delta\phi/\Delta T = -2.4 \times 10^{-3}$ eV/deg which is nearly an order of magnitude greater than that observed for the CsW system.

The sign of $\Delta\phi/\Delta T$ for the CsFW system is such that the dipole moment per adsorbed Cs must increase with temperature. This implies that either the dipole length and/or the net transfer of electronic charge to the substrate must increase with temperature. The idea that CsF forms a dipolar complex erected by the surface fields of the stubstrate put forth by Dykman[8] and expanded by others[9] is not supported by our value of $\Delta\phi/\Delta T$. Their model predicts a decreasing value of dipole moment with temperature whereas we observed an increasing value. It appears that a clearer picture of the nature of the adsorbed complex is necessary before the rather large temperature coefficient of work function can be understood.

Field Instability of the CsFW System

It was observed for CsFW, that in the range of work function values below 2.0 eV if the electric field F_a (for emitting electrons) was made sufficiently high, the emission current I began to decrease with time. Further, it was noted that the rate of decrease of the field emission current increased with F_a as shown in Figure 9 for T = 77°K. This phenomenon did not preclude measurement of ϕ by Fowler-Nordheim plots provided values of F_a and, hence, I were kept sufficiently low. The time dependent diminution in I with F_a was accompanied by a dimming of the bright emission from

the 112 planes as shown in Figure 6 (d). Generally, after the current had diminished, the original conditions could be restored by heating to ~115°K, although the temperature required for complete restoration increased as more such cycles were completed. It was also observed that after the emitted current diminution, say at 77°K, no restoration could be effected by reversing the field polarity.

A most interesting study of the temperature dependence of this phenomenon, shown in Figure 10, revealed a decrease in the rate and a leveling off of I with time with increasing temperature. At 115°K, as shown in Figure 10, very little net change in I occurs with time. We believe that the apparent negative activation energy for the rate of change of this process with time is due to a concomitant thermally initiated restoration process. This is supported by the fact that even at low temperatures (e. g., 77 - 90°K) the current slowly returns to its initial value as shown by spot checks of the value of I periodically with time after relaxing the field.

From the experimental observations of this phenomenon obtained thus far we have concluded that field desorption of negative fluoride ions F^- is responsible for the decrease in I with applied field. We picture the removal of F^- to cause a local net decrease in the dipole moment μ of a CsF complex thereby increasing ϕ. If we assume at the coverage at which this phenomenon occurs an excess of F exists relative to Cs, the work function is given by

$$\phi = \phi_s - g\pi\left[\mu_{Cs}\sigma_{Cs} - \mu_F\sigma_F\right], \qquad (8)$$

where σ_{Cs} and σ_F refer to the Cs and F coverage respectively, ϕ_s is the substrate work function and g is 2 or 4 depending on whether image or polarized dipoles are assumed. Clearly for ϕ to become smaller at a given value of σ_{Cs} upon addition of F, the increase in μ_{Cs} must override the increase in the $\mu_F \sigma_F$ term. Conversely, removal of F at a given coverage of Cs will cause ϕ to increase.

The fact that restoration occurs at such low temperature rules out the migration of F from the shank of the emitter where fields are too low to promote desorption of F. In fact even Cs is rather immobile at the restoration temperature of 115°K so that gross mobility of either Cs or F may be ruled out of the restoration process. A possible explanation is that only F^- from sites adjacent to adsorbed Cs are removed by field desorption and, provided that F^- exists in larger concentration than Cs, the Cs need only migrate a few lattice sites to be under the influence of remaining adsorbed F and re-exhibit the enhanced dipole moment.

The field desorption of negative halogen ions has been reported by Kirchner[10] who observed $C\ell^-$ desorption from $KC\ell$ layers on W. An examination of the energetics involved in field desorption of negative ions leads to the following expression for the activation energy E of desorption:

$$E = E_o + \phi - A_e - e^{3/2} F_a^{1/2} + aF_a + bF_a^2, \qquad (9)$$

where the symbols have the following meaning:

E_o - zero field activation energy of desorption

A_e - electron affinity of F

e - electronic charge

a and b - constants

The term linear in F_a comprises the field dipole interactions and field induce work function changes while the term quadratic in F_a involves field induced dipole interactions. The lowering of the Schottky saddle, represented by the $F_a^{1/2}$ term, is the dominate term so that a lowering of E and increase in rate with applied field is expected as observed in Figure 9. Clearly, the large values of A_e for F and small values of ϕ obtained in this system are conducive to field desorption of negative ions.

In view of the very low temperatures required for restoration it appears difficult to perform a quantitative investigation of the temperature dependence of the rate of F^- field desorption. If temperatures lower than 77°K are employed the high fields required to initiate desorption would be prohibited because of excessive field emission. By assuming a linear relationship between the change in work function with coverage, i.e., $\Delta\phi \propto \sigma_o - \sigma$ and recognizing that Equation (1), at constant F_a, can be written in terms of the ratio of the current I/I_o at ϕ_o and ϕ, then the following expression can be obtained:

$$\ln I/I_o = C_1' (\phi_o^{3/2} - \phi^{3/2}) \cong -C_2' \phi_o^{1/2} \Delta\phi \cong C_3' (\sigma - \sigma_o) \qquad (10)$$

where $\Delta\phi = \phi - \phi_o$. Thus, one can view the variation of $\ln I/I_o$ with time in Figure 9 as proportional to the coverage change of F with time. The rapid increase in rate of desorption (i.e., $d(\ln I/I_o)/dt$) with electric field is, thus, expected in view of Equation (9) and the following first order rate equation which normally characterizes field desorption:

$$-d(\ln I/I_o)/dt \propto -d\sigma/dt = k_o \sigma e^{-E/kT}, \qquad (11)$$

where k_o is the frequency factor. We therefore conclude that field desorption of F^- is the most likely explanation of the observed emitted current instability.

SUMMARY

The ability of F to greatly reduce the work function and increase the thermal stability of Cs on W is demonstrated by these results. Work function values of 0.97 eV and stable up to $\sim 500^{\circ}K$ have been obtained. Migration studies indicate complete dissociation of the CsF on adsorption so that surface migration of Cs occurs in the usual range of 150 - $250^{\circ}K$ while F does not become mobile until $T > 380^{\circ}K$. Adsorption and desorption of Cs on an FW layer, formed by impinging CsF on a W surface at $1200^{\circ}K$, is completely reversible leaving the FW layer unchanged.

Finally for CsFW layers exhibiting values of $\phi < 2.0$ eV and at sufficiently high applied fields, the removal of F^- by field desorption occurs. Complete restoration of the slightly field desorbed CsFW surface occurs, however, at $115^{\circ}K$.

REFERENCES

1. L. W. Swanson, et al., Final Report, Contract NASW-458, Field Emission Corp. (1963).

2. L. W. Swanson, et al., Final Report, Contract NAS3-2596, Field Emission Corp. (1964).

3. E. D. Wolf, Twenty-Fifth Ann. Conf. Physical Electronics, Cambridge, Massachusetts (March 1965) and private communication.

4. D. Zimmerman and R. Gomer, Rev. Sci. Instr. 36, 1046 (1965).

5. R. H. Good and E. W. Müller, Handbuch der Physik 21, 176 (1956).

6. M. Silver and R. S. Witte, J. Chem. Phys. 38, 872 (1963).

7. R. Gomer and J. K. Hulm, J. Chem. Phys. 27, 1363 (1957).

8. I. M. Dykman, Ukr. Fiz. Zh. 1, 81 (1956).

9. L. K. Tower, NASA Technical Note, TN D-3223.

10. F. Kirchner and H. A. Ritter, Z. Natmforschg. 11a, 35 (1956).

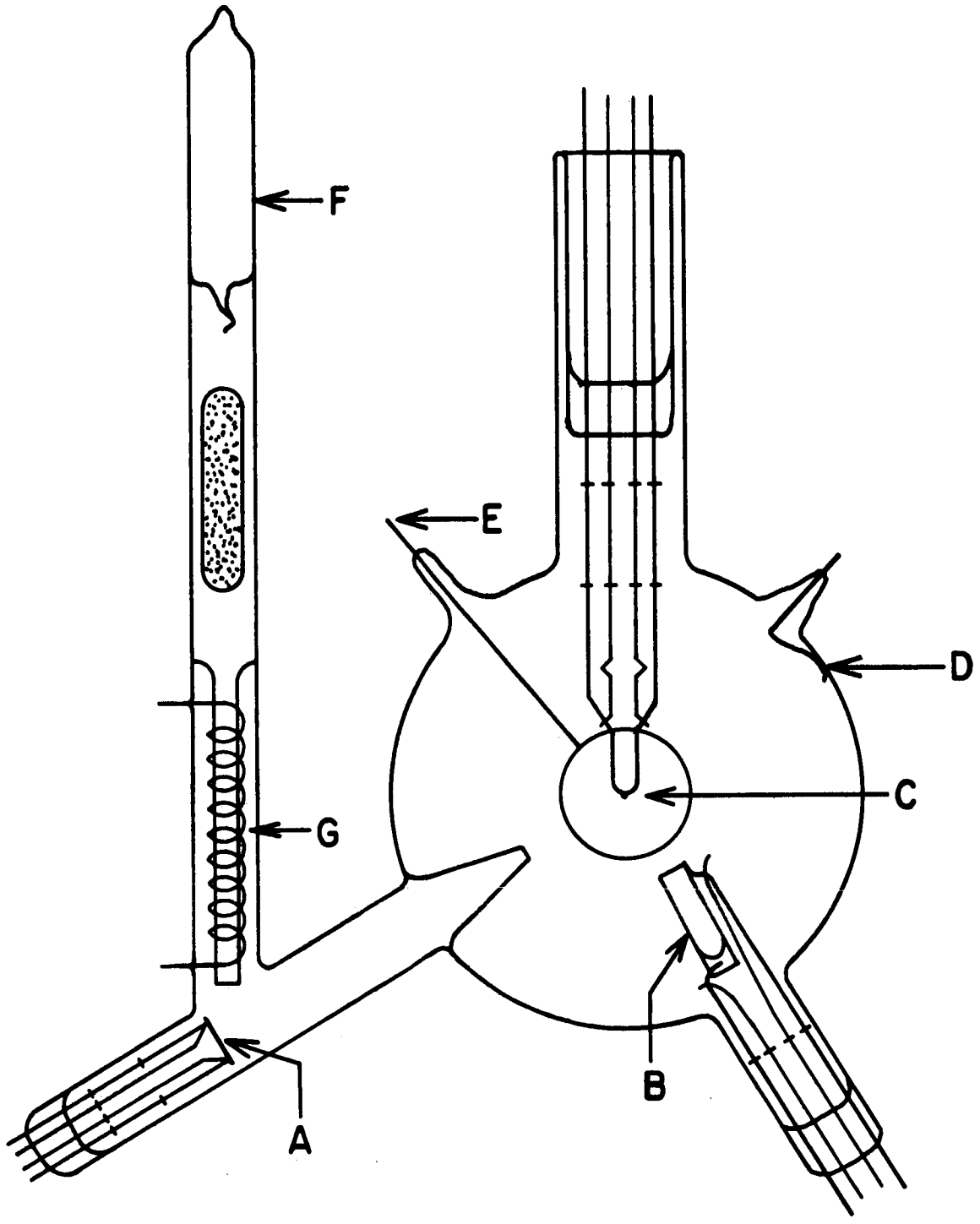

Figure 1. Front view diagram of field emission microscope for investigation of cesium and fluorine on tungsten. A, cesium source; B, fluorine source (heatable platinum crucible containing cesium fluoride); C, emitter assembly; D, electrical connection to conductive coating; E, anode ring; F, cesium reservoir; G, secondary cesium source.

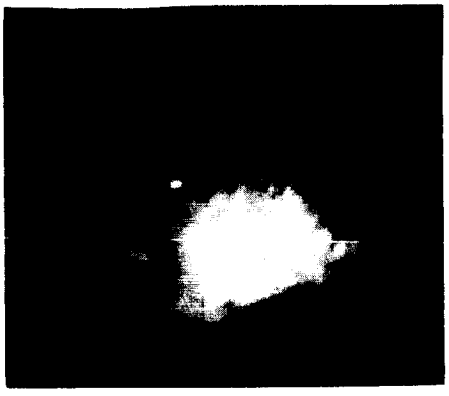

(a)
Initial dose at 77°K

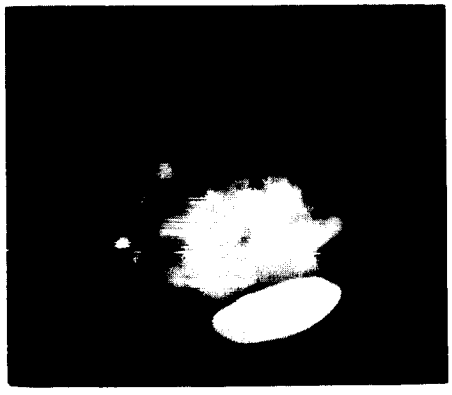

(b)
T=142°K

(c)
T=220°K

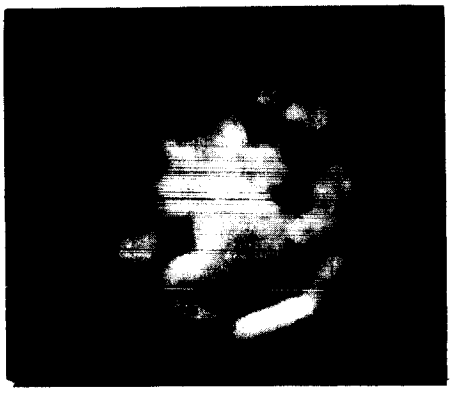

(d)
T=354°K

(e)
T=384°K

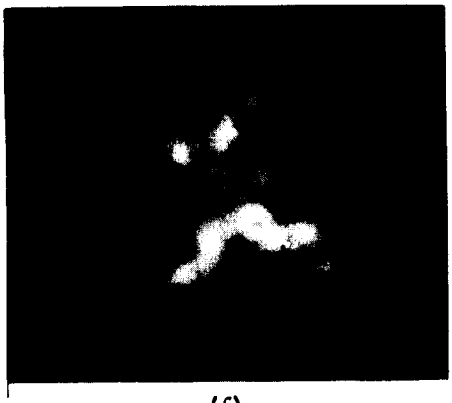

(f)
T=487°K

Figure 2. Sequence of patterns showing migration of a single CsF dose across a W surface. Patterns (c) and (d) are typical Cs on W patterns.

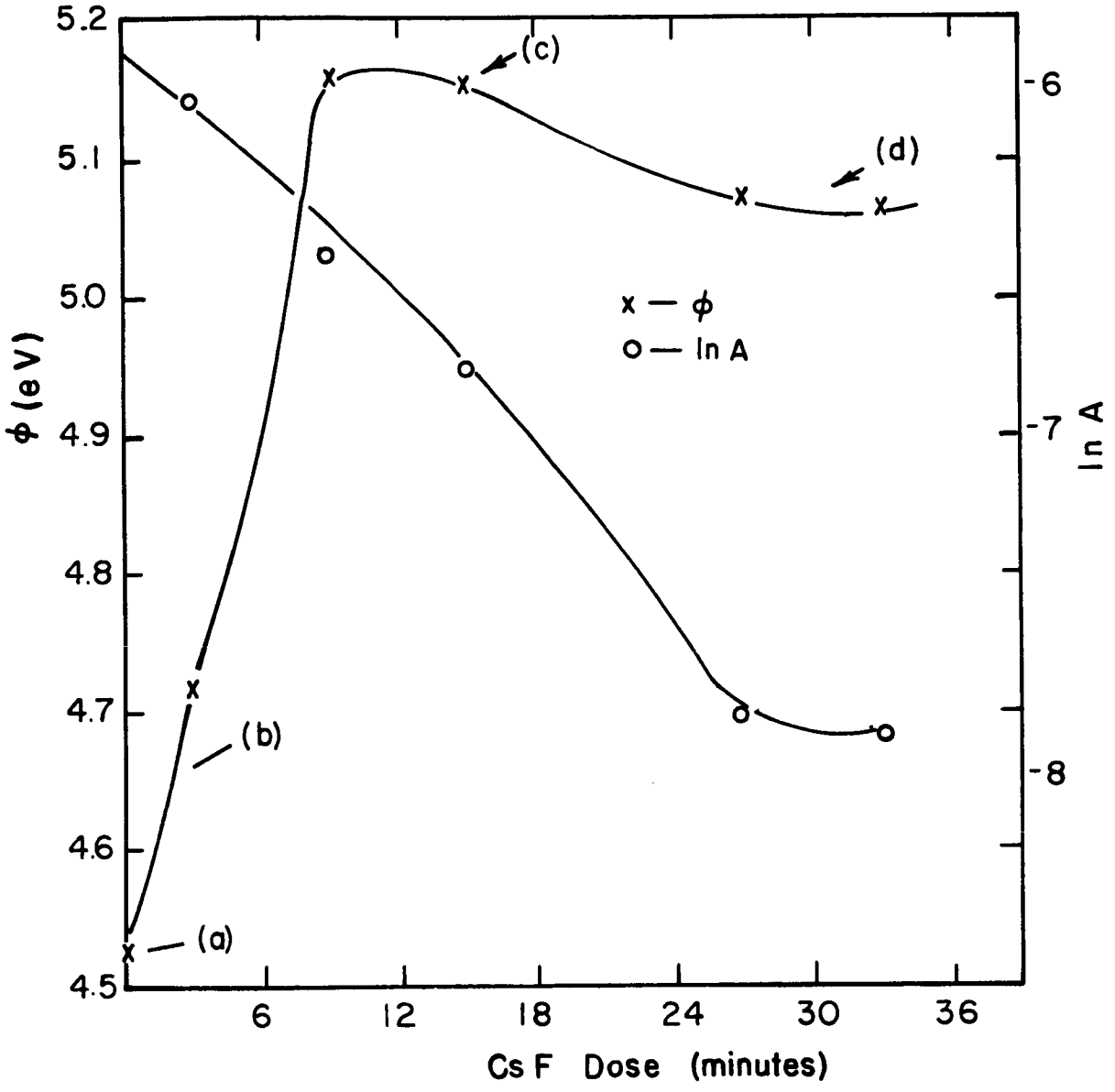

Figure 3. Curves show the variation of ϕ and $\ln A$ as a function of amount of Cs F impinged on a W surface held at 1090°K during deposition. Corresponding patterns indicated on ϕ curve are given in Figure 4.

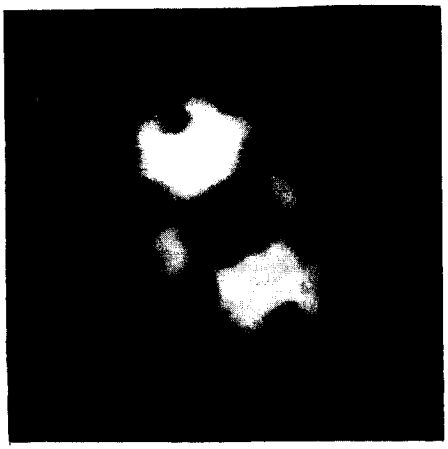

(a)

Clean W

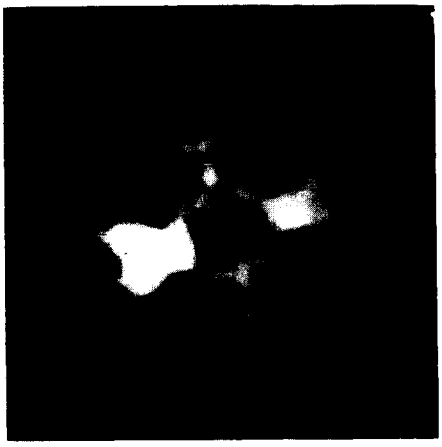

(b)

ϕ=4.65 eV

(c)

ϕ=5.15 eV

(d)

ϕ=5.05 eV

Figure 4. Field emission patterns corresponding to various amounts of F on W as indicated in the ϕ curve of Figure 3.

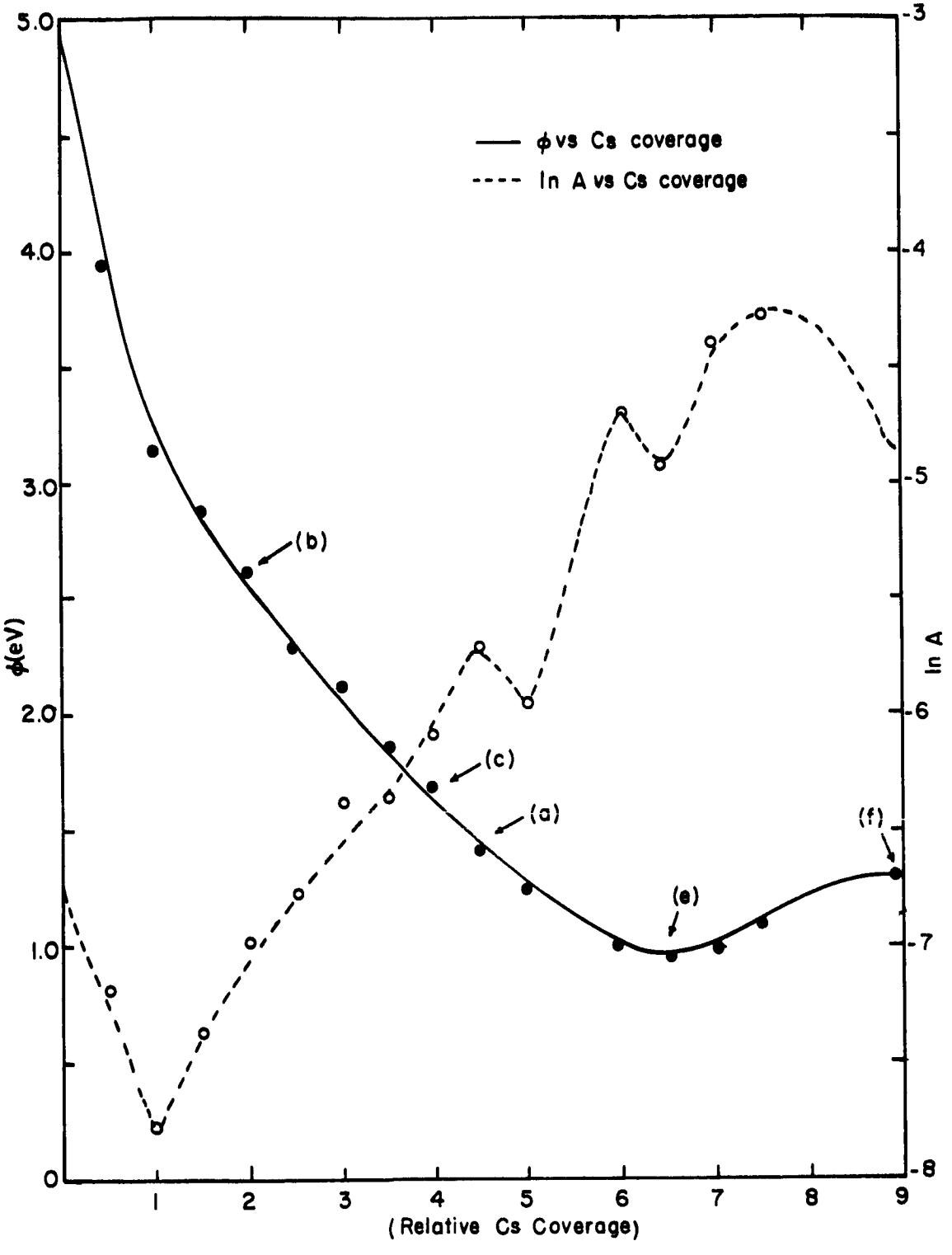

Figure 5. Curves show the variation of ϕ and $\ln A$ with Cs coverage on a FW surface exhibiting an initial work function of 4.97 eV. Corresponding patterns indicated on ϕ curve are given in Figure 6.

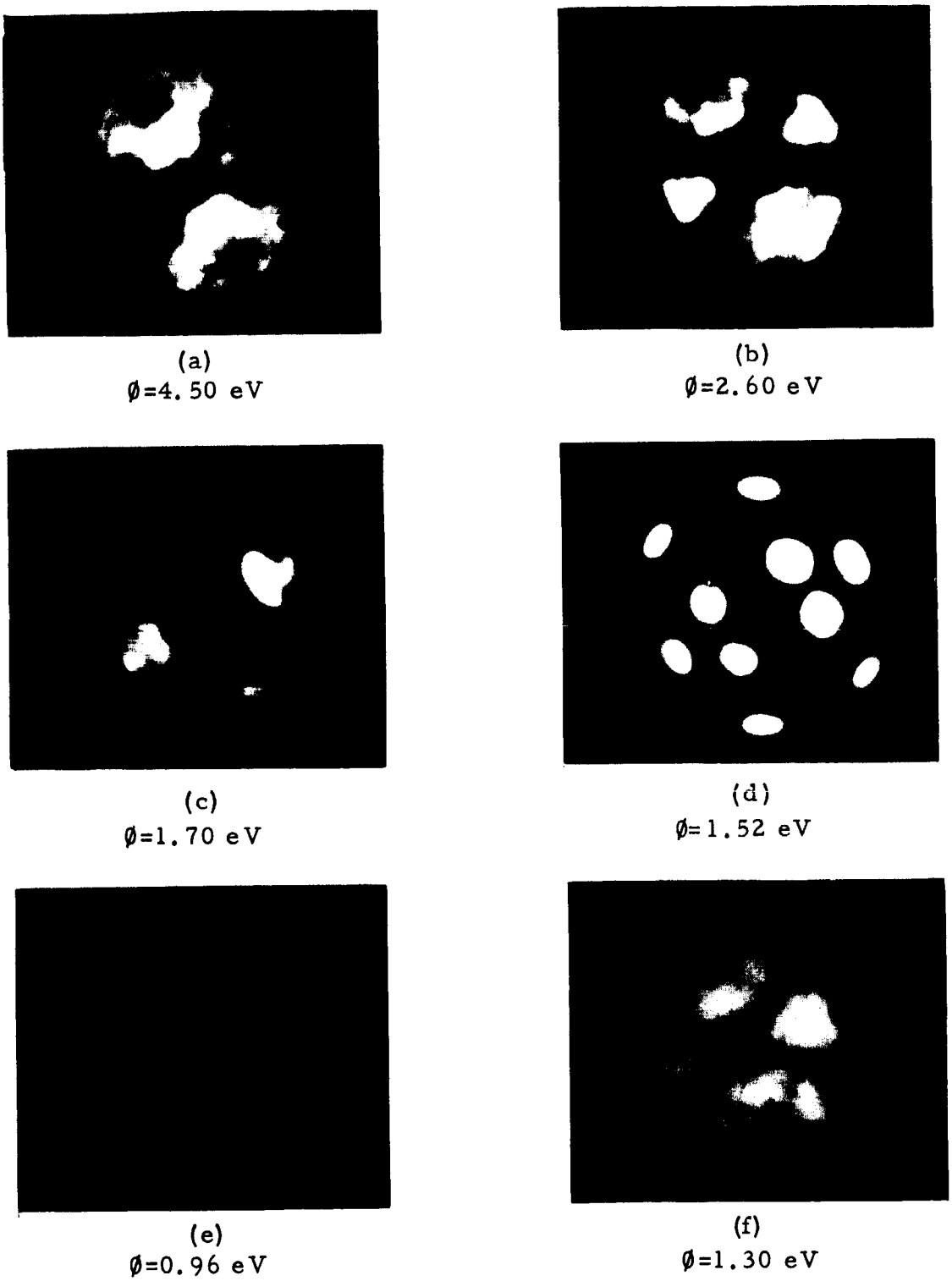

(a)
ϕ=4.50 eV

(b)
ϕ=2.60 eV

(c)
ϕ=1.70 eV

(d)
ϕ=1.52 eV

(e)
ϕ=0.96 eV

(f)
ϕ=1.30 eV

Figure 6. Field emission patterns corresponding to various amounts of Cs on a FW surface as indicated on the ϕ curve of Figure 5.

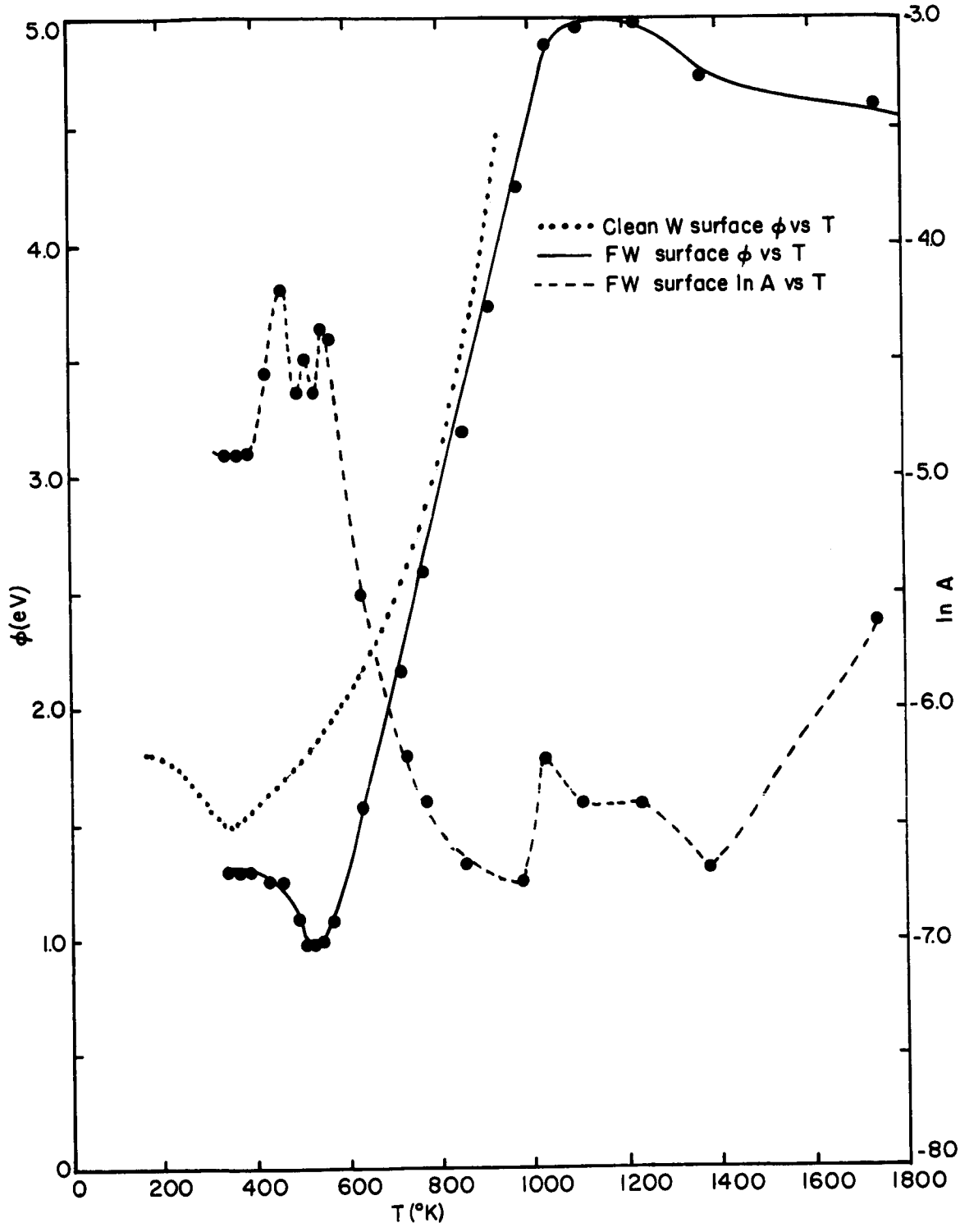

Figure 7. Curves show the variation of ϕ and $\ln A$ upon heating the fully covered surface of Figure 5 for 60 second intervals at the indicated temperatures. Note the work function $\phi = 4.97$ eV of the original FW surface is obtained at 1100°K. Also shown for comparison is the ϕ vs T curve for Cs on clean W.

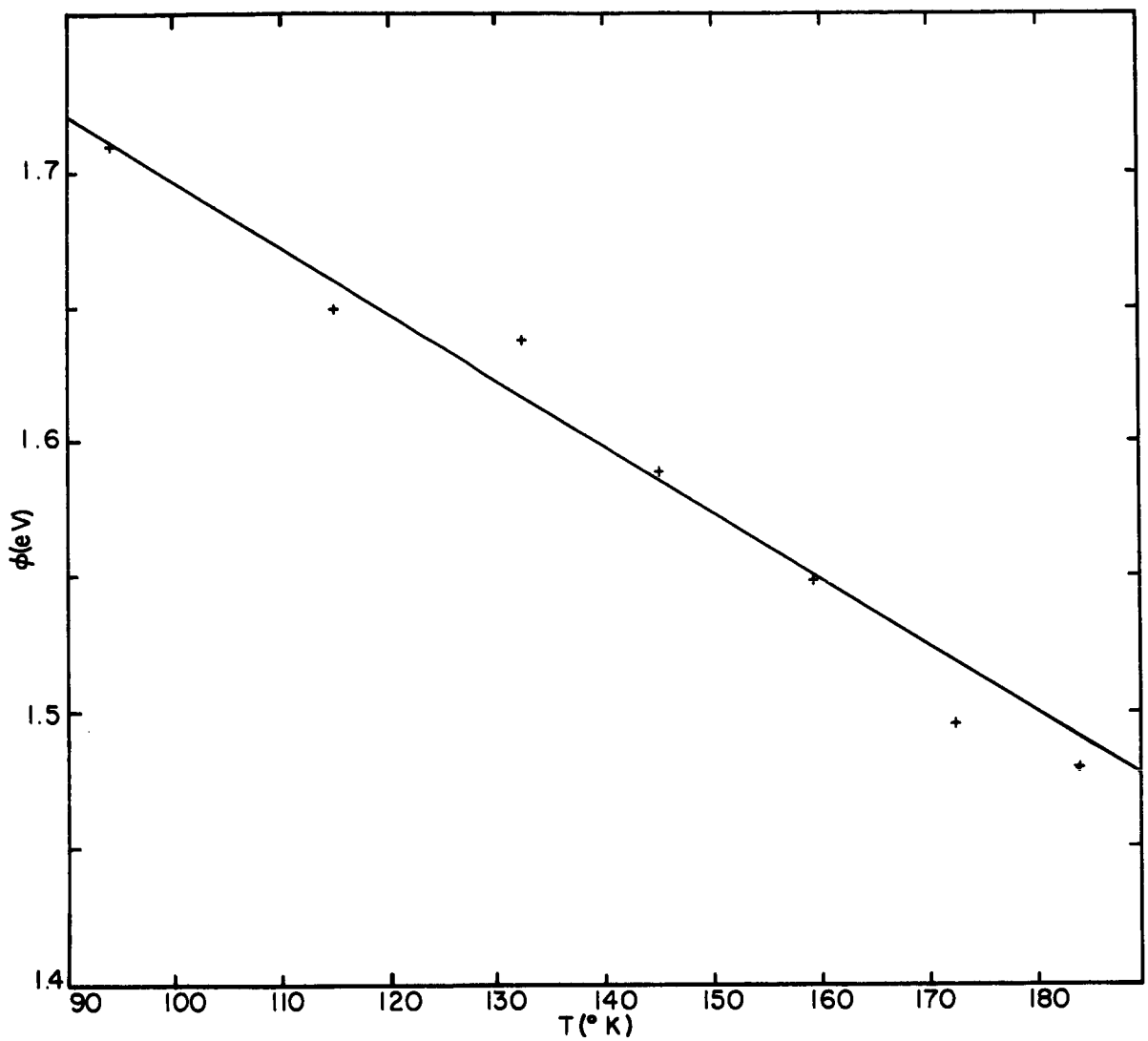

Figure 8. Curve shows the temperature dependence of ϕ for a CsFW surface.

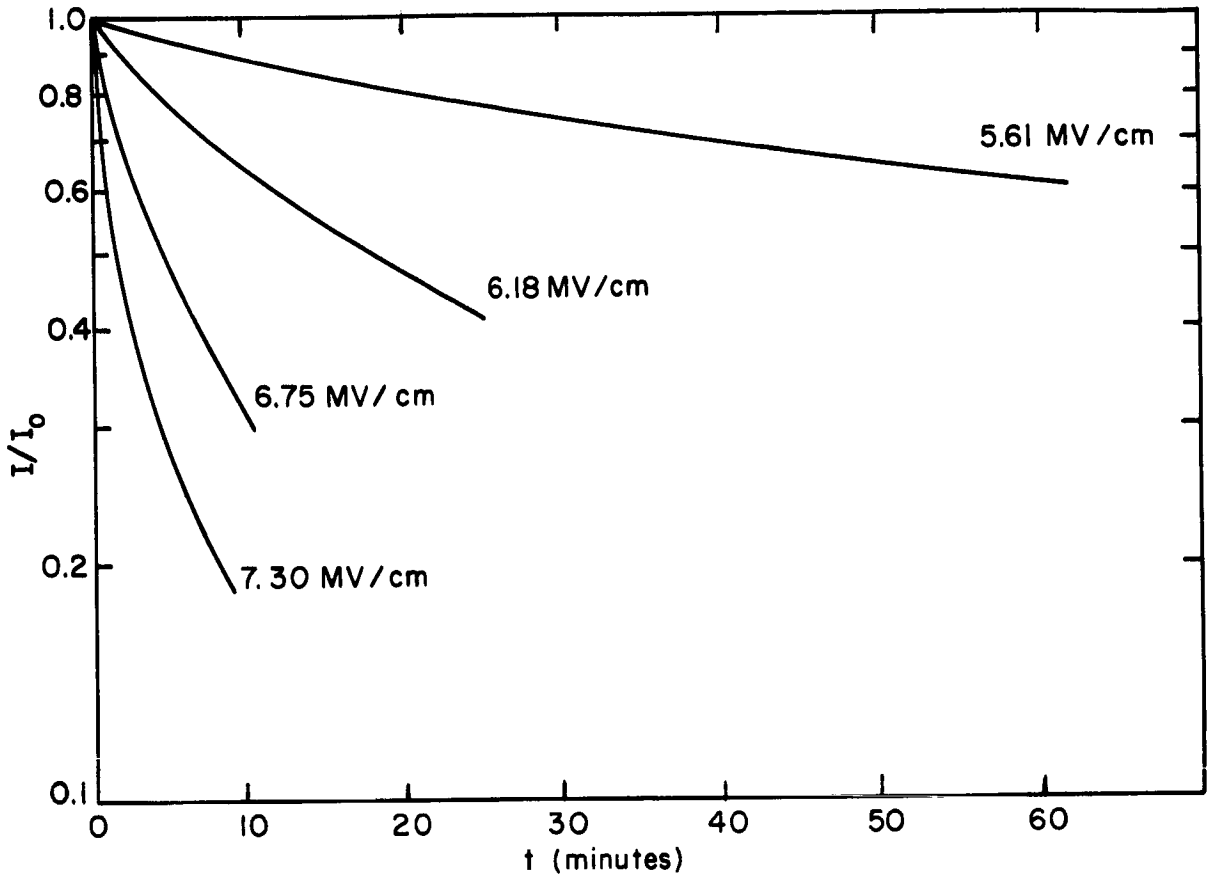

Figure 9. Curves show the variation of the relative field emission current with time at various applied field strengths for a CsFW surface of initial work function $\phi = 1.30$ eV and $T = 77^{\circ}K$.

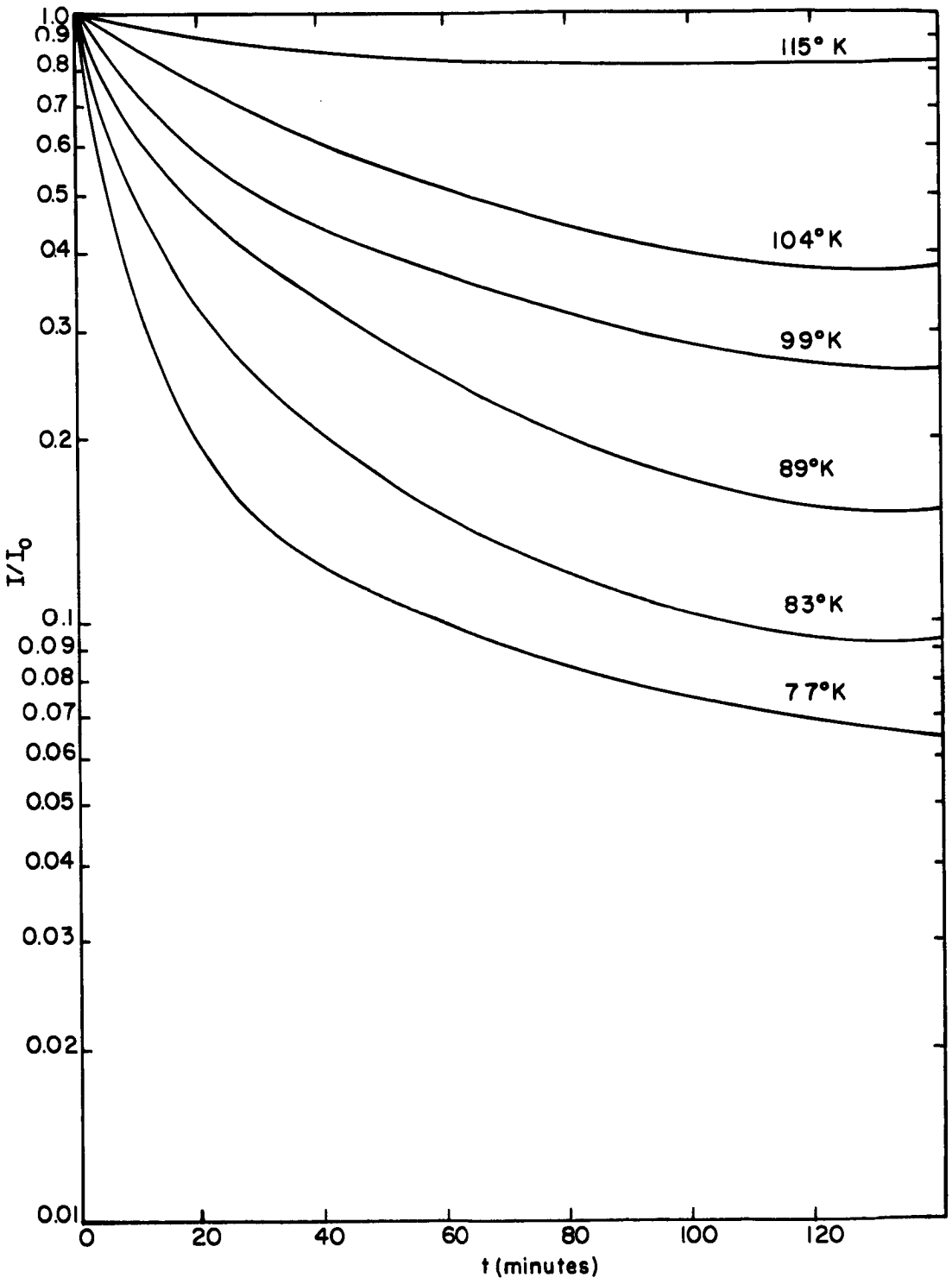

Figure 10. Curves show the variation of relative field emission current with time at various temperatures for a CsFW surface of initial work function 1.25 eV and F = 5.68 MV/cm.